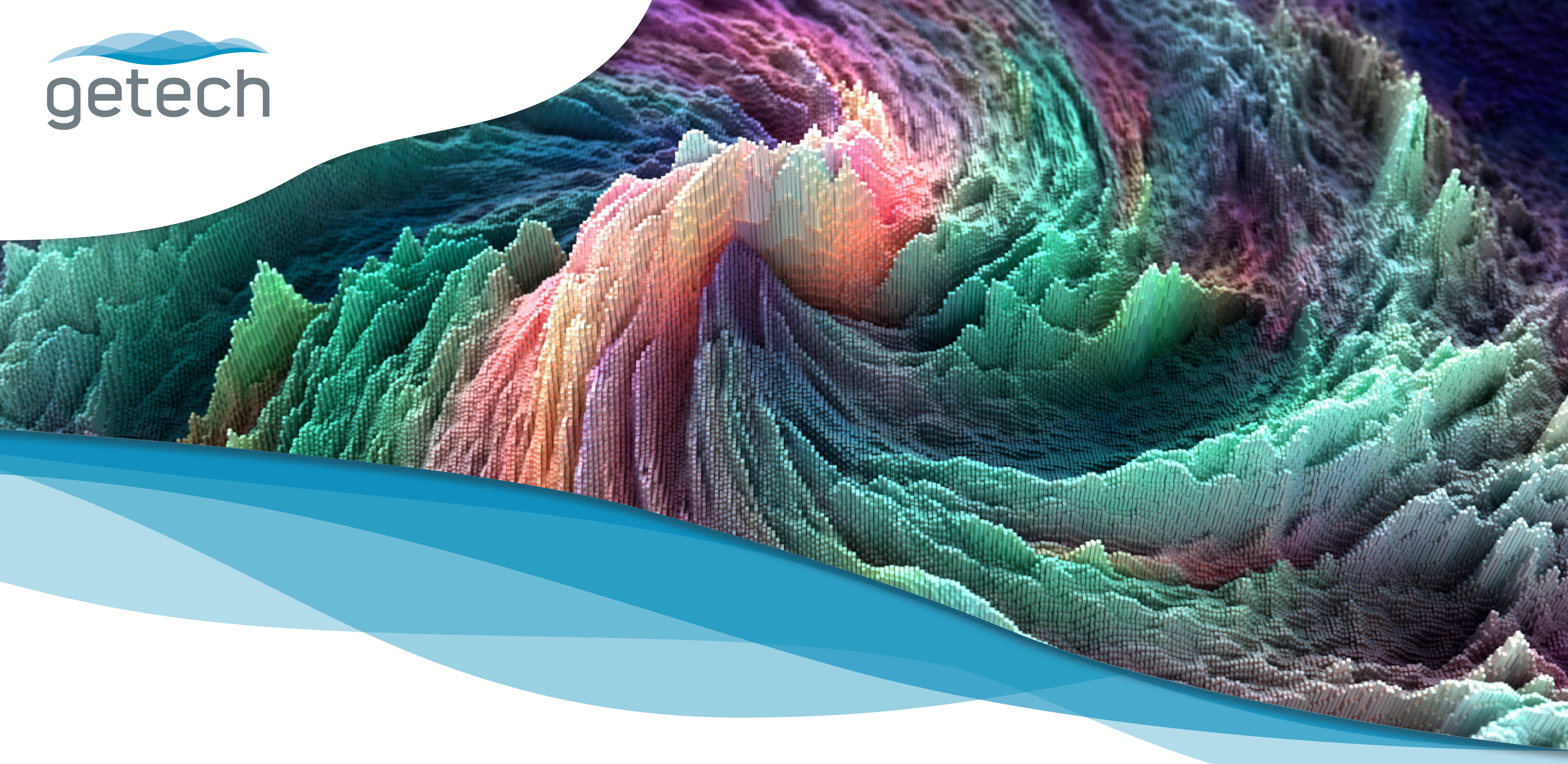

Organic Facies Prediction and Risking of Jurassic Source Rocks, Offshore Nova Scotia

EXECUTIVE SUMMARY

This report presents the results of the Jurassic source rock prediction study undertaken by Getech Group plc on behalf of OERA.

Lower Jurassic source rock horizons recognised across the North Atlantic, along with inconclusive well observations within the Scotian Basin, have led to considerable supposition on the occurrence of more oil-prone lower Jurassic source rocks contributing to hydrocarbons in the Scotian Basin. These are in addition to the more widely recognised Tithonian source that has charged the gas and condensate discoveries found on the Scotian Shelf.

The aim and objective of this study was to predict the distribution of Tithonian and Early Jurassic (Toarcian, Pliensbachian, Sinemurian, Hettangian) source rocks offshore Nova Scotia, based on biogeographic principles derived from modern environments, and palaeoenvironmental interpretations derived from palaeogeographic mapping and Getech's proprietary organic facies prediction (OFP) modelling. In order to ground-truth the model predictions against true data values, the wider region of the European Tethys was initially used to predict (pre-maturation) Total Organic Carbon (TOC) content and Hydrogen Index (HI) of sediments deposited. Subsequent higher resolution modelling was undertaken for the Hispanic Corridor. Source rock risk maps were constructed by taking into account the palaeogeographic, palaeogeological and palaeoocean boundary conditions that would have influenced source rock deposition. The resulting maps will provide a spatial understanding of both the how and where favourable conditions existed for source rock development at the time of deposition.

To provide both the inputs and calibration data for the gross depositional environment mapping (GDE) and the OFP models, extensive data was provided by OERA, and used alongside Getech's internal databases (Globe, Regional Reports) and public domain data.

Gross Depositional Environment (GDE) maps were generated for each of the five proposed source intervals to provide a spatial understanding of coastlines, bathymetry and depositional environments. These maps, have incorporated the tectonic and structural morphology of the depositional basin to identify potential depocentres that would have been favourable for fine-grained source rock deposition, as well as those areas such as intra-basinal highs where fine-grained accumulation would have been less likely.

The Hettangian, Sinemurian and Pliensbachian intervals were deposited during the late syn-rift to early post-rift stage, prior to the first occurrence of oceanic crust in the Central Atlantic, and portray a gradual encroachment of the Tethys Sea. The seaway separating Nova Scotia from Morocco was relatively narrow (~250 km at its widest) and was relatively shallow. Due to the hot and dry climate, the shallow seaway was repeatedly evaporated, resulting in the precipitation of extensive salt and minor anhydrite deposits in the Hettangian. Continued restricted shallow marine conditions established mixed clastic-carbonate sedimentation in the Sinemurian and Pliensbachian. Getech's Multi-Sat gravity data (2019) has enabled us to visualise a series of gravity lows, which may represent former Triassic-Lower Jurassic grabens inboard of the Naskapi, Mohican and Oneida Grabens. These inboard co-eval fluvial-lacustrine continental rift basins stood above the level of the invading Tethys Sea and were subsequently eroded during the break-up unconformity.

The Toarcian represents deposition during the early thermal subsidence stage, immediately after the break-up unconformity and creation of the oceanic crust at the onset of the opening of the Atlantic Ocean. Transgressive shallow water to tidally influenced dolomites and clastics were deposited in a shallow, warm, agitated and extensive ramp system that extended across the Scotian Basin.

The Tithonian interval represents the pinnacle of a Jurassic carbonate reef, bank and platform environments that had formed in the Middle Jurassic and thrived along the basin hinge line on the Lahave Platform. Concurrent with carbonate deposition, increased Late Jurassic clastic input led to the establishment of the Sable and Shelburne delta complexes.

Organic Facies Prediction (OFP) was carried out for the wider Tethys region, utilising Getech's palaeographical and bathymetric reconstitutions as boundary conditions for the modelling. A suitable oxygen minimum zone scenario was defined to capture the widespread anoxia that was evident in the Lower Jurassic epicontinental basins of the Tethys. Initial results showed a good agreement with the data collected for constraining the models, with the modelled TOC values correlating well with the range of published values for the region.

Although this initial Tethys modelling provided favourable correlations, the relatively long, narrow seaway of the Hispanic Corridor within which the Nova Scotia region was located during the Lower Jurassic, is likely to have experienced very different oceanographic conditions to the adjacent Tethyan epicontinental shelf area. As a result of these environmental differences, as well as the lack of data to constrain the oceanographic conditions at the time, it was necessary to refer to modern analogues to define the oceanographical conditions on which to base the higher resolution models for the Hispanic Corridor, with focus on Nova Scotia. Four analogues were identified: Red Sea, Gulf of California, Saanich and the Black Sea. All four scenarios were modelled for each time interval and the most appropriate identified.

Due to the shallow water depths of the Hispanic Corridor Basin at the time of deposition, the water depths of the Red Sea, Gulf of California and Saanich were deemed too deep to be the most accurate analogue for the Lias Hispanic corridor. Therefore, the Black Sea model was considered most appropriate in terms of oceanographic conditions and has been subsequently applied to the source rock risk maps.

The construction of the source rock risk maps involved the stacking of the gross depositional environment maps, with the organic content (TOC), richness (HIA) and oxygen levels derived from the Black Sea OFP model runs.

For each risk map, three conceptual categories of favourable, less favourable and unfavourable were used to classify the source rock parameters. The assignment of each category were based purely on the results of the OFP modelling and GDE mapping results.

The results of the source rock risk mapping for the five Jurassic intervals are shown in Figure 1. The risk maps show the extent of favourable to unfavourable conditions for source rock deposition. However, the risk maps have not taken into account:

- if there was sufficient accommodation space for sediment accumulation;
- potential thickness;
- any post-depositional process that may have perversely(or conversely) affected source rock development and preservation, or;
- maturity of each source interval.

When these extra factors are added, the extent of a productive (and effective) source horizon is likely to be smaller.

Despite being a recognised source rock interval in the Sable Island area, the risk map for the Tithonian interval shows "less favourable" conditions for source rock development when compared with the four Lower Jurassic horizons (Figure 1). This is due to relatively low predicted TOC and HIA (in the modelling results), which are a result of the geometry of the offshore region during deposition. The inboard region consists of a very shallow carbonate platform, bounded by a steep foreslope, where water depth dramatically increased. As a result, the OFP models a significant reduction in sedimentation rate and Carbon Delivery Flux (CDF) with consequently reduced TOC and HI. Additionally, in the Tithonian, the geography and oceanography has changed from a restricted narrow seaway to a fully open marine setting. Therefore, using the Black Sea modelling results will not be as appropriate for this scenario. However, it is important to consider that "less favourable" areas on the risk maps (shown on Figure 1) do not necessarily preclude the possibility of source rock development, only that the prevailing depositional conditions (defined by the palaeogeographical reconstruction) result in moderate to low modelled TOC and HI values; these lower values can still equate to moderate to good source rock potential, but are not as favourable as the very good-excellent potential shown in the "favourable" classification. An example of this is the Annapolis discovery, which lies withing the "less favourable" mapped area for the Tithonian, but there is indirect evidence of a Tithonian source horizon (albeit overmature).

"Less Favourable" to "Unfavourable" conditions were mapped across the palaeo-onshore regions for all five Jurassic horizons. This is due to the lack of direct or modelled data to support a favourable classification. The Abenaki, Sable and Huron Sub-basins playa facies that formed part of the Hettangian salt basin, along with Sinemurian and Toarcian low energy, high salinity coastal areas away from the clastic input, are considered to provide limited favourable conditions for source rock development. This is highlighted by analysis of oil stains from the Mic Mac J-77 and D-89 wells that demonstrates some evidence of a Lower Jurassic source. Elsewhere, the GDE mapping for the palaeo-onshore areas generally show high energy, coarse clastic deposition. These environments typically lower the preservation of organic matter and are likely to have been unfavourable for source rock deposition.

In summary, all four lower Jurassic intervals show favourable conditions for source rock development. Due to the shallow low oxygen conditions, coupled with the high CDF and sedimentations rates predicted, the margins of the marine basin show widespread favourable conditions for organic rich sediments to have been deposited. The Hettangian has the smallest area of favourable conditions, as the water depths were too shallow and mainly within the oxic zone as a result of it being in the early development of the Hispanic corridor. As the Hispanic corridor widened and deepened during the Sinemurian to Toarcian, a greater area of the offshore region fell within the optimum PZE depositional conditions for organic rich sedimentation, therefore the spatial extent of favourable source rock development increases during the later stages of the Lower Jurassic.

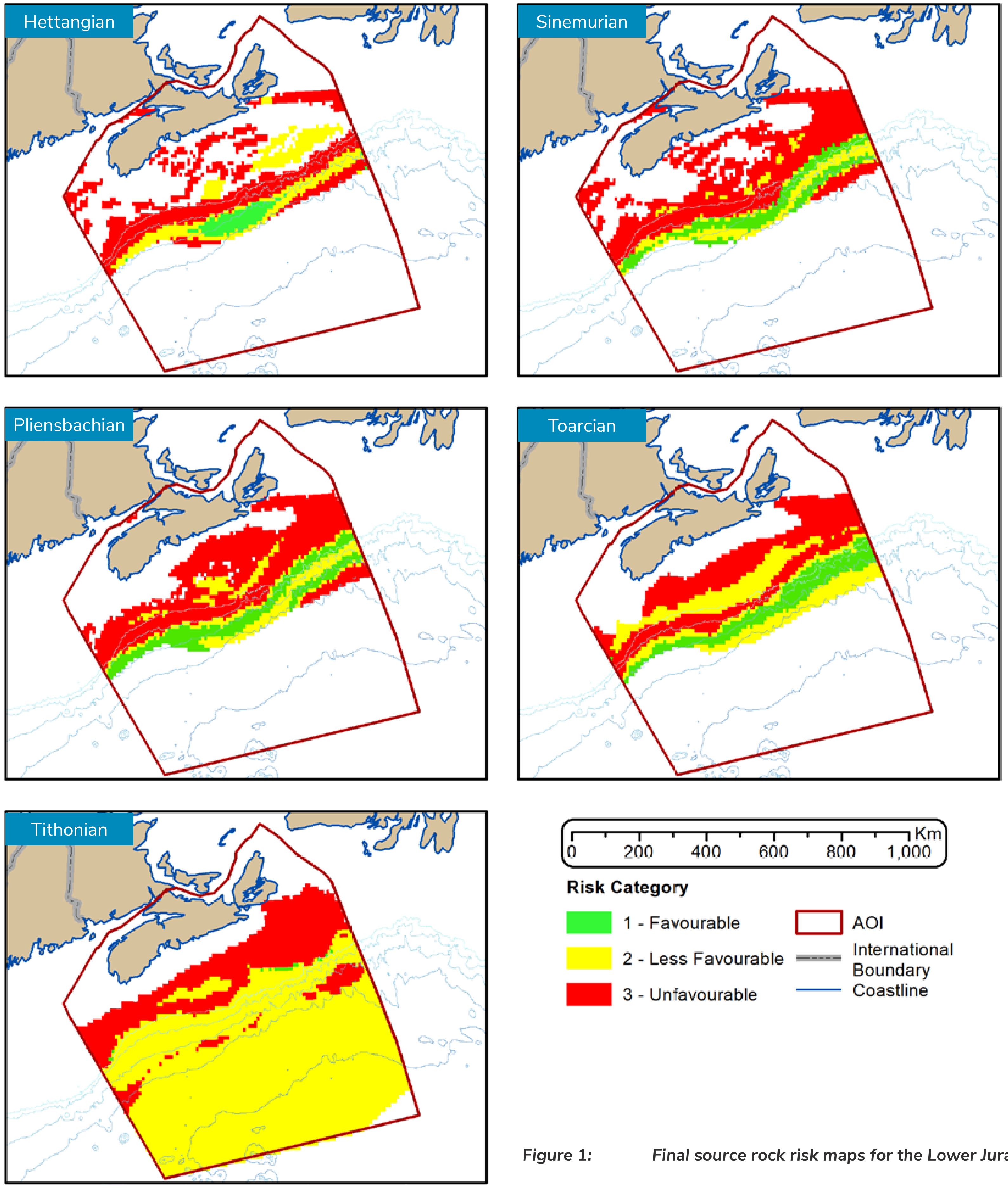

Figure 1: Final source rock risk maps for the Lower Jurassic and Tithonian intervals.

TABLE OF CONTENTS

1. INTRODUCTION

This report presents the results of the Jurassic source rock prediction study undertaken by Getech Group plc on behalf of OERA.

According to the Play Fairway Analysis series of reports (Beicep-Franlab, 2011-2019), there are a total of five source rock intervals on the Scotian Margin: intra-Aptian (mid Cretaceous), Valanginian (early Cretaceous), Tithonian (Late Jurassic), Callovian (mid Jurassic), and Pliensbachian (Early Jurassic). Basin modelling results from the same studies suggest that the two most important source rocks are the Tithonian and the Pliensbachian. Of these two, the Tithonian is well documented, with penetrations in seven wells, whereas the Pliensbachian has never been directly observed; its presence is only inferred from sparse biomarker data in oils and fluid inclusions, isotopic data in seafloor seeps, and circumstantial evidence from conjugate margins in Portugal and Morocco.

From inconclusive well observations and other recognised Lower Jurassic source horizon across the North Atlantic, there has been considerable supposition on the occurrence of a more oil prone lower Jurassic source rock contributing to hydrocarbons in the Scotian Basin.

The aim of this work was to predict the depositional distribution of Tithonian and early Jurassic (Toarcian, Pliensbachian, Sinemurian, Hettangian) source rocks offshore Nova Scotia (Figure 1.1), based on biogeographic principles derived from modern environments, and palaeoenvironmental interpretations derived from palaeogeographic mapping, palaeoclimate and palaeooceanographic models. In order to ground-truth the model predictions against true data values, the wider region of the European Tethys (Figure 1.2) has been included, where several known Lower Jurassic source rocks have been observed and there is sufficient data to compare model results to ensure a good regional model fit against know data values.

1.1 PROJECT OBJECTIVES

Covering the Tithonian, Toarcian, Pliensbachian, Sinemurian, Hettangian stages, the project consists of four main objectives:

1.1.1 DATA COMPILATION & REVIEW

Integrating all data from OERA and Getech, as well as undertaking a full literature search for additional data to provide both the inputs and calibration data for the Palaeoenvironmental mapping and the OFP models. Data was made available by OERA along with Getech's internal database (Globe, Regional Reports) and public domain data. The types of data compiled included:

- Petroleum fairway analysis (PFA) reports (Beicep-Franlab, 2011; 2014; 2015; 2016; 2019a; 2019b)
- GSC Basins database
- CNSOPB-DMC database (well/biostratigraphy reports)
- Proprietary well reports & data supplied by OERA

1.1.2 GROSS DEPOSITIONAL ENVIRONMENT (GDE) MAPS

Construction of GDE maps for each of the five source rock intervals. By integrating Getech's understanding of the region's palaeogeography, findings from published literature and data provided by OERA into a regional geological model for each of the time intervals to identify potential depocentres that would have been favourable to fine-grained source rock deposition, as well as those areas such as intra-basinal highs where fine-grained accumulation would have been less likely.

1.1.3 ORGANIC FACIES PREDICTION (OFP) MODEL

Using Getech's proprietary Organic Facies Prediction (OFP) to predict initial (pre-maturation) Total Organic Carbon (TOC) content and Hydrogen Index (HI) of sediments deposited. This will focus on the AOI shown in Figure 1.1, but in some cases will cover a wider area (approx. North and Central Atlantic; Figure 1.2) to provide greater regional context and calibration within the Area of Interest.

1.1.4 SOURCE ROCK RISK MAPS

Source rock potential risk maps have been constructed by taking into account the palaeogeographic, palaeogeological and palaeocean boundary conditions that would have influenced source rock deposition. These maps will provide a spatial understanding of both the how and where favourable conditions existed for source rock development at the time of deposition.

1.2 DELIVERABLES

The deliverables are in digital format and consist of the following:

- A technical report in PDF format
- An Esri ArcGIS MXD project and geodatabase v.10.5

The Esri ArcGIS Digital Maps for the five Jurassic timeslices, include the following:

- Gross Depositional Environments Maps:
  - Broader scale palaeogeographic reconstructions for the North and Central Atlantic for the Jurassic timeslices (provided in palaeoposition)
  - The higher resolution GDE maps for the area covered in Figure 1.1 highlighting areas of potentially mud-rich depositional environment (provided in palaeoposition)
- Models of Climate and Ocean Boundary Conditions and Organic Facies Prediction (OFP) (provided in palaeoposition)
  - Oxygen ocean boundary conditions for different oxygen scenarios
  - Models of initial (pre-maturation) Total Organic Carbon (TOC)
  - Content and Hydrogen Index (HI) of sediments deposited
  - Coastal upwelling based on assessment of general circulation model climate data
- Source Rock Presence Risk Maps (provided in Present Day position)

The projection used for Esri ArcGIS Digital Maps for the all the palaeo-projected data is GCS WGS 1984; and for the Present Day data NAD 1927 UTM Zone 20N.

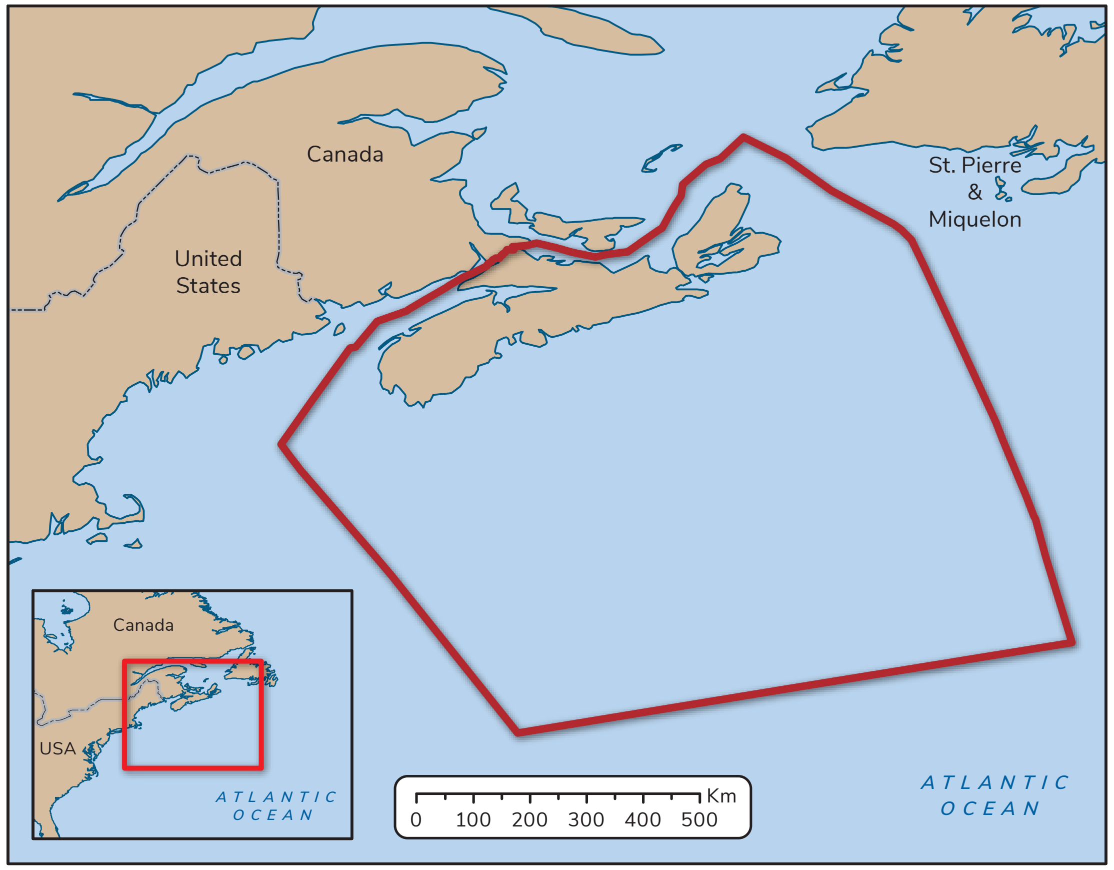

Figure 1.1: ***The area of interest used for the gross depositional environment mapping and source rock risk maps (Chapters 2 and 4).***

Figure 1.2: ***The European Tethys area (shown as an example on the Hettangian timeslice) was included in the data collection and baseline organic facies prediction models (Chapter 3).***

2. GROSS DEPOSITIONAL ENVIRONMENT MAPPING (GDE)

2.1. INTRODUCTION

A series of paleoenvironmental maps have been generated for each of the five proposed source rock time intervals:

- Tithonian
- Toarcian
- Pliensbachian
- Sinemurian
- Hettangian

The paleoenvironmental maps generated for each of the proposed source rock intervals will then form the base maps for the Organic Facies Prediction (OFP) modelling.

Getech has evaluated the existing coastline, bathymetric, and gross depositional environment interpretations in our Mega Regional Explorer Paleogeography reconstructions built on Getech Plate Model 4.1, against the OERA supplied data (see Section 2.3) and additional literature data and interpretations collected for any potentially lower confidence areas. Coastlines, bathymetry and gross depositional environments, especially for potentially mud-rich depositional environments, have been refined to honour the higher resolution local data.

2.2. APPROACH & METHODOLOGY

Gross Depositional Environments (GDE) maps provide a powerful predictive tool for extending interpretations beyond the extent of existing data (e.g. wells, outcrop) by providing explorationists with a visual link between tectonics and spatial relationship of depositional environments. The GDE maps have been generated using a series of well-constrained methodologies (Figure 2.1). The underlying concept is to map contemporary base level. The maps are therefore designed to represent those areas both above base level which are in the erosional realm and also potentially supplying sediment to those areas below base level where deposition takes place. Palaeodrainage provides a reconstruction of the transport pathways connecting source to sink areas on land.

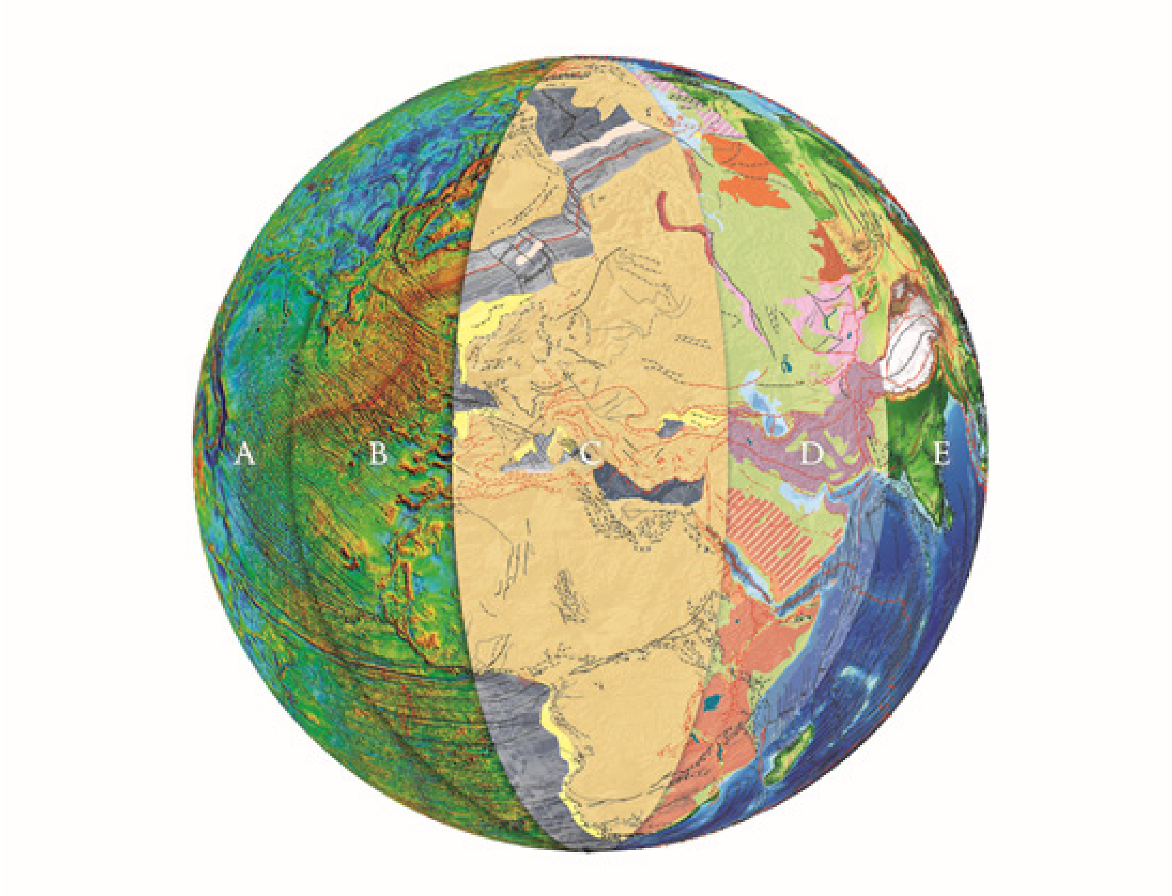

Figure 2.1: A graphical representation of the workflow that represents the layers from which the palaeogeographies are built up within Globe.

A) Potential field data set; B) potential field data are used to pick lineaments for a global structural coverage; C) structures define the boundaries for the plate polygons and terranes; D) using the plate model and interpreted structures, environments and lithologies are mapped, and E) environments are boundaries used by drainage and DEMs for both onshore and offshore.

Palaeogeographic mapping involves four main stages (Figure 2.1):

- Structural mapping
- Plate modelling
- Gross depositional environment (GDE) mapping
- Drainage analysis

Using Getech's Global Plate model (Version 4.1), the structural elements, points data, and other relevant geological data are rotated onto the appropriate timeslices and used to constrain the depositional environments. Structures have been rotated to their reconstructed positions for each timeslice, based on whether they were present at the time specified and also whether they were active (motion during interval) or inactive (no evidence of motion during the timeslice interval).

The palaeoenvironments were then drawn around these structural elements to the edge of the interpreted contemporary depositional limit (whether preserved or not at the Present Day). Areas of upland tectonophysiographic terrains (above base-level) were assigned to their thermomechanical origin and age of activity relative to the timeslice in question (See Section 2.4.2). The mapped GDEs, provide reconstructions of the palaeolandscape, and combined with drainage pattern evolution analysis enables us to reconstruct the palaeodrainage.

Figure 2.2 (Right): Wells with key wells labelled (top) and line data (bottom) used for GDE mapping; Scotian margin.

2.3. DATA

Geological data sets have been used to underpin and constrain the GDE maps. Data was made available by OERA along with Getech's internal database (Globe, Regional Reports) and public domain data. The types of data compiled include:

- From OERA
  - Seismic-surface and isopach grids from the Petroleum fairway analysis (PFA) reports (Beicep-Franlab, 2011; 2014; 2015; 2016; 2019a; 2019b)
  - Digital versions of the GDE grids from the PFA Studies
  - Biostratigraphy reports for selected Moroccan Wells
- From Getech:
  - Palaeogeographic data (Globe mega-regional palaeogeographies)
  - Data from pertinent Getech Regional Reports, especially "Tectonic Evolution of the North Atlantic: Implications for Prospectivity".
- Publicly available Well Data (environmental and lithological data; Figures 2.2; 2.3 & Table 2.1)
  - Petroleum fairway analysis (PFA) reports (Beicep-Franlab, 2011; 2014; 2015; 2016; 2019a; 2019b)
  - GSC Basins database
  - CNSOPB-DMC database (well/biostratigraphy reports)
- Cross-section (Seismic, structural, well correlations; Figures 2.2 & 2.3)
  - Getech internal database
  - PFA reports (Beicep-Franlab, 2011; 2014; 2015; 2016; 2019a; 2019b)
  - Literature review
- Literature review
  - Open file reports (downloaded from OERA, CNSOPB, GSC, Geoscan)
  - Published papers

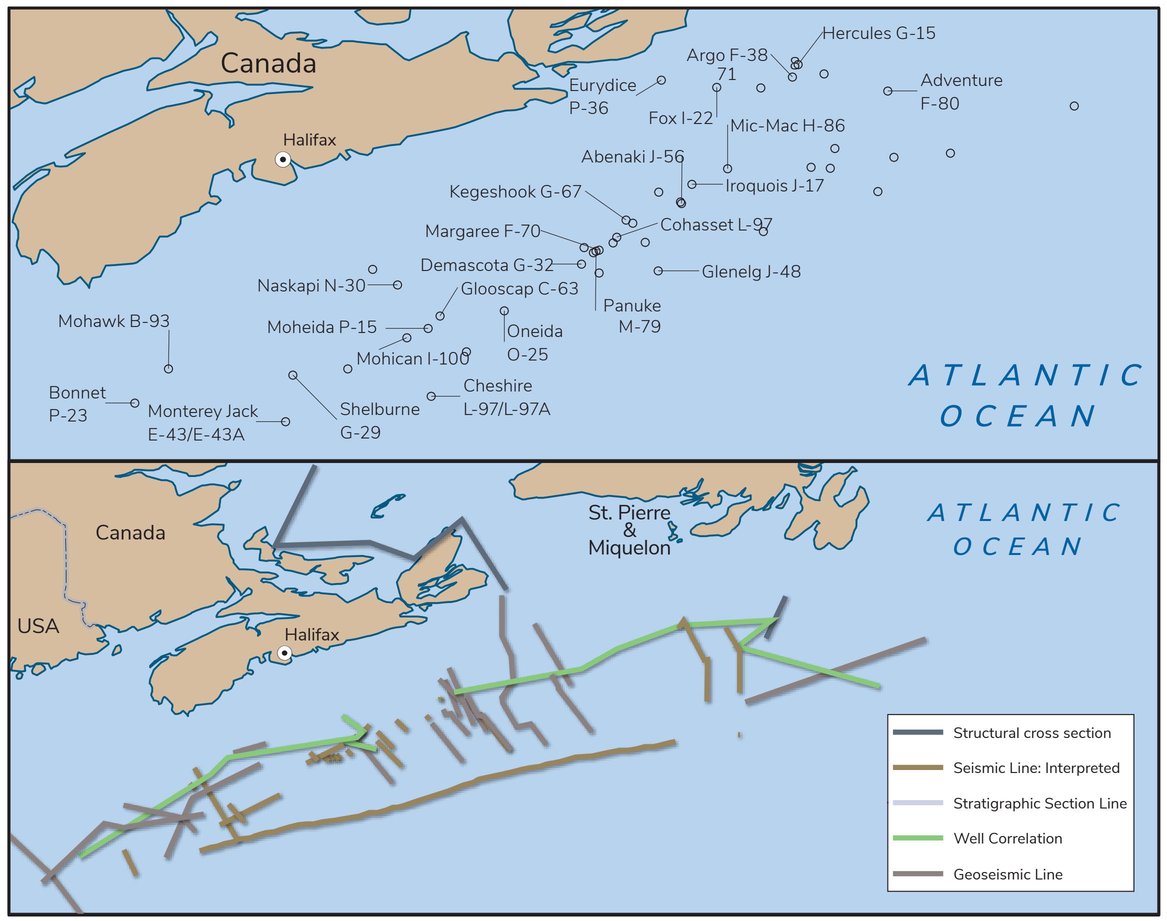

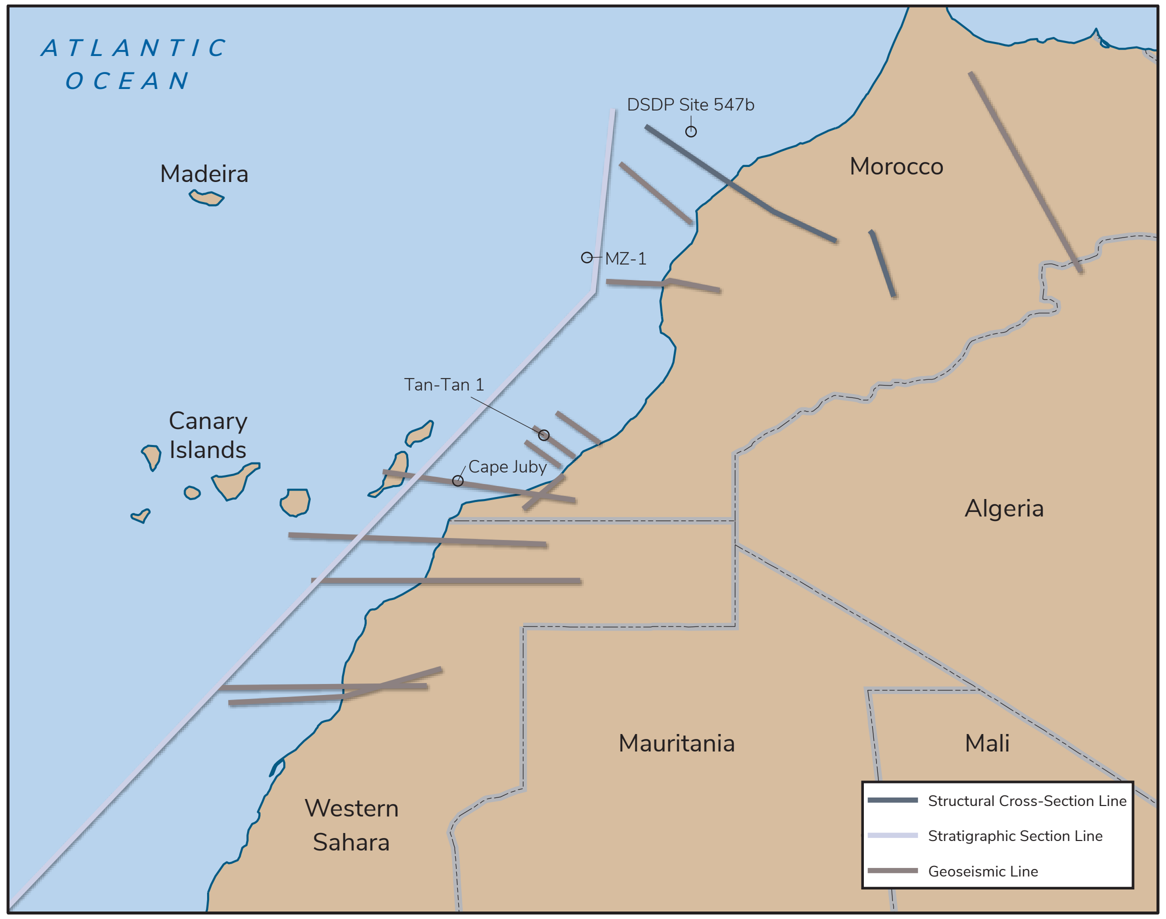

Figure 2.3 (Left): Well and line data used for GDE mapping; Moroccan margin.

2.3.1 DATA RELIABILITY AND RESOLUTION

The point data used in the construction of the GDE maps represents a variety of reliabilities and resolutions (Figure 2.4). Each data point is placed on the map and is presumed to represent a single observation. However, the time presented by each locality varies, due in part to dating and correlation uncertainties. Consequently, the recorded information for a locality may represents a temporal resolution that spans more than one geological stage. For example, the map might show sandstones for a particular formation at a particular locality that is dated as Hettangian–Sinemurian. The conceptual 'time-plane' cuts this unit at some point within this section, although the poorly resolved dates means that it is impossible to say exactly where. The more points there are, the greater the uncertainty, which means that there is no guarantee that two adjacent data points plotted on a map were actually coeval.

Additionally, differentiating the ages of the Lower Jurassic strata across the Scotian margin is problematic as biostratigraphic recovery is poor (Weston et al., 2012). For example, beneath the occurrence of Middle Jurassic markers Glooscap C-63, Mohican H-100, and Moheida P-15, the Iroquois and/or Mohican Formations are nearly barren, with only palynomorphs of Jurassic age that do not allow the distinction of Middle Jurassic from Early Jurassic. In the revised biostratigraphy study of the Scotian margin by Weston et al. (2012), no clear biostratigraphic signal of Early Jurassic was detected in any of the wells they studied, even contrary to earlier studies, and was therefore assigned an indeterminate, possibly Jurassic, age to these intervals. Table 2.1 shows the collation of wells that were used to constrain the five Jurassic GDE's across the Scotian margin. For wells where the biostratigraphy reports stated that the interval was barren and/or indeterminate, environmental and lithological information collected was allotted based on the assigned formation name.

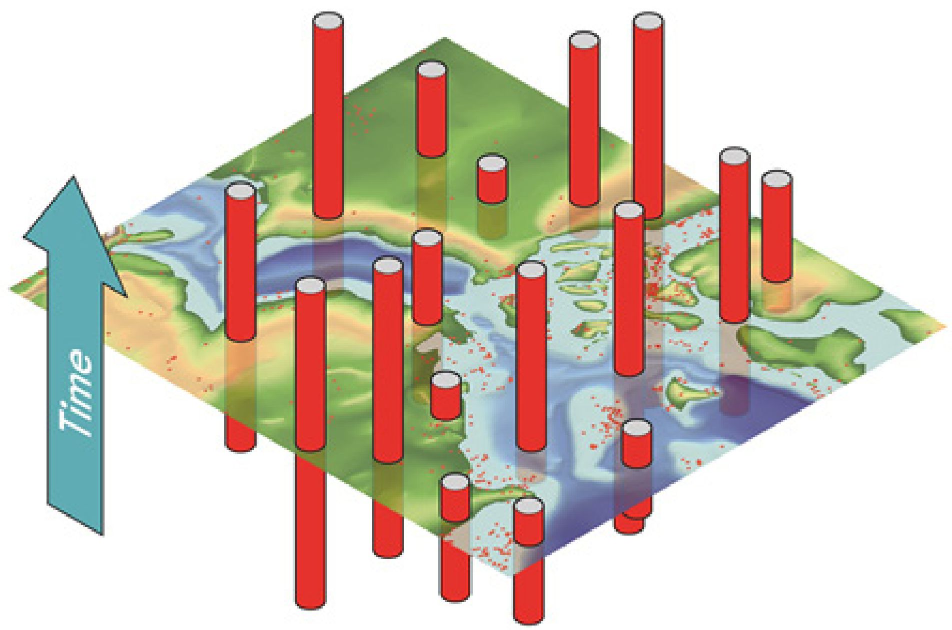

Figure 2.4: ***The data points are placed on a map and represent a single location. Each point represents a variety of reliabilities and temporal resolutions, with the red cylinders showing examples of the temporal grain of data that may be used to construct a timeslice map (Markwick & Valdes, 2004).***

Well	Environment Data	Lithological Data	Tithonian	Toarcian	Plienbachian	Sinemurian	Hettangian
Abenaki J-56	y	y	Mic-mac/Missisauga	Mohican	Iroquois	Iroquois	
Abenaki L-57		y	ABSENT	Iroquois	Iroquois	Argo	Argo
Acadia K-62	y	y	Anenaki	Iroquois	Iroquois	Argo	
Adventure F-80			ABSENT		Iroquois/Argo	Iroquois/Argo	Argo
Albatross B-13	y	y	Anenaki				
Alma F-67	y	y	mic mac				
Argo F-38	y	y	Mic Mac	Iroquois	Iroquois	Iroquois/Argo	Argo/Red beds
Bandol-1			ABSENT				
Bonnet P-23	y	y	Anenaki	Iroquois	Iroquois	Iroquois	
Chippewa G-67	y	y	Mic Mac	ABSENT	ABSENT	ABSENT	Argo ~
Cohasset L-97			Mic-mac/Missisauga	Iroquois	Iroquois	Iroquois	
Como P-21	y		Anenaki				
COST G-1			mic mac				
Cost G-2			mic mac	Mohican/Iroquois	Mohican/Iroquois		
Crow F-52	y	y	ABSENT	Mohican	Mohican/Iroquois	Mohican/Iroquois	ABSENT
Dauntless D-35	y		mic mac				
DEMASCOTA G-32	y		Anenaki				
Dover A-43	y		Mic Mac	?Mohican	?Mohican		
East Wolverine G-37			ABSENT				
Emerillon C-56			ABSENT				
Eurydice P-36	y	y	ABSENT	Iroquois	Iroquois	Iroquois/Argo	Argo/Red beds
Fox I-22	y	y	Mic Mac	ABSENT	ABSENT	ABSENT	ABSENT
Glooscap C-63	y	y	Anenaki/Missisauga	Mohican	Mohican/Iroquois	Iroquois	Glooscap volcs/Argo
Hercules G-15	y		Mic Mac	Iroquois	Iroquois	Argo	Argo
Hesper P-52	y	y	mic mac				
Huron P-96	y	y	Mic-mac/Missisauga	Iroquois	Iroquois	Iroquois/Argo	Argo
Iroquois J-17	y	y	Missisauga	Iroquois	Iroquois	Iroquois	Argo
Jason C-20				Iroquois	Iroquois	Argo	Argo
Kegeshook G-67	y	y	Anenaki				
Margaree F-70	y	y	Anenaki				
Marquis L35	y	y	Anenaki				
Mic-Mac H-86			mic mac				
Mohawk B-93	y	y	Mohawk	ABSENT	ABSENT	ABSENT	ABSENT
Moheida P-15			Anenaki	Iroquois	Iroquois		
Mohican I-100	y	y	Baccaro Fm	Iroquois	Iroquois	Iroquois/Argo	Argo
Naskapi N-30	y	y	Mic-mac	?Mohican	?Mohican	ABSENT	ABSENT
Oneida O-25	y	y	Baccaro Fm	Mohican	Mohican		
Panuke M-79			Anenaki				
Primrose N-50	y	y				Argo	Argo
Queensland M-88	y	y					
Sambro I-29			ABSENT	ABSENT	ABSENT	ABSENT	
Shelburne G-29	y	y	Verril canyon				
South Griffin J-13	y	y	Mic mac/misane				
Thebald I-94	y	y	Missisauga				
West Esperanto B-78	y	y	mic mac				
Glenelg J-48	y		Verril canyon				
Monterey Jack E-43		y	Verril canyon				
Cheshire L-97		y	Verril canyon				
	Full Biostratigarphic recovery						
	Indeterminate						
	Not penetrated						
	Absent						
	Palyontological recovery only						

Table 2.1: ***Reference wells used for the Jurassic GDE's. Full biostratigraphic age assignments was possible for the Tithonian for many of the wells. Only a small number of wells have penetrated the Lower Jurassic, with no wells that can demonstration accurate age constraints.***

2.4 LEGEND

Figure 2.5 shows the Legend for the GDE maps.

GDEs are separated into two main categories;

- Depositional environments (areas below base level)
- Tectonophysiographic terranes (areas above base level).

2.4.1 DEPOSITIONAL ENVIRONMENTS

GDEs combine the depositional environment and the lithology deposited. The GDEs are separated into the following types:

- Continental, which includes alluvial, fluvial, floodplains, aeolian, wetlands, etc.
- Lacustrine
- Delta top
- Coastal/transitional, which includes coastal, sabkhas, lagoons, mangroves, saltmarshes, inter-tidal, supra tidal etc.
- Marine environments: shallow shelf (<50 m), deep shelf (50–200 m), carbonate platform/ramp slope and basin floor.

As the depositional environments are mapped to their original depositional extent (prior to any subsequent erosion), the GDEs have been further differentiated into preserved or inferred and eroded, with the eroded category representing areas where the strata has been subsequently eroded.

- Shading of the lithologies displayed are also subdivided:
- Subcrop – Lithologies observed by well penetration
- Inferred – Secondary information; Lithologies from published data but does not have specific spatially precision.

2.4.2 TECTONOPHYSIOGRAPHIC TERRANES

Tectonophysiographic terranes (TPTs) are related to a specific tectonic regime defined by a series of mantle and crustal processes or driving geodynamic forces. These are areas above base level that are mapped and coded so that the last uplift mechanism in the local area is accounted for.

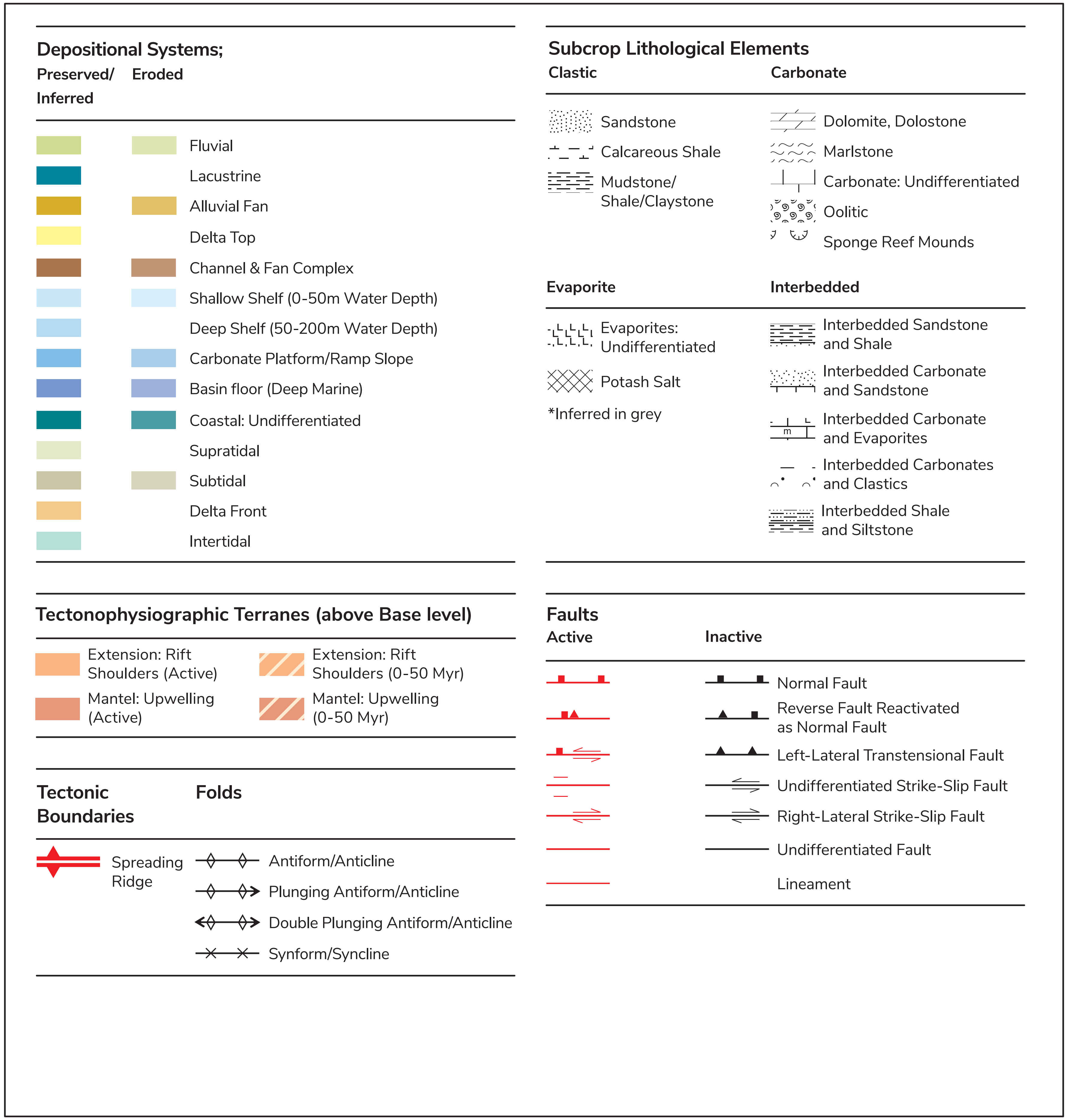

Figure 2.5a: GDE map legend.

Figure 2.5b: Legend for the Getech Globe regional insert maps.

2.5 BACKGROUND

The Present Day Nova Scotian margin is the result of a complex evolution since the Proterozoic. A collage of terranes (Figure 2.6) were rifted from Gondwana in the Palaeozoic and were progressively accreted to the North American and European continents during the Caledonian, Appalachian and Variscan orogenies. In eastern North America, these orogenies contributed to a period of continental growth prior to the formation of the supercontinent Pangaea. The consequence of these orogenies is that there is a wide zone of weakened crust stretching from Newfoundland to the Gulf of Mexico. The sutures between terranes are key crustal weaknesses, which are reactivated as rift faults from the Triassic.

The distribution of Palaeozoic terrane accretion is probably the reason why Triassic syn-rift sedimentation is mainly restricted to the North American margins (Labails et al., 2010). Rifting here occurs in the wide zone of accreted terranes, where pre-existing weakness along the sutures allows for easier rifting than on the African margins, where rifting is adjacent to the craton.

The Nova Scotia margin lies outboard of three accretionary domains: the Meguma, Avalon and Gander domains. These are, respectively:

- Cambrian and Ordovician deep marine deposits
- A Neoproterozoic continental fragment
- Gondwanan origin arc terranes

All of these domains crossed the Iapetus and Rheic oceans and were accreted to North America. The Moroccan margin lies outward of the younger Atlas Mountains, which appear to form along pre-existing faults, suggesting that Morocco behaved as a microplate during the early Central Atlantic opening. This likely explains why Morocco is the only location where Triassic syn-rift is observed on the African side of the Central Atlantic (Labails et al., 2010).

2.5.1 RIFTING AND BREAKUP

Sedimentary basins around the Central Atlantic region have Triassic continental red beds at the base of structural grabens as part of the basin fill (Figure 2.7). These are indicative of the early phases of continental rifting; they are more prominent on the North American margins, extending from the Gulf of Mexico to the Grand Banks region offshore Newfoundland. At the Triassic-Jurassic boundary, the whole area was influenced by the eruption of the Central Atlantic Magmatic Province (CAMP). Eruption of large-scale volcanism is commonly associated with the end of rifting and onset of sea floor spreading. In the Central Atlantic, the first oceanic crust appears to be significantly younger than the CAMP volcanics, suggesting continental rifting continued post-eruption.

The oldest magnetic polarity reversal anomaly in the Central Atlantic segment is chron M25r (Klitgord & Schouten, 1986), which corresponds to 156 Ma, according to Gradstein et al. (2012). M25 lies between 300 and 400 km outboard of the limit of oceanic crust (LOC), so forms a younger bound on the oldest oceanic crust in the segment. Upper Triassic red beds throughout eastern North America and the Gulf of Mexico represent continental rifting as a pre-cursor to Central Atlantic seafloor spreading and put an older limit on the age of oceanic crust. Furthermore, the CAMP crosses the Triassic-Jurassic boundary and is related to the earliest stages of Pangea break-up (e.g. Marzoli et al., 1999). Commonly, the first oceanic crust in the Central Atlantic is interpreted as 180 Ma, an interpretation we follow for Getech's Global Plate Model. Alternatively, Labails et al. (2010) propose 190 Ma as the first occurrence of oceanic crust. Selecting 180 Ma as the break-up age is consistent with spreading rates of 12–13 mm/yr from 180 Ma to the first magnetic reversal chron, matching with spreading rates calculated from M-series magnetic anomalies M25r to M0 (between 156 and 126 Ma). Other interpretations suggest an initial period of oceanic crust accumulation followed by a ridge jump to the east prior to M25r. This interpretation accounts for the asymmetry between the two sides of the central Atlantic Ocean, but is conflicted by a lack of magnetic anomalies and no obvious evidence for an extinct mid-ocean ridge in Getech's Multi-Sat gravity data.

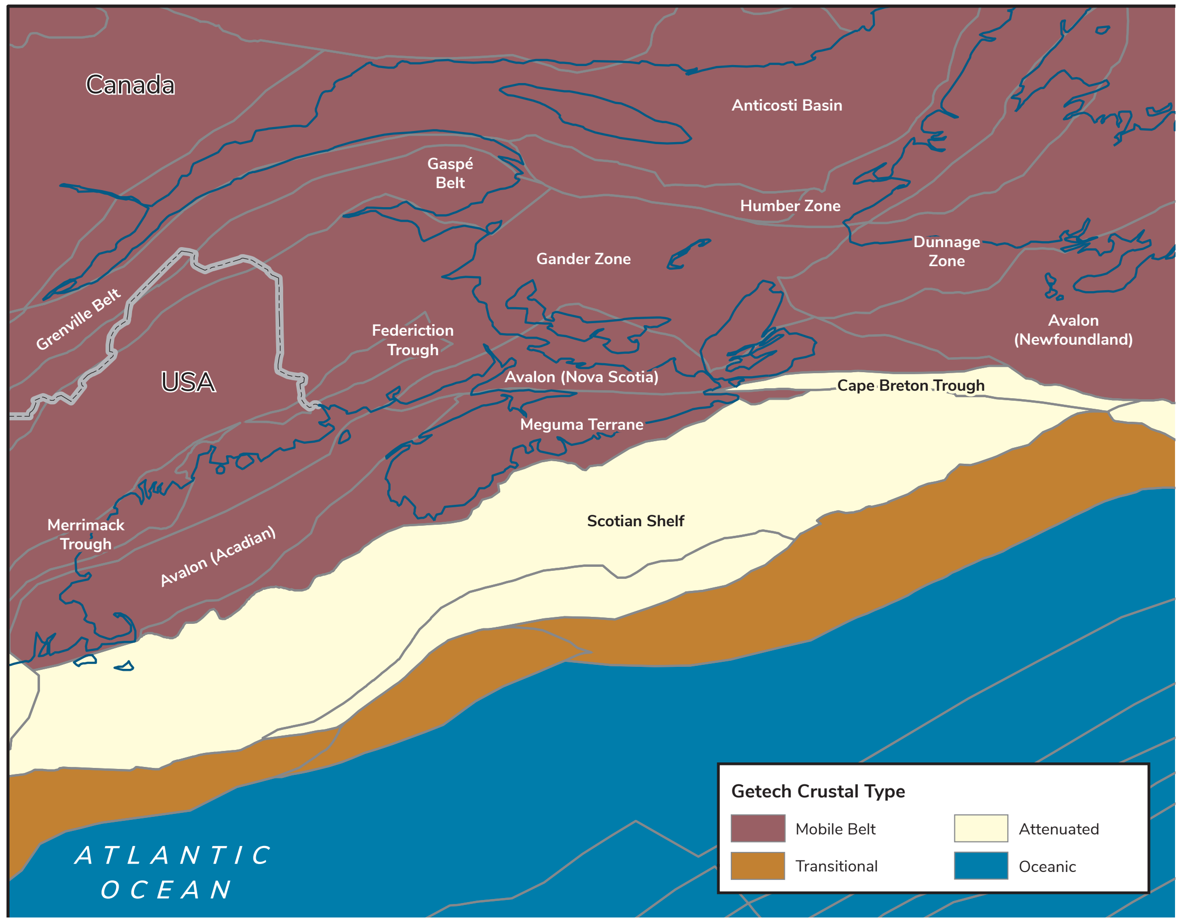

Figure 2.6 (Left): Crustal architecture for the Nova Scotian Margin.

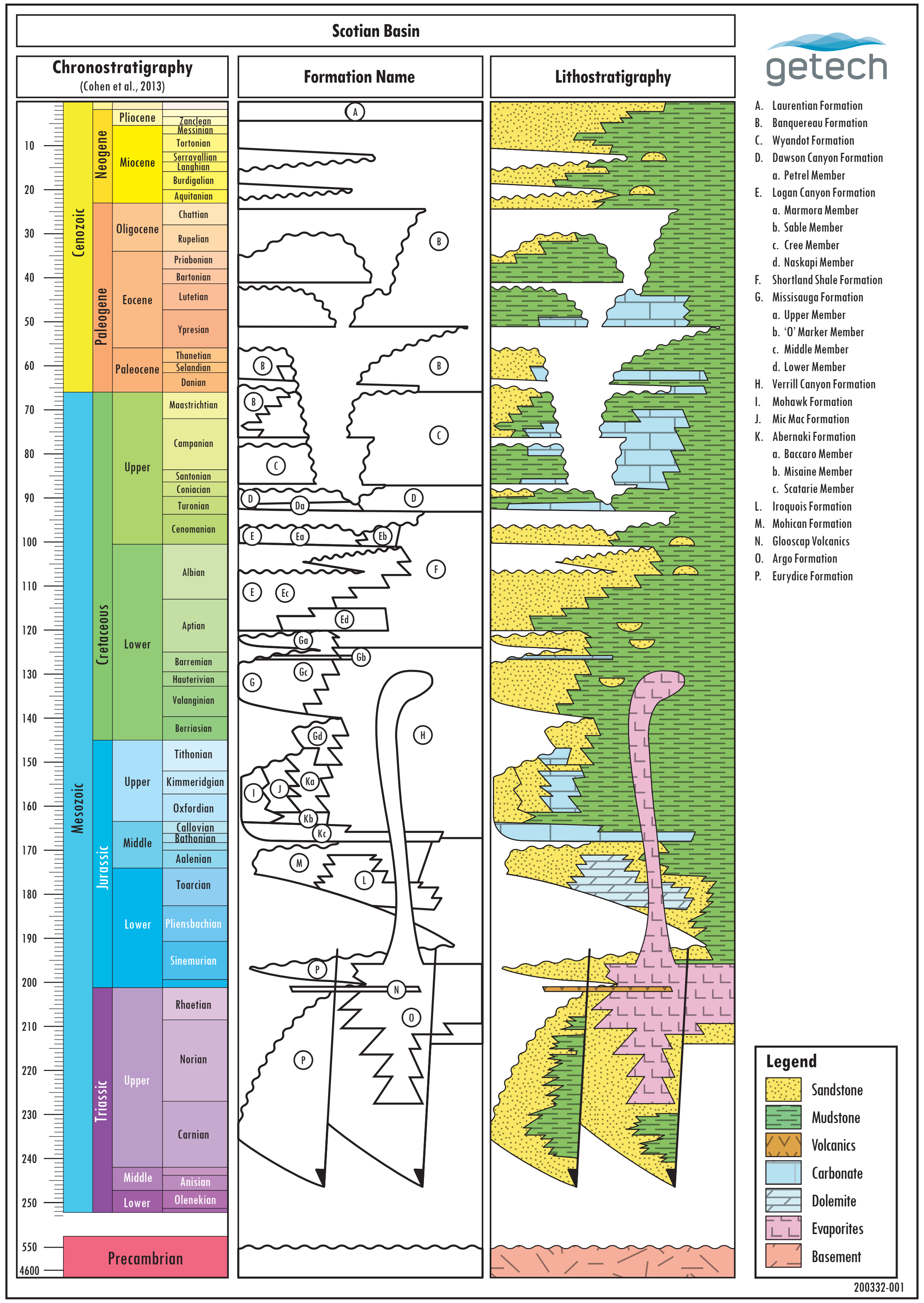

Figure 2.7: Stratigraphy of the Scotian margin. (Modified from Weston et al., 2012 and Deptuck & Althiem, 2018).

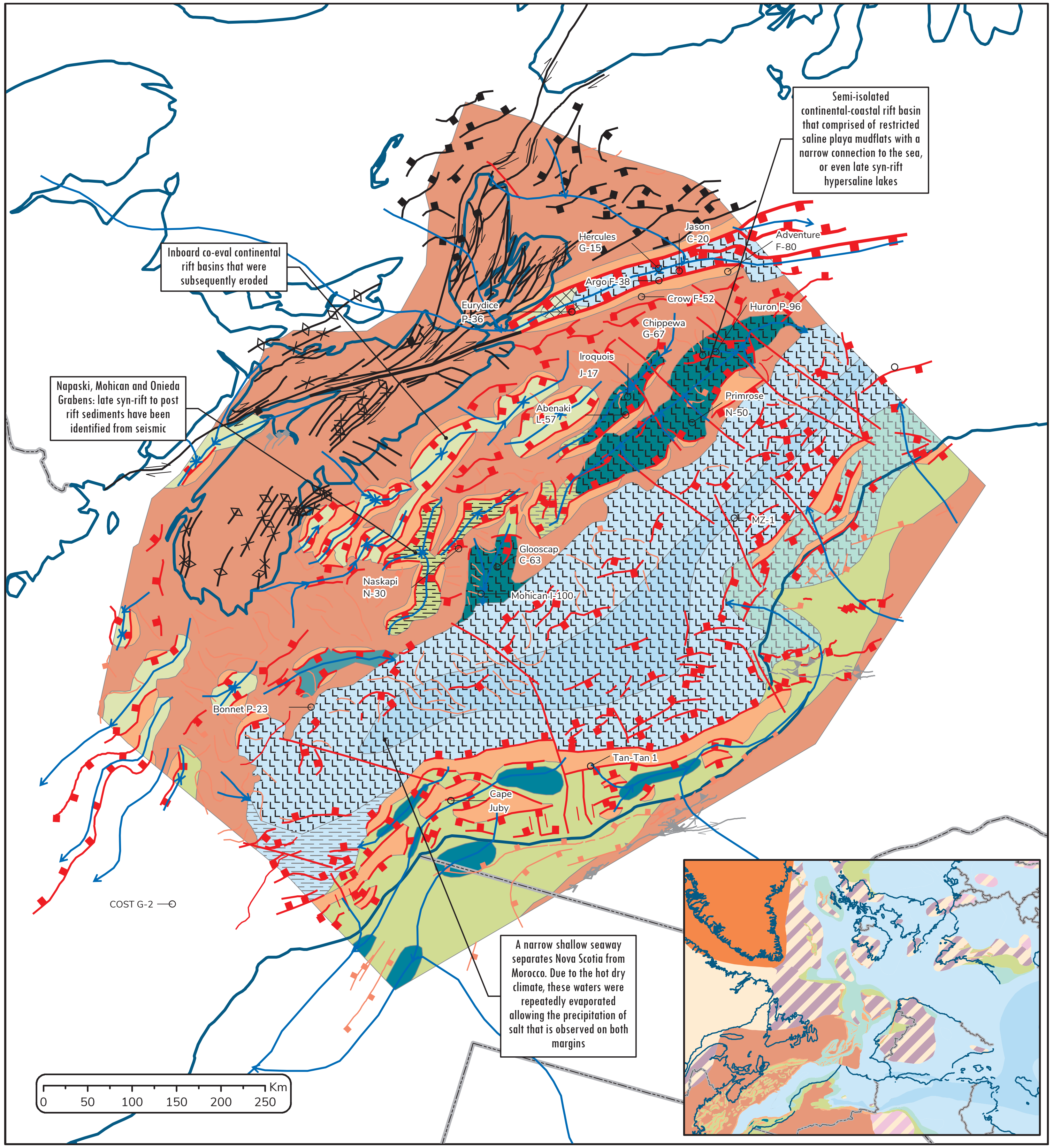

Figure 2.8: ***Gross depositional environment and palaeodrainage map for the Hettangian. Insert (bottom right) shows the regional context (From Getech's Atlas of global Palaeogeographies).***

2.6 HETTANGIAN

At the Triassic-Jurassic boundary, the whole area was influenced by the eruption of the Central Atlantic Magmatic Province (CAMP). On seismic, this corresponds to the J200 marker and shown, at Glooscap C-63, to correspond to the reflection response from a 152 m thick basalt layer emplaced conformably above Late Triassic strata (Deptuck & Altheim 2018). Overlying these volcanics, the syn-rift succession continued across the Scotian and Moroccan margins. The Hettangian GDE presented in Figure 2.8, represents the late syn-rift period of deposition after the CAMP volcanics.

Within the Naskapi, Mohican and Oneida Grabens, late syn-rift to post-rift sediments have been identified by Deptuck and Altheim (2018) from seismic. Outside of these grabens, the succession has been entirely removed by the post-rift unconformity. Inboard of the grabens mapped by Deptuck and Altheim (2018), Getech's Multi-Sat gravity data (2019) has enabled us to visualise a series of gravity lows that may represent former Triassic-Lower Jurassic grabens, which were then subsequently eroded. These co-eval continental rift basins stood above the level of the invading Tethys Sea and would have perhaps contained fluvial-lacustrine red-bed deposits (Eurydice Formation).

Some caution must be used on the confidence of these landward inboard rift basins. There are onshore exposures of Upper Paleozoic rocks (Windsor Group) around St Margaret's Bay – near some of these landward rift basins, as well as onshore basins like the Kennetcook, Musquodoboit, and Shubenacadie Basins (Deptuck, 2021 per comms.). This suggests that some of these gravity lows could instead correspond to the remnants of older rift basins that pre-date the opening of the Atlantic. However, an interval of Paleozoic tectonically folded strata also underlies Triassic strata in the Oneida Graben (Deptuck & Altheim 2018), and therefore may not preclude such basins from being reactivated in the Triassic and forming local depocenters that have subsequently been eroded. If the overlying Triassic rift successions were completely removed (as would be expected for them being further landward), these older strata may be very hard to distinguish from basement on seismic profiles.

Due to limited well penetration and uncertainties in the dating of Lower Jurassic strata, there still remains conjecture on the origin of the evaporites, as to whether they are marine or continental (Leleu et al., 2016). Renewed Late Triassic rifting further to the north and east in the Grand Banks/Iberia region led to the first incursions of marine waters from the eastern Tethys paleo-ocean into the interconnected syn-rift basins, including the Annapolis, Shelburne and Laurentian Sub-basins and similar conjugate rift basins on the Moroccan margin. By the Hettangian, restricted shallow marine conditions across these sub-basins were established, and, due to the hot dry climate, these waters were repeatedly evaporated, resulting in the precipitation of extensive salt and anhydrite with some mixed clastic - carbonate sedimentation (Jansa et al 1980; Beicep-Franlab, 2015; Wade & MacLean, 1990). Landward of the mapped Hettangian coastline, a series of rift basins - the Abenaki, Sable and Huron Sub-basins - are observed on seismic horizon mapping with thick intervals of halite increased accommodation accumulating (Beicep-Franlab, 2011; Deptuck & Altheim 2018). Rather than being part of a central marine salt-basin, deposition in these more proximal basins may have been in a semi-isolate, more continental-coastal regime and comprise of restricted saline playa mudflats with a narrow connection to the sea, or even late syn-rift hypersaline lakes (Deptuck & Altheim 2018; Leleu et al., 2016).

The seaway separating Nova Scotia from Morocco has been mapped on the Hettangian GDE as relatively narrow (~250 km at its widest) and is also relatively shallow, with water depths only reaching beyond 50 m in the very centre.

The fluvial successions in Morocco have not been studied in any significant detail. In the Essaouira Basin, the Bougadine Formation extends into the Hettangian and comprises of red beds (Tari et al., 2012a). Palaeoflow indicators show that the fluvial systems flowed from east to west (Tari et al 2012b).

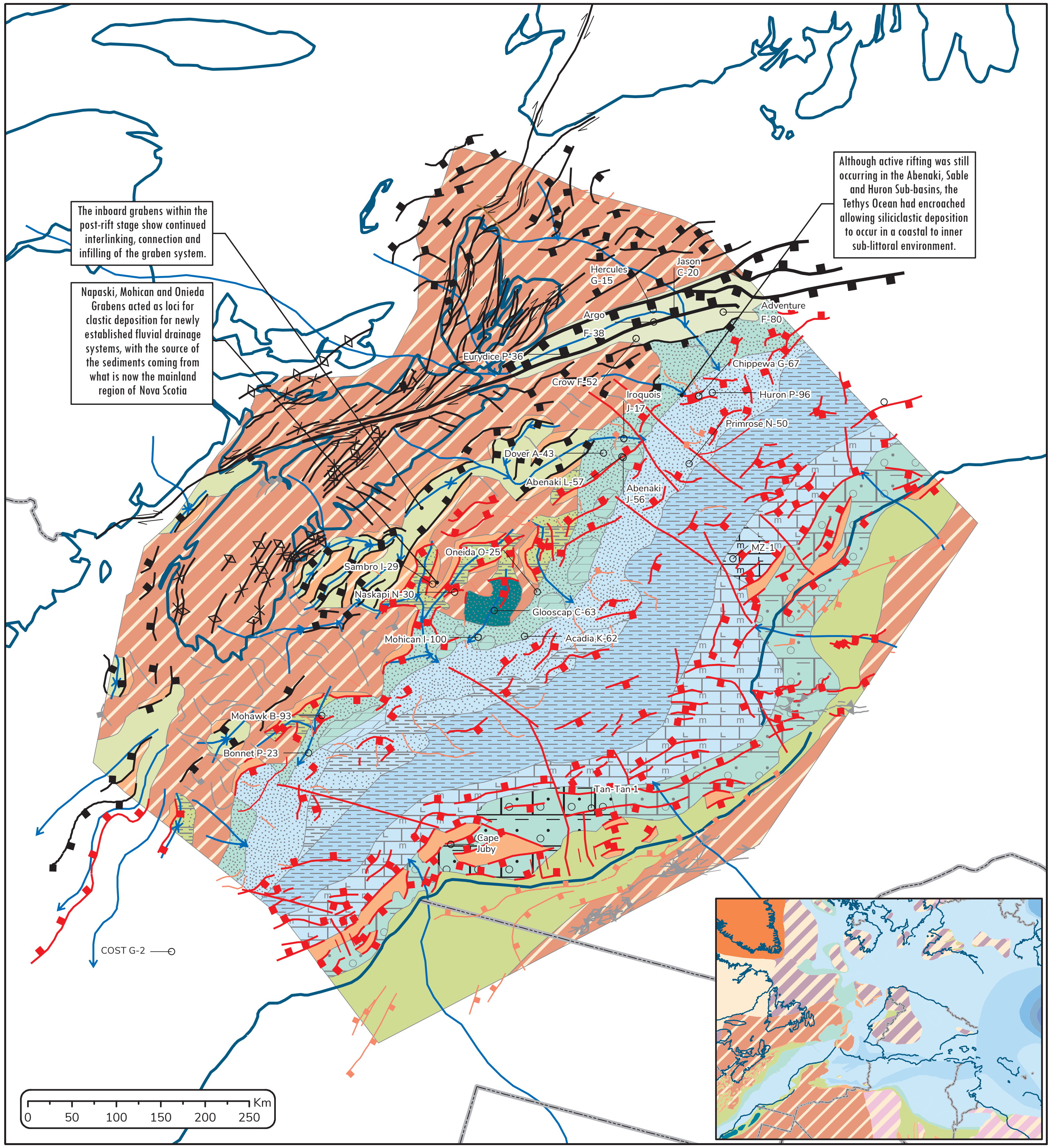

Figure 2.9: ***Gross depositional environment and palaeodrainage map for the Sinemurian. Insert (bottom right) shows the regional context (From Getech's Atlas of global Palaeogeographies).***

2.7 SINEMURIAN

The Sinemurian GDE shown in Figure 2.9 represents a late syn-rift to early post-rift stage, prior to the first occurrence of oceanic crust in the Central Atlantic. Deposition in the early Sinemurian may have been similar to the Hettangian, with the continuation of salt deposition within marine to non-marine environments (Beicep-Franlab 2011; 2014; 2015; Weston et al., 2012; Figure 2.6) . The Sinemurian GDE is more representative of the late Sinemurian, when deposition of the Scotian margin became more dominated by siliciclastic sedimentation.

We have speculated that the inboard grabens (landward of the Naskapi, Mohican and Oneida Grabens that were still actively rifting during the Sinemurian) were now within the post-rift stage, where associated extension-driven accommodation localized along border faults has become inactive with accommodation space driven by post-rift thermal subsidence. This post-rift stage further enhanced interlinking, connection and infilling of individual grabens. This succession was subsequently removed in its entirely by the post-rift unconformity. Examples of more than one distinct rift axis that are diachronous in age have been observed in other areas during the opening of the Atlantic ocean. In the Newfoundland-Iberian rift, Alves et al., (2009) identified two rift axes across the West Iberian margin. The first 'inboard' rift axis (Oxfordian) extends from the Porto Basin to the Alentejo Basin, while the second rift axis (Berriasian/Valanginian) is located on the outer proximal margin. In Getech's South Atlantic report (2018), GDE mapping along the west African coast from Gabon to the Kwanza Basin (Angola) demonstrated two rift axis, with an earlier Berriasian inboard rift axis, as shown in Figure 2.10 (left) and a later Aptian rift axis located on the outer margin (Figure 2.10; right). In both the North and South Atlantic examples, the post-rift stage was also reached earlier in the inboard rift axis.

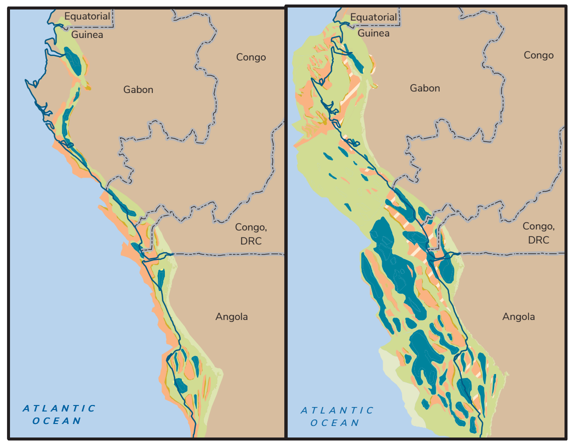

Figure 2.10: ***Dual rift axis in West Africa during the opening of the South Atlantic. The inboard rift system (left), became active during Berriasian. By the later Aptian (right), active rifting had switched to the outboard margin and the inner rift axis had become inactive (Getech, 2018).***

The continental basins shown on the GDE map acted as loci for clastic deposition for the newly established fluvial drainage systems, with the source of the sediments coming from the Present Day mainland region of Nova Scotia (Kitson et al., 2005). While not yet encountered in wells, the age of this succession can be inferred to be mid- to late Sinemurian to early Pliensbachian since it conformably overlies the Argo Formation and is later truncated by the younger break-up unconformity.

The seaway between Nova Scotia and Morocco is still relatively narrow (~250 km at it widest) and also remains relatively shallow (although slightly deeper than the Hettangian).

The deep water (outer shelf/upper bathyal) environment of deposition suggested for the late Sinemurian to early Pliensbachian sediments in the DSDP 547B cores (Hinz et al.,1984) is not corroborated by the data recorded in internal GSCA data (Beicep-Franlab, 2014). The micropalaeontological recoveries recorded from the DSDP 547B samples in Riegraf (1984), Luterbacher and Leckie (1984) and Hinz et al. (1984) are similar to those recorded in the Early Jurassic section of Heron H-73 Well and are typical of deposition close to a marshy coastal plain in an open marine shelf setting (Beicep-Franlab, 2014).

2.8 PLIENSBACHIAN

The Pliensbachian GDE shown in Figure 2.11 represents the early post-rift stage prior to the first occurrence of oceanic crust in the Central Atlantic. The depositional environments are expected to have shown a similar distribution to that of the Sinemurian, with the continuation of siliciclastic dominated deposition.

The Scotian and Moroccan margins were now within the post-rift stage where associated extension-driven accommodation localized along border faults became inactive, with accommodation space driven by post-rift thermal subsidence. This resulted in widespread fluvial deposition across the Lahave Platform as the siliciclastic Mohican Formation infilled the grabens and overlapped basement highs. Much of the continental deposition was subsequently eroded during the immediate and/or co-eval break-up unconformity and Upper Jurassic Avalon Uplift. Potentially, only minor amounts of Pliensbachian sediment have been preserved in the Oneida, Napaski and Mohican Graben (Deptuck & Altheim 2018; Wade, 1991), however sediments of this age are not proven due to uncertainties in the dating of Lower Jurassic sediments and they have not been penetrated in wells within these grabens.

During the late Pliensbachian, carbonate deposits (Iroquois Formation) start to develop along the coast of the Scotian margin (Wade & MacLean 1991, Weston et al., 2012).

The Lower Jurassic successions in Morocco have not been studied in any significant detail. As syn-rift activity gradually declined, marine carbonate/siliciclastic overlying the syn-rift sequence was controlled by thermal subsidence. The rhythmic nature of sedimentation, of limestone, sandstone and claystone/siltstone observed in the Tan-Tan 1 and Cape Juby-1 wells suggests a stable, shallow marine, coastal environment in which sedimentation was in equilibrium with the creation of accommodation space (Weston, 2019b; 2019c).

The presence of sandstones implies input from a clastic source. Deposition was anticipated to be under nearshore to marginal marine conditions, relatively close to the shoreline, in an overall carbonate ramp setting Weston, 2019b; 2019c).

The seaway between Nova Scotia and Morocco still remained narrow. Although the seaway as a whole remains a relatively shallow bowl, the area where water depths reaches beyond 50 m has increased in size.

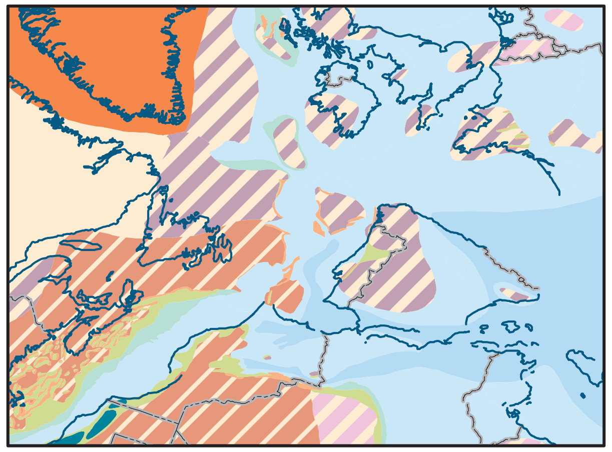

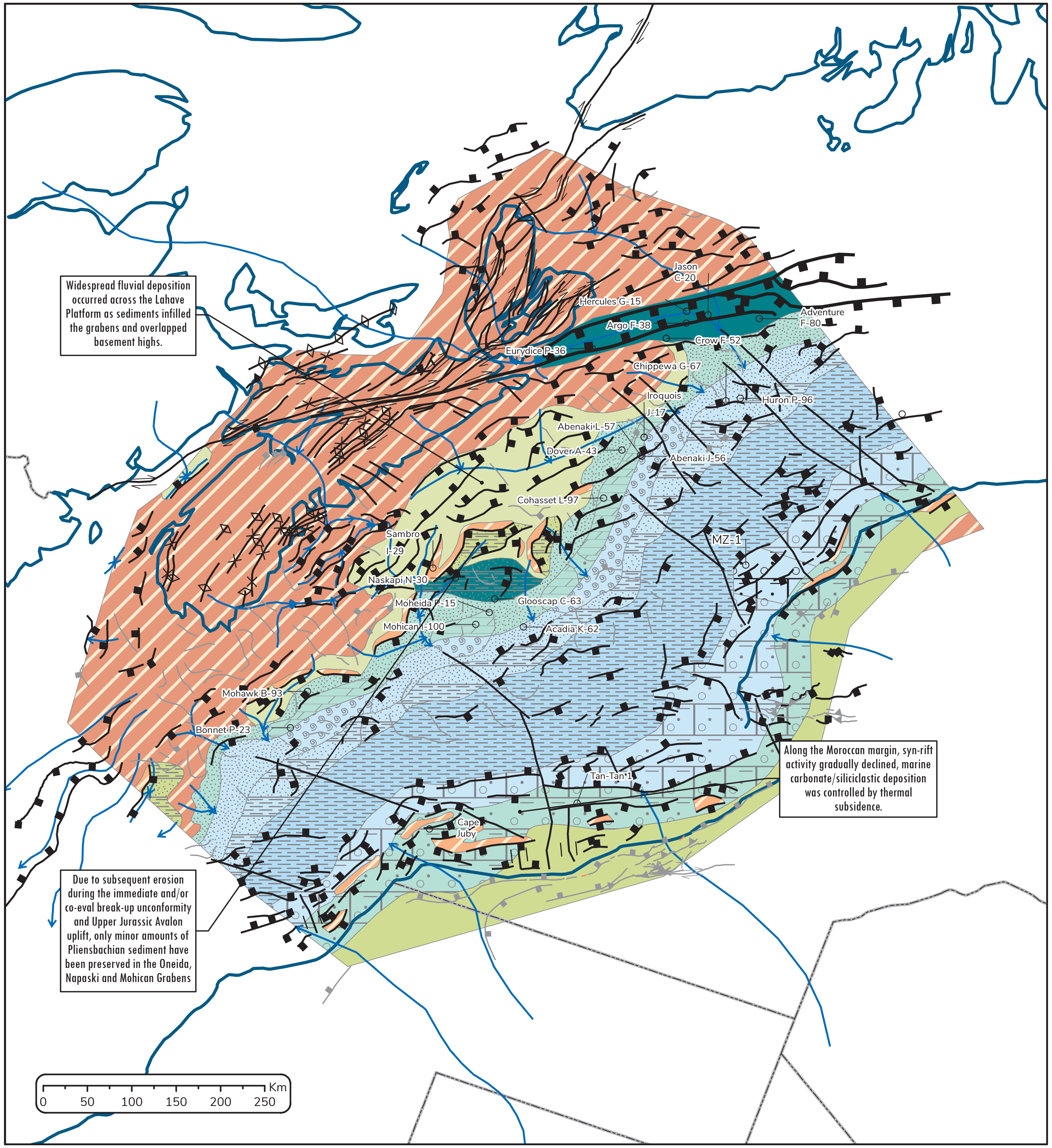

Figure 2.11: Gross depositional environment and palaeodrainage map for the Pliensbachian. Insert (left) shows the regional context (From Getech's Atlas of Global Palaeogeographies).

2.9 TOARCIAN

The Toarcian GDE shown in Figure 2.12 represents the thermal subsidence stage, immediately after the break-up unconformity and creation of oceanic crust and the opening of the Atlantic Ocean. As a result of the final continental separation event (break-up unconformity), the Scotian margin that had earlier consisted of a heavily faulted, complex terrane of grabens and basement highs underwent a significant degree of peneplanation (Kitson et al., 2005).

Transgressive shallow water to tidally influenced dolomites and clastics were deposited in a shallow, warm, agitated and slightly restricted sea, across an extensive ramp system that extended across the Scotian shelf down to the Scotian slope, (Beicip-Franlab, 2011; Kitson et al., 2005; Wade and MacLean, 1990). Development of larger river systems across the Scotian Basin allowed the Sable Delta to start to develop. The proximal, fluvial-deltaic dominated part of the shallow ramp in the north-western area of the Scotian margin consists of thick sequences of interbedded sandstones and shales (Mohican Formation; Beicip-Franlab, 2011; Wade & MacLean, 1990). The fine muds from this succession were transported by marine processes into silty-shale channel and fan complexes and were deposited on the distal ramp in deeper waters (Kitson et al., 2005; Beicep-Franlab, 2011). These fans and channels slowly infilled basinal lows and cover new oceanic crust.

Along the west Scotian shelf border (between Bonnet to Cohasset) intertidal dolostones were deposited (Iroquois Formation) within the inner ramp area and prograded seaward into open marine carbonates and/or clastics deposited on the middle/inner area of the ramp system. The shallow-marine inner to middle ramp area extended at least as far as 50 km beyond the edge of the Present Day Scotian shelf (Beicep-Franlab, 2015). Hemipelagic marlstone, shales and minor limestones were deposited on the deep marine outer ramp and basin floor.

During the Toarcian and continuing in to the middle Jurassic, the combination of sea-floor spreading, thermal subsidence and global sea level rise caused the Atlantic Ocean to become broader and deeper (Kitson et al., 2005). However, recent paleoenvironmental results from Cheshire L-97 Well show that pre J165 water depth were still less than 100m in the Bajocian. Biostratigraphy analysis for the MZ-1 Well in Morocco suggests deposition within a low energy, bathyal depositional setting with relatively poorly oxygenated bottom conditions, which was probably upper bathyal (Weston, 2019a).

The Toarcian Moroccan margin is similar to the Pliensbachian, with marine carbonate/siliciclastic deposition along a stable margin. Siliciclastic deposition in the Tan-Tan 1 Well was in an ephemeral marginal marine, coastal environment that was periodically subject to subaerial exposure (Weston, 2019b). Speculative siliciclastic turbidite, and calciturbidite channel and fan complexes may have been deposited on the distal ramp (Tari et al., 2012a).

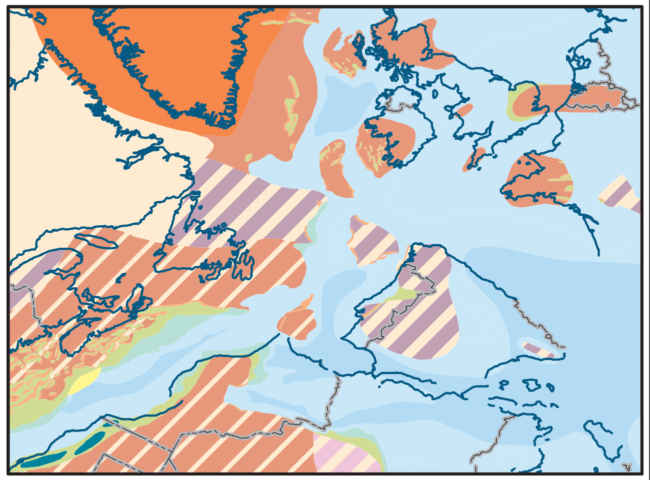

Figure 2.12 (Right): Gross depositional environment and palaeodrainage map for the Toarcian. Insert (above) shows the regional context (From Getech's Atlas of Global Palaeogeographies).

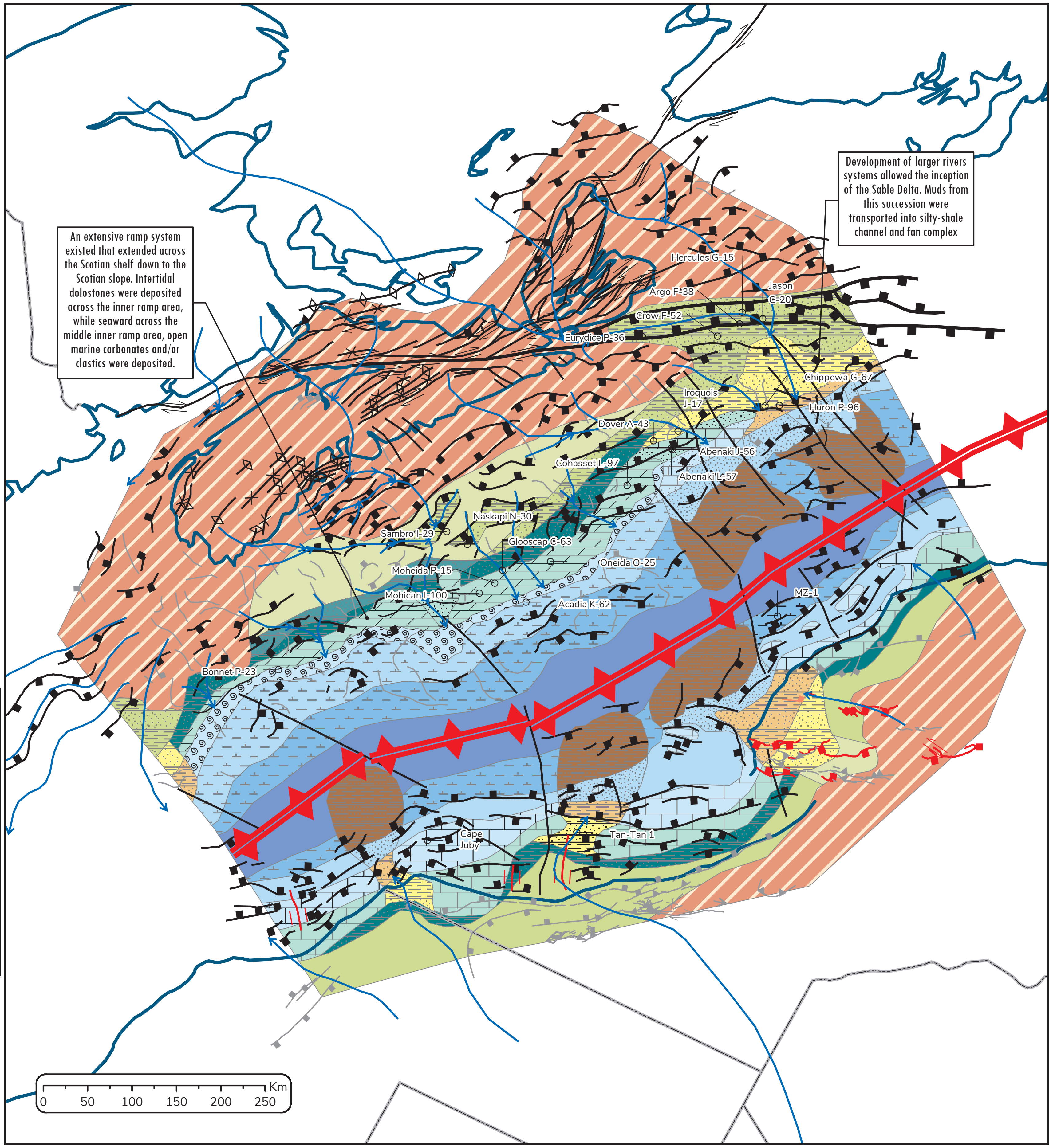

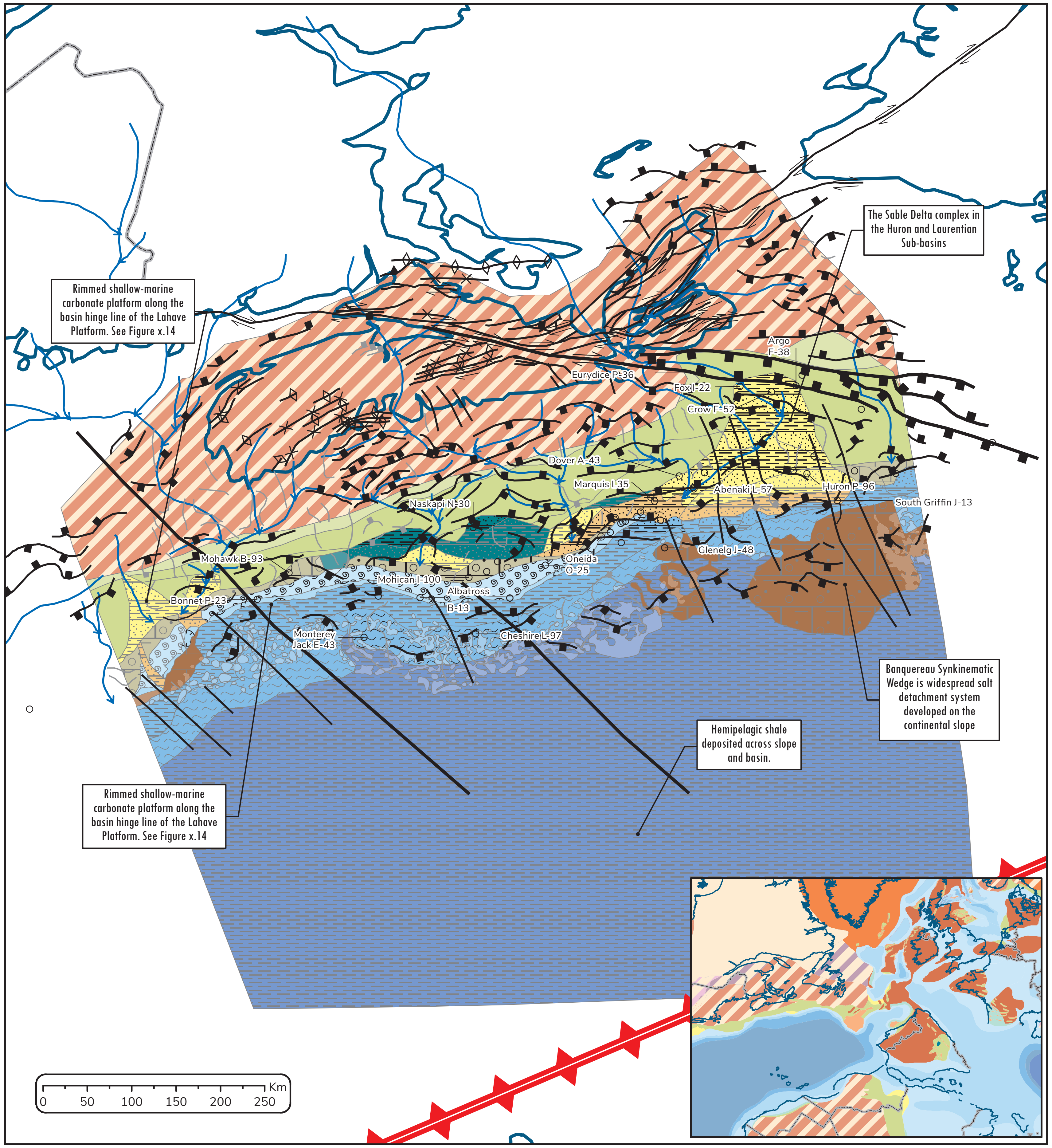

2.10 TITHONIAN

A sequence boundary is observed within the Tithonian (Beicep-Franlab, 2011; Weston et al., 2012; MacLean & Wade 1990). The lower Tithonian is dominated by carbonate sedimentation of the Abenaki Formation, while the upper Tithonian is dominated by siliciclastics of the lowermost Mississauga Formation (Weston et al., 2012; MacLean & Wade 1990). For the Tithonian GDE (Figure 2.13), we have mapped below the sequence boundary, as this time frame corresponds to a maximum flooding period, which would have favoured the development of source rocks (Beicep-Franlab, 2011).

Figure 2.13 (Left): Gross depositional environment and palaeodrainage map for the Tithonian. Insert (below-right) shows the regional context (From Getech's Atlas of Global Palaeogeographies).

The lower Tithonian interval corresponds to the continued development of a rimmed shallow-marine carbonate platform that had thrived along the basin hinge line of the Lahave Platform since the Middle Jurassic (Kitson et al., 2005; MacLean & Wade 1996). The Abenaki Formation (Baccaro Member) has been studied in much detail by Eliuk (1978), Weissenberger et al. (2000) and Kitson et al. (2005), amongst others, and later in the PFA 2011 study, where a specific breakdown was established in the Baccaro Member, taking into account the existing data and extensive publications over the last 20 years. By the Tithonian, the Baccaro Member had developed the morphology of a reefal carbonate platform, with the geometry changing upwards into an open-marine mixed carbonate clastic steepened ramp (Figure 2.14).

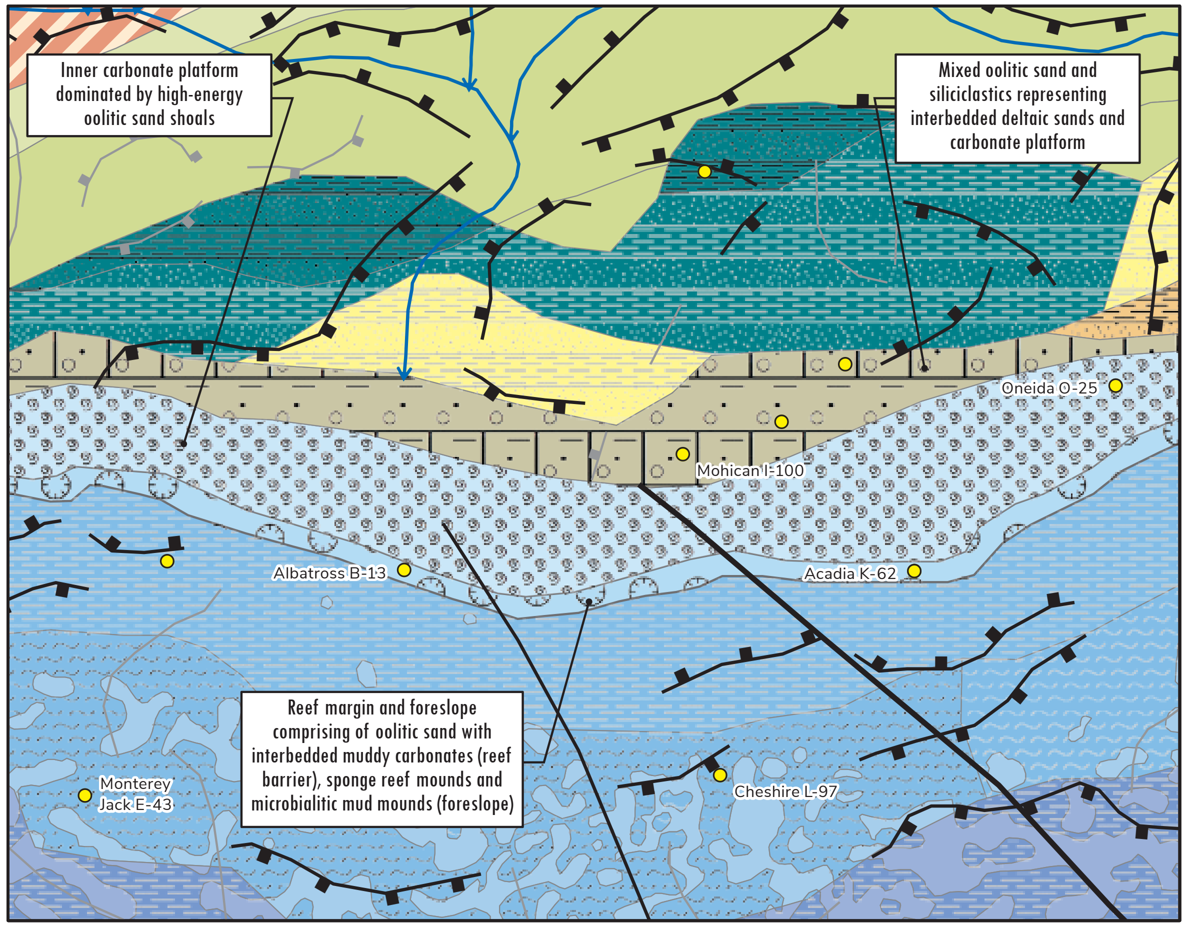

Figure 2.14: Enlargement of the carbonate platform area between Bonnet P-23 and Oneida O-25.

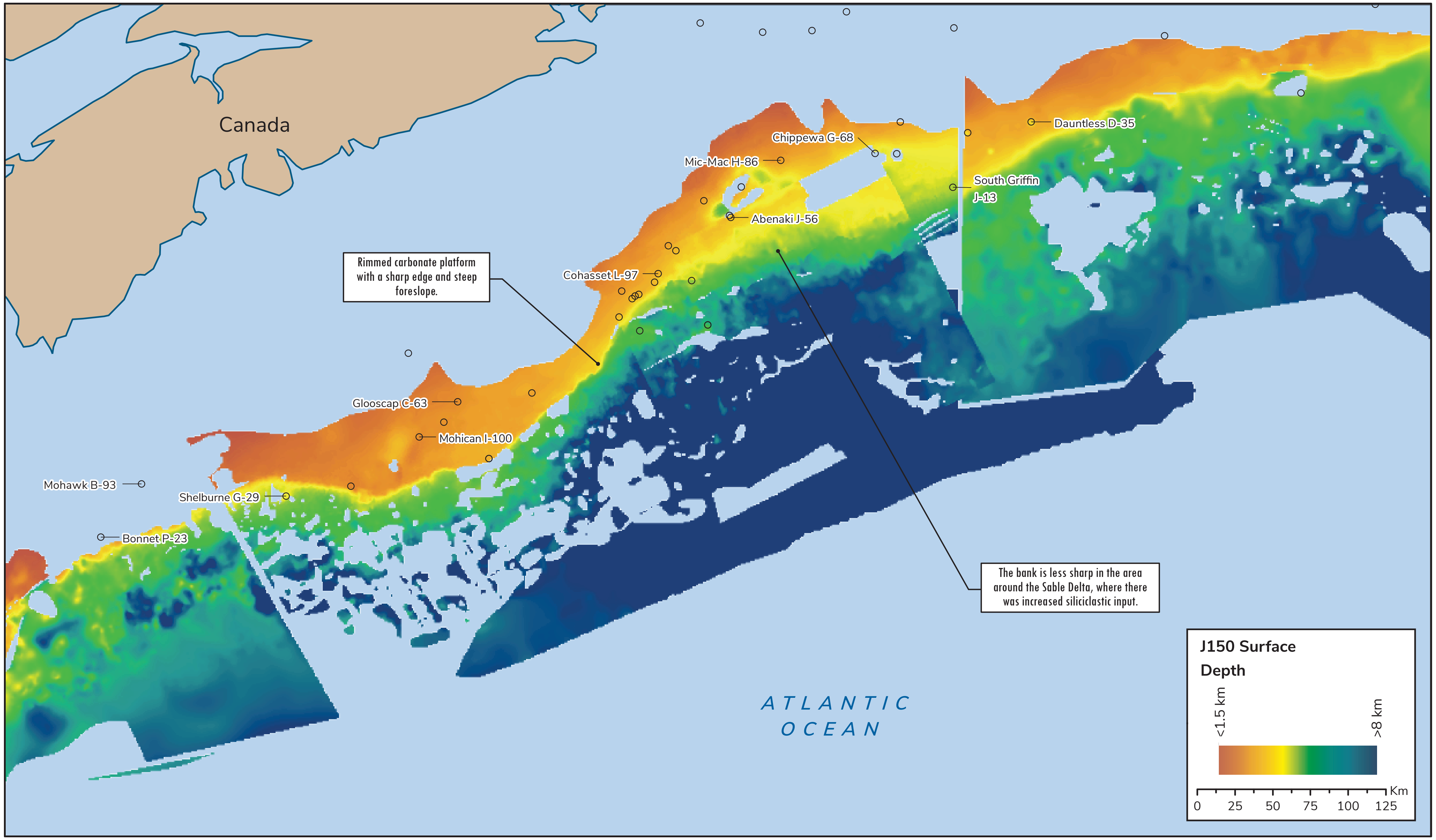

Figure 2.15: ***Structure map of the J150 surface.***

Seismic structural maps of the J150 surface (Figure 2.15) show quite clearly the carbonate platform with a sharp edge and steep foreslope. The bank is less sharp to the east and west edges where there was increased siliciclastic input (Beicep-Franlab, 2011; 2014; 2015; 2016; 2019a; 2019b; Deptuck & Alheim, 2018)

Concurrent with carbonate deposition, increased Late Jurassic clastic input from the east was in response to the Avalon Uplift, and led to the establishment of the mixed energy (current and tidal) Sable Delta complex in the Laurentian Sub-basin (Beicep-Franlab, 2015). In the southwest, a similar progradation of sediments occurred at the vicinity of the U.S.-Canada border (Shelburne Delta). Well and seismic data also suggest minor deltaic complexes between the Sable and Shelburne deltas.

During periods of sea level lowstand, rivers down-cut into the exposed shelf with shelf-edge delta complexes. Turbidity currents, mass sediment flows and large slumps carried large volumes of sands, muds and carbonates into deep-water.

The Banquereau Syn-kinematic Wedge (BSW) is a widespread salt detachment system that developed on the continental slope. It was deposited during the Middle to Upper Jurassic so was time-equivalent to the Oxfordian-Tithonian Mic Mac Formation and largely pre-dates the latest Jurassic development of the Avalon Uplift (Ings & Shimeld, 2006; Albertz et al., 2010).

From the Middle Jurassic to the Paleogene , widespread salt deformation and expulsion of salt occurred across the slope area of the Scotian margin creating a wide range of detached and undetached allochthonous salt bodies. During the Tithonian, contemporaneous salt tectonics allowed mini salt-basins to form, but also subsequent salt tectonics will have resulted in other areas of Tithonian deposition to be eroded.

2.11 SUMMARY

- Available well data, existing GDE maps and published seismic profile images were used as points of constraint and were then applied, along with the Getech's own palaeodrainage reconstructions, to extrapolate the depositional environments for the Tithonian, Toarcian, Pliensbachian, Sinemurian and Hettangian across the AOI. In turn, these form the input base maps for the Organic Facies Prediction (OFP) modelling.
- For both the Scotian and Moroccan margins, the data used in the construction of the GDE maps represent a variety of reliabilities and temporal resolutions. A limited number of wells have sampled Lower Jurassic strata. This, combined with differentiating the ages of the Lower Jurassic strata (or even as Lower Jurassic strata as a whole) due to poor biostratigraphic recovery, would understandably limit ground truthing to Lower Jurassic GDEs.
- The Hettangian, Sinemurian and Pliensbachian GDE's represent the late syn-rift to early post-rift stage, prior to the first occurrence of oceanic crust in the Central Atlantic. The Hettangian GDE represents syn-rift deposition after the CAMP volcanics, with rifting waning over the Sinemurian and Pliensbachian. The Pliensbachian represents deposition immediately before or co-eval with the break-up unconformity. The Toarcian represents the thermal subsidence stage, immediately after the break-up unconformity and creation of the oceanic crust and the opening of the Atlantic Ocean.
- Getech's Multi-Sat gravity data (2019) has enabled us to visualise a series gravity of lows which may represent former Triassic-Lower Jurassic grabens inboard of the Naskapi, Mohican and Oneida Grabens. These inboard co-eval continental rift basins stood above the level of the invading Tethys Sea and were subsequently eroded during the break-up unconformity.
- Based on examples observed in other areas during the opening of the Atlantic ocean, we have speculated more than one distinct rift axis across the Scotian margin that are diachronous in age. The inboard grabens (landward of the Napaski, Mohican and Onieda Grabens) reached the post-rift stage during the ?Sinemurian, where associated extension-driven accommodation localized along border faults became inactive, and accommodation space driven by post-rift thermal subsidence. The Naskapi, Mohican and Oneida Grabens and other seaward grabens reached this post-rift stage by the ?Plienbachian.
- The lower Jurassic GDE's portray a gradual encroachment of the Tethys Sea. In the Hettangian, the interconnected syn-rift basins (including Annapolis, Shelburne and Laurentian Sub-basins) and similar conjugate rift basins on the Moroccan margin had been flooded and evaporites were deposited. The Abenaki, Sable and Huron Sub-basins were semi-isolated, with a more continental-coastal depositional regime that consisted of restricted saline playa mudflats, or even late syn-rift hypersaline lakes. By the Sinemurian, the Tethys Sea had encroached these sub-basins, allowing siliciclastic deposition to occur in a coastal environment to inner sub-littoral environment.
- Newly established fluvial drainage systems allowed more widespread fluvial deposition along the Lahave Platform during the Sinemurian to Pliensbachian. As the siliciclastic Mohican Formation infilled the grabens and overlapped basement highs, the Scotian margin became more siliciclastic dominated.
- By the Toarcian, the development of larger rivers systems across the Scotian Basin allowed the Sable Delta to develop. Away from this foci of clastics, transgressive shallow water to tidally influenced dolomites were deposited in an extensive ramp system that extended across the Scotian shelf down to the Scotian slope.
- Between the Hettangian and Pliensbachian, the developing seaway between Nova Scotia and Morocco remained narrow (~250 km at the widest part), with a geometry of a relatively asymmetrical shallow bowl. Areas where water depths reaches beyond 50 m were present throughout this time and gradually expanded in area. The deep water (outer shelf/upper bathyal) environment of deposition suggested for the Late Sinemurian to Early Pliensbachian sediments in the DSDP 547B cores is not corroborated with similar palaeontology recorded in the early Jurassic section of Heron H-73, and are instead thought to be typical of deposition close to a marshy coastal plain in an open marine shelf setting.
- By the Toarcian and continuing into the Middle Jurassic, the combination of sea-floor spreading, thermal subsidence and global sea level rise caused the Atlantic Ocean between the Scotian margin and Morocco to become broader and deeper. However, recent paleoenvironmental results from Cheshire L-97 show that pre J165 water depth in that area were still less than 100 m in the Bajocian.
- Excessive water depths are not necessarily needed for source rock development. The existence of water depths beyond the storm wave base under restrictive marine conditions for all of the Lower Jurassic GDEs, confirms that at least depositional environments that are conducive for the development of source horizons were present.
- The Tithonian GDE represent the pinnacle of a Jurassic carbonate reef, bank and platform environments that had formed and thrived along the basin hinge line on the Lahave Platform since the Middle Jurassic. Concurrent with carbonate deposition, increased Late Jurassic clastic input from the east led to the establishment of the mixed energy (current and tidal) Sable and Shelburne delta complexes.

2.12 REFERENCES

Albertz, M., Beaumont, C., Shimeld, J. W., Ings, S. J. & Gradmann, S. (2010). An investigation of salt tectonic structural styles in the Scotian Basin, offshore Atlantic Canada: 1. Comparison of observations with geometrically simple numerical models. Tectonics 29, TC4017.

Alves, T. M., Moita, C., Cunha, T., Ullnaess, M., Myklebust, R., Monteiro, J. H. & Manuppella, G. (2009). Diachronous evolution of Late Jurassic–Cretaceous continental rifting in the northeast Atlantic (west Iberian margin). Tectonics 29, TC4003.

Beicip-Franlab (2011). Play fairway analysis atlas, offshore Nova Scotia Canada. Offshore Energy Research Association (OERA).

Beicip-Franlab (2014). Play Fairway Analysis: Laurentian Sub-basin, Canada. Offshore Energy Research Association (OERA).

Beicip-Franlab (2015). Play Fairway Analysis: SW Nova Scotia Expansion Atlas. Offshore Energy Research Association (OERA).

Beicip-Franlab (2016). Play Fairway Analysis: Central Scotian Slope Atlas. Offshore Energy Research Association (OERA).

Beicip-Franlab (2019a). Play Fairway Analysis: Shelburne Sub-Basin Play Fairway Analysis Update. Offshore Energy Research Association (OERA).

Beicip-Franlab (2019b). Nova Scotia-Morocco Conjugate Biostratigraphy Project. Offshore Energy Research Association (OERA).

CNSOPB (2021). Canada-Nova Scotia Offshore Petroleum Board Data Management Centre. https://cnsopbdigitaldata.ca/iseisview/dmc

Deptuck, M. E. & Altheim, B. (2018). Rift basins of the central LaHave Platform, offshore Nova Scotia. CNSOPB Geoscience Open File Report 2018-001MF.

Eliuk, L. S. (1978). The Abenaki Formation, Nova Scotia Shelf, Canada - A depositional and diagenetic model for a Mesozoic carbonate platform. Bulletin of Canadian Petroleum Geology 26 (4), pp. 424-514.

Gradstein, F., Ogg, J., Schmitz, M. & Ogg, G. (2012). The Geologic Time Scale 2012. Elsevier.

Getech Group plc (2017). Digitial Atlas of Global Palaeogeography: Globe 2017.

Getech Group plc (2018). South Atlantic, G1801.

Getech Group plc (2019). Getech's Global Gravity 2018v3.

Hinz, K., Winterer, E. L., Baumgartner, P. O., Bradshaw, M. J., Channell, J. E. T., Jaffrezo, M., Jansa, L. F., Leckie, R. M., Moore, J. N., Rullkötter, J., Schaftenaar, C., Steiger, T. H., Vuchev, V. & Wiegand, G. E. (1984). Initial Reports of the Deep Sea Drilling Project, Volume 79. National Science Foundation, Washington D.C.

Ings, S. J. & Shimeld, J. W. (2006). A new conceptual model for the structural evolution of a regional salt detachment on the northeast Scotian margin, offshore eastern Canada. American Association of Petroleum Geologists Bulletin 90 (9), pp. 1407-1423.

Jansa, L. F., Bujak, J. P. & Williams, G. L. (1980). Upper Triassic salt deposits of the western North Atlantic. Canadian Journal of Earth Sciences 17 (5), pp. 547-559.

Kidston, A. G., Brown, D. E., Smith, B. M. & Altheim, B. (2005). The Upper Jurassic Abenaki Formation Offshore Nova Scotia: A Seismic and Geologic Perspective. Canada-Nova Scotia Offshore Petroleum Board 1.

Klitgord, K. D. & Schouten, H. (1986). Plate kinematics of the central Atlantic. In: Vogt, P. R. & Tucholke, B. E., The Western North Atlantic region. The Geological Society of America. The Geology of North America M, pp.351-375.

Labails, C., Olivet, J. -L., Aslanian, D. & Roest, W. R. (2010). An alternative early opening scenario for the Central Atlantic Ocean. Earth and Planetary Science Letters 297 (3-4), pp. 355-368.

Leleu, S., Hartley, A. J., van Oosterhout, C., Kennan, L., Ruckwied, K. & Gerdes, K. (2016). Structural, stratigraphic and sedimentological characterisation of a wide rift system: The Triassic rift system of the Central Atlantic Domain. Earth and Planetary Science Reviews 158, pp. 89-124.

Markwick, P. J. & Valdes, P. J. (2004). Palaeo-digital elevation models for use as boundary conditions in coupled ocean-atmosphere GCM experiments: a Maastrichtian (late Cretaceous) example. Palaeogeography, Palaeoclimatology, Palaeoecology 213, pp. 37-63.

Marzoli, A., Renne, P. R., Piccirillo, E. M., Ernesto, M., Bellieni, G. & de Min, A. (1999). Extensive 200 My old continental flood basalts of the Central Atlantic Magmatic Province. Science 284, pp. 616-618.

Natural Resources Canada (2021). The BASIN Database. Government of Canada. https://basin.gdr.nrcan.gc.ca/wells/index_e.php.

Riegraf, W., Luterbracher, H. & Leckie, R. M. (1984). Jurassic foraminifers from the Mazagan Plateau. In: Hinz, K. & Winterer, E. L. Initial reports of the Deep Sea Drilling Project, Leg 79. U.S. Government Printing Office, pp. 671-702.

Tari, G., Jabour, H., Molnar, J., Valasek, D. & Zizi, M. (2012). Deep-water exploration in Atlantic Morocco: Where are the reservoirs? In: Gao, D. Tectonics and sedimentation: Implications for petroleum systems. American Association of Petroleum Geologists Memoir 100, pp. 337-355.

Tari, G., Brown, D. E., Jabour, H., Hafid, M., Louden, K. & Zizi, M. (2012). The Conjugate margins of Morocco and Nova Scotia. In: Roberts, D. G. & Bally, A. W. Phanerozoic Passive margins, Cratonic Basins and Global Tectonics Map. Regional Geology and Tectonics 1C, Elsevier, pp. 285-323.

Wade, J. A. (1991). Lithostratigraphy 2: Pre-Mesozoicbasement, and Mohican Formation and equivalents. East coast basins Series: Scotian Shelf. Geological Survey of Canada.

Wade, J. A. & MacLean, B. C. (1990). The geology of the southeastern margin of Canada. In: Keen, M. J. & Williams, G. L. Geology of the Continental Margin of Eastern Canada. Geological Survey of Canada, pp169-238.

Weston, J. F., MacRae, A., Ascoli, P., Cooper, K. E., Fensome, R. A., Shaw, D. & Williams, G. L. (2012). A revised biostratigraphic and well-log sequence-stratigraphic framework for the Scotian Margin, offshore eastern Canada. Canadian Journal of Earth Sciences 49, pp. 1417-1462.

Weston, J., 2019a. Biostratigraphic Study of the Mazagan-1 (MZ-1) well, Mazagan Block, Mazagan Basin, offshore Morocco. Weston Stratigraphical Limited.

Weston, J., 2019b. Biostratigraphic Study of the Tan Tan-1 well, Agadir-Tarfaya Basin, offshore Morocco. Weston Stratigraphical Limited.

Weston, J., 2019c. Biostratigraphic Study of the Cap Juby-1/ST#4 well, Tarfaya Basin, offshore Morocco. Weston Stratigraphical Limited.

Weissenberger, J., Harland, N., Hogg, J. & Sylonyk, G. (2000). Sequence stratigraphy of Mesozoic Carbonates, Scotian Shelf, Canada. Conference: GeoCanada 2000 – The Millenium Geoscience Summit, Joint Convention of the CSPG, CSEG, GAC, MAC, CGU & CWLS, Calgary, Alberta.

3. OFP MODELLING

3.1 INTRODUCTION

The ability to establish areas where organic-rich sediments may have been potentially deposited in the past is a fundamental aspect of the exploration workflow. The risks associated with accurately predicting source rock presence and quality are determined ideally by detailed analysis of observed data; however, these data are often lacking, especially in frontier areas. In the absence of such data, theoretical predictive models can play an important role.

The Organic Facies Prediction (OFP) Model was developed for predicting the initial (pre-maturation) total organic carbon (TOC) content and hydrogen index (HI) of sediments. It was designed to work anywhere with minimal data so that it could be of value in frontier exploration areas where information is sparse or where limited/clustered data make interpolation and extrapolation difficult.

The Scotian Basin and wider Hispanic corridor region has very limited data regarding the potential for Lower Jurassic source rock deposition. This is largely due to the lack of well penetrations down to Lower Jurassic strata. The presence of effective petroleum systems along the Scotian margin suggest the presence of a viable source rock; however, evidence of this is yet to be obtained. In the absence of adequate well data, it is necessary to examine alternative approaches to establish if the conditions during the Lower Jurassic were suitable for organic-rich facies to be deposited.

The OFP model has been employed to predict the initial TOC and HI of the Hispanic Corridor sediments during the Early Jurassic and Tithonian based on the gross deposition environment reconstructed in Chapter 2. The GDE's provide the environment and - most importantly - the bathymetry for the model to calculate against.

In order to ground the model predictions against true data values the wider region of the European Tethys has been included. A number of actual or potential source rocks have sufficient published data which could be compared with OFP results to ensure a reasonable regional performance of the model.

3.2 MODELLING PRINCIPLES AND METHODOLOGY

To model TOC and HI, we need to know - or at least be able to estimate - the primary productivity and water depth to first calculate a Carbon Delivery Flux (CDF). We also need to understand variations in preservation in response to carbon flux, sedimentation rate and dissolved oxygen. These data are often not directly accessible from ancient sediments (or with the desirable accuracy), so we must turn to data from modern environments and sediments to help us understand and quantify these factors and their relationships. We can then apply this knowledge to ancient palaeogeographies by making the assumption that the fundamental relationships are relatively unchanged through geological time. Although many things may differ between the modern world and the past, we believe this approach has value and is capable of producing viable predictions given the overall levels of uncertainty.

The OFP Model utilises published equations for the key input preservation and dilution (IPD) relationships (Figure 3.1), plus a number of custom ones based on reanalysis of published marine sediment data. The model was developed with multiple options to accommodate a number of different potential scenarios. This is so it can be applied and calibrated to generate more precise regional predictions where the local conditions are better known, giving the model the potential to achieve much greater predictive power.

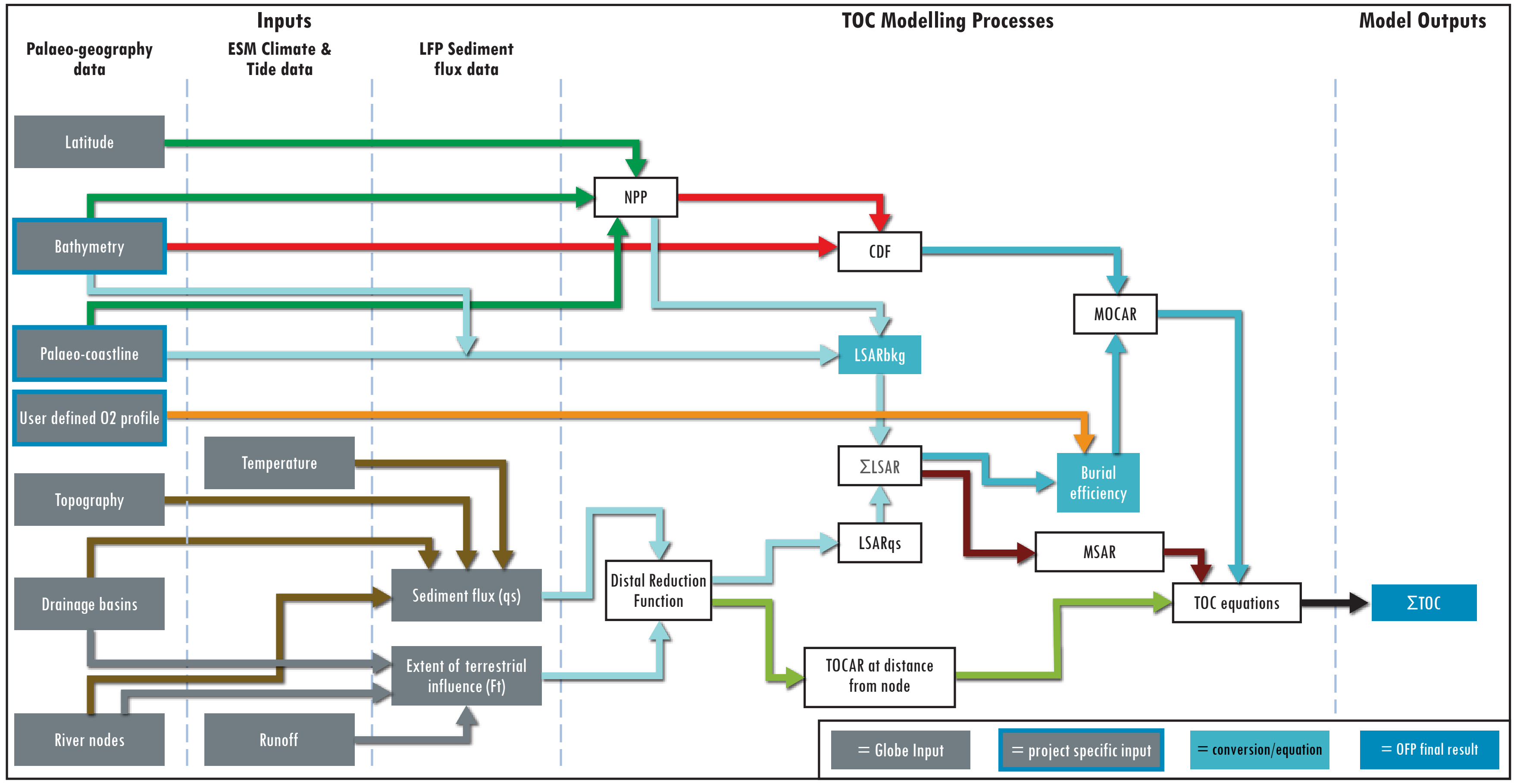

Figure 3.2: A summary of the OFP model processes for calculating TOC.

Figure 3.1 (Below): An illustration of key inputs required to model TOC using the IPD approach.

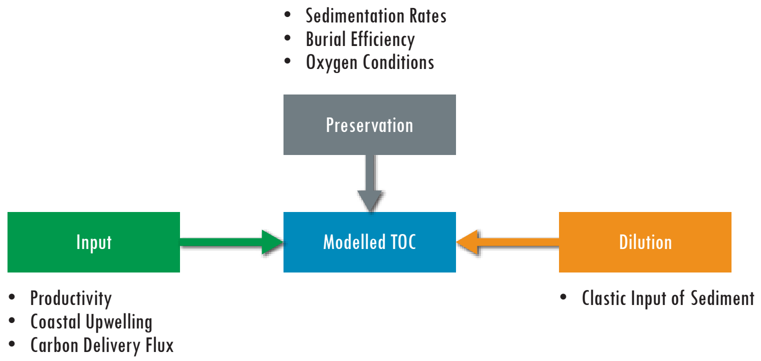

The relationships of the key variables were often harvested from data in multiple papers on different geographic areas and, thus, represent very generalised trends that might not necessarily apply well in a given specific area; conversely, some may be biased by data from a specific region. Use of global data invariably results in a larger error bar than if they had come from just one region where all factors would be expected to be more uniform. Obvious outliers were filtered to help remove noise. New data are constantly being produced and methodologies are revised, so no algorithms based on empirical relationships can ever be considered to be fixed in stone.

In order to predict the TOC content or the HI, the model first simulates net primary productivity (NPP), which is based on latitude, water depth and distance from the coastline. Given productivity values, CDF can then be estimated from the modelled water depth. The productivity values are also used in Getech's custom equation for predicting background offshore sedimentation rate (LSARbkg), along with depth and distance from land. Sedimentation rates and carbon flux values allow us to estimate Burial Efficiency (BE), and from the BE and CDF, we can then derive a marine organic carbon accumulation rate (MOCAR). Conversion of linear into mass sediment accumulation rates then provides us with everything we need to calculate location specific TOC estimates using the basic (arithmetic) TOC equation. A schematic of the approach for TOC values is shown in Figure 3.2.

3.2.1 NET PRIMARY PRODUCTIVITY (NPP)

Palaeoprimary productivity (PPP) is typically an unknown value for ancient sediments. Quantitative estimates of PPP require TOC values, sedimentation rates, sediment densities and porosities (and there are at least 10 different published equations). If these input data were all known, there would be no need for a TOC prediction. PPP calculations are not routine, and published examples come mostly from a small number of academic studies. In most cases, we need a different approach to PPP estimation.

The algorithm we use to derive the productivity estimate is based on a global map of the mean of 8 years of modern annual mean productivity values derived using the remote sensing carbon-based productivity model (CBPM; Westberry et al., 2008). The key advantages of the remote sensing data are the greater and more consistent temporal and spatial coverage, compared to conventional shipboard measurements. The CBPM was adopted because it is considered to be the best model currently available (O'Malley, pers. com., 2012) and also because the overall range of values was found to be more comparable to measured values than those from the main (older) alternative model (the VGPM model of Behrenfeld and Falkowski, 1997). At least partly due to the better sampling, remote sensing values are typically greater than conventional shipboard measurements.

Only the NPP data that matched sites from which other modern sediment calibration data were available were included in the analysis (to help ensure a more cohesive data set). These NPP values were then regressed with depth, distance from land and latitude to provide an algorithm that could be used with any palaeogeography and DEM.

The best regression results for the modern data were obtained by treating data from each hemisphere separately.

It was considered that modern hemisphere difference would be unlikely to remain constant through time due to changes in climate, ocean circulation and continental configuration.

Furthermore, because there were more calibration data available for the northern hemisphere, the northern hemisphere NPP trend was calculated and then mirrored about the equator.

3.2.2 CARBON DELIVERY FLUX (CDF)

The OFP Model can calculate CDF using any of 22 equations (published or derivatives) based on water depth and NPP. When using the modern sediment equations for calibration purposes, the CDF values used were either ones based on near-bottom sediment trap data or calculated values where the CDF was reconstructed from the sum of the Organic Carbon Accumulation Rate (OCAR) plus the carbon oxidised, where the latter was based on pore water and/or diagenetic modelling by the authors of the data set. Although OFP necessarily uses 'top-down' predictions of CDF (from NPP and water depth) in its ancient predictions, relevant OFP equations were calibrated using only documented 'bottom-up' CDF values as these are thought to be more reliable.

Top-down equations presume that the OM preserved in the sediment was supplied only vertically from waters where the NPP was estimated. This is a significant simplification, as there are obviously also lateral fluxes due to currents, resuspension and nepheloid gravity flows (especially on the inner shelf and on topographic slopes) to consider. The magnitude of these lateral fluxes is very poorly constrained even at the Present Day (and, of course, OM is not a conservative property). The true CDF (bottom-up) is often likely to be higher than any top-down estimate, and the latter are thus relatively conservative estimates.

All published carbon flux equations, which are based primarily on open-ocean data, are not valid for depths of less than 100 m, and no equation is likely to be meaningful at depths of less than 50 m (where the formation or preservation of basinal source rock facies also becomes increasingly unlikely). To provide some estimate for palaeowater depths of between 50 and 100 m, we have improvised a separate algorithm utilising Wassmann's (1990) equation for estimating carbon export below 50 m, plus a linear interpolation between this and the ordinary equation-predicted flux for 100 m. At depths shallower than 50 m, the water column is likely to be fully mixed and unsuitable for source rock deposition, and any organic-rich sediment deposited is less likely to survive any subsequent erosion.

3.2.3 LINEAR SEDIMENT ACCUMULATION RATE (LSAR)

Sedimentation rates are crucial for assessing BE in oxic facies and dilution in all facies. The linear rates (thickness/time) can be converted into mass sediment accumulation rates (MSAR) using linear (or multiple) regression of modern LSAR and MSAR.

All sedimentation rates used in modelling TOC are short-terms ones (mostly expressed in cm/ka). This is because these are the rates relevant to the duration of the processes that influence the production, deposition and preservation of OM. The TOC content of immature sediments is 'locked in' relatively soon after burial. Although longer term (geological) rates might be important for preserved total thicknesses, they are not what control the TOC content.

OFP splits sedimentation rates into two components: the background (LSARbkg) and local fluvial LSARqs related to sediment discharge from river nodes.

3.2.3.1 LSARBKG

The LSARbkg is not just a biogenic pelagic rate, but the mean sedimentation rate for any sediment that is not related to a specific fluviodeltaic point source (river mouth).

This estimate of LSAR is based upon a multiple linear regression analysis of published modern marine sediment data. Being based on modern sediments, these are short-term values and essentially uncompacted, but these are the rates that are most relevant to the short-term processes that influence OM deposition and preservation. They will overestimate the long-term sediment accumulation rate.

3.2.3.2 LSARQS

The combination of the Getech drainage modelling, climate model results and sediment flux modelling based on the BQART model (Syvitski & Milliman, 2007) allows us to estimate the sediment discharge from each river node (Qs).

With some pragmatic assumptions, these data can be converted into distance-varying estimates of linear and mass sedimentation rates (LSARqs and MSARqs) of fluvially derived sediment. The LSARqs are only calculated for areas within a radial distance of river mouths and are derived using a proxy based on the relationship between river discharge and the distance offshore at which modern δ13C values indicate the fraction of terrestrial OM falls to zero (ZFt), shown in Figure 3.3a.

To convert sediment discharge (Qs) into an estimated sedimentation rate (LSARqs), we have to know the area over which the annual mass of sediment coming from the node is deposited. The indirect proxy we use for this is the ZFt radial distance, which is estimated using a Schultz and Calder (1976) type equation, which is then edited, supplemented and modified to extend it to a greater range of discharge without it reaching a premature asymptotic maximum.

This equation links the ZFt to river water discharge (Q), and, thus, the terrestrial influence of larger rivers extends further offshore than smaller ones (to a maximum of about 300 km based on the Amazon profile perpendicular to the coast).

A 3D geometry must be assigned to the sediment body deposited within the ZFt in order to relate the mass and area to a volume and thus thickness (via user-defined density and porosity values). It is assumed that the debouching annual fluvial sediment load forms a semi-conical 180° fan, especially over extended periods of time (due to distributary switching, changing coastal morphology, etc.).

Using basic conical geometry, we can determine the height of the apex of the sediment cone with twice the fluvial sediment (half cone) volume, which will be equivalent to the annual sediment increment at the node (cm/a). We not only need the height of the apex of the cone, but to calculate this correctly, we also need the volume of the full cone. The LSARqs is then assumed to decrease offshore radially and linearly with distance from its maximum at the apex of the cone (the node) to its minimum (zero) at the ZFt distance, where only the background LSAR is recorded (Figure 3.3c).

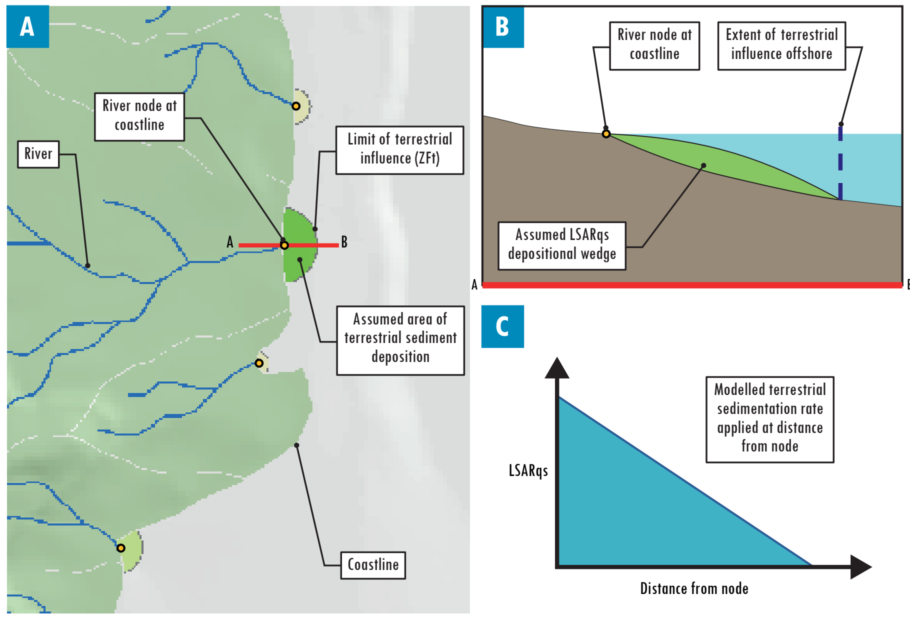

Figure 3.3: ***Schematic showing a) how the extent of terrestrial influence is mapped by the model, b) schematic cross section of assumed wedge and limit of terrestrial influence, c) modelled terrestrial sedimentation rate from node to limit of terrestrial influence.***

3.2.3.3 INTEGRATION OF LSARBKG AND LSARQS (∑LSAR)

For the default LSARbkg equation, the distance used is distance from coast (Dc in degrees). For the fluvial sedimentation rates, the distance used is that from the river node (Dn in km). Within the ZFt radius, the Dn and Dc thus need to be known for each grid point, but only the Dc offshore of the ZFt. Within the ZFt radius, the LSARbkg and LSARqs could be considered to combine in either a summative fashion (both present and summed) or a replacive one (the background is entirely replaced by LSARqs at Dn < ZFt if the LSARqs is greater than the background), as represented in Figure 3.4. A replacive model has been utilised for this study.

The ZFt decreases with discharge, and thus, for smaller rivers fewer grid points. The overall impact on the maps will vary with the proximity of the coastline to the centre of the grid cell. Small rivers always dominate on a global scale, and, as their ZFt is generally only about 40 km or less, terrestrial influence has a limited spatial effect on TOC & HI predictions.

3.2.4 BURIAL EFFICIENCY

BE is the Organic Carbon Accumulation Rate (OCAR) divided by the CDF, expressed as a percentage. This is the fraction of the carbon flux that survives early diagenesis to be preserved in the sediment (generally at burial depths of 50–100 cm). There may be subsequent slow degradation with further burial, but the rates are low and the diagenetic signal will become smaller than that associated with changes through time. It has been found that this parameter covaries with sedimentation rate (Henrichs & Reeburgh, 1987), although it may also be influenced by other variables, including carbon flux and oxygen regime (Tyson, 2001), and, thus, oxygen exposure time (Hartnett et al., 1998).

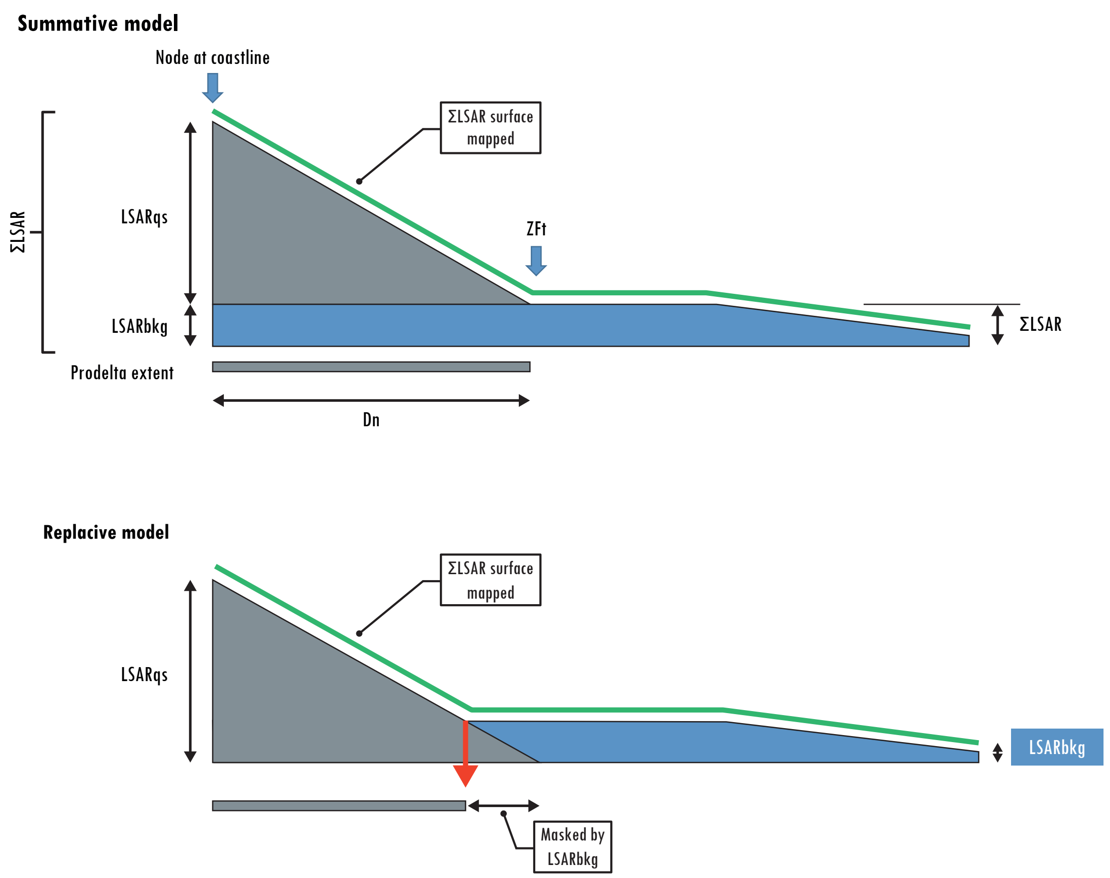

Figure 3.4: ***Schematic showing the two different possible methods of integrating the fluvial sediment flux with the background sediment flux.***

3.2.5 TOC

3.2.5.1 MARINE TOC (MTOC)

This is the TOC calculated using the fundamental IPD equation (Tyson, 2005):

TOC = ((Input x Preservation)/(Input x Preservation x OMF) + Mineral Dilution) x 100

where OMF is the conversion from TOC to OM (1.8 is used here).

As the MTOC equation above requires an estimate of the CDF, which is not possible when water depth is less than 50 m, a different approach is required in order to avoid large areas of the shelf on the maps remaining blank. For most of these shallow-water areas, we have utilised the median TOC value of modern marine sediments based on a database of published values (1.57%, n = 1,846)

Using the constant MTOC value of 1.57% for much of the shallow shelf means that there is often an unrealistically abrupt change in the ∑TOC values at the 50 m isobath (especially as the CDF at 50–100 m may be an overestimate). It does, however, ensure that the oxic coastal facies are shown as having a lower quality organic facies.

3.2.5.2 TERRESTRIAL TOC (TTOC)

Despite the additional flux of terrestrial OM from rivers, TOC values are rarely more than 2–3% in most prodelta muds (for samples unbiased by macroscopic plant debris). For simplicity, we assume that at the river node the terrestrial fraction (Ft) is 100%, and, thus, that the TOC here represents just TTOC. We also assume that the TTOC has a value of 3% at all river nodes. The TTOC is multiplied by the MSARqs value (derived from the fluvial Qs) to give the terrestrial organic carbon accumulation rate (TOCAR) at the river node. As the sedimentation rate (MSARqs) decreases with distance from the river node, the TOCAR thus also decreases proportionately. The TTOC can be calculated from the TOCAR and the MOCAR and omfMSAR values (and the OM factor); it varies from 3% at the river node to zero at or beyond the ZFt distance. Redeposition beyond the Zft, including that achieved by gravity currents, storms and alongshore drift, is not taken into account.

3.2.5.3 MARINE AND TERRESTRIAL TOC (∑TOC)

The final mapped TOC values represent the ∑TOC, which is the sum of the MTOC and TTOC. At depths greater than 50 m and beyond the ZFt radius, the ∑TOC corresponds to the MTOC, but within the ZFt radius, it is a mixture of marine and terrestrial carbon.

3.2.6 HYDROGEN INDEX (HI)

The HI is derived from Rock-Eval pyrolysis and is a measure of the oil-proneness of the organic matter (its remaining generative potential), which reflects its origin, preservation state, and maturity. Maturity is not considered here because we are only dealing with initial properties controlled by environmental factors. Hydrogen Index can be estimated in two main ways. The first is a simple conversion of a predicted MTOC values into an HI using a HI versus TOC relationship derived from an analogue or available immature sediment data (HIA). The second approach uses independent assessment of marine and terrestrial HI values and then integrates these to derive an overall HI (∑HI) using a mixing calculation.

3.2.6.1 HI BY ANALOGUE (HIA)

Hydrogen Index shows a positive and asymptotic logarithmic (LN) relationship with TOC because TOC is also used in calculating the HI (S2 /%TOC x 100); there is thus a linear correlation between HI and LogTOC, and also between S2 (mgHC/g rock) and TOC (Langford & Blanc-Valleron, 1990). The analogues chosen for modelling can be documented source rock facies, regionally or temporally relevant source rocks, or based on locally available data. With this approach HIA values will only change if the MTOC is changed, or if a different TOC v HI equation is selected.

Initially, 14 natural logarithmic and one polynomial equation have been provided to estimate a HIA from a predicted MTOC, based on a range of calibration sets for marine source rock facies that exhibit a range of maximum HI (from about 300 to 700). Because the regression-predicted mean HI is being used, natural noise is stripped out, and the resulting HIA will inevitably be less varied than real data. The equations are also constrained to yield a minimum of 50 mgHC/gTOC (approximately equivalent to inertinite) and a maximum equal to the mean HI calculated from the slope of S2/%TOC x 100 (where S2 is derived from HIA x MTOC/100, for MTOC values of 2-6%). Although the mean slope-derived HI is constant for each HIA equation, the HIA estimated by the equation (like measured HI values) changes with MTOC (specifically its magnitude relative to the TOC intercept) and is typically lower than the mean slope value (on average by about 100 mgHC/gTOC; Tyson, 2006).

In effect, the calculated HIA corresponds to a mixing between two components (an HI applicable at TOC values ≤ intercept, and the slope HI applicable to the more reactive component whose addition results in TOC values > intercept). The low TOC background component (often refractory terrestrial OM) does not just disappear if redox or productivity changes result in an increase in MTOC, but it does become progressively diluted. The calculated TOC intercept is generally thought to reflect either a mineral matrix effect leading to adsorption and, thus, underestimation of part of the S2, and/or a change to a lower HI organic facies at lower TOC. Adsorption phenomena are not contested here, but these are usually demonstrated for a constant OM composition and laboratory experiments where the observed TOC reflects only mineral dilution. An OM mixing origin is favoured here because in real world samples the slope of S2/TOC often decreases at low TOC, conforming to a different trend that often does pass through the origin or closer to it (although the inherently higher scatter at low TOC and S2 often decreases the r2). Microscopy also often indicates a clear change in OM character at lower TOC (e.g.

reduced AOM/phytoclast ratio and/or AOM fluorescence). Often the trend through the higher S2 and TOC values does not therefore remain constant at lower TOC and, thus, should only be extrapolated with caution to a TOC intercept less than the observed. Assuming the HI at and below the TOC intercept value has a value of 50 mgHC/gTOC, the relative difference between the HI calculated by such a mixing model shows over 99% agreement with the calculated HIA. The TOC intercept value is only an approximation of the TOC at which the organic facies changes. In some cases, where preservation as well as kerogen mixing is changing with TOC, or there is more than one component contributing significantly to the S2, more than two organic facies may also be present.

3.2.6.2 MIXING MODEL APPROACH: ∑HI

A schematic of this approach is shown in Figure 3.5. The initial HI of terrestrial OM (THI) is typically low (50-200, gas-prone), whereas the HI of plankton–derived marine OM (MHI) can range from <100 to 700 depending upon its preservation (and thus be gas- or oil-prone). The huge majority of OM in marine sediments is of marine phytoplankton/bacterial origin. Adjacent to rivers this MOM is supplemented by the supply of TOM, but the greater supply of siliciclastic sediment often elevates LSAR into a range where the predominant overall impact of the rivers is one of dilution. Although MOM is initially oil-prone when produced (higher MHI), its actual HI preserved in the sediment depends on its preservation state, which will be determined by oxygen exposure time (OET).

Modern sediment deltaic and estuarine carbon isotopic equations permit the estimation of the relative terrestrial OM fraction (Ft) for a given distance from river nodes. The suitable equations are few and also all based on low to mid latitude rivers (e.g. the Amazon, Mobile, and Tay), with no consideration of vegetation type. The Ft at a given distance varies with river discharge, and four equations have been used to provide Ft estimates for low, medium, high and very high discharge rivers.

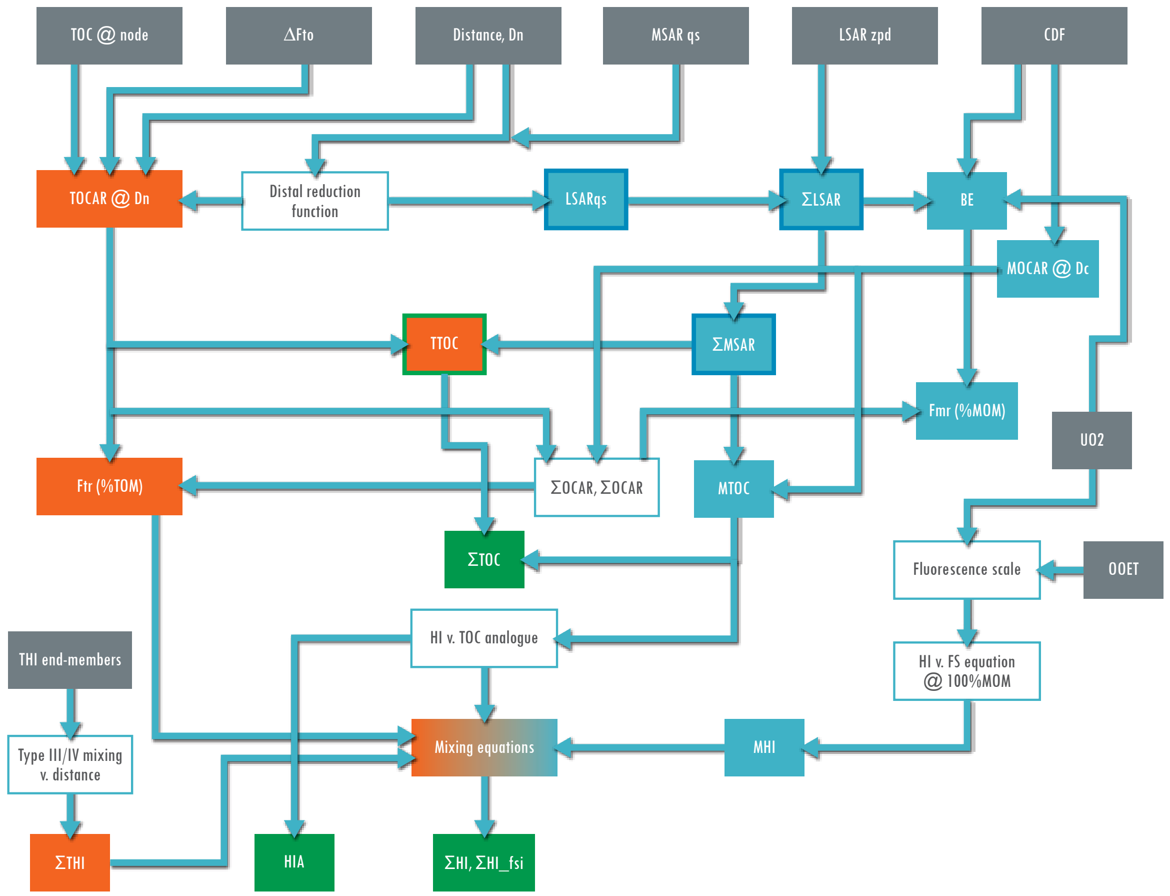

Figure 3.5: ***Schematic showing how OFP calculates Hydrogen Indicies.***

We refer to these estimates as the original Ft (Fto), as they are the value initially generated by the modern equations.

For realistic modelling, one cannot use estimates of percentage Fto based on modern isotopic studies directly to model ancient TOM. This is because the marine and terrestrial OM fluxes can both vary independently and do not have a fixed total (∑TOC or ∑OCAR, neither of which may be reported). The ancient factors controlling the MOM and TOM supply and preservation may not be the same as in the Present Day studies, and thus their percentages would also thus differ. If TOM supply was constant but the MOM preservation increased (e.g. due to higher productivity or dysoxia-anoxia), the %TOM would fall, and the %TOM also ought to increase if MOM preservation were reduced. We thus derive a recalculated Ft (Ftr) from independently modelled TOCAR and MOCAR trends and this will differ from the original Ft (Fto) values.

If we assume the mean OMF was more or less the same for both marine and terrestrial post-early diagenetic OM, the Ftr to be used in the HI mixing model is thus:

Ftr = TOCAR/(TOCAR+MOCAR)

Whatever the TOM flux supplied by the river, and the resulting TOCAR, both of which may be very high, we know it usually produces surprisingly consistent overall TOC values that are rarely more than 2-3% in most prodelta muds (for samples unbiased by macroscopic plant debris). The overall TOC = TTOC if we assume the Ft is 100%; we can make this TTOC a user-defined constant (applied to all nodes), and then combine it with the calculated MSARqs to derive an estimate of the TOCAR at the node.

It is next necessary to consider how the TOCAR decreases with increasing distance (Dn) away from the river node. We can base this on just the MSARqs alone as TOCAR equals %TTOC/100 x MSARqs).

For gridpoints that are within the ZFt radius at the node, this TTOC value will only correspond to the user assigned TTOC value (≤3%), and then decrease linearly (at varying rates) to 0% at the ZFt. Although some TOM may in fact escape beyond the ZFt, its amount will be small and its distribution unknown; along with aeolian TOM fluxes it will probably contribute to a minor refractory background TOC in distal sediments that is of negligible significance for HI.

Once separate TTOC and MTOC values have been calculated from the MOCAR and TOCAR (Figure 3.6), we need to estimate the HI values associated with each so that we can use them in the ∑HI mixing model. For the marine HI (MHI) end-member value we assume a redox-related control, as commonly implied by geological observations. There are no adequate data to derive a direct relationship between MHI and the full range of O_2 values (and even if there were, modern sediment HI values may not be directly comparable with ancient ones). Instead, we use the Fluorescence Scale (FS) of Tyson (2006) as a proxy for preservation that has been correlated with HI. The FS parameter was based on palynofacies observations on ancient immature or early mature sediments under blue light fluorescence and found to reflect redox regimes inferred from other observations (like bioturbation, macrofossils and sediment colour); its use here does not require microscopy data as it is only being used as a scaling function.

The FS1-FS5 range typical of marine facies has been equated with dissolved oxygen ranges expressed in the non-linear ROx (rescaled oxygen) scale of Tyson (2001; 2005), to give a greater sensitivity to lower O_2 values. As there are only five marine FS values, once beyond the ZFt (where there is only MOM) this would result in only five unique HI values for any given HI versus FS equation. To avoid this, a continuous estimate of ROx is derived from the UO_2 using a polynomial equation (based on the upper limit of O_2 for each ROx value).

This ROx is then used in a linear regression to estimate a continuous rather than categorised estimate of FS. This in turn is used in the HI versus FS equations to provide a continuous estimate of MHI.

The more oxygenated the regime the lower the inferred FS, and the lower the associated MHI. For oxic environments, the length of duration of exposure to oxygen is also of importance and to incorporate this effect a rule is included that uses the estimated OOET1 value (oxic oxygen exposure time). OOET1 uses the equation of Wenzhofer and Glud (2002) which predicts the oxygen penetration depth (OPD) from water depth and primary productivity, and then combines this with the sedimentation rate (LSARz or LSARzpd) to estimate the OOET. Where OOET1 is greater than a specific value (default 500 years) for any oxic facies with ROx >5 (O_2 >2ml/L) the continuous FS value is set to a low value that generally gives an MHI <100. This should help to replicate the observed low HIs in oxic condensed sections (including the modern oxic deep ocean). The default threshold OOET1 value of 500 years was based upon some model trials.

The MHI end-member value can be calculated given the FS and assuming 0%Ft (100%Fm) via one of six different marine sediment HI v FSI equations (Tyson, 2006) provided.

The absolute variation in terrestrial HI (THI) is typically less than for MHI. We can model lateral variation in THI using a basic distance-based mixing model. This is guided by the observations that normal "coaly" vitrinite commonly has an HI of around 200 mgHC/gTOC whereas dispersed marine phytoclast populations are more typically associated with an HI of about 100. Inertinite (Type IV kerogen) is generally considered to have a HI of about 50 mgHC/gTOC, and the fraction of inertinitic phytoclasts tends to increase distally due to selective preservation or transportation, regardless of the basal redox regime (although based on phytoclast colour, it seldom seems to become dominant, except perhaps when OET is very high).

Given the default two end-member values the default distance-based mixing model produces a range in THI from ~200 at the node to ~100 at the ZFt. The user can adjust the four settings of this THI mixing model if they desire (e.g. perhaps to simulate more oil-prone terrestrial OM if this were applicable, as in the Cenozoic of SE Asia).

Once the MHI and THI are known, the overall combined ∑HI can either be calculated using a mixing of the MHI and THI according to the Fmr/Ftr ratio (the default), or via one of the six analogue-derived FSI equations and the Fmr but not the estimated THI value (∑HI_fsi). If the TOC is grain size adjusted (TOCgsa), the ∑HI values are automatically decreased because MOCAR is reduced and the Fmr/Ftr ratio modified.

The mixing approach thus accounts for a redox-preservation effect on MHI, the impact of phytoclast variation on THI, and the mixing of TOM and MOM (at Dn<ZFt). Unlike most models, neither the marine or terrestrial end-member is assumed to have a constant HI. Mixing of TOM and MOM is generally a relatively localised and proximal effect, and thus it is applied only adjacent to river nodes within the ZFt radius. Note also that because the absolute THI value is much lower than the MHI of well preserved MOM, the overall magnitude of the mixing effect on ∑HI will be diminished in dysoxic-anoxic facies.

However, as the majority of dysoxic-anoxic facies are probably located beyond the ZFt, at any given location the ∑HI may often be a function of only preservation or mixing, rather than both simultaneously. If the MOM is poorly preserved (high O_2, low FS) and has a low MHI, the resulting convergence in MHI and THI values means that mixing will also have less apparent impact on ∑HI.

A decrease in MTOC will lower the HIA, even though mixing is not used per se in the HIA approach. This is because the HIA v TOC calibrations often effectively incorporate a degree of such mixing at the lower end of the TOC range.

3.3 WEST TETHYS OFP MODEL WORKFLOW AND SETTINGS

Due to the lack of regional data from the Hispanic Corridor, it is necessary to look beyond the Hispanic Corridor to the adjacent West Tethys region for reliable known source rock data to constrain model results with. As the OFP model was developed with multiple options to accommodate a number of different potential scenarios, it is possible to calibrate the model specifically to the West Tethys region to give a much greater predictive power.

There are a number of options for the various equations employed by the OFP model. Figure 3.2 shows each parameter that has to be calculated to predict TOC. For each parameter in that step wise process, there are a number of published and custom equations that can be selected to calculate that one parameter. Table 3.1 lists the workflow and each of the settings selected for the West Tethys model runs, with explanations of how and why that specific setting has been applied.

Customised region specific bathymetries, palaeocoastlines have been generated for modelling boundary conditions, along with calculating the sediment flux and extent of terrestrial influence utilising the specific regional inputs above and general circulation climate model data (shown in Figure 3.2).

For this study, two scenarios have been run; one using the 'standard' LSARbkg equation to predict sedimentation rate, the other using a fixed low sedimentation rate of 1 cm kyr^{-1} (Table 3.1, step 5). This latter scenario is to represent a condensed section setting and provide a maximum TOC prediction (for low O_2 CS, minimum for oxic CS). The former standard sedimentation rate yields a more central (median) TOC prediction due to dilution.

The two different approaches to calculating HI (described in the previous methods section) have also been applied to show the variance between the two methods (Table 3.1 step 5).

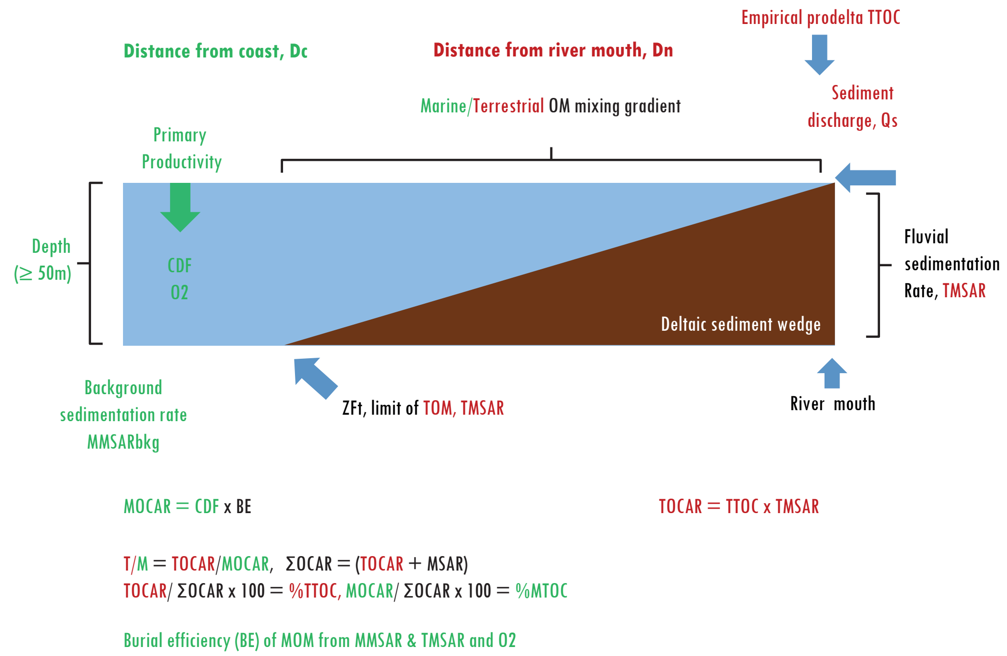

Figure 3.6 (Left): ***Schematic showing how OFP integrates MTOC and TTOC. Green indicates marine components and brown indicates terrestrial components.***

Workflow	Model setting/ equation applied	Notes
1. Literature Review	N/A	Review of Jurassic North Atlantic and European Lias source rock properties carried out to assess model performance
2. Input data	Data required: DEM, palaeocoastline, sediment flux and terrestrial influence data	Customised region-specific DEMs, palaeocoastlines have been generated along with predictions of fluvial sediment flux and the extent of terrestrial influence. See Chapter 2 for further details
3. NPP equation	Mirrored	Generalised trend with water depth, distance from land and latitude, based on the greater amount of modern sediment data from the northern hemisphere and then mirrored at the equator.
4. CDF equation	Pace et al. 1987	Appears to perform better at shelf depths than some, and in both oxic and anoxic regimes.
5. LSARbkg equation	Scenario: 1. Getech custom 2. Fixed condensed section	1. Uses depth, distance from land and the estimated palaeoproductivity (NPP) 2. Sedimentation rate is fixed at average condensed sedimentation rate of 1 cm kyr-1
6. Inclusion of fluvial LSAR	Included terrestrial sediment flux and extent of terrestrial influence Node over lap rule applied	Allows a simplified estimate of terrestrial OM supply and dilution effects adjacent to river mouths. Where river nodes overlap, the model uses the highest predicted fluvial LSAR value.
7. LSARbkg cap in shallow proximal settings	None applied	
8. Oxygen profile set	OMZ applied between 100-200m depths	Most suitable to capture anoxic continental shelf basins that are evident in the later Lias. See Section 3.5 for further details
9. BE equation	Scenario: 1. Tyson 2006 2. Variable O_2 cs	
10. TOC type	Tyson 2005	Input-Preservation-Dilution model.
11. HI method	Two scenarios: 1. Mixing Model 2. Analogue	1. Based on non-linear relationship of O_2 and HI 2. Based on non-linear relationship with TOC using data from an appropriate analogue (Toarcian Whitby Mudstone Formation)
12. Results		

Table 3.1: ***Model settings applied to the West Tethys region for each step of the OFP workflow.***

3.4 LITERATURE REVIEW

The first step in the OFP workflow (shown in Table 3.1) is to gather data and review published literature in order to compare and ground truth theoretical model predictions. If a reasonable regional fit is evident, it gives confidence that the predictive model has value where there is no data available.

Regional data from the Hispanic Corridor is sparse, with very few wells penetrating Lower Jurassic sections. Therefore, it is necessary to look beyond the Hispanic Corridor to the adjacent West Tethys region for reliable known source rock data.

Over 200 data entries covering the five time slices across 143 locations were collected to produce an integrated database of existing source-rock data from Getech, OERA and published literature (Figure 3.7). These can then be rotated back to their palaeoposition allowing comparison with the OFP model predicted values.

The data points in the source rock database represent a variety of reliabilities and resolutions. Each data point is placed on the map and is assumed to represent a location's single observation.

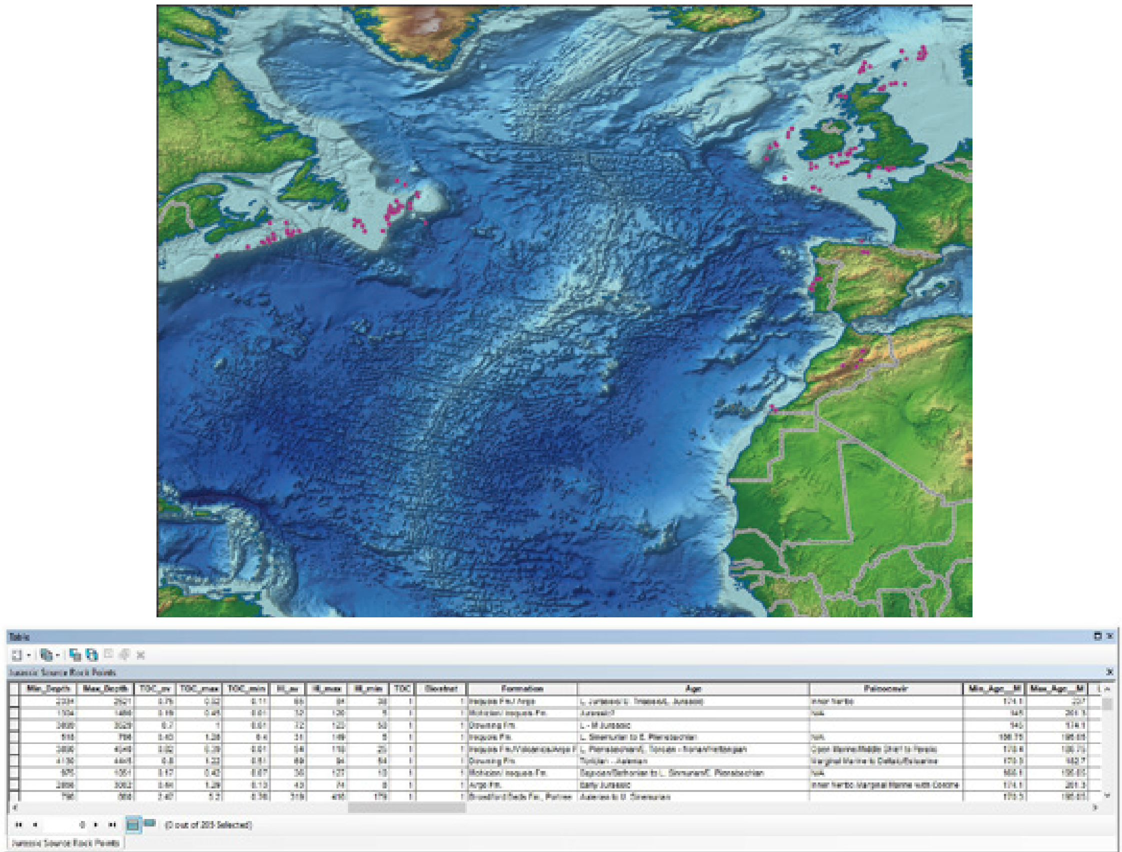

Figure 3.7: Integrated points data base containing source rock information for North Atlantic source rocks. Data has been complied from Getech, OERA and published literature.

However, the time span presented by each locality varies, due in part to dating and correlation uncertainties. Many samples have poor temporal resolution, with age ranges covering 3-4 stages of the Lower Jurassic, e.g. Hettangian to Toarcian or 'Lias'. It is therefore difficult to determine in many cases which stage that sample truly represents. It is important to consider these uncertainties when carrying out data/model comparisons. Further uncertainties in the data can be introduced by drilling contaminants and selective sampling.

Other useful sources of source rock data can be compiled from published literature. Getech's Source Rock Atlas provides the mapped spatial extent of known source rock units, these can also be rotated back to palaeoposition to give an better indication of the minimum spatial extent of source rock deposition during the relevant stage (Figure 3.8).

Additionally published literature can provide useful regional/unit source rock information without giving specific point values or spatial extent (Figure 3.9 & Table 3.2).

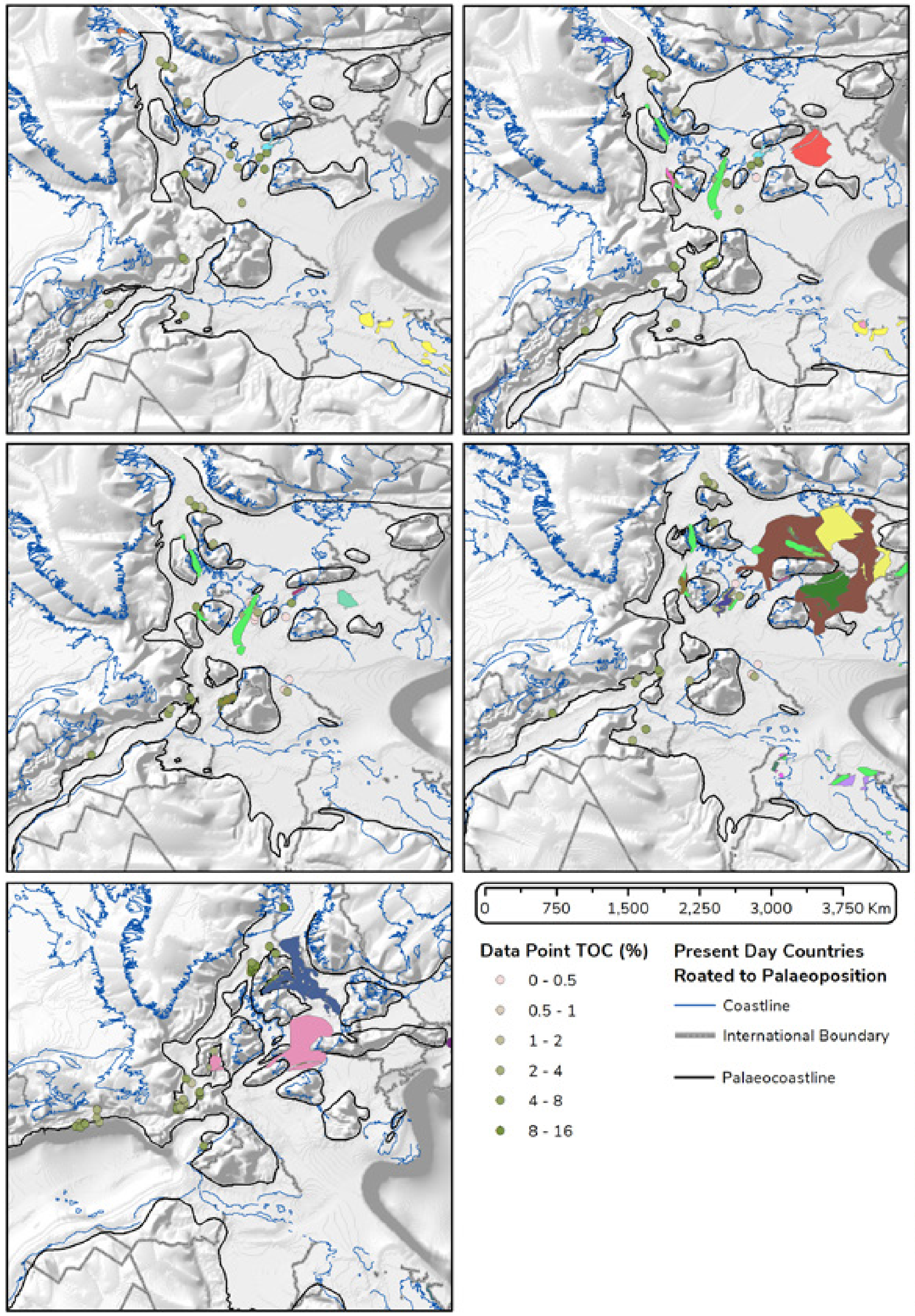

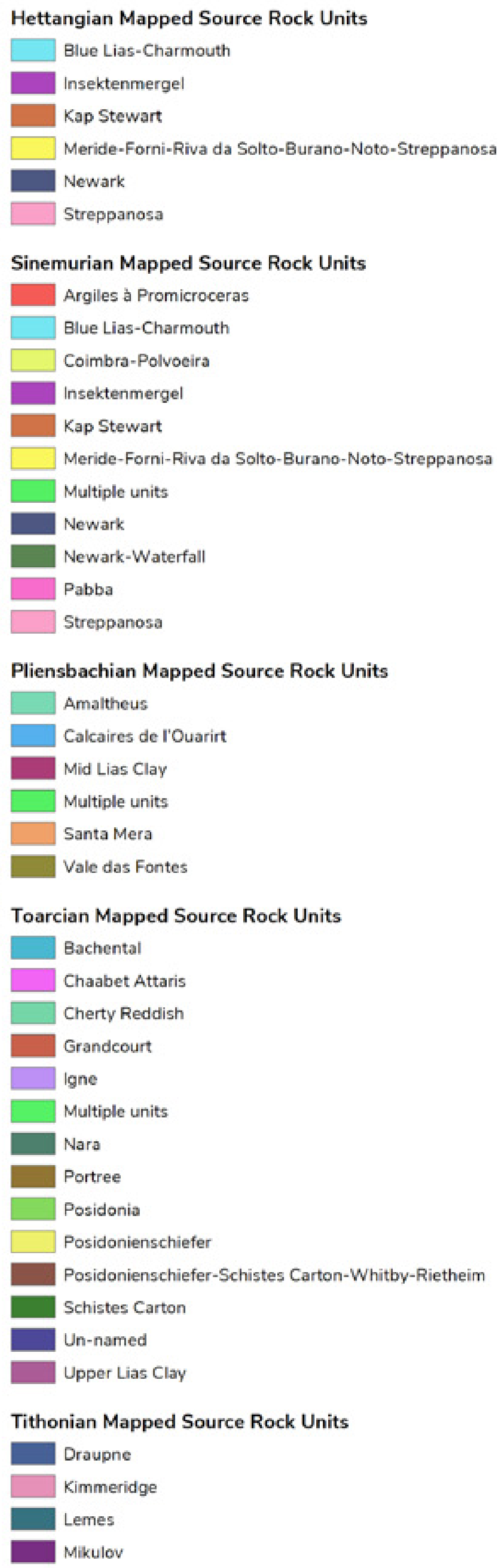

Figure 3.8: Mapped spatial location of age relevant source rock units from Getech Source Rock Atlas and TOC point data maximum or average where data maximum data was absent. All data has been rotated back to the palaeoposition of each relevant stage. Palaeocoastline is shown in black with the Present Day coastline and country boundaries show in blue and dashed grey, respectively.

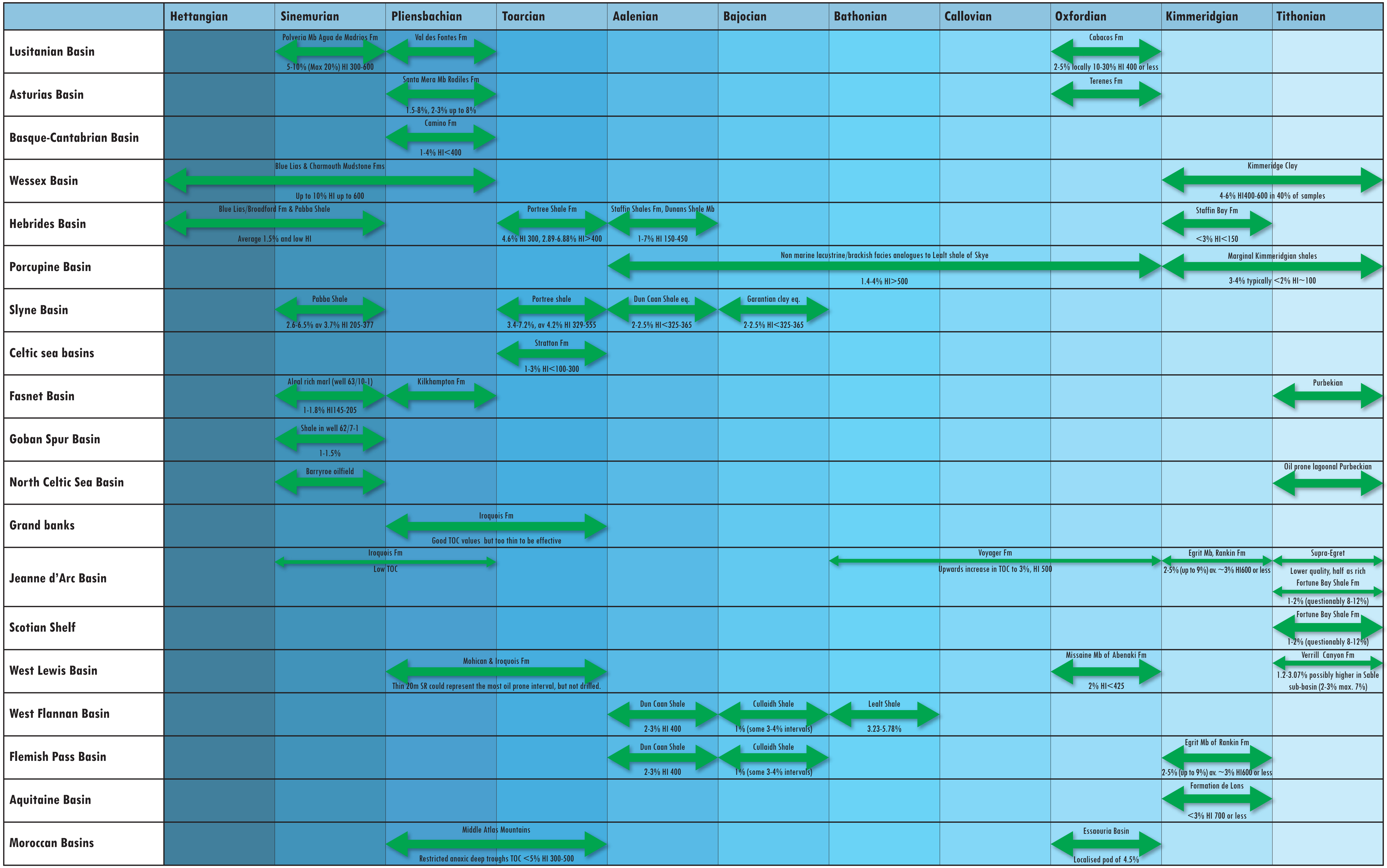

Figure 3.9: *Review of Jurassic North Atlantic source rocks. With TOC values reported as %. Summary of Getech North Atlantic source rock review (Getech Group plc, 2016).*

Stage	Location	TOC reported for source rock facies	Source
Hettangian - Sinemurian	Blue Lias facies in Dorset and Somerset	2.3-10% (average 5.7%)	Weedon 1986
		2-10% (mostly 2-6%)	Paris et al. 2010; Clemence et al 2010; Ruhl et al 2010
		2-8%	Deconinck et al. 2003
		2-10%	Nava Cedilo & Abbott 2017
		2-10% (<=15%)	Houben et al. 2017
		2-8%	Weedon et al. 2018
	Ireland	<= 4%	Scotchman 2001
	South Germany	5-12%	Hougard et al. 2021
		1-6% (average 2.2%)	Quan et al 2008
		1-6 % (<=13%)	Pross 2012
	Paris Basin	<=3%	Bessereau & Guillocheau 1994
		<=3.5%	Hanzo & Espitalie 1993
Sinemurian	Poveira Member if the Agua de Madiros Fm, Lusitanian	5-10% (maximum >20%)	Monticone et al. 2012, Hanzo & Espitalie 1993
	Pabba Shale, Slyne Trough	2-4%	Trueblood 1992
	Paris Basin	<=2%	Monticone et al. 2012
Pliensbachian	Paris Basin	<=4%	Monticone et al. 2012
	Val des Fontes Fm, Lusitanian	often 5–10% or less	Silva & Duarte 2015
	Santa Mera Mbr, Rodiles Formation, Asturias	1.5-8%	Gómez et al. 2016
	Belemnite Marl, Wessex	1-5%	Weedon & Jenkyns 1990
	Camino Fm, Basque-Cantabrian	mostly 1-4%	Quesada et al. 2005; Gómez et al. 2016
	Aït Moussa, Middle Atlas, Morocco	<=4.7%, 1-6%	Assaoud et al. 2001; Sachse et al. 2012
Toarcian	Peniche (peak values)	2.6-10%	Fantasia et al. 2019
	Asturias Basin	1-3%	Gomez and Goy, 2011
	Basque-Cantabrian (Castillo Pedroso Formation)	1-2%	Quesada et al. 2005
	Portree Shale, Hebrides	3-5%	Scotchman and Thomas 1995 ; Scotchman 2001
	Portree Shale, Slyn	3-7%	Scotchman and Thomas 1995 ; Silva et al.2017
	Austria (Bachental)	3-13%	Neumeister et al. 2015, 2016, 2020
	SW Germany	6-12%	Moldowan et al. 1986
		4-12%	Prausss et al. 1991
		5-11%	Rohl et al. 2001
		4-14%	Schmid-Rohl et al. 2002
		2-15%	Frimmel et al. 2004, Rohl & Schmid-Rohl. 20
		4-16%	Berner et al. 2013
		2-14%	Song et al. 2015
		5-15%	Ruvalcaba Baroni etal. 2018
Toarcian	NW Germany	5-12%	Littke & Rullkotter 1987
		9-13%	Littke_et al 1991
		11% Av	Littke_et al. 1991b
		4-12%	Horsfield et al. 2010
		2-18%	Ruvalcaba Baroni et al. 2018
	Swiss Jura	2-13% (av.7%)	Gorin & Feist-Burkhardt 1990
		2-12%	Montero-Saerrano et al. 2015
		3-11%	Fantasia et al. 2018
		2-12%	Fantasia et al. 2019
	Paris Basin	4-12%	Hollander et al. 1991
		2-7%	Hanzo & Espitalie 1993
		4-6%	Bessereau & Guillocheau 1994
		4-9%	Katz 1995
		3-6%	Monticone et al. 2012
		5-12%	Lezin et al. 2013
		3-11%	Hermoso et al. 2013
		4-15%	Ruebsam et al. 2016
		2-9%	Bruneau et al. 2018
	Other France: Causses Basin	3-6%	Fonseca et al. 2018
	Other France: Quercy	2-9%	Fonseca et al. 2018
	Other France: Beaujolais	4-10%	Suan et al. 2013
	UK, Yorks, etc. (immature-early mature)	4-13%	Saelen et al. 1996
		5-18%	McArthur et al. 2008
		4-18%	Kemp et al. 2011, Song et al. 2015
		3-10%	Caswell & Coe 2012 (Leicestershire)
		4-16%	Hudson 2015 (Lincolnshire)
		4-15%	Dickson et al. 2017
		2.5-18%	McArthur 2019
	Luxembourg	4-8%	Robl et al. 1992
		5-22%	Hermoso et al. 2014
		5-9%	Song et al. 2017
	West Netherlands	6-19%	van Bergen et al. 2011
		3-18%	Trabucho et al. 2012
		4-11%	van Bergen et al. 2013
		4-18%	Song et al. 2017
	Hungary	2-15%	Ruebsam et al. 2018 (Rekavolgy Fm)
		4-13%	Varga et al. 2007 (Rekavolgy Fm)
		1-3%	Polgari et al. 2016 (Urkut Manganese ore)

Table 3.2: ***Published values of European Lias source rocks.***

3.5 WEST TETHYS REGIONAL SPECIFIC INPUTS

To tailor the model from a global approach to the specific region of interest, modified bathymetries and palaeocoastlines from the detailed GDEs reconstructed in Chapter 2 have been integrated into global palaeogeographies.

These geographies determine the depth and distance aspects that OFP uses to calculated the various parameters necessary to generate a prediction of TOC. Figure 3.10 shows the regional specific 0.5 degree bathymetric grids and palaeocoastlines that have been used as model inputs.

It is not plausible to apply a single oxygen profile on a global scale, given the wide variabilities in modern and ancient oceans. However, an ocean oxygen profile can be employed at a smaller regional scale where oxygen conditions are more likely to be less variable. An oxygen minimum zone (OMZ) approach was most applicable for this region, given the prevalence of anoxia in the deeper shelf basins particularly in the Toarcian and Pliensbachian, but not in the deep Tethys. The oxygen profile applied is shown below in Figure 3.11, with oxygen versus depth values specified in Table 3.3.

Once the oxygen profile is defined, the model can then intersect it with the input bathymetries to define a sea floor oxygen value (Figure 3.12). These oxygen values are then utilised by the burial efficiency equation as shown in (Figure 3.2).

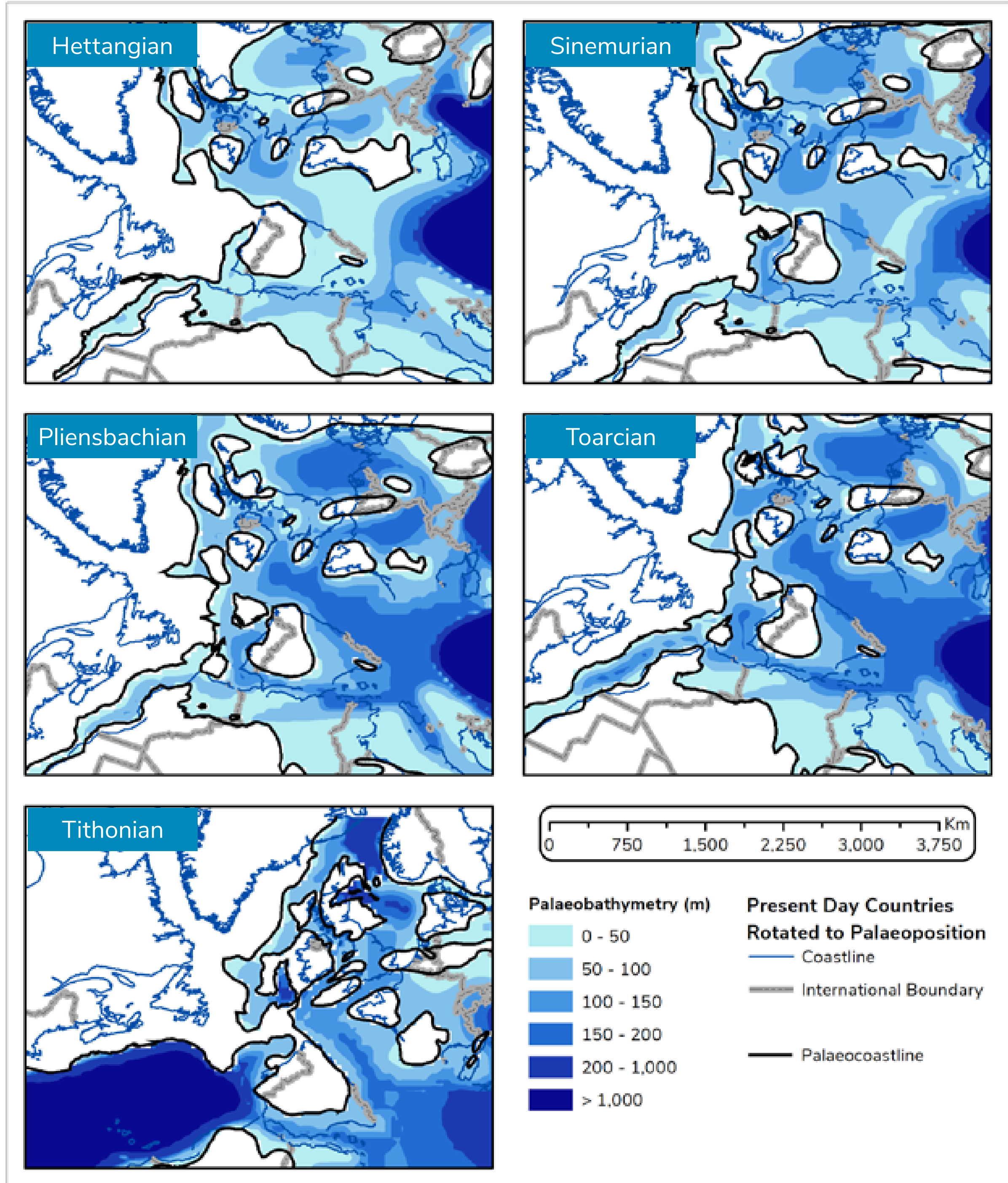

Figure 3.10: Lower Jurassic and Tithonian bathymetries and palaeocoastlines (shown in black) used for the West Tethys regional OFP modelling. The Present Day coastlines and country boundaries are shown in blue and dashed grey.

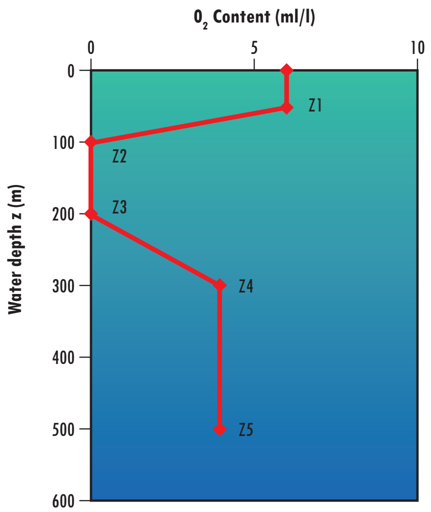

Figure 3.11: The oxygen profile applied to the OFP model for the West Tethys.

	Depth of zone (m)	Oxygen value (ml/l)
Z1	50	6
Z2	100	0.01
Z3	200	0.01
Z4	300	4
Z5	Sea bed	4

Table 3.3: The oxygen values used to create the oxygen profile set in the OFP model for the West Tethys.

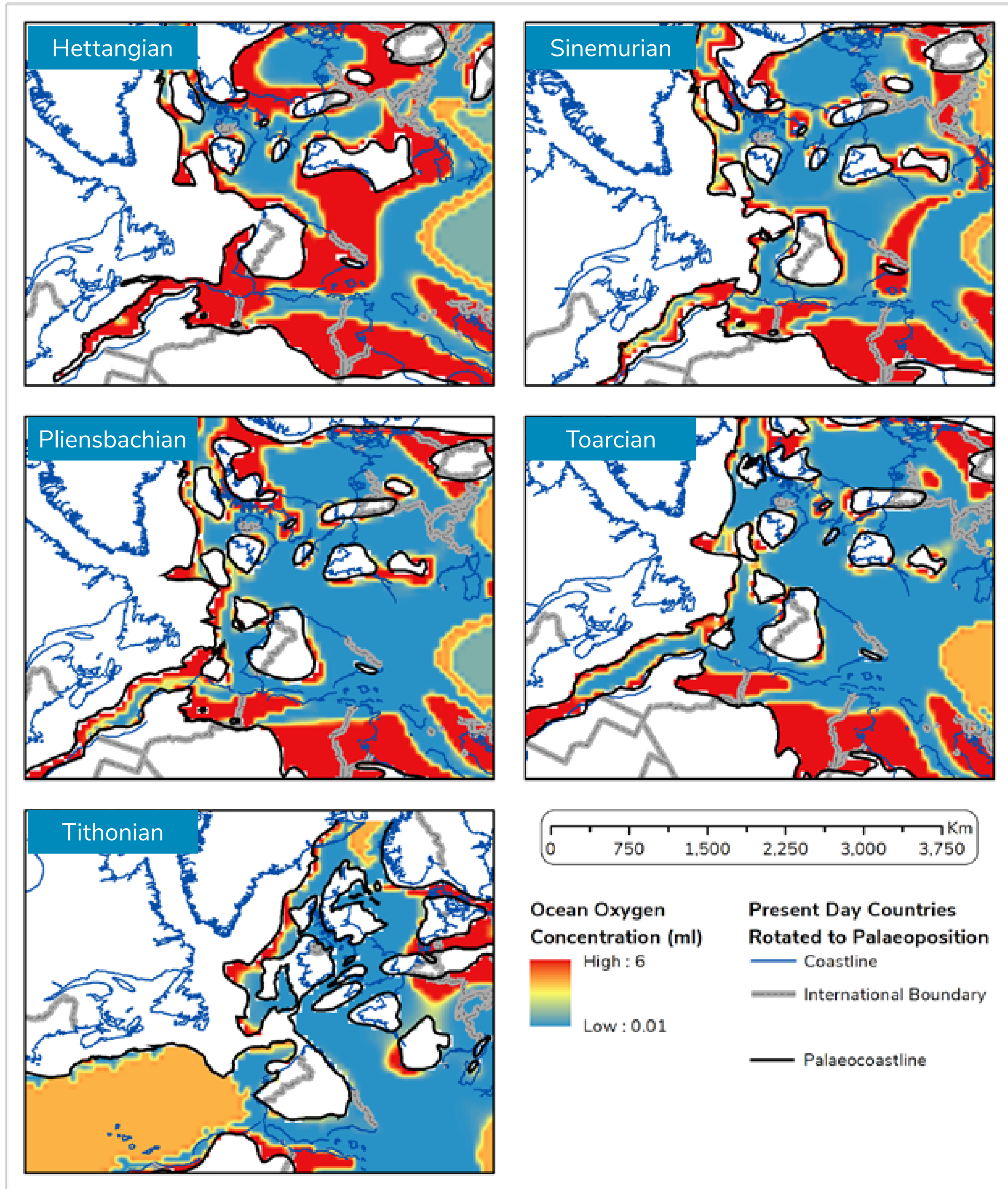

Figure 3.12: Lower Jurassic and Tithonian oxygen values for the West Tethys determined by the oxygen vs depth profile in Figure 3.11.

3.6 WEST TETHYS RESULTS

3.6.1 TOC

This section presents the results from the large-scale model runs of the West Tethys region, where there is more abundant data to compare to model results. Figure 3.13 shows the 'standard sedimentation rate' scenario, where the sedimentation rate is calculated in the model using the productivity, depth and distance from the coastline. Figure 3.14 shows the 'condensed section' scenario, where the sedimentation rate is fixed at 1 cm kyr^{-1}. This broadly corresponds to the average sedimentation. rate observed in most condensed sections.

The purple lines show the outlines of know mapped source rock as shown in Figure 3.8. The associated HI results are shown in Figures 3.15-3.18.

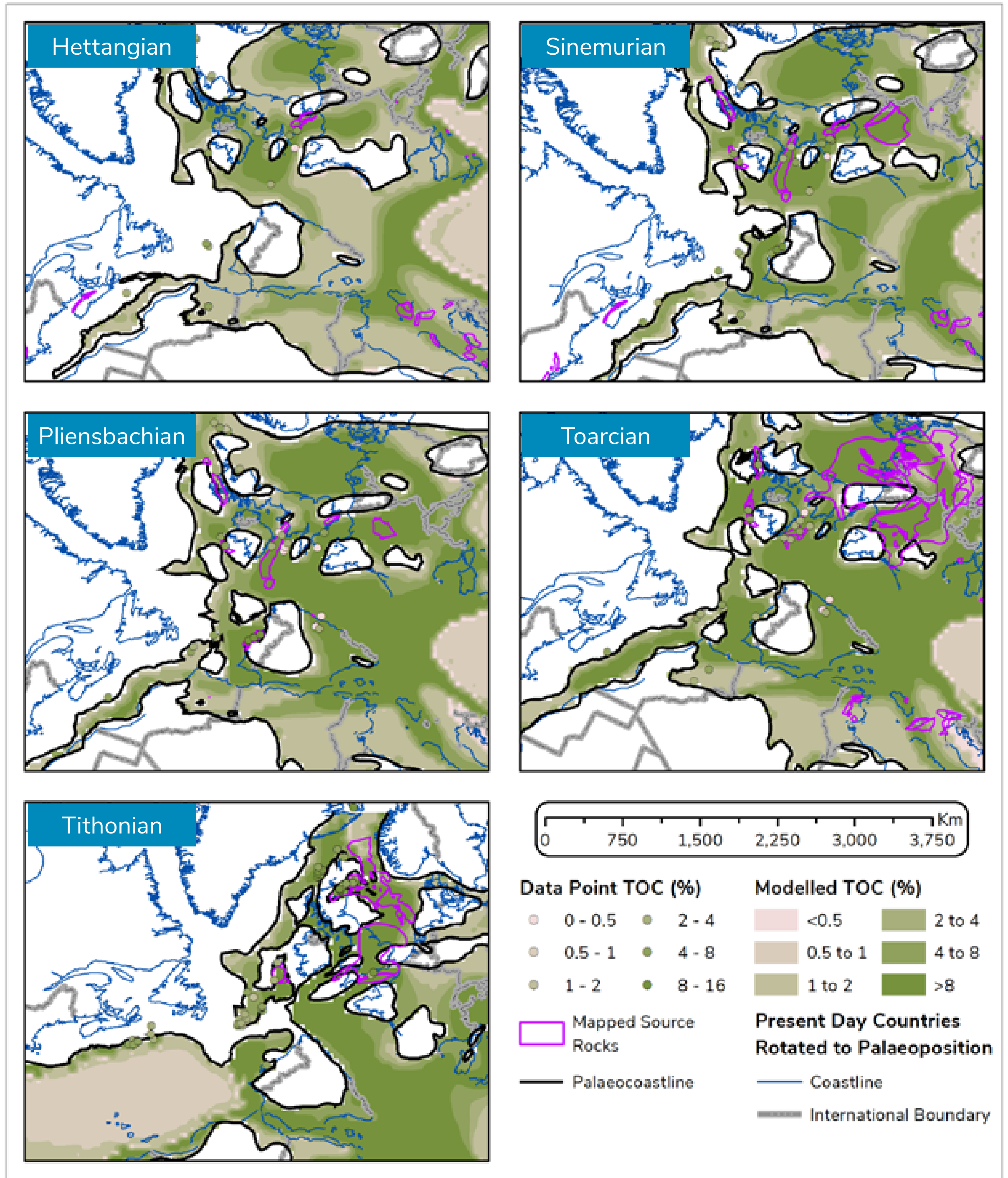

Figure 3.13: Modelled TOC for standard sedimentation rate scenario.

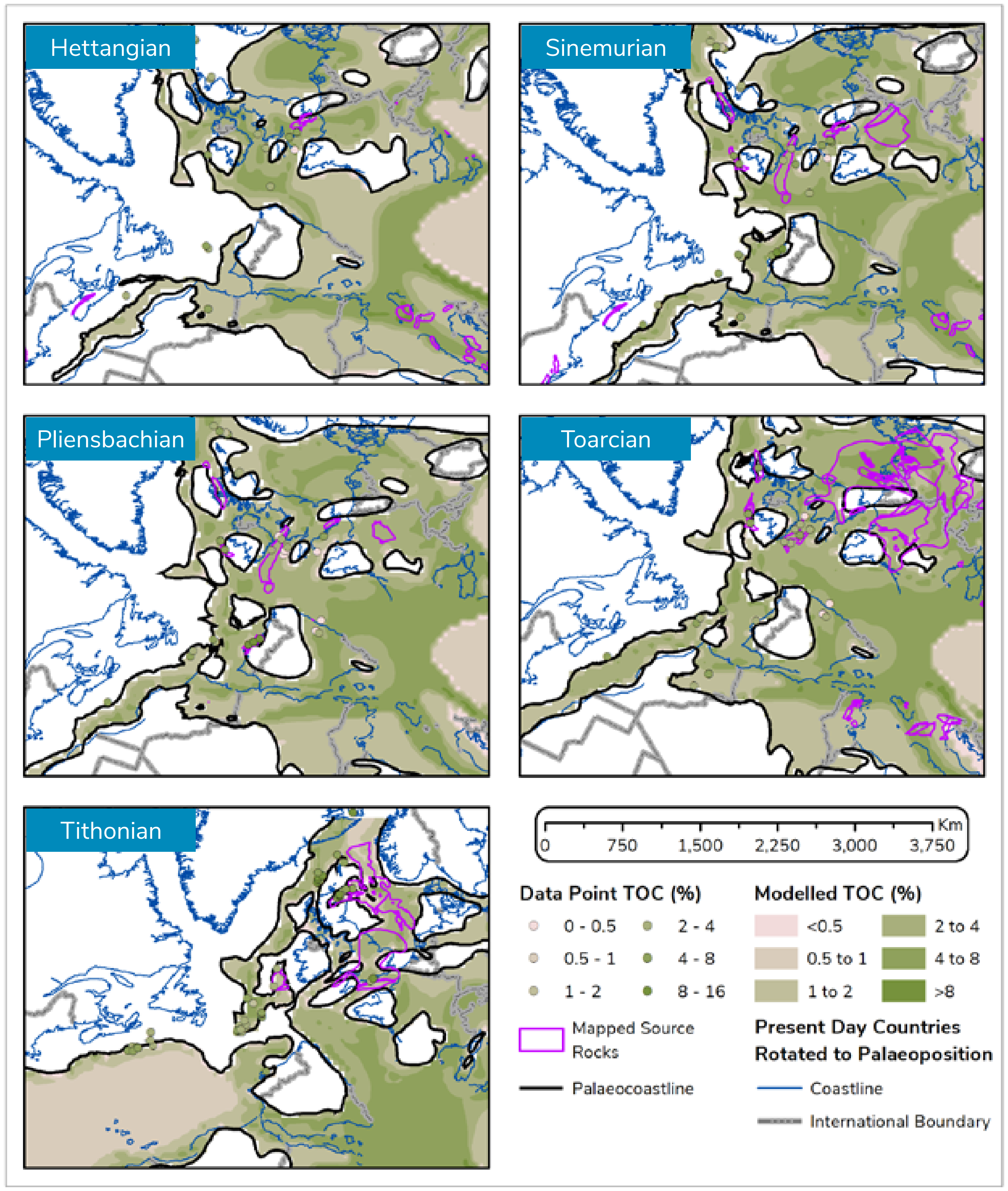

Figure 3.14: Modelled TOC for condensed section scenario.

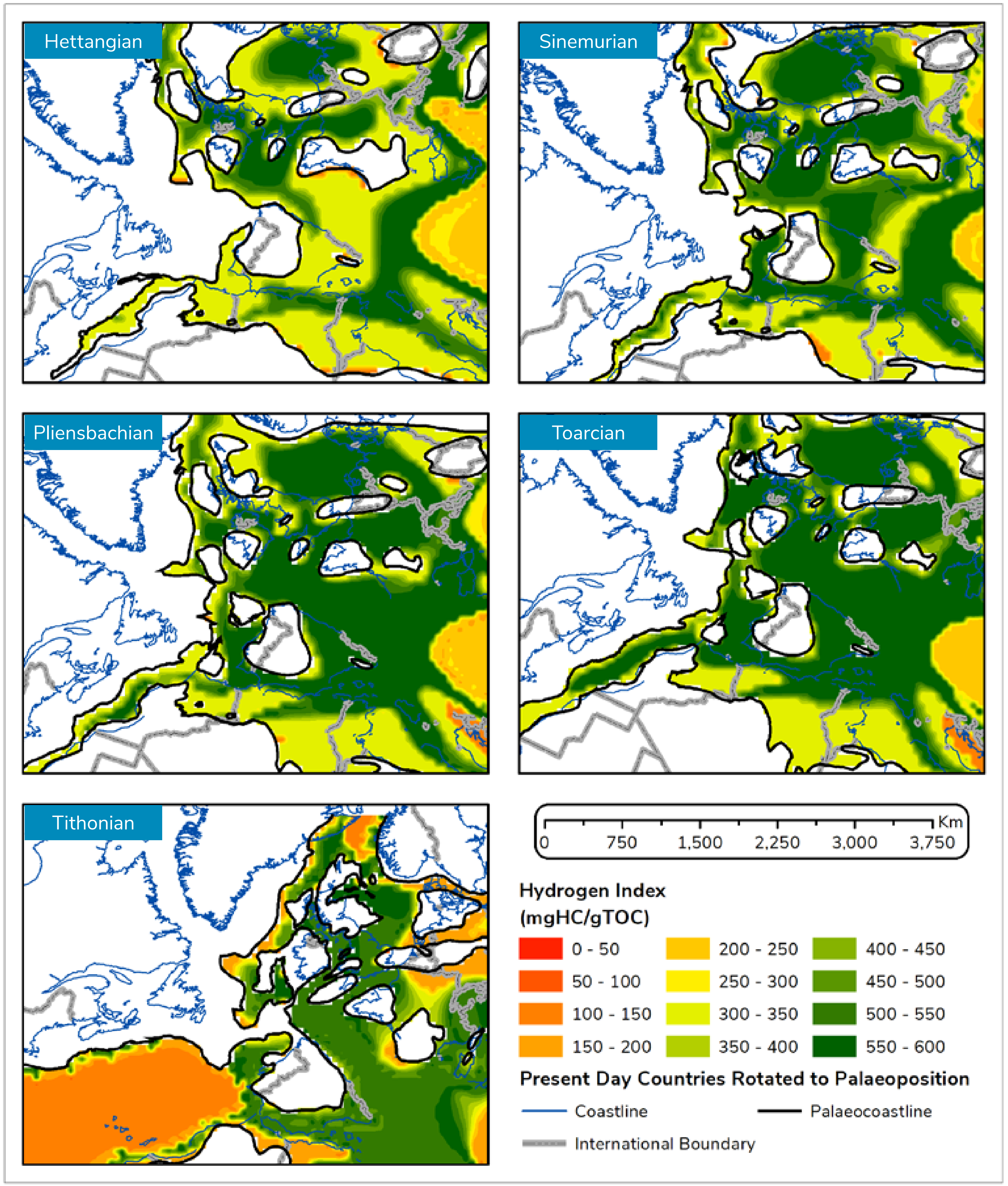

Figure 3.15: *Modelled Hydrogen Index for standard sedimentation rate scenario and analogue TOC approach.*

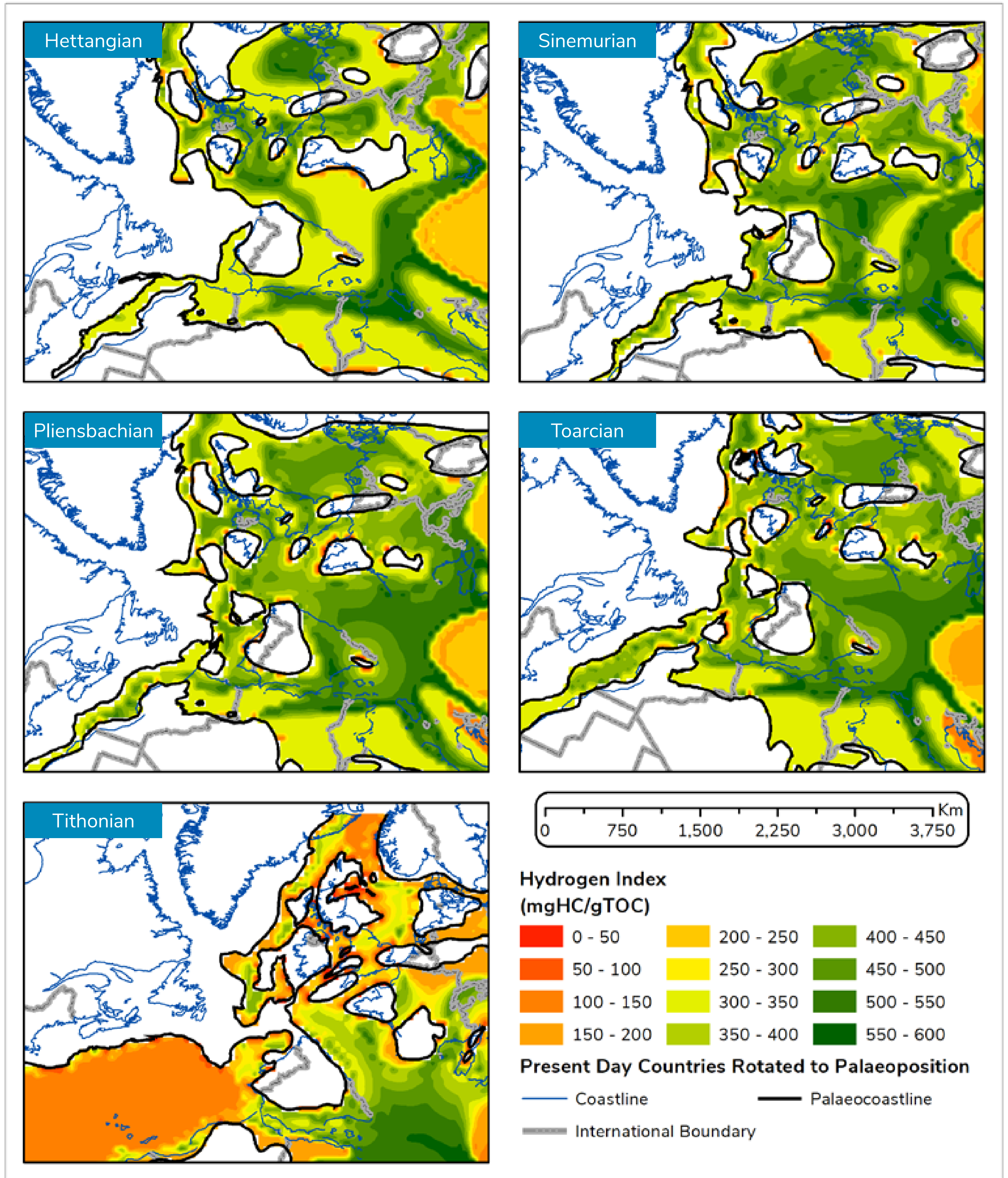

Figure 3.16: *Modelled Hydrogen Index for condensed section scenario and analogue TOC approach.*

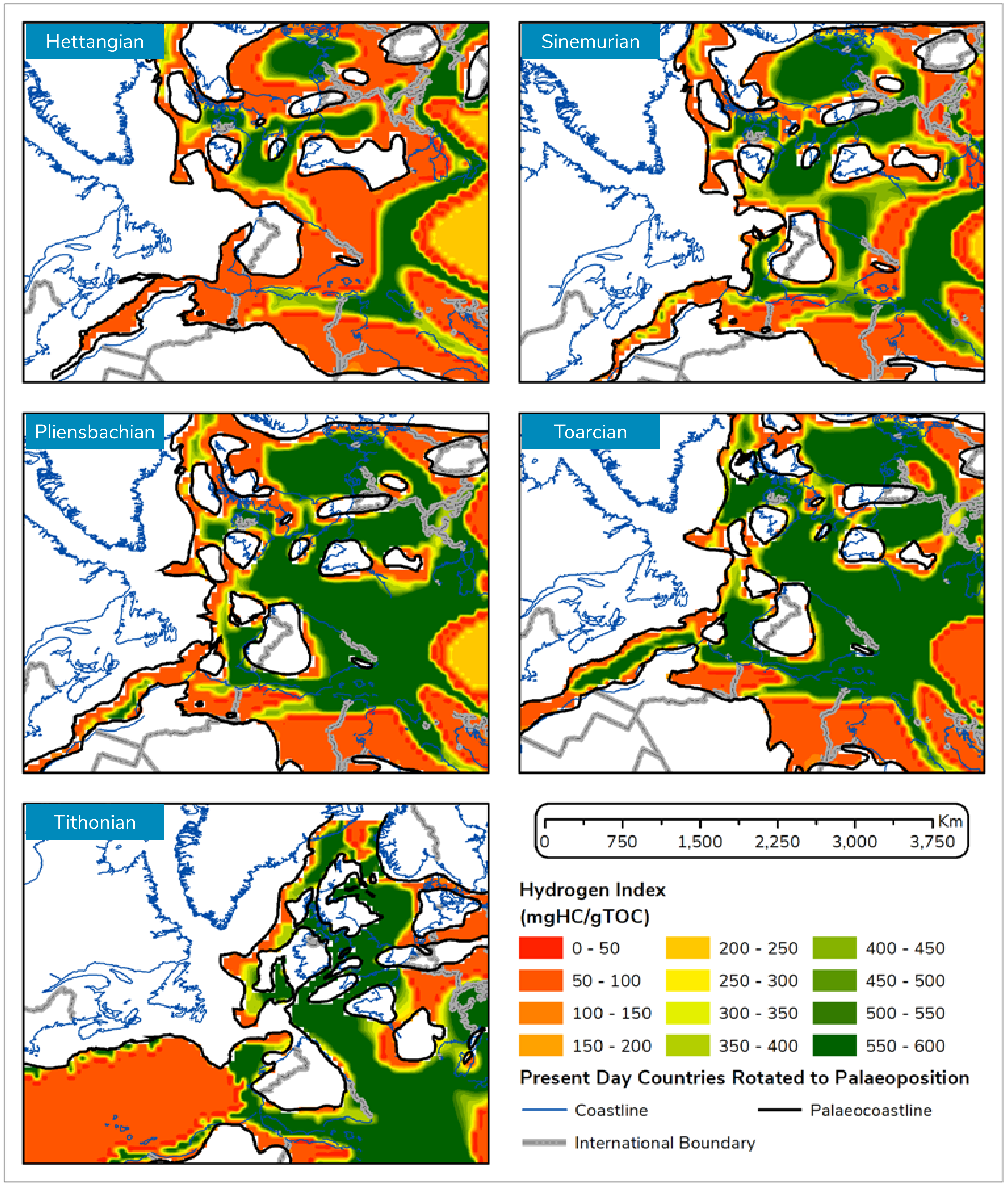

Figure 3.17: *Modelled Hydrogen Index for standard sedimentation rate scenario and mixing model approach.*

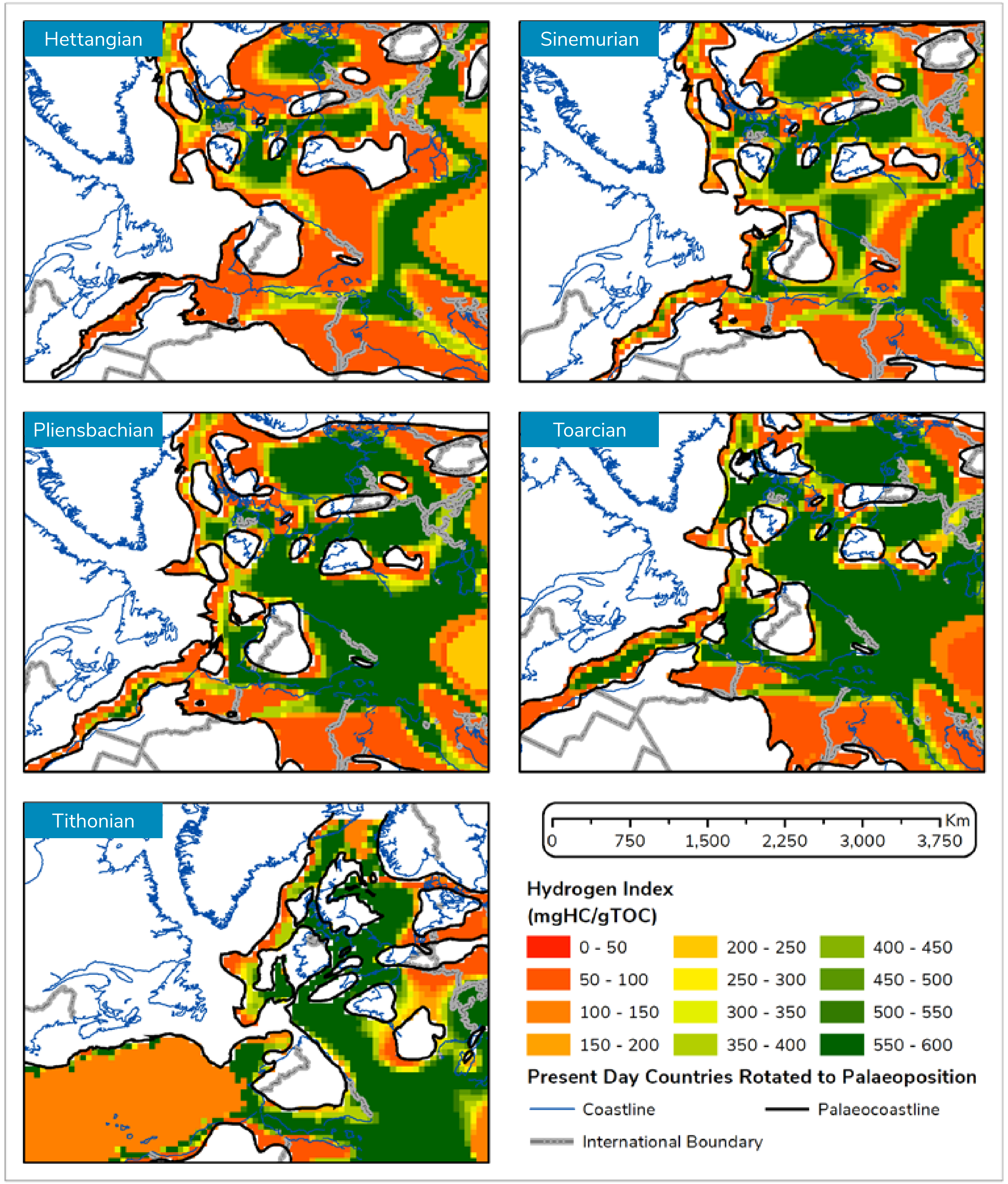

Figure 3.18: *Modelled Hydrogen Index for condensed section scenario and mixing model approach.*

3.7 LIAS TOC RESULTS AND DATA FROM SOURCE ROCK FACIES

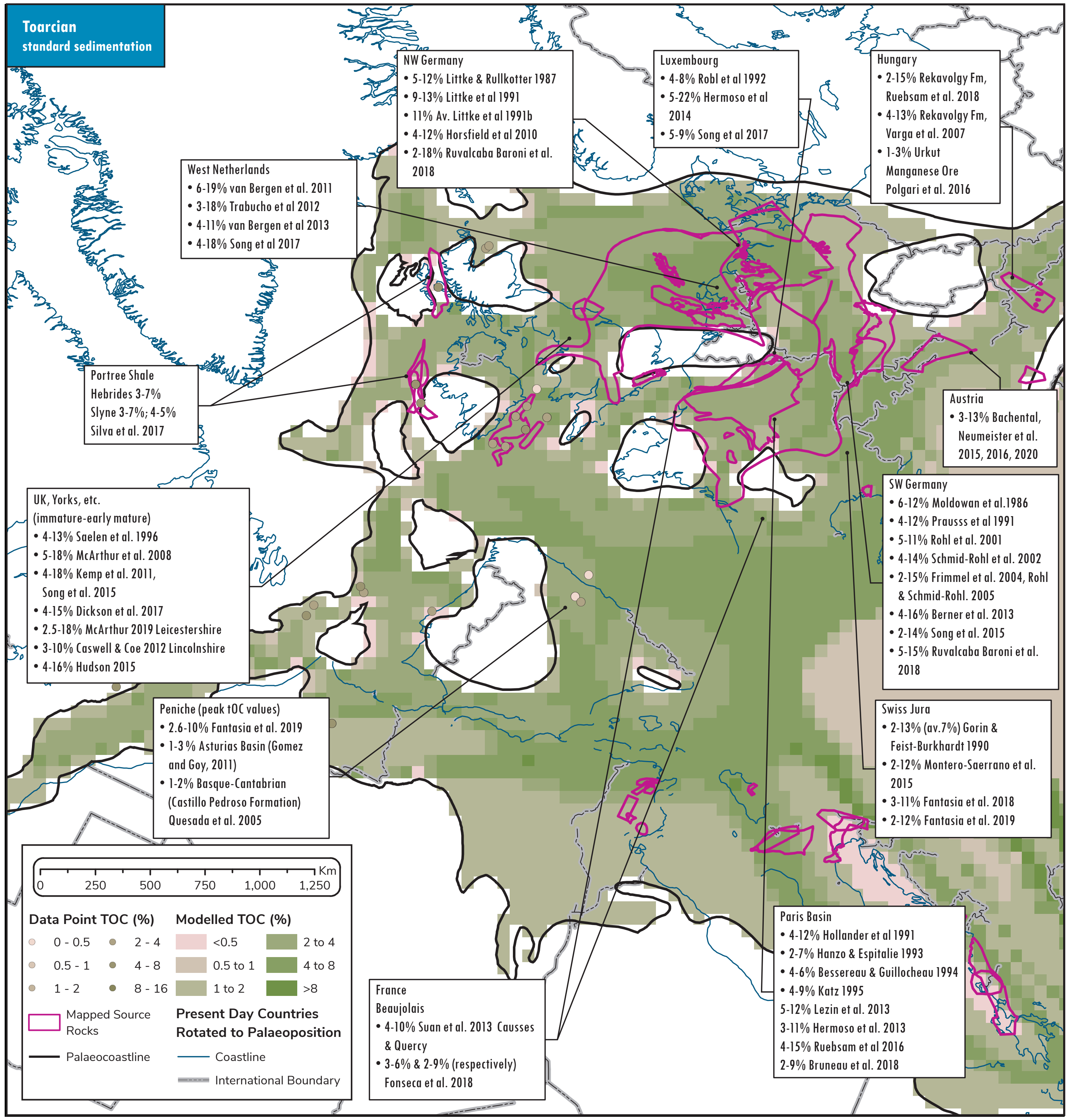

Figure 3.19: Modelled Toarcian TOC compared to reported TOC values in published literature.

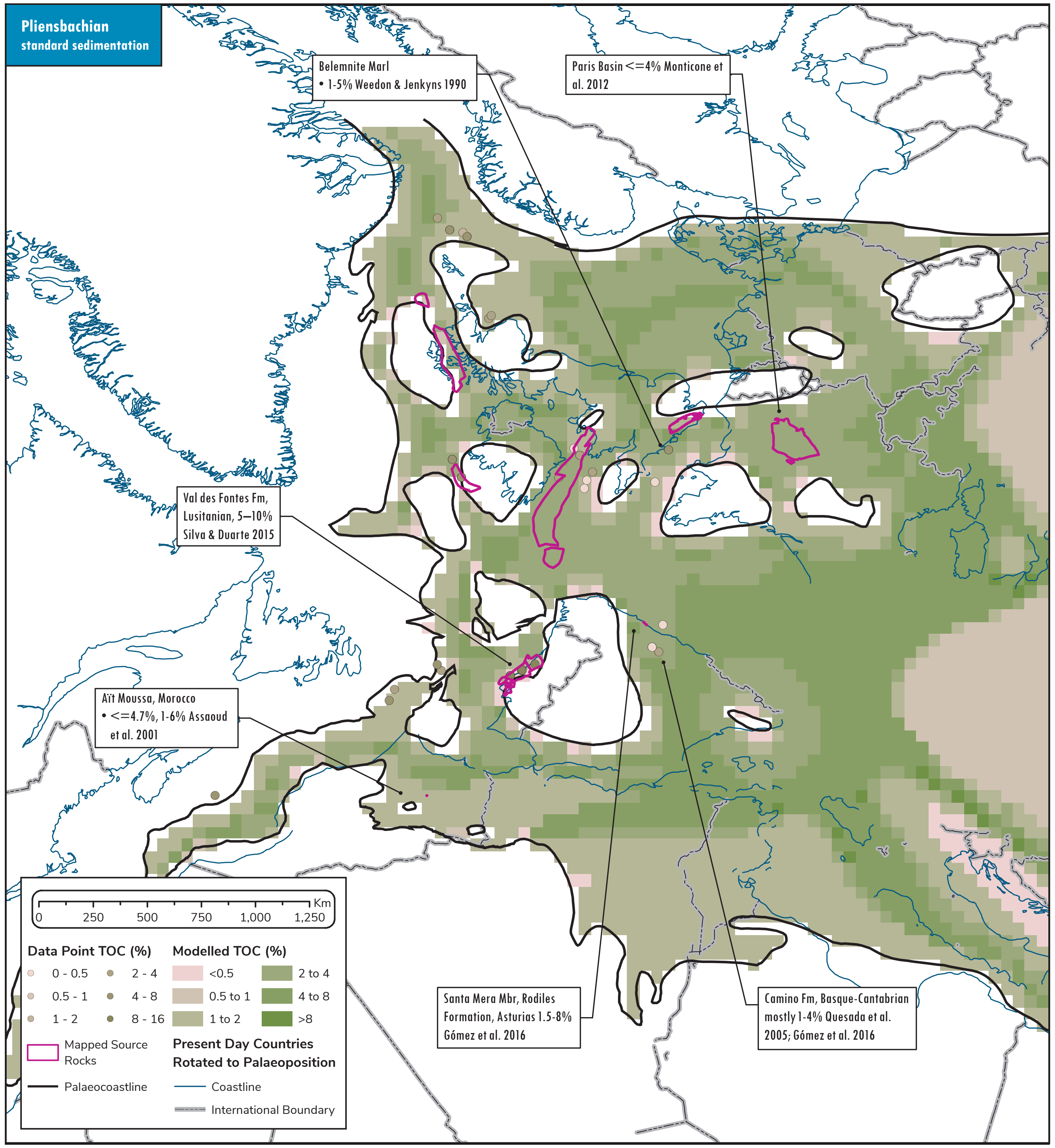

Figure 3.20: Modelled Pliensbachian TOC compared to reported TOC values in published literature.

Characteristic TOC ranges of European Lias black shale facies reported in the literature are summarised for specific basins or regions. Much of the range in observed values falls between the predicted TOC for the standard sedimentation rate (Figures 3.19 - 3.22) and the condensed section values.

There are several reports of photic zone euxinia (PZE) in European Lower Jurassic, especially in the Toarcian where PZE is documented in France (van Breugel et al. 2006), Austria (Reinhardt et al. 2018), Germany (Schwark & Frimmel 2004), Luxembourg (Song 2015) and the UK (Sælen et al. 2000; French 2014).

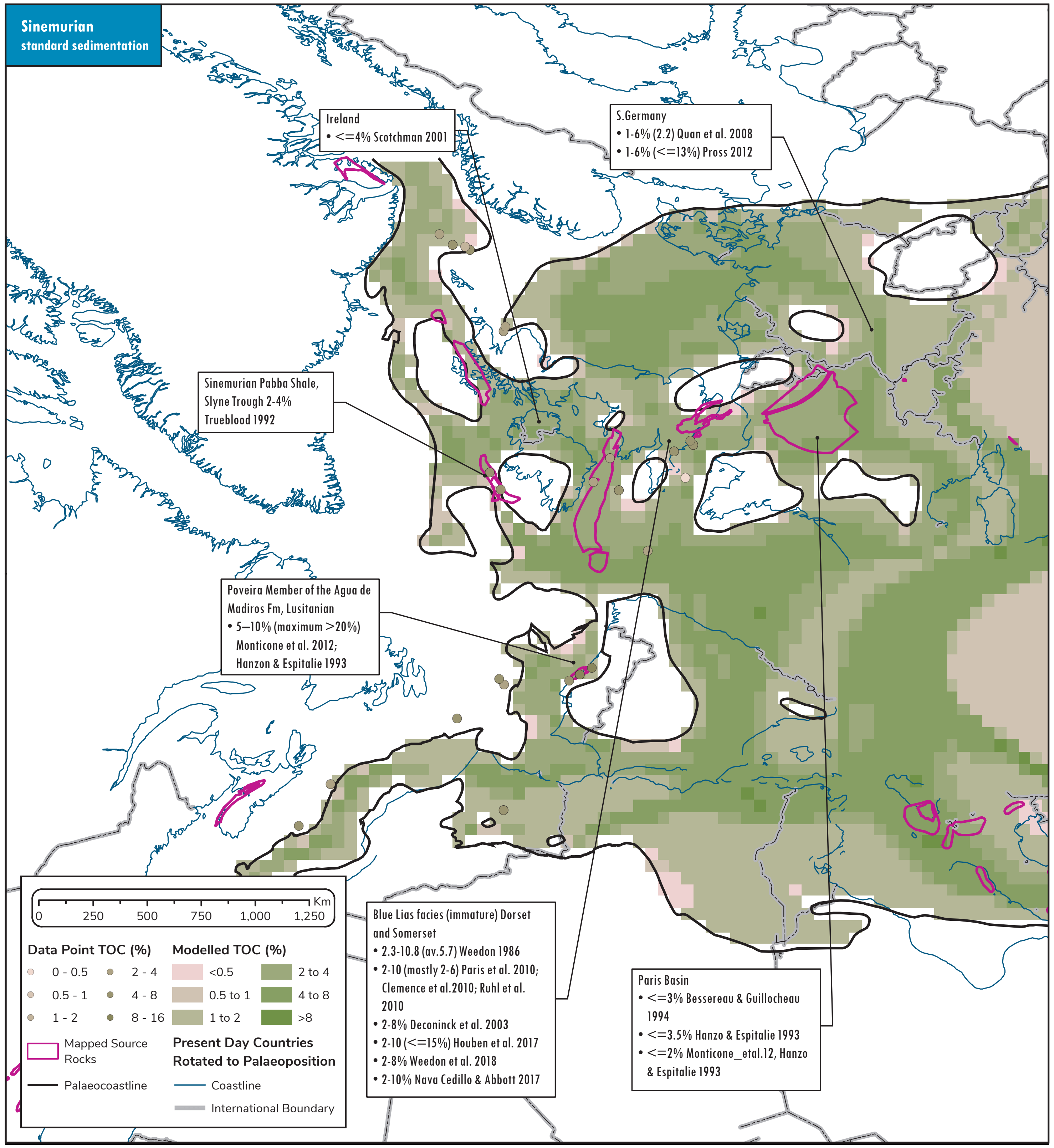

Figure 3.21: ***Modelled Sinemurian TOC compared to reported TOC values in published literature.***

Evidence for earlier episodes of PZE in Europe come from Rhaetian-Hettangian sections in Germany, Luxembourg and the UK (Jaraula et al. 2013; Richoz et al 2012; van de Schootbrugge et al 2013; Blumenberg et al 2016; Schwab & Spangenberg 2007). Further evidence for PZE is also found in the Sinemurian Blue Lias of Lyme Regis (Nava Cedillo & Abbott 2017).

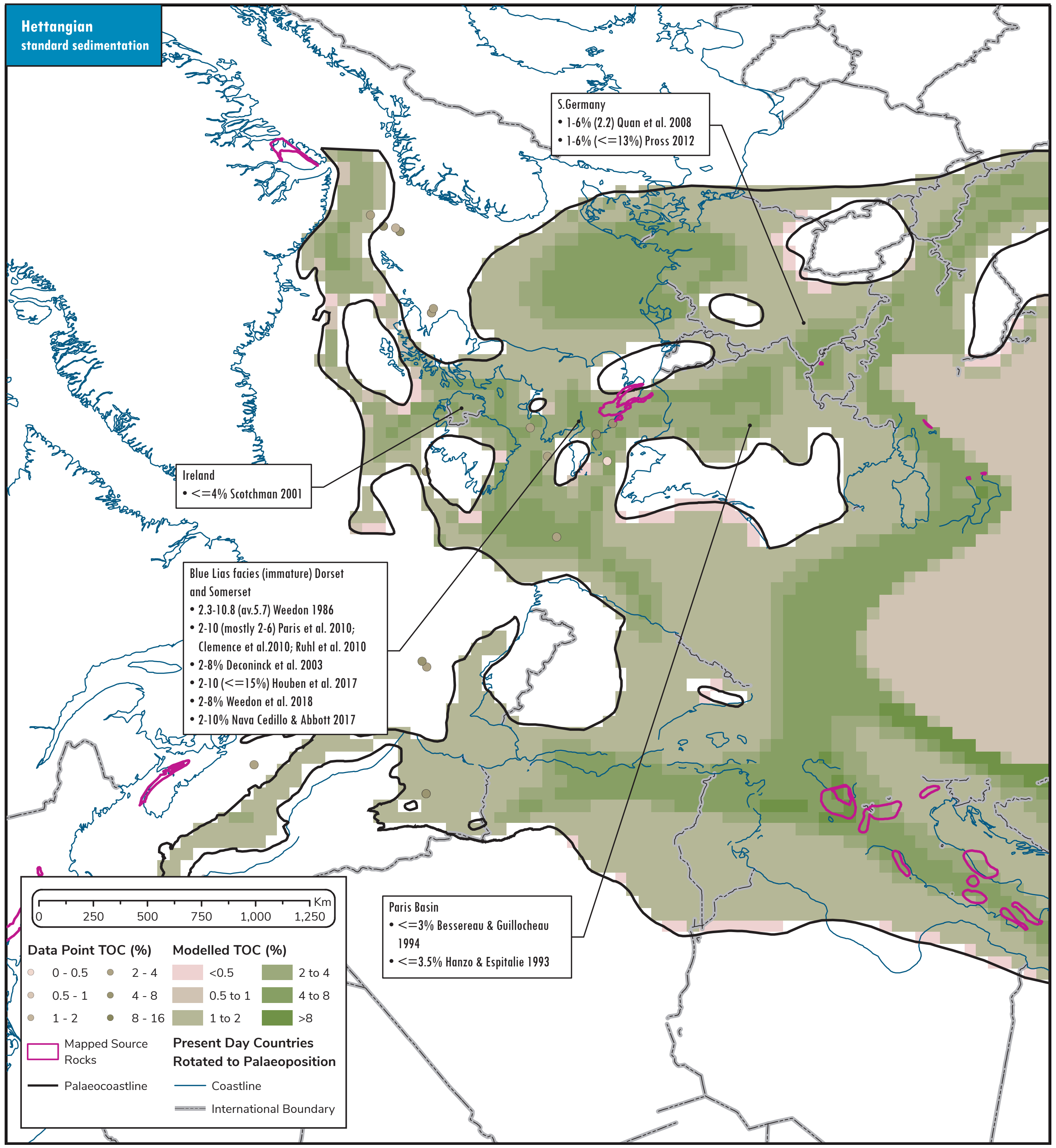

Figure 3.22: ***Modelled Hettangian TOC compared to reported TOC values in published literature.***

The widespread occurrence of PZE on the European shelf during the Lias suggests optimal preservational conditions were probably common. Although as yet unproven, these conditions may have extended to the geographically restricted Hispanic Corridor, as utilised in the OFP modelling.

3.8 HIGH RESOLUTION HISPANIC CORRIDOR MODEL SETTINGS AND INPUTS

The TOC results from the Tethyan regional model show reasonable agreement with reported values for known source rock facies. This agreement allows for confidence that model is predicting plausible results at the regional scale. However, the offshore Nova Scotian area of specific interest is not necessarily best represented by the model settings applied to the greater region.

The regional and more detailed GDE maps (Chapter 2) show that the offshore Nova Scotian area sits within a relatively small, narrow and restricted seaway. The depth and nature of any sill is unknown, but the seaway may have experienced different oxygen conditions to the European shelf and Tethys.

A marine connection eastward is inferred for the Hispanic Corridor on biogeographic grounds, but the potential prevailing oxygen conditions of the deeper Hispanic Corridor during the Lias are unknown. It is therefore appropriate to consider any possible Present Day analogues.

The only modern analogues for long and thin marine basins in an early ocean opening stage are the Red Sea and Gulf of Mexico. The length and width of these basins are also comparable to those of the Hispanic Corridor, and their dry to arid climatic settings are also similar. However, their depths are considerably greater.

Most of the Red Sea has an oxygen minimum zone; it is comparatively thin (100-150 m) by OMZ standards, and shifts seasonally. The lowest oxygen values are generally around 0.5 ml/L (dysoxic). There are no known descriptions of the nature of the sediments intersecting the OMZ depths. The only known organic-rich sediments (up to 6% TOC and Type II kerogen) are those in the anoxic hypersaline brine deeps (which originate from dissolution of Miocene evaporites). This may reflect the oligotrophic and primarily oxic nature of the basin. Outside of the deeps, the bottom waters are oxic and the sediments organic-poor. The brine deeps mostly occur in the basin axis in waters deeper than 2000 m and are individually small; there are over 20, with reported sizes of 12 to 78 km^2 and brine pools of 11-366 m vertical extent. Their depth occurrence is far greater than the Lias Hispanic Corridor palaeobathymetry. The organic-rich sediments appear cyclical, related to Quaternary palaeoclimate and productivity shifts.

The Gulf of California (e.g. the Guaymas Basin) is much deep than the Hispanic Corridor. Its OMZ is imported from the adjacent Pacific, where it forms in response to the Eastern Boundary Upwelling System of the California Current. Organic-rich, source rock type sediments occur where the OMZ intersects the sea floor. The top of the OMZ (and only that part of it) is compatible with the Hispanic Corridor depths. This scenario is not unlike that used for the original OMZ-based Getech predictions.

The only other long and thin basins are fjordic in nature, and are generally much smaller and with a glacially determined morphology and bathymetry. Saanich Inlet on Vancouver Island is an example of a salinity-stratified seasonally anoxic silled basin with a positive water balance and estuarine circulation. Its depth is compatible with the Getech Hispanic Corridor palaeobathymetry. It could perhaps be scaled up to Hispanic Corridor size to simulate an anoxic basin (rather than OMZ) scenario. In this case the sill depth would be arbitrary. The chemocline would be much more abrupt than the transition seen in the case of an OMZ, and the bottom water might only be seasonally anoxic, as in Saanich Inlet (although organic-rich sediments still result). There is a question about the palaeoclimatic regime, and whether a positive water balance could be maintained, although the occurrence of Hettangian lacustrine black shales in East Berlin Formation of the Newark Basin, may indicate more humid conditions in part on the USA side.

Overall, two scenarios for the Hispanic Corridor seem most suitable. The first is the partial entry of OMZ waters westwards from the adjacent Tethys Ocean (where an OMZ certainly occurred in the Toarcian). Whether the corridor was deep enough for this is uncertain; it may not have been deep enough for sub-OMZ bottom water penetration. Using the actualistic depths for the top of the OMZ in the Gulf of California or Red Sea, only the Toarcian would have been deep enough in the Getech palaeobathymetry to achieve suboxic and anoxic conditions associated with elevated TOC and hydrogen indices. The extent of upwelling in the adjacent Tethys may have influenced the intensity of the OMZ. The second scenario is that the corridor is a stratified silled basin that developed anoxic bottom waters, perhaps most likely due to the ponding of saltier waters produced by evaporation rather than a freshened water lid due to runoff. Both scenarios could perhaps have occurred for the western and eastern parts of the corridor, respectively. It is possible that the deeper parts of basin could have been separated into smaller and more restricted pull-apart basins (as in both the Gulf of California and the Red Sea deeps). Sill depths would be highly speculative.

An alternative option was suggested by Bishop (pers. comm 2021). Based on reports of biomarker evidence of photic zone euxinia (PZE) in the European Lias (especially the Toarcian), it was suggested using the modern Black Sea as an analogue. The average depth at which PZE occurs in the central Black Sea is around 80 m, although for more marginal settings the average PZE depth is about 114 m. However, because the OFP model uses O_2 and not PZE, an actualistic Black Sea analogue requires that the top of the anoxic zone should be based on the overlying so-called "suboxic layer" rather than the chemocline/PZE depth. It contains no sulfide and no or extremely low or undetectable O_2. In OFP, this will also impact the organic facies to the same extent as the sulfidic anoxic zone. The chemocline fluctuates by tens of metres on seasonal and shorter timescales, so the depth boundary between the two is always blurred. This final Black Sea PZE and suboxic layer scenario represents the most extreme anoxic scenario to be modelled.

All four potential analogues described were modelled to test the different hypothetical oxygen scenarios for the Lias Hispanic Corridor:

1. The Red Sea - OMZ
2. Gulf of California - OMZ
3. Saanich – anoxic bottom water
4. Black Sea – euxinic bottom water

These oxygen profiles are shown in Figure 3.23 with their defined oxygen values vs depth highlighted in the table below each profile.. For the depth regime of the Hispanic Corridor the initial Tethys OMZ model is not unlike the Black Sea model in principle, but with a deeper chemocline.

The OFP model for each scenario was run using both a standard sedimentation rate and a condensed section sedimentation rate as previously done in the Tethyan model runs. All other settings remain the same as for the Tethyan model runs, only the O_2 scenario varies in each run.

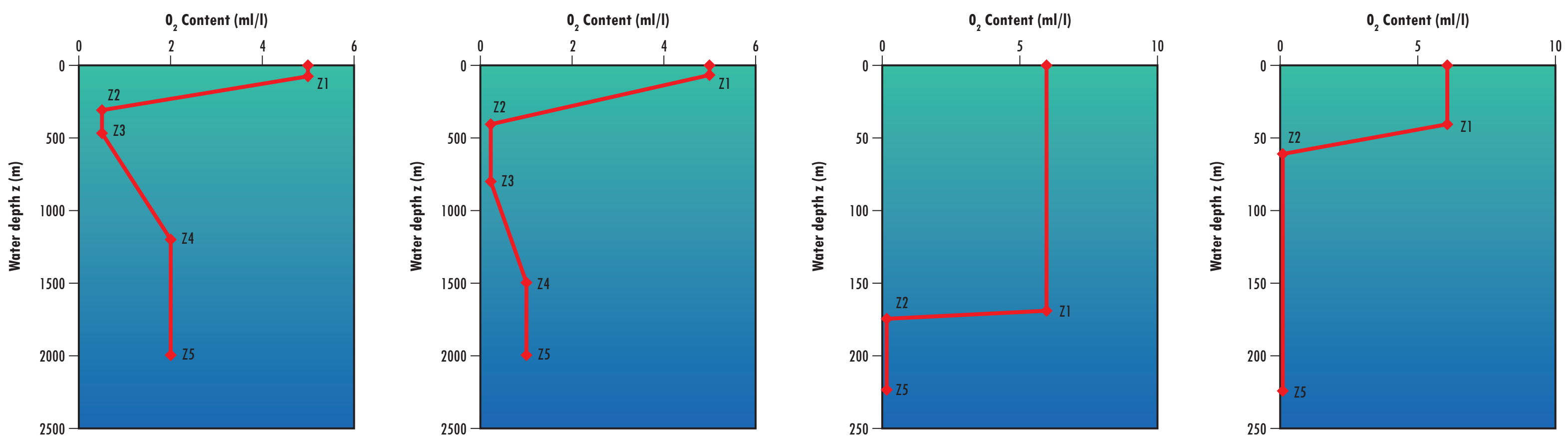

Red Sea (OMZ)	Depth	02
Z1	65	5
Z2	300	0.5
Z3	450	0.5
Z4	1200	2

GoC (OMZ)	Depth	02
Z1	50	5
Z2	400	0.2
Z3	800	0.2
Z4	1500	1

Saanich (BW)	Depth	02
Z1	170	6
Z2	175	0.01
Z1 & Z2 – Depth to chemoline		

PZE + suboxic layer	Depth	02
Z1	65	7
Z2	300	0.02

Figure 3.23: Analogue ocean oxygen profiles for the Lias Hispanic Corridor with defined oxygen vs depth values shown in the tables below each profile. 1) Red Sea. 2) Gulf of California, 3) Saanich and 4) Black Sea PZE and suboxic layer.

3.8.1 BATHYMETRIC INPUTS

Figure 3.24 shows the high resolution bathymetric grids that have been generated based on the gross depositional environments mapped in Chapter 2. These grids have been generated at a 0.1x0.1 degree grid scale to capture more detailed features of the basin bathymetry during each stage.

3.8.2 OCEAN OXYGEN MAPS

The Present Day analogue ocean oxygen profiles described in Section 3.8 and shown in Figure 3.23 have been intersected with the bathymetries in Figure 3.24 to determine the oxygen values at the sediment water interface.

This had been carried out for each of the four oxygen scenarios for each of the 5 stages of the study. The resulting 20 ocean oxygen maps can be seen in Figure 3.25 (on the next page).

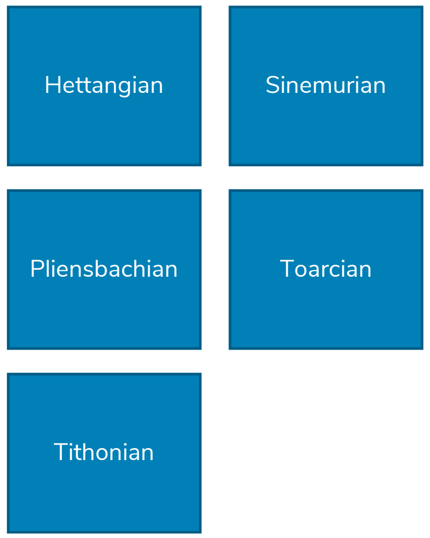

Figure 3.25 (next page): Oxygen conditions at the sea bed based on the high resolution bathymetries shown in Figure 3.24 and the Present Day ocean oxygen analogues described in Section 3.8. The map legend is show to the right and the image layout for each of the resulting stages and oxygen scenarios is shown in the grid below:

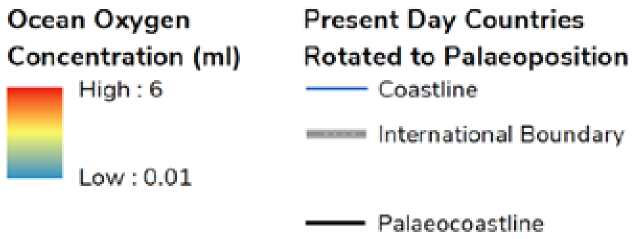

Hettangian Red Sea	Sinemurian Red Sea	Pliensbachian Red Sea	Toarcian Red Sea	Tithonian Red Sea
Hettangian Gulf of California	Sinemurian Gulf of California	Pliensbachian Gulf of California	Toarcian Gulf of California	Tithonian Gulf of California
Hettangian Saanich	Sinemurian Saanich	Pliensbachian Saanich	Toarcian Saanich	Tithonian Saanich
Hettangian Black Sea	Sinemurian Black Sea	Pliensbachian Black Sea	Toarcian Black Sea	Tithonian Black Sea

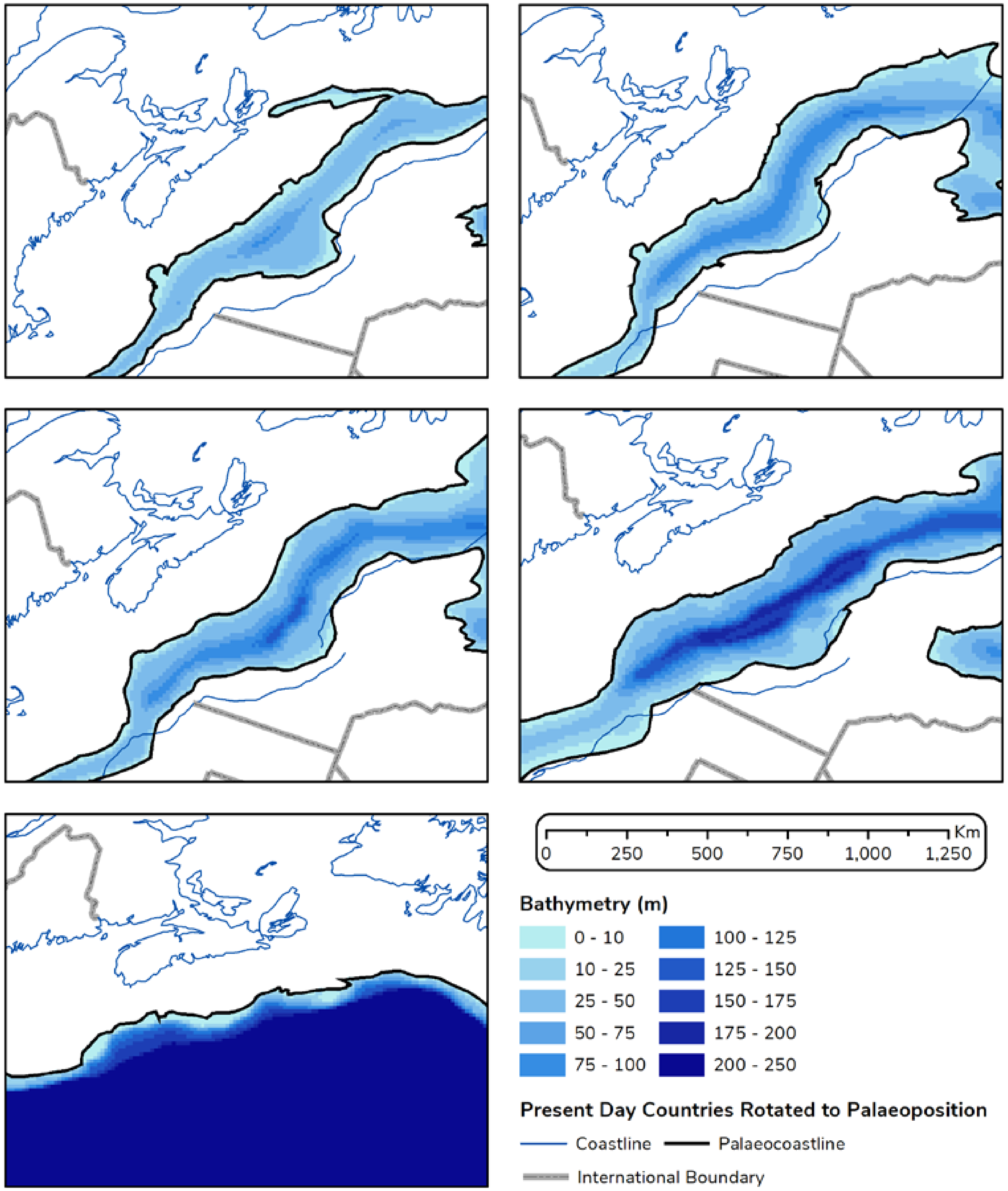

Figure 3.24: High resolution bathymetric grids used in OFP modelling the layout is as shown in top-left grid:

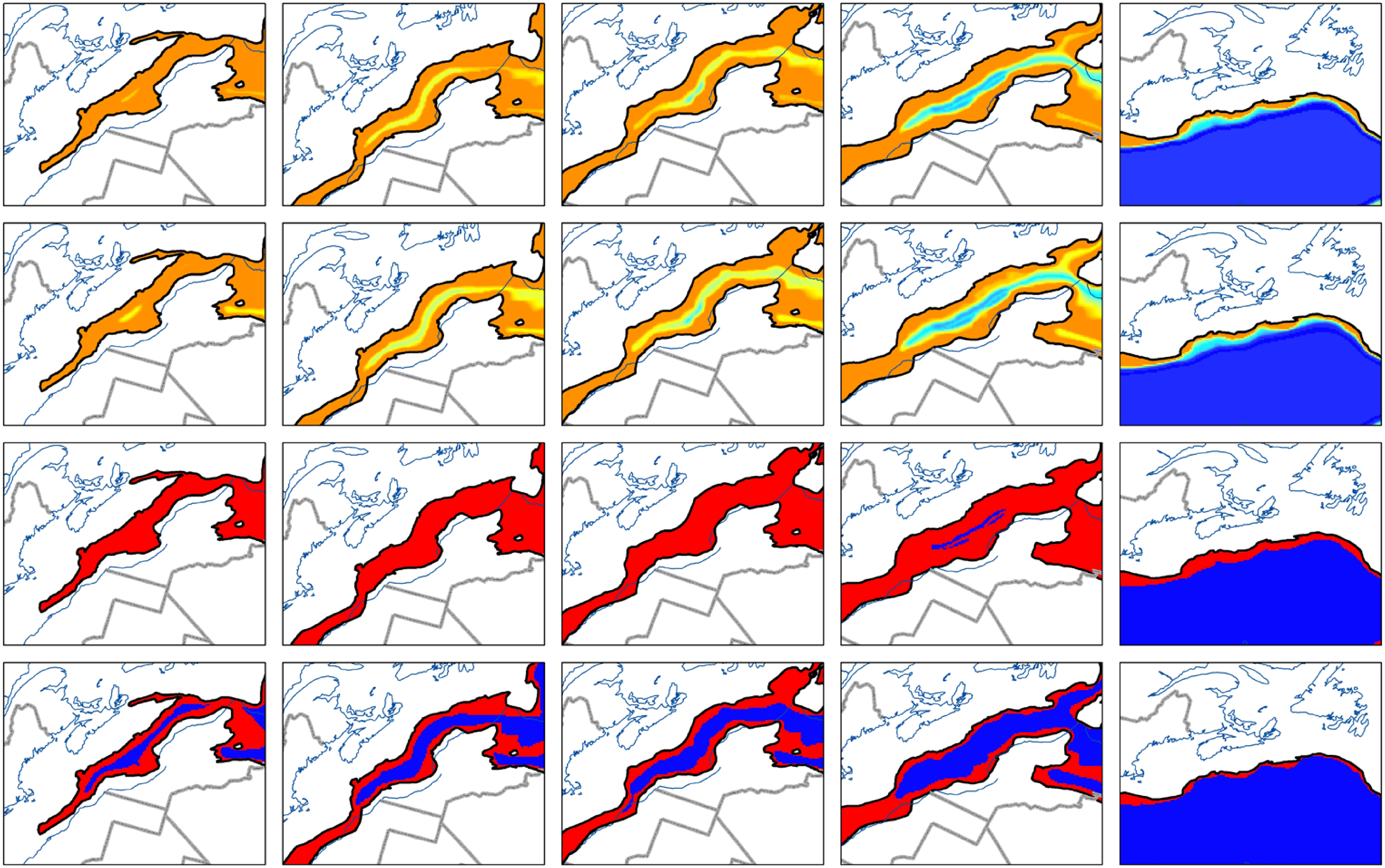

3.9 HIGH RESOLUTION HISPANIC CORRIDOR RESULTS

3.9.1 HETTANGIAN

Figure 3.26 shows the Hettangian TOC results of the OFP model runs for each of the four oxygen scenarios discussed from top to bottom, with the images to the left showing results for the condensed section sedimentation rate runs and the images to the right the results for the standard (zpd) sedimentation runs. The associated HIA and ∑HI results are presented in Figures 3.27 and 3.28 respectively.

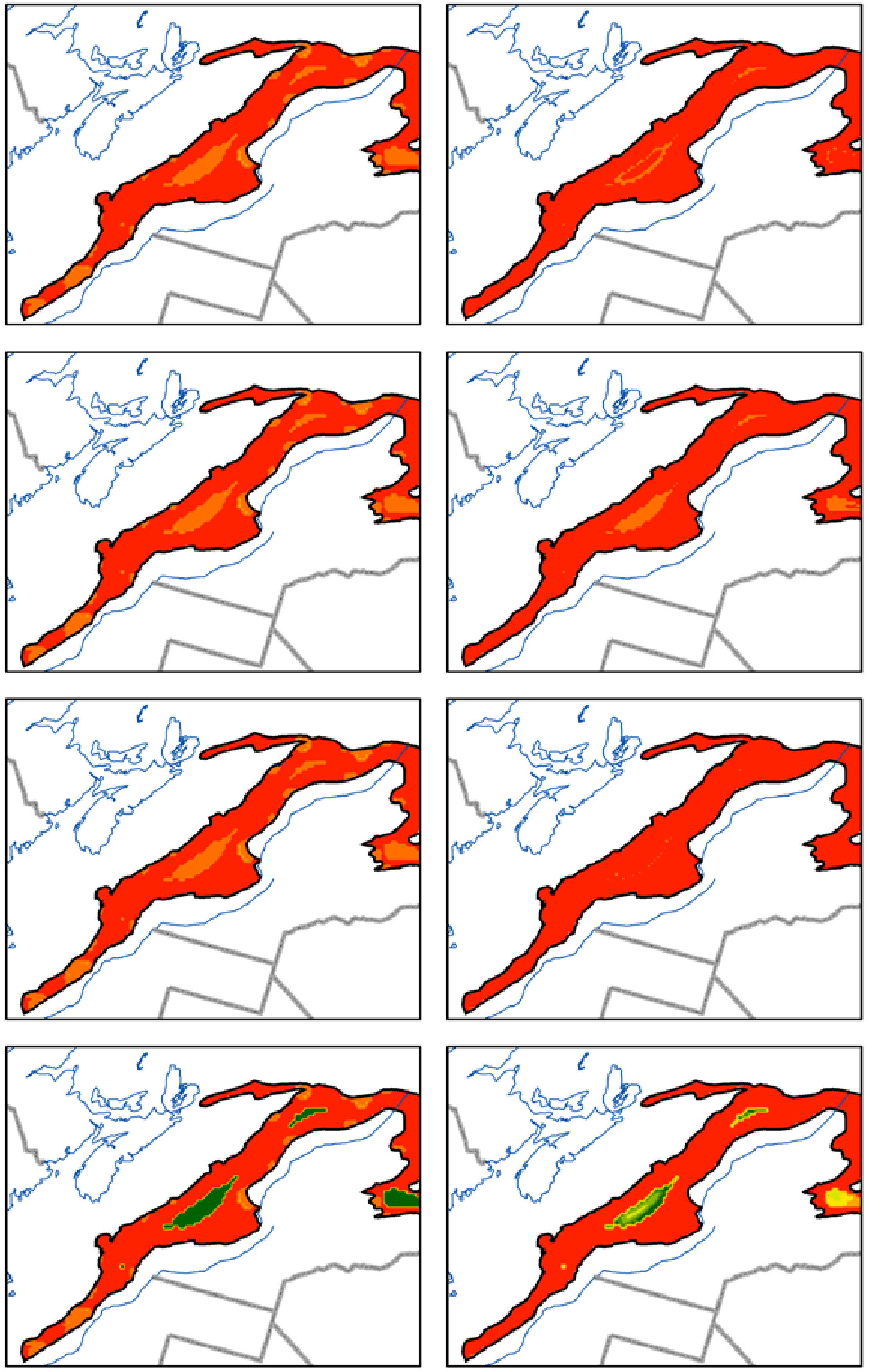

Figure 3.26: Predicted TOC for the Hettangian.

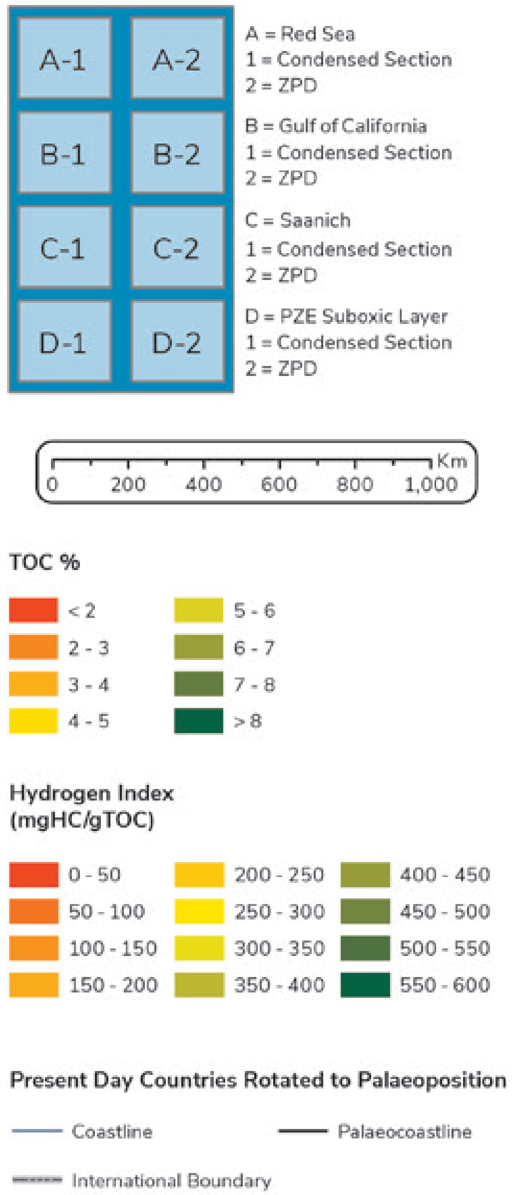

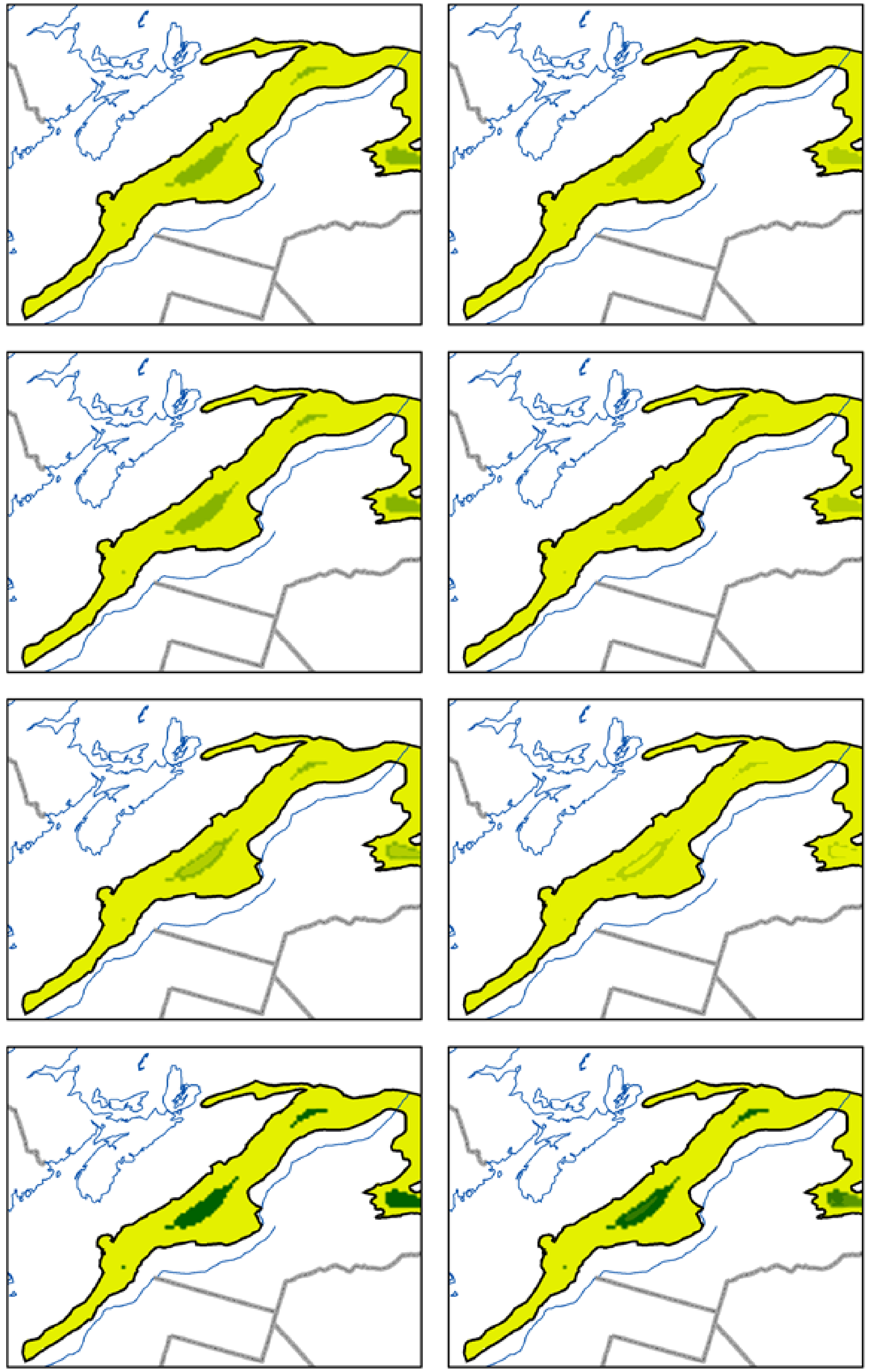

Figure 3.27: Predicted HI using analogue approach for the Hettangian.

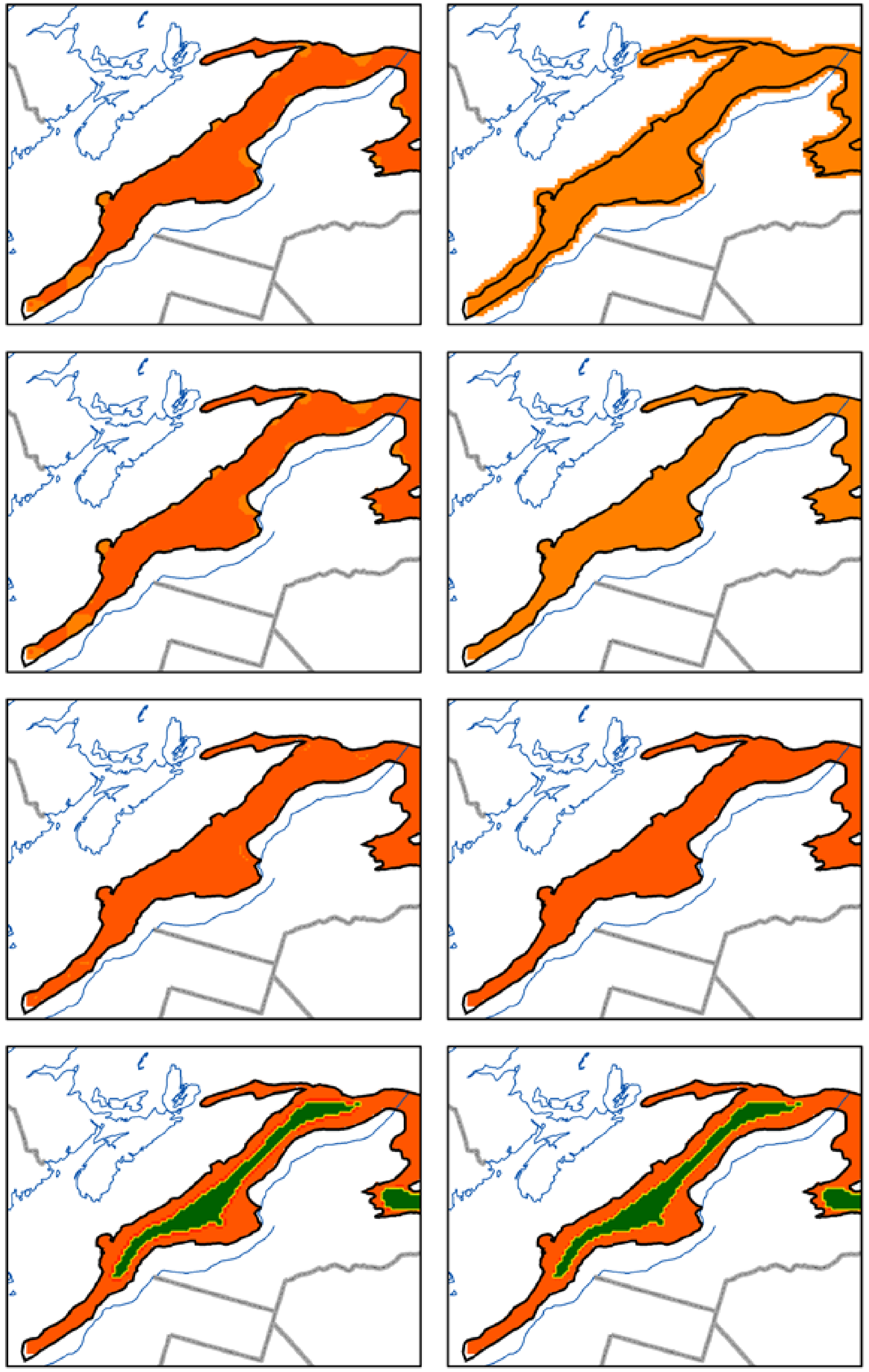

3.9.2 SINEMURIAN

Figure 3.29 shows the Sinemurian TOC results of the OFP model runs for each of the four oxygen scenarios discussed from top to bottom, with the images to the left showing results for the condensed section sedimentation rate runs and the images to the right the results for the standard (zpd) sedimentation runs. The associated HIA and ∑HI results are presented in Figures 3.30 and 3.31 respectively.

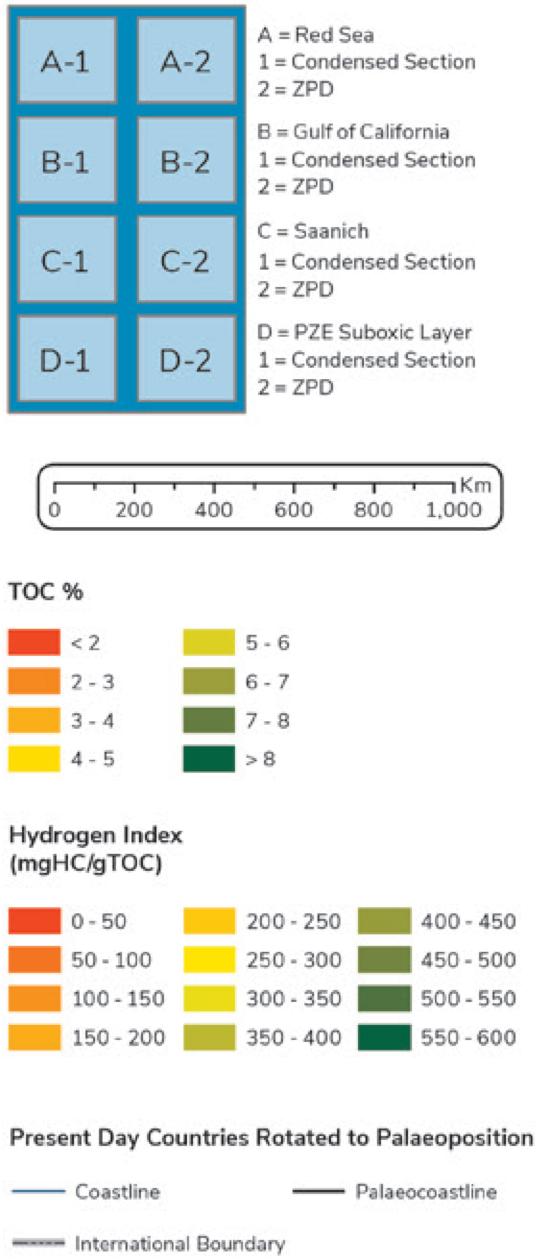

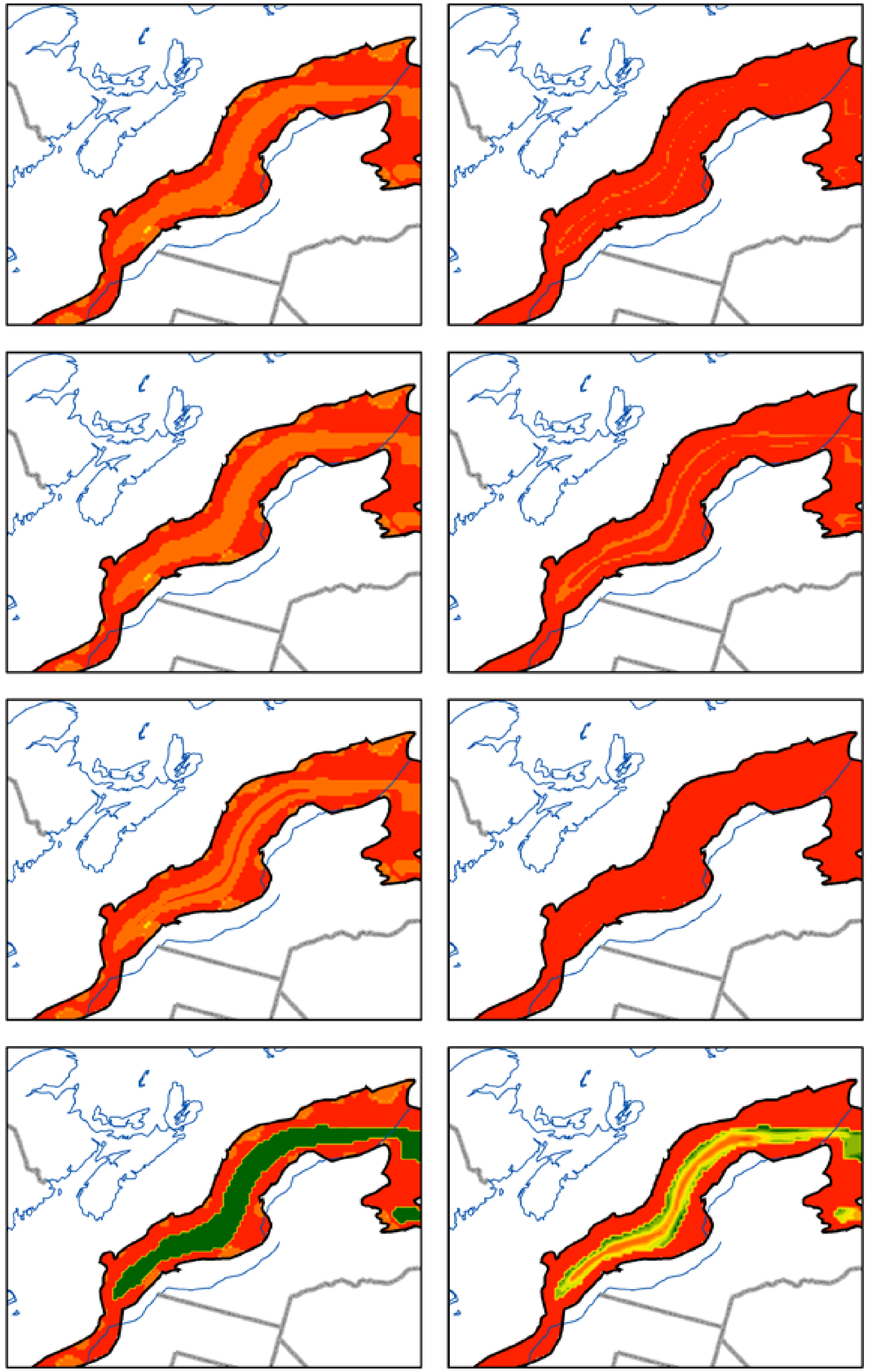

Figure 3.28: Predicted HI using mixing model approach for the Hettangian.

Figure 3.29: Predicted TOC for the Sinemurian.

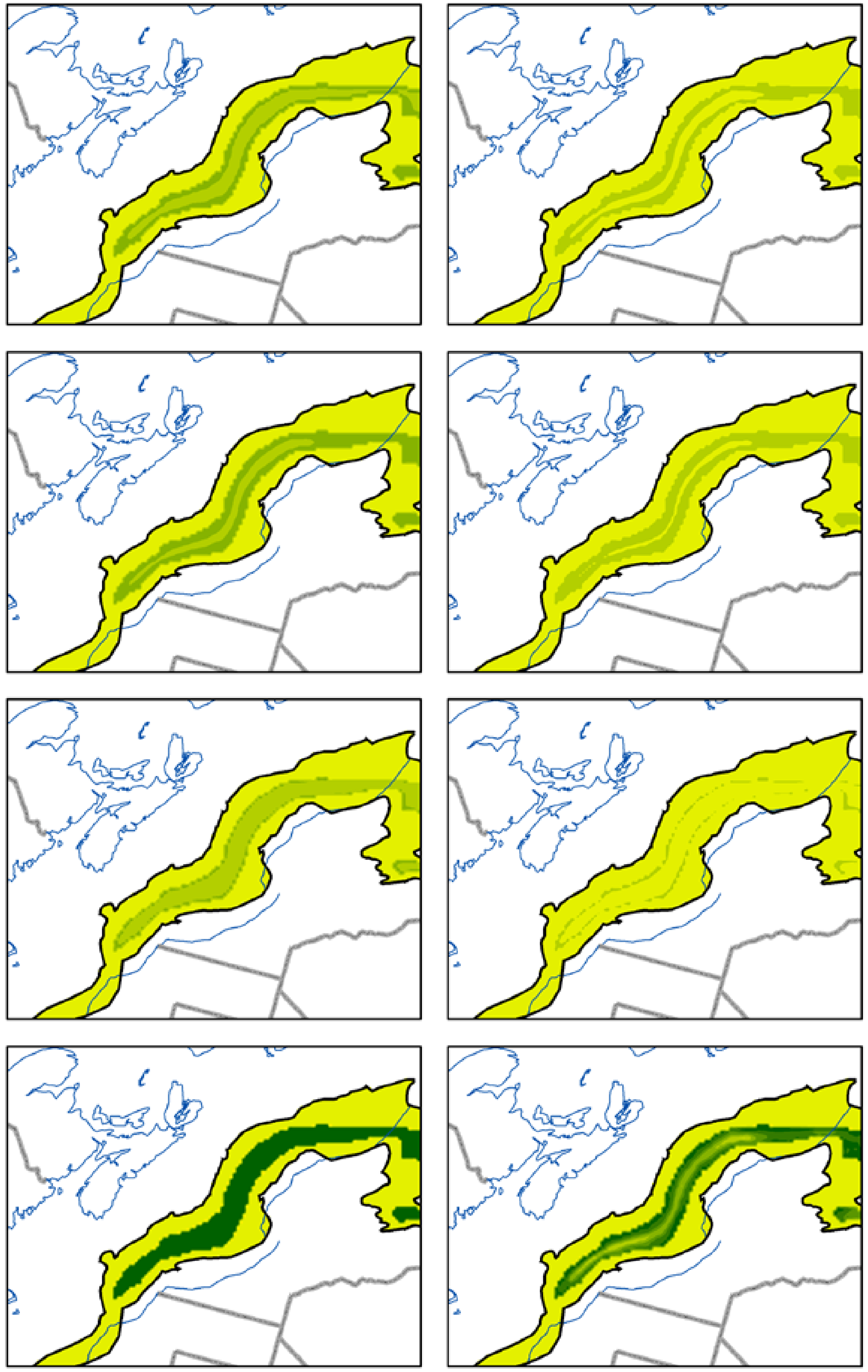

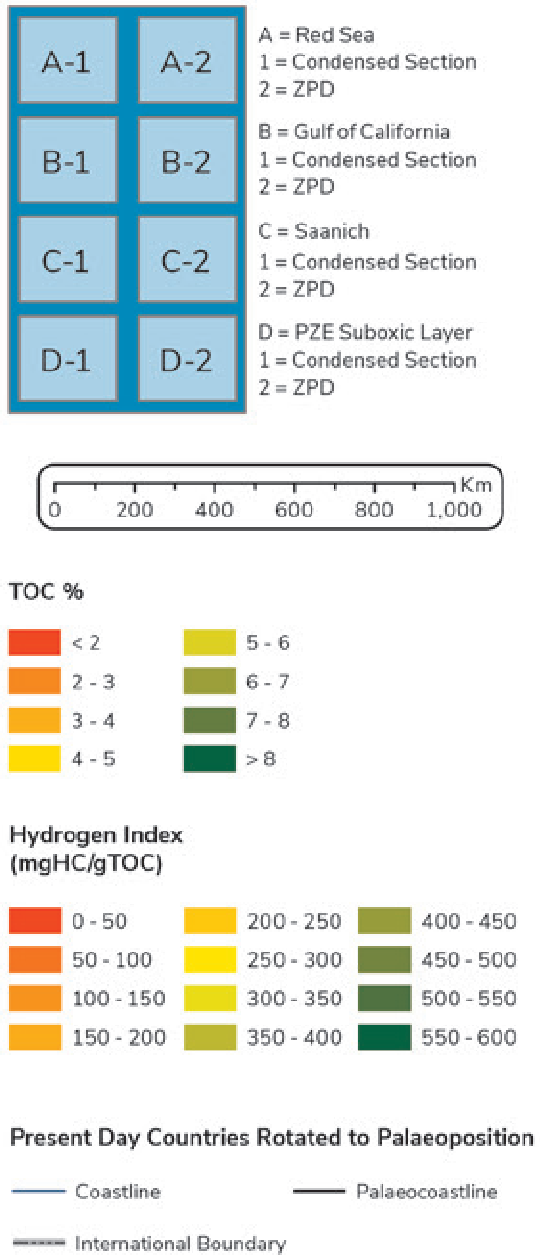

Figure 3.30: Predicted HI using analogue approach for the Sinemurian.

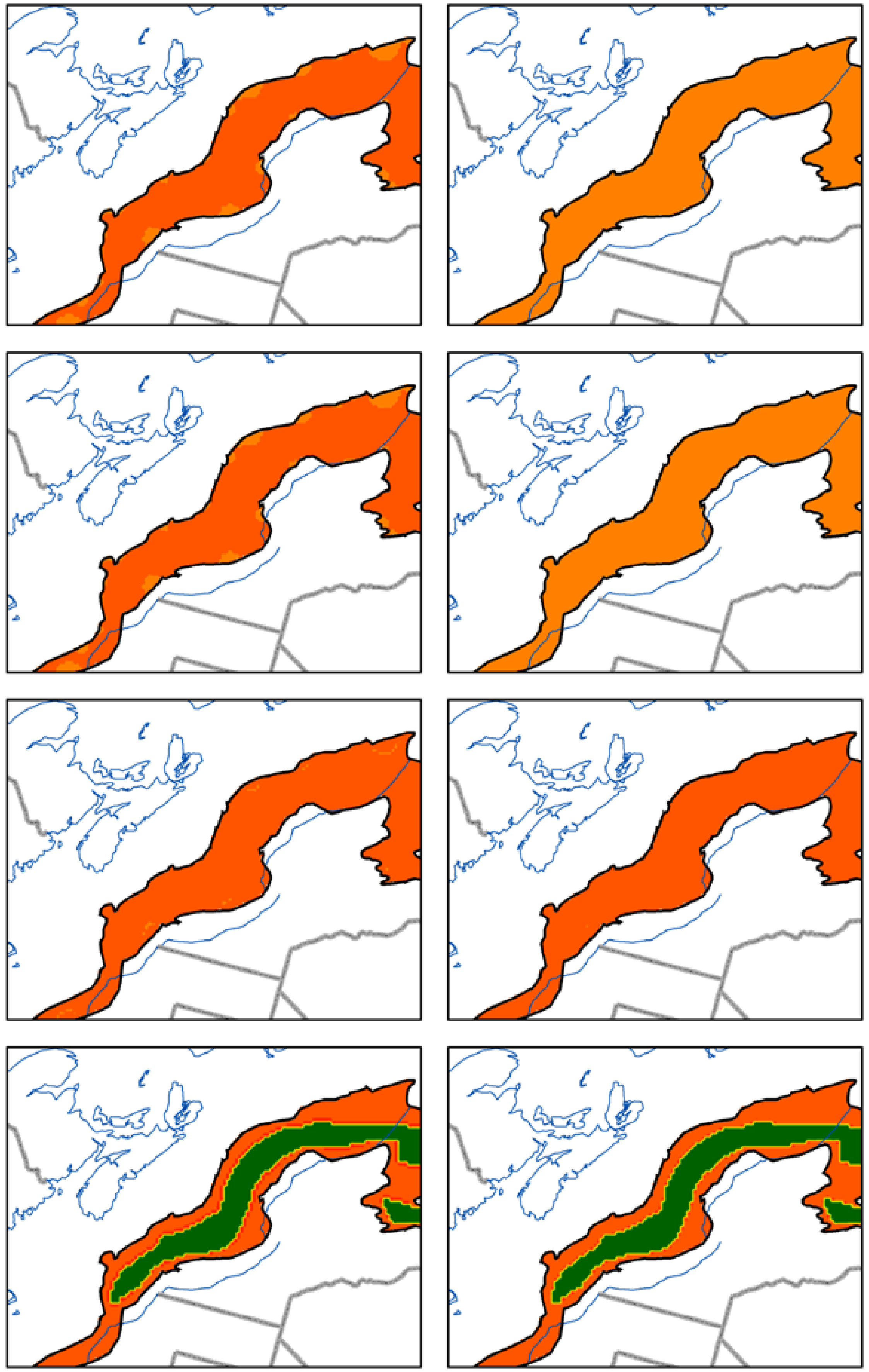

Figure 3.31: Predicted HI using mixing model approach for the Sinemurian.

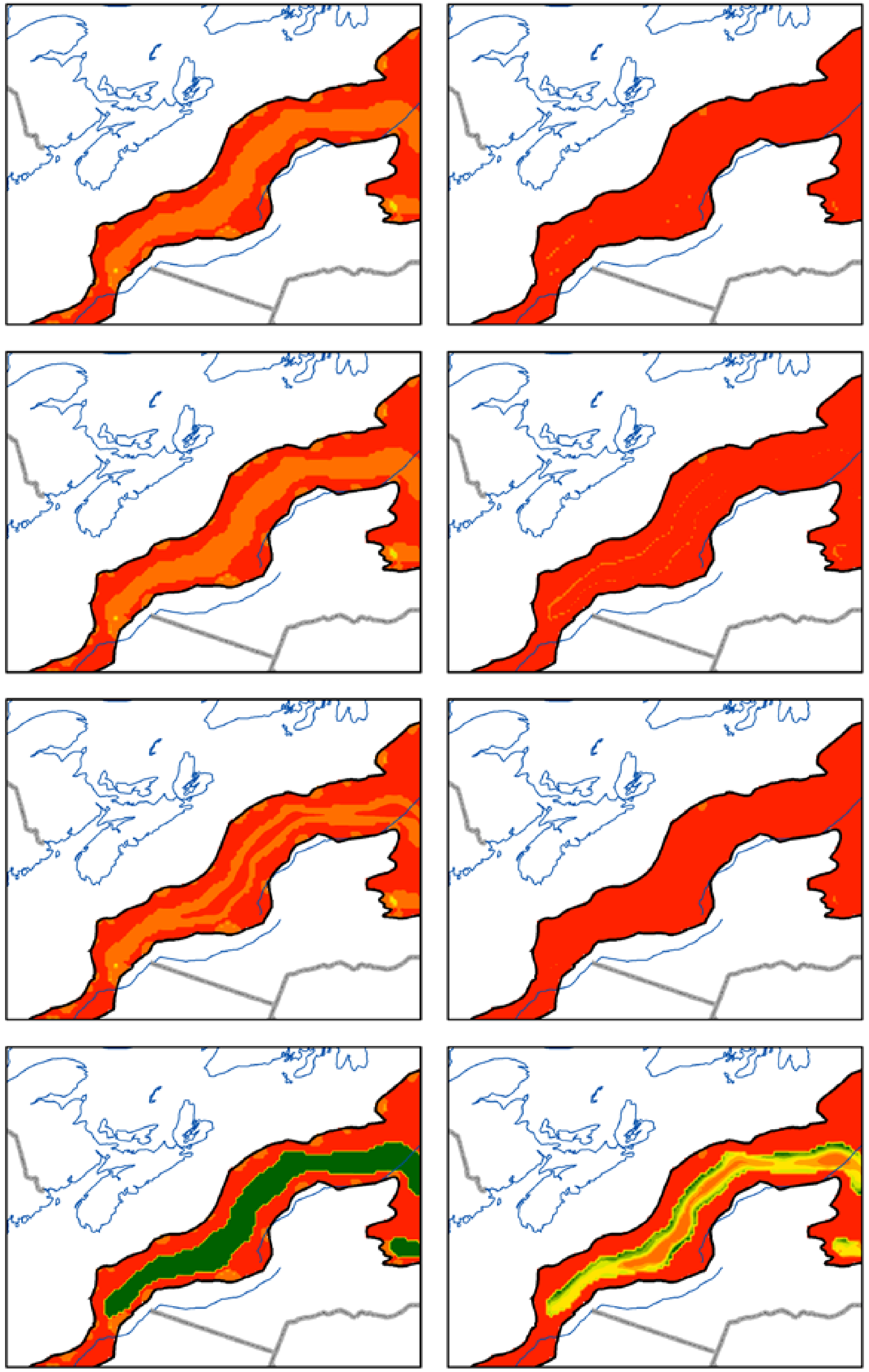

3.9.3 PLIENSBACHIAN

Figure 3.32 shows the Pliensbachian TOC results of the OFP model runs for each of the four oxygen scenarios discussed from top to bottom, with the images to the left showing results for the condensed section sedimentation rate runs and the images to the right the results for the standard (zpd) sedimentation runs. The associated HIA and ∑HI results are presented in figures 3.33 and 3.34 respectively.

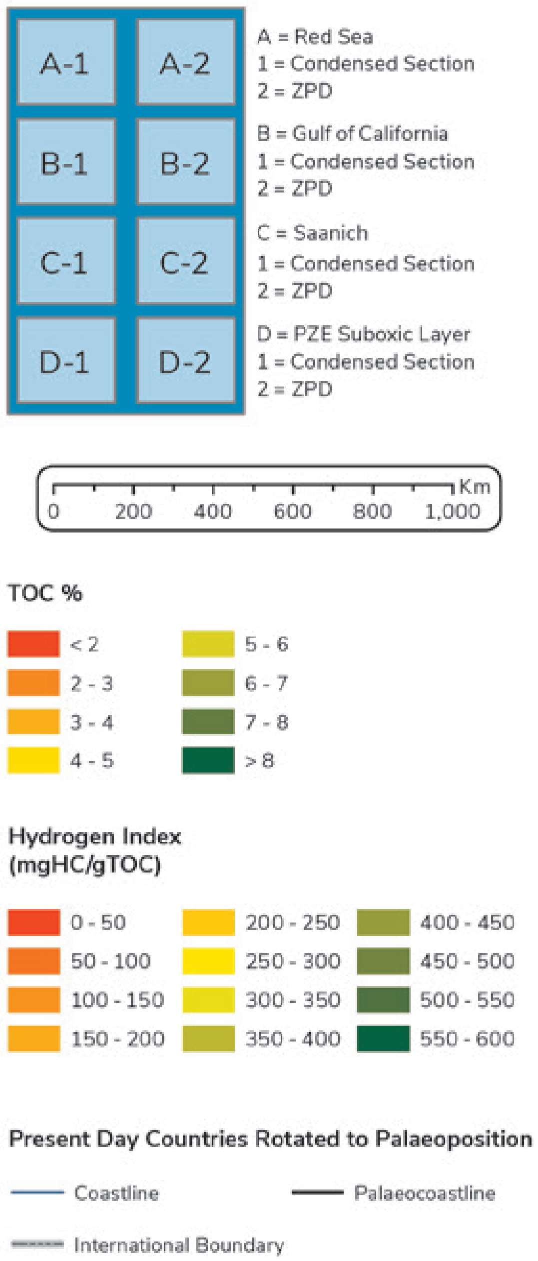

Figure 3.32: Predicted TOC for the Pliensbachian.

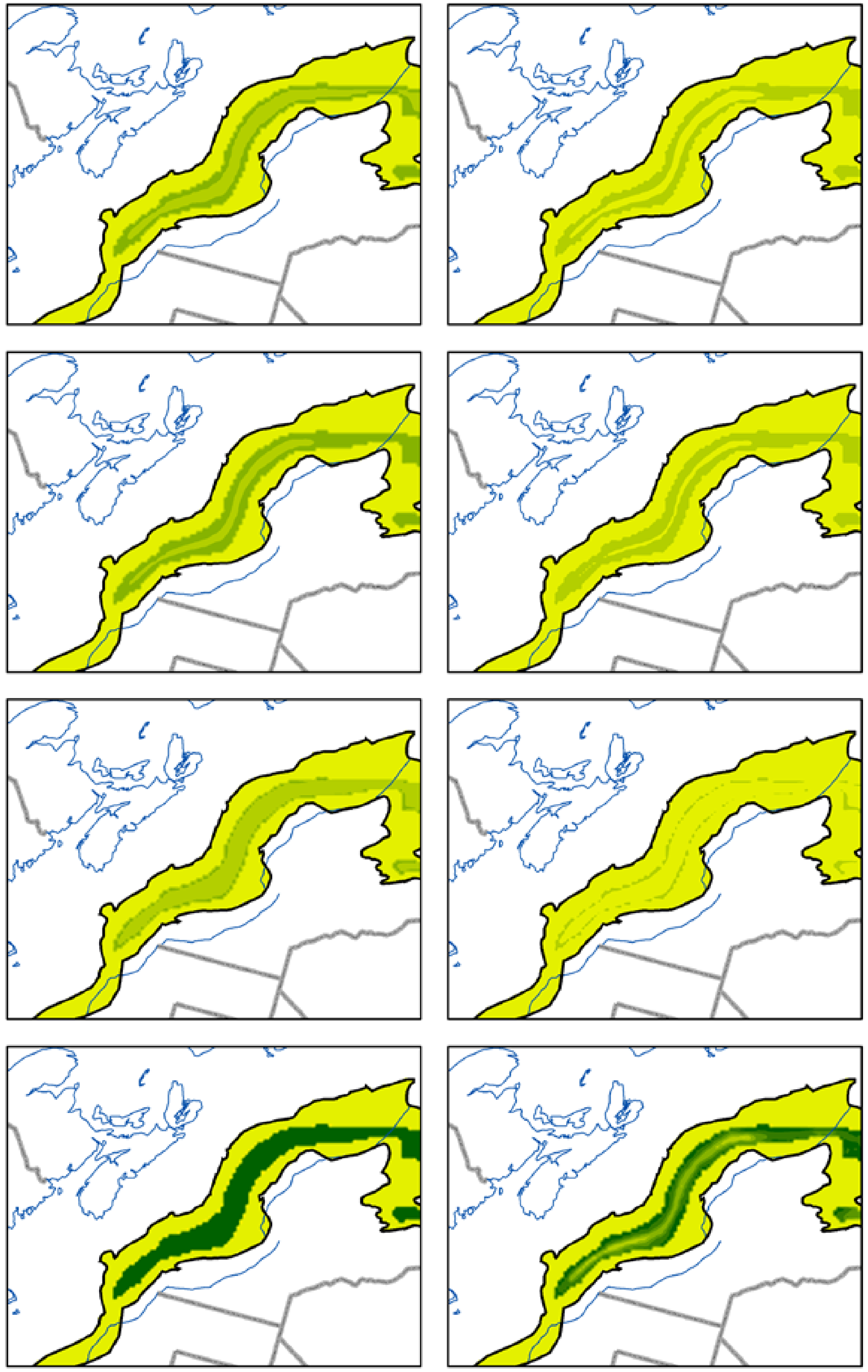

Figure 3.33: Predicted HI using analogue approach for the Pliensbachian.

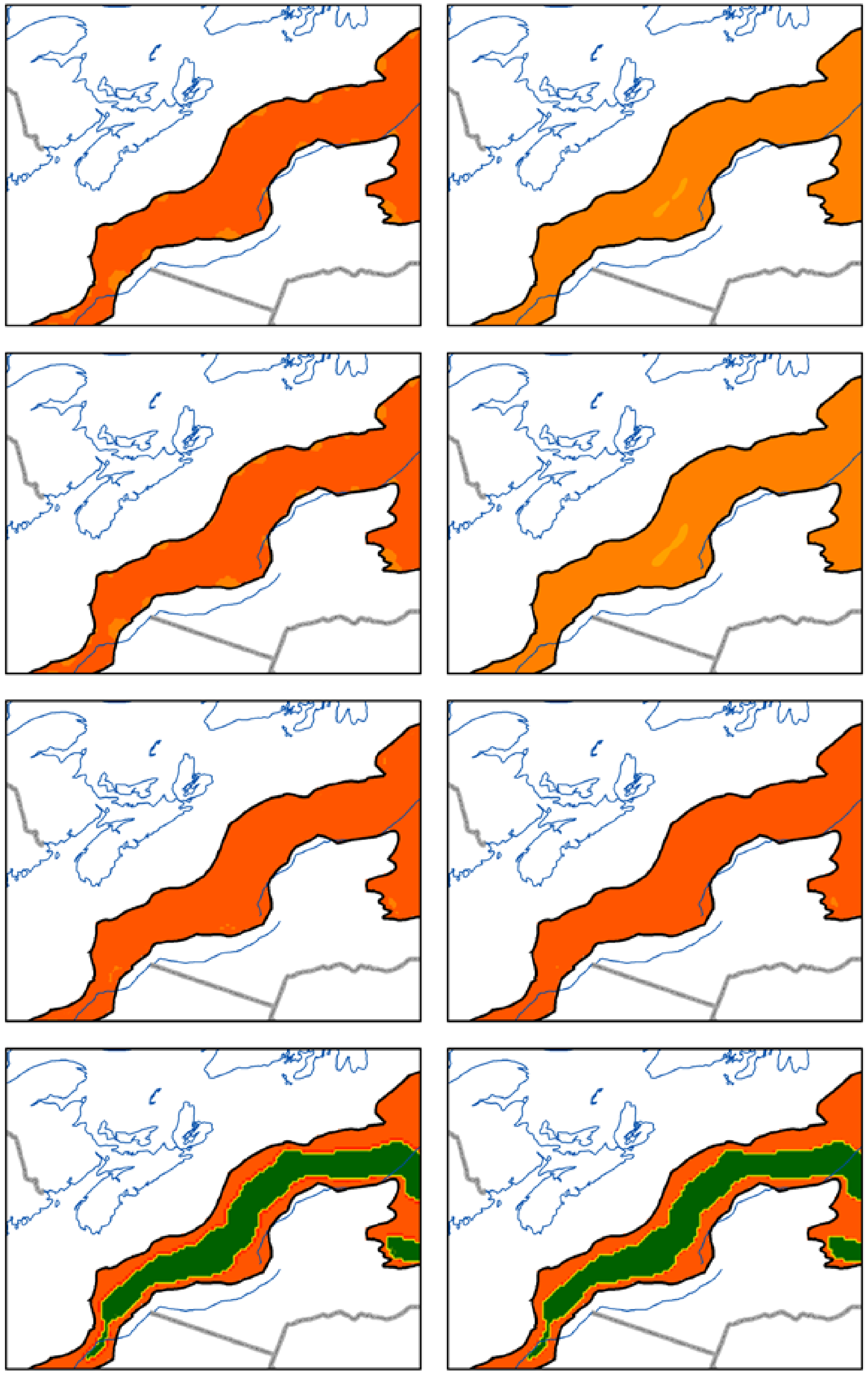

3.9.4 TOARCIAN

Figure 3.35 shows the Toarcian TOC results of the OFP model runs for each of the four oxygen scenarios discussed from top to bottom, with the images to the left showing results for the condensed section sedimentation rate runs and the images to the right the results for the standard (zpd) sedimentation runs. The associated HIA and ∑HI results are presented in Figures 3.36 and 3.37 respectively.

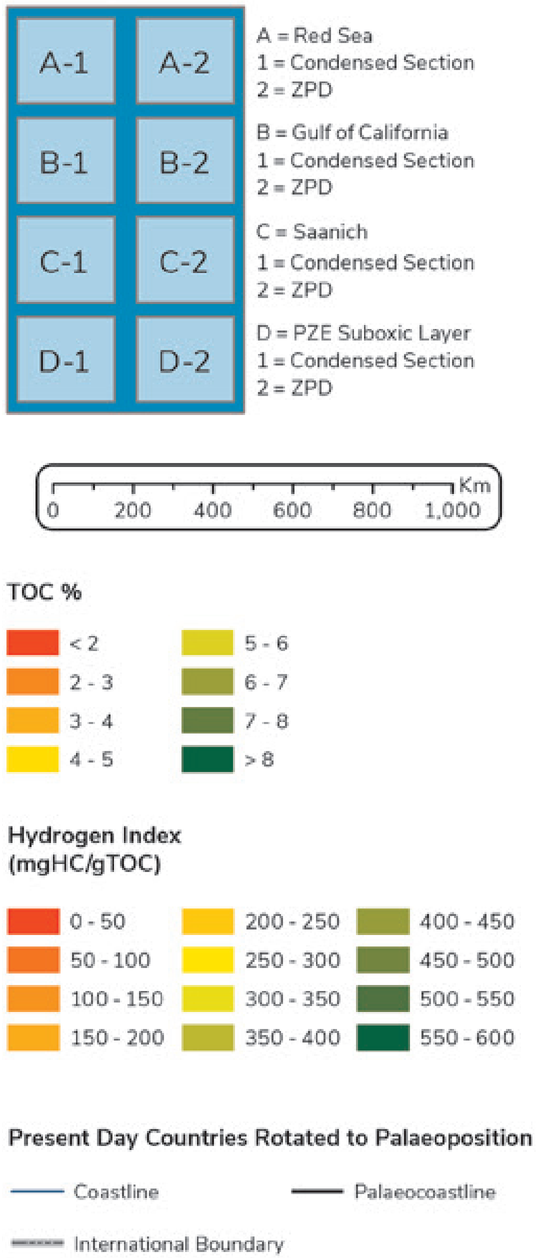

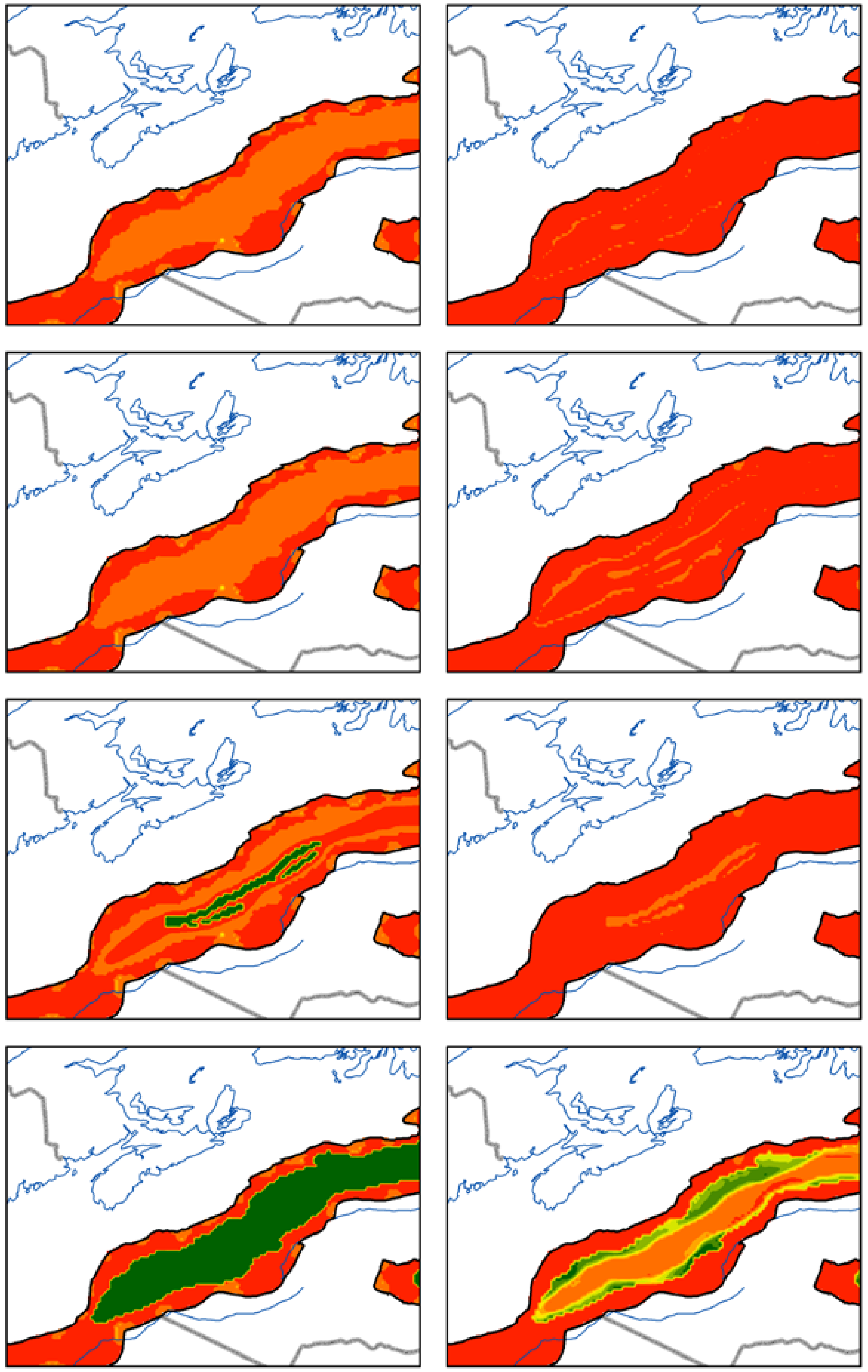

Figure 3.34: ***Predicted HI using mixing model approach for the Pliensbachian.***

Figure 3.35: ***Predicted TOC for the Toarcian.***

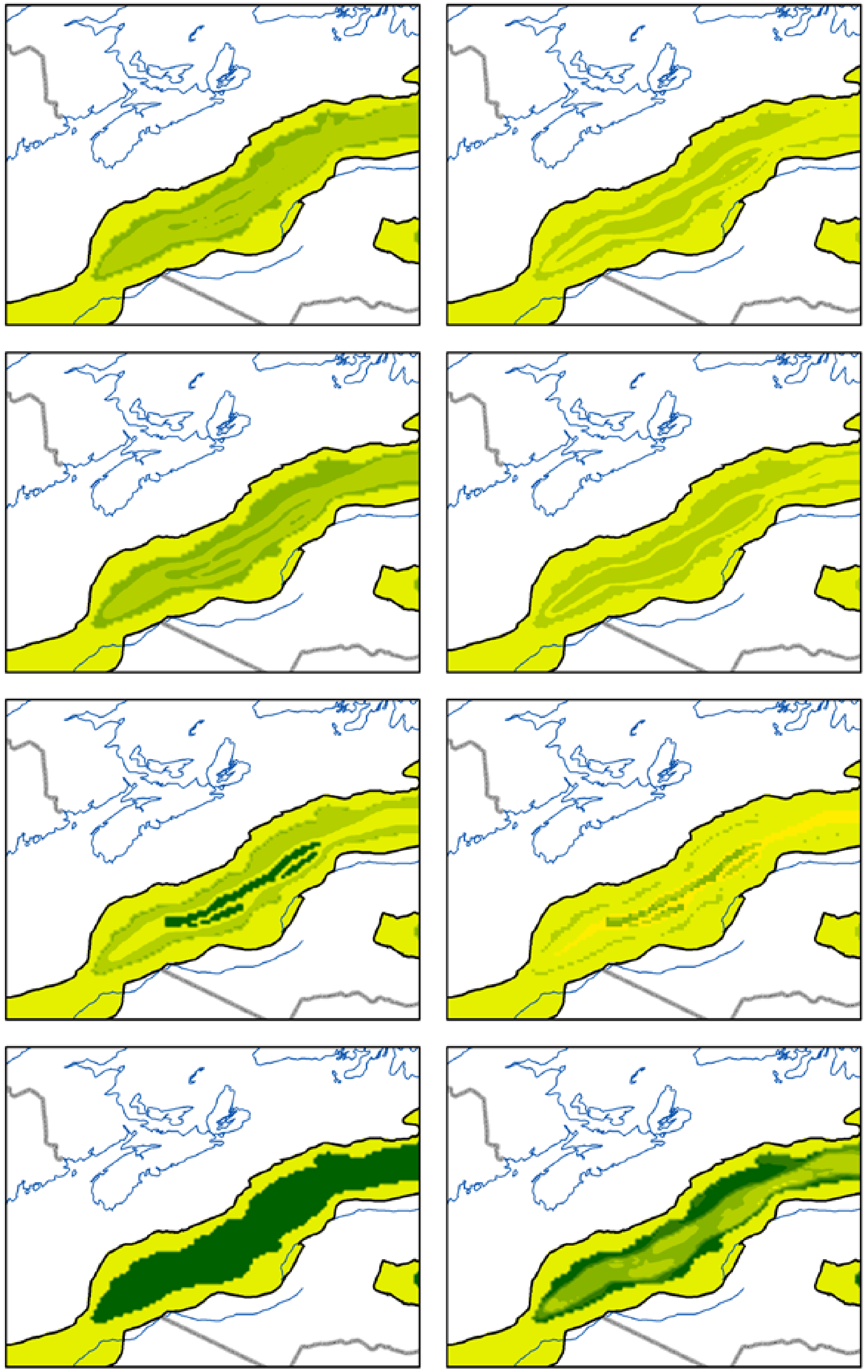

Figure 3.36: Predicted HI using analogue approach for the Toarcian.

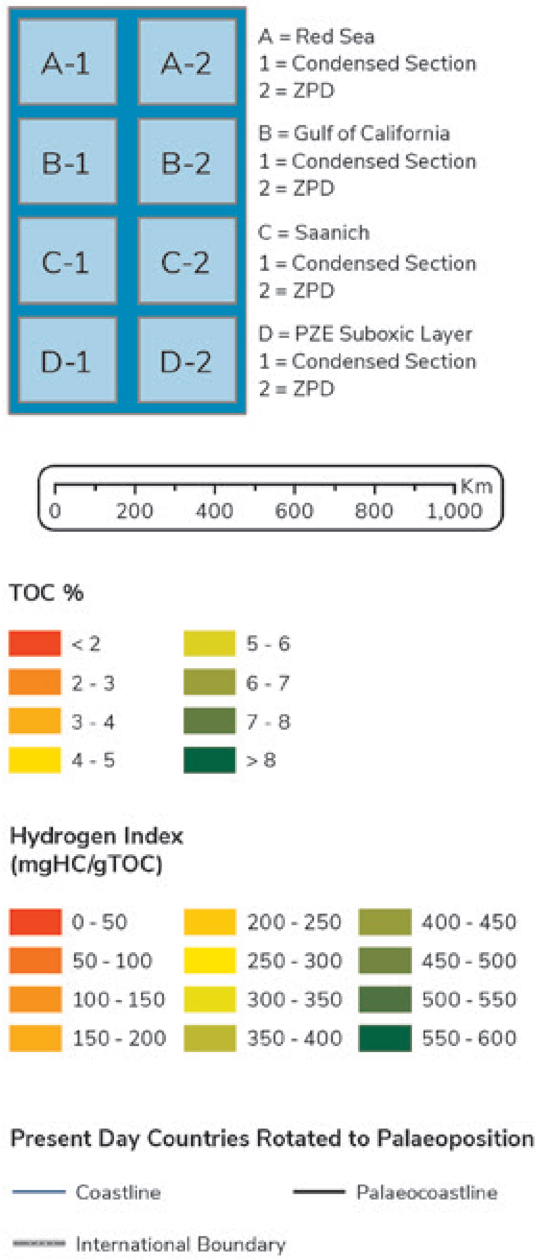

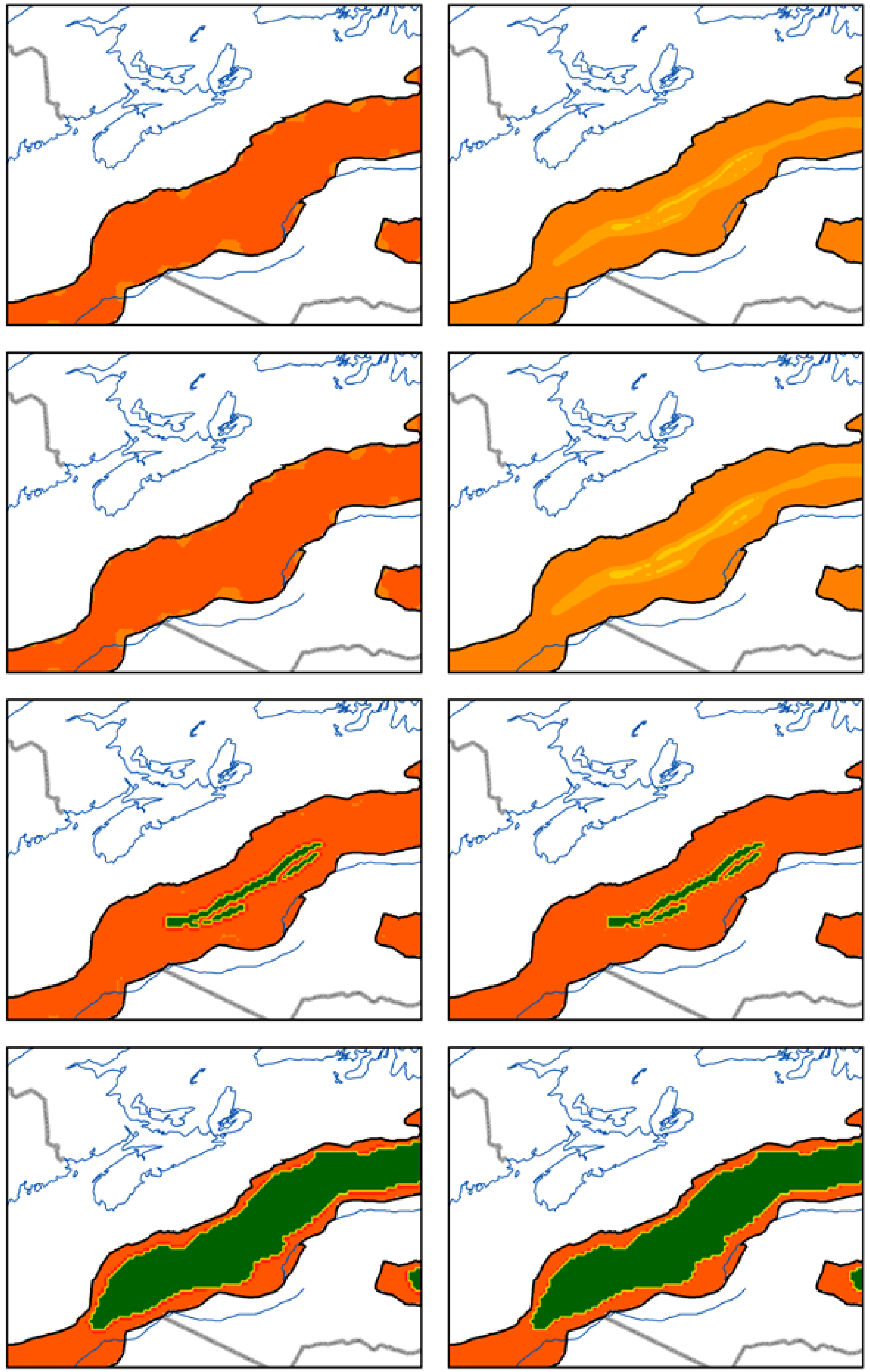

Figure 3.37: Predicted HI using mixing model approach for the Toarcian.

3.9.5 TITHONIAN

Figure 3.39 shows the Tithonian TOC results of the OFP model runs for each of the four oxygen scenarios discussed from top to bottom, with the images to the left showing results for the condensed section sedimentation rate runs and the images to the right the results for the standard (zpd) sedimentation runs. The associated HIA and ∑HI results are presented in Figures 3.40 and 3.41 respectively.

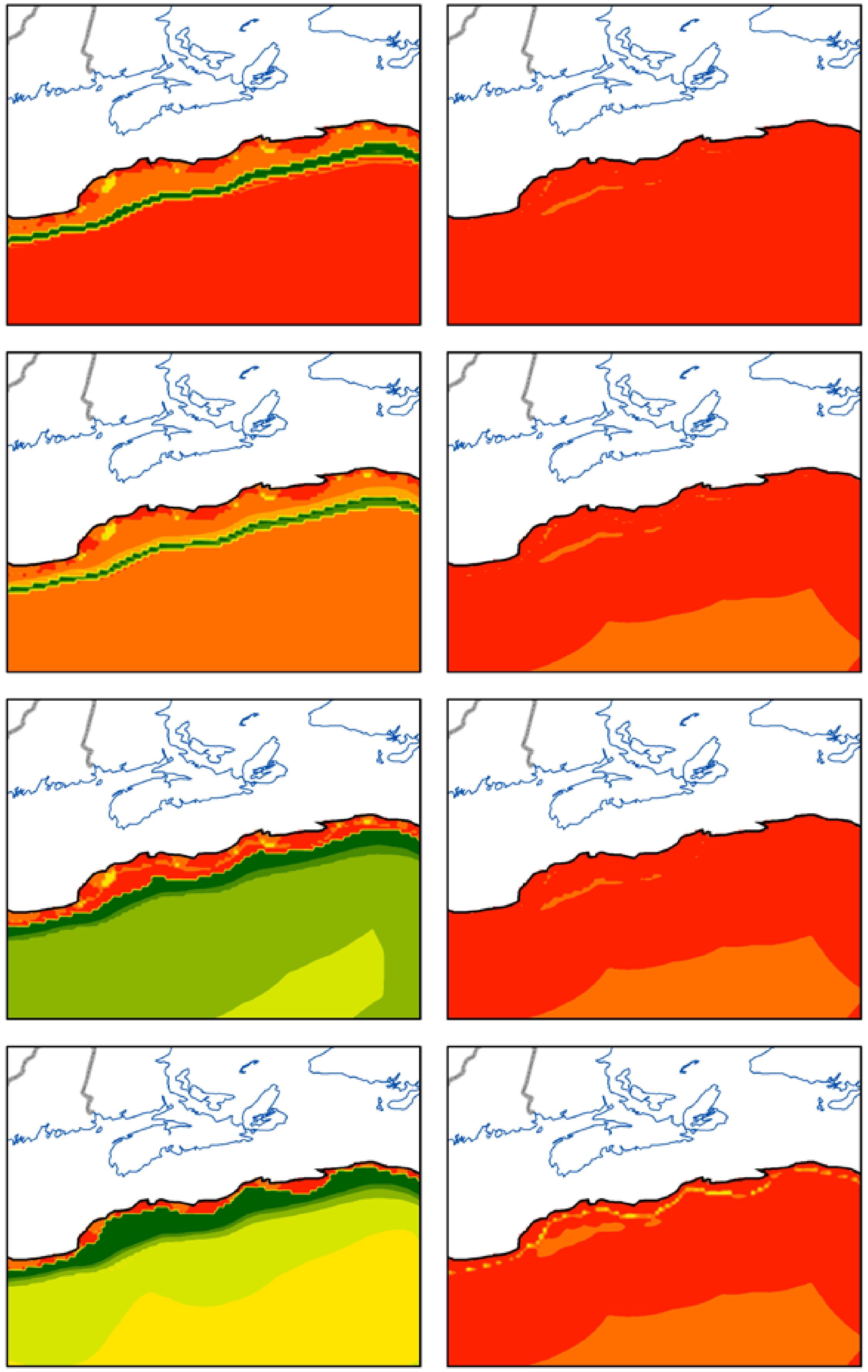

Figure 3.39: ***Predicted TOC for the Tithonian.***

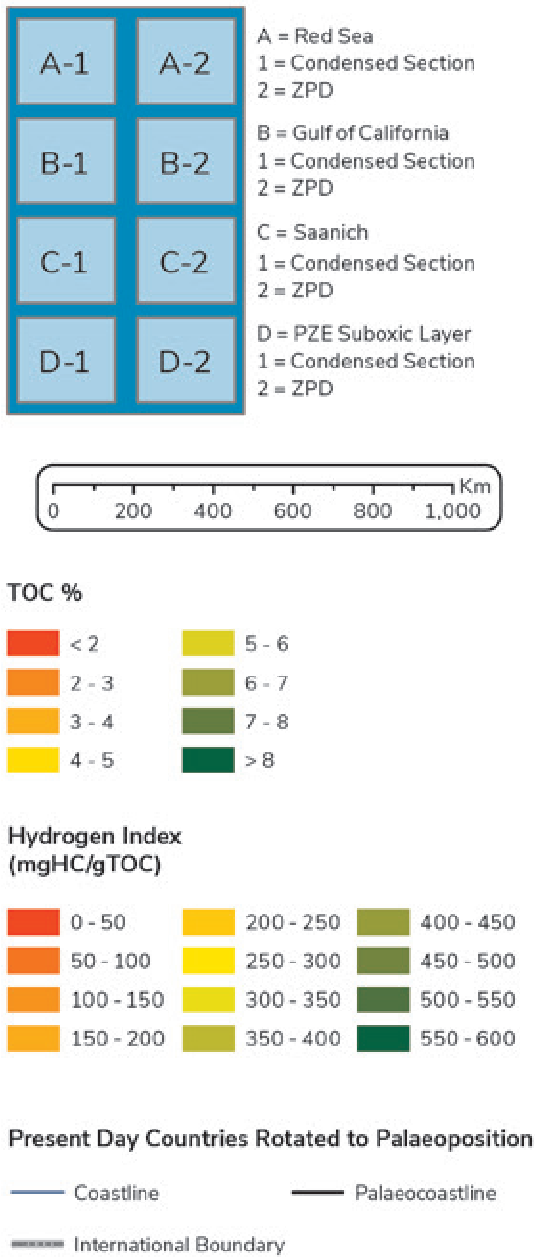

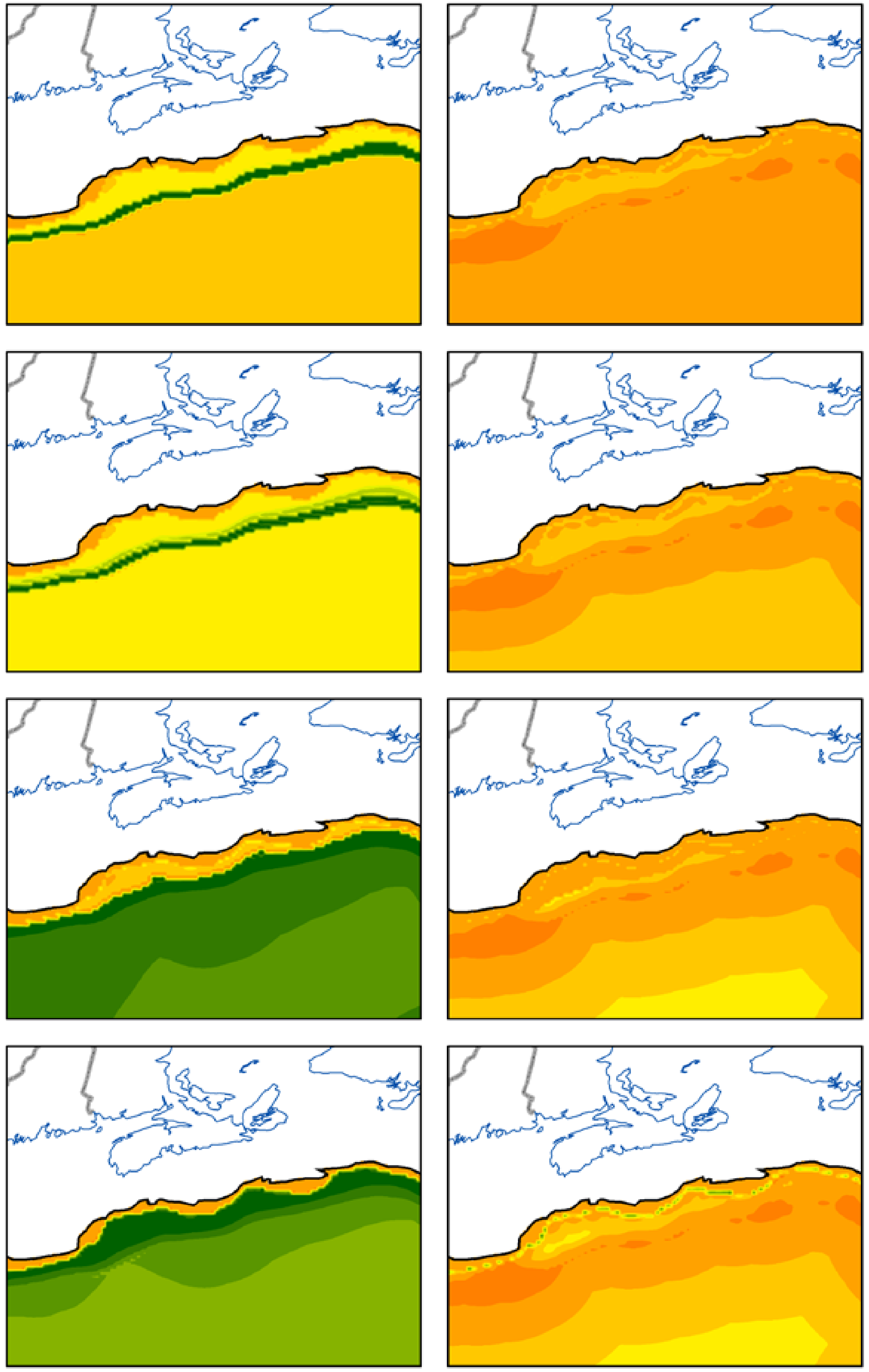

Figure 3.40: ***Predicted HI using analogue approach for the Tithonian.***

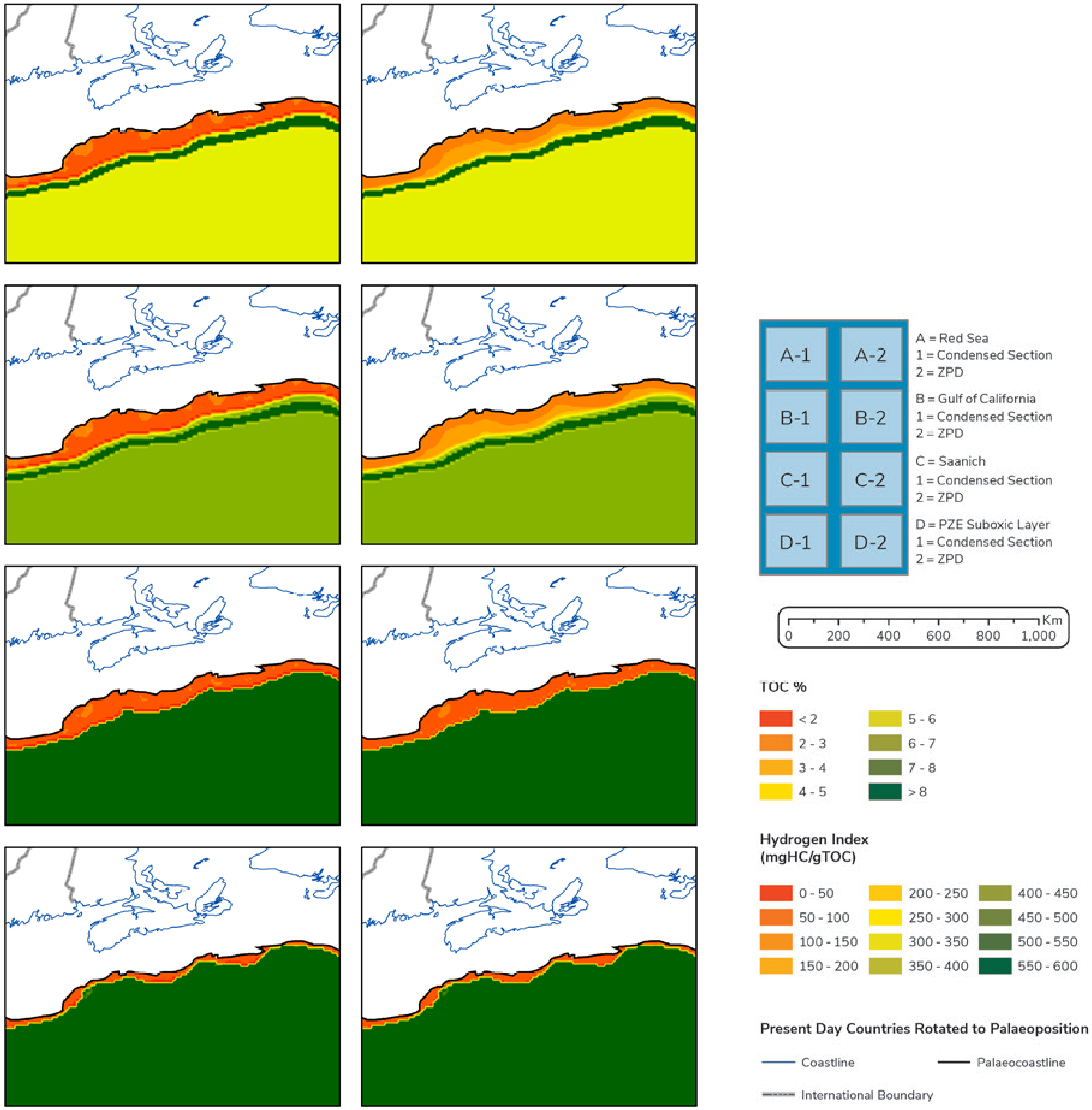

Figure 3.41: Predicted HI using mixing model approach for the Tithonian

3.10 OFP MODELLING DISCUSSION AND RECOMMENDATIONS FOR THE LIAS HISPANIC CORRIDOR

The closest Present Day analogues for long and thin marine basins in an early ocean opening stage are the Red Sea and Gulf of Mexico. Despite the attraction of using these tectonic analogues, the OMZ conditions of these modern analogues relate to specific oceanographic factors which one cannot presume would be appropriate for the area of interest (AOI).

Furthermore, the Hispanic Corridor is much shallower than these basins, even during the Toarcian. It is unlikely that the corridor was deep enough for a more oxygenated sub-OMZ layer to exist, meaning that it is more likely that conditions were uniform below the chemocline, probably with a warm saline bottom water.

The initial OMZ settings applied for the Tethys model runs was purely in order to reflect the probable deep oxic bottom water in the Western Tethys; however, this lies outside the AOI, and thus the initial model differs little, in principle, from the bottom water models (Saanich model (deepest chemocline, least source rock extent) and Black Sea "PZE" model (shallowest chemocline, greatest source rock extent)). For the depths in the AOI, the initial Tethys OMZ model and the Black Sea "PZE" model are not that different. The Black Sea model is the most optimistic in terms of source rock potential.

As the OFP model predicts a single snapshot in time, it is unable to reflect the variability of conditions throughout the entire stage. It is therefore useful to consider a number of different scenarios to attempt to get a sense of possible range of predicted values. In this instance, the condensed section results provide a good sense of maximum estimates and the standard (zpd) sedimentation rate, where dilution moderates the TOC, gives a sense of "median" predictive values.

In order to proceed with a single scenario for risk mapping, the most suitable of the eight modelled scenarios must be determined.

Given the depth limitations and the specific oceanographic conditions of the modern tectonic analogues (Red Sea and Gulf of California), these are least likely to best represent the conditions of the Lias Hispanic Corridor. It is therefore likely that a bottom water model is best suited. Although much shallower than the tectonic analogues, the Saanich deep chemocline model is still not shallow enough. Despite lacking a similar geometry and tectonics setting the Black Sea PZE plus suboxic layer model depth has been defined using data from the margins of the basin where water depths are suitably similar to those of the reconstructed Hispanic Corridor during the Lias.

The Black Sea LSARzpd model output is probably the best single choice to be applied in the risk mapping. The results from this scenario are optimistic, although not outlandishly so given the widespread dysoxia-anoxia during the Lias, especially in the Toarcian, and the confined nature of the basin. The sediments could be strongly cyclic, and it is uncertain how long the conditions set in the model would have persisted, and thus how much thickness of source rock might have accumulated. Some constraint could be gained from analysis of the better studied sections in adjacent regions (typical thicknesses, typical durations, ratios of oxic to dysoxic-anoxic sediments, sedimentation rates, etc.). A more detailed comparison of the observed TOC range with the predicted TOC range (using LSARzpd and LSARcs sedimentation rates) would allow a quantification of model effectiveness.

3.11 REFERENCES

Assaoud, S., A. Chalouan, and H. Belayouni, 2001, Intérêt pétrolier des bassins liasiques de la bordure nord-ouest du craton africain: exemple le bassin moyen atlasique marocain: Africa Geoscience Review, v. 8, no. 1–2, p. 211–222.

Behrenfeld, M. J., and P. G. Falkowski (1997). Photosynthetic rates derived from satellite- based chlorophyll concentration, Limnology and Oceanography, v. 42, no. 1, p. 1–20.

Berner, Z. A., H. Puchelt, T. Nöltner, and U. Kramar, 2013, Pyrite geochemistry in the Toarcian Posidonia Shale of south-west Germany: evidence for contrasting trace-element patterns of diagenetic and syngenetic pyrites: Sedimentology, v. 60, no. 2, p. 548–573, doi:10.1111/j.1365-3091.2012.01350.3.

Bessereau, G., and F. Guillocheau, 1994, Sequence stratigraphy and organic matter distribution of the Lias of the Paris Basin, in J. Mascle, ed., Hydrocarbon and petroleum geology of France: Berlin, Springer, Special Publication of the European Association of Petroleum Geoscientists, p. 107–119, doi:10.1007/978-3-642-78849-9_7.

Bruneau, B., M. Villié, M. Ducros, B. Chauveau, F. Baudin, and I. Moretti, 2018, 3D numerical modelling and sensitivity analysis of the processes controlling organic matter distribution and heterogeneity—a case study from the Toarcian of the Paris Basin: Geosciences, v. 8, no. 11, p. 1–17, doi:10.3390/geosciences8110405.

Caswell, B. A., and A. L. Coe, 2012, A high-resolution shallow marine record of the Toarcian (Early Jurassic) Oceanic Anoxic Event from the East Midlands Shelf, UK: Palaeogeography, Palaeoclimatology, Palaeoecology, v. 365–366, p. 124–135, doi:10.1016/j.palaeo.2012.09.021.

Clémence, M.-E., A. Bartolini, S. Gardin, G. Paris, V. Beaumont, and K. N. Page, 2010, Early Hettangian benthic–planktonic coupling at Doniford (SW England): palaeoenvironmental implications for the aftermath of the end-Triassic crisis: Palaeogeography, Palaeoclimatology, Palaeoecology, v. 295, no. 1–2, p. 102–115, doi:10.1016/j.palaeo.2010.05.021.

Deconinck, J.-F., S. P. Hesselbo, N. Debuisser, and O. Averbuch, 2003, Environmental controls on clay mineralogy of an Early Jurassic mudrock (Blue Lias Formation, southern England): International Journal of Earth Sciences, v. 92, no. 2, p. 255–266, doi:10.1007/s00531-003-0318-y.

Dickson, A. J., B. C. Gill, M. Ruhl, H. C. Jenkyns, D. Porcelli, E. F. Idiz, T. W. Lyons, and S. H. J. M. van den Boorn, 2017, Molybdenum-isotope chemostratigraphy and paleoceanography of the Toarcian Oceanic Anoxic Event (Early Jurassic): Paleoceanography, v. 32, no. 8, p. 813–829, doi:10.1002/2016PA003048.

Fantasia, A., K. B. Föllmi, T. Adatte, J. E. Spangenberg, and E. Mattioli, 2019, Expression of the Toarcian Oceanic Anoxic Event: new insights from a Swiss transect: Sedimentology, v. 66, no. 1, p. 262–284, doi:10.1111/sed.12527.

Fantasia, A., K. B. Föllmi, T. Adatte, J. E. Spangenberg, and J.-C. Montero-Serrano, 2018, The Early Toarcian oceanic anoxic event: paleoenvironmental and paleoclimatic change across the Alpine Tethys (Switzerland): Global and Planetary Change, v. 162, p. 53–68, doi:10.1016/j.gloplacha.2018.01.008.

Fantasia, A., T. Adatte, J. E. Spangenberg, E. Font, L. V. Duarte, and K. B. Föllmi, 2019, Global versus local processes during the Pliensbachian–Toarcian transition at the Peniche GSSP, Portugal: a multi-proxy record: Earth-Science Reviews, v. 198, no. 102932, p. 1–16, doi:10.1016/j.earscirev.2019.102932.

Fonseca, C., J. G. Mendonça Filho, C. Lézin, L. V. Duarte, and P. Fauré, 2018, Organic facies variability during the Toarcian Oceanic Anoxic Event record of the Grands Causses and Quercy basins (southern France): International Journal of Coal Geology, v. 190, p. 218–235, doi:10.1016/j.coal.2017.10.006.

Frimmel, A., W. Oschmann, and L. Schwark, 2004, Chemostratigraphy of the Posidonia black shale, SW Germany. I. Influence of sea-level variation on organic facies evolution: Chemical Geology, v. 206, no. 3–4, p. 199–230, doi:10.1016/j.chemgeo.2003.12.007.

Getech Group, plc, 2016. Tectonic evolution of the North Atlantic: implications for prospectivity. G1604.

Gómez, J. J., and A. Goy, 2011, Warming-driven mass extinction in the Early Toarcian (Early Jurassic) of northern and central Spain. Correlation with other time-equivalent European sections: Palaeogeography, Palaeoclimatology, Palaeoecology, v. 306, no. 3–4, p. 176–195, doi:10.1016/j.palaeo.2011.04.018.

Gorin, G. E., and S. Feist-Burkhardt, 1990, Organic facies of Lower to Middle Jurassic sediments in the Jura Mountains, Switzerland: Review of Palaeobotany and Palynology, v. 65, no. 1–4, p. 349–355, doi:10.1016/0034-6667(90)90085-w.

Hanzo, M., and J. Espitalié, 1993, Relation entre matière organique et sédimentation dans le Lias de Lorraine (France): Comptes Rendus Académie des Sciences Paris, Série II, Mécanique, physique, chimie, sciences de l'univers, sciences de la terre, v. 316, no. 7, p. 945–950.

Hartnett, H. E., Keil, R. G., Hedges, J. I. & Devol, A. H. (1998). Influence of oxygen exposure time on organic carbon preservation in continental margin sediments. Nature, 391 (6667), pp. 572-574.

Henrichs, S. M. & Reeburgh, W. S. (1987). Anaerobic mineralization of marine sediment organic matter: rates and the role of anaerobic processes in the oceanic carbon economy. Geomicrobiology Journal, 5 (3-4), pp. 191-237.

Hermoso, M., F. Minoletti, and P. Pellenard, 2013, Black shale deposition during Toarcian super-greenhouse driven by sea level: Climate of the Past, v. 9, no. 6, p. 2703–2712, doi:10.5194/cp-9-2703-2013.

Hermoso, M., D. Delsate, F. Baudin, L. Le Callonnec, F. Minoletti, M. Renard, and A. Faber, 2014, Record of Early Toarcian carbon cycle perturbations in a nearshore environment: the Bascharage section (easternmost Paris Basin): Solid Earth, v. 5, no. 2, p. 793–804, doi:10.5194/se-5-793-2014.

Hollander, D. J., G. Bessereau, S. Belin, A. Y. Huc, and J.-P. Houzay, 1991, Organic matter in the early Toarcian shales, Paris Basin, France: a response to environmental changes: Revue de l'Institut Français du Pétrole, v. 46, no. 5, p. 543–562.

Horsfield, B., R. Littke, U. Mann, S. Bernard, T. A. . Vu, R. di Primio, and H.-M. Schulz, 2010, Shale gas in the Posidonia Shale, Hils area, Germany, AAPG annual meeting, New Orleans: 31 pp. https://www.searchanddiscovery.com/pdfz/documents/2010/110126horsfield/ndx_horsfield.pdf.html

Houben, S., S. Nelskamp, T. Goldberg, R. M. C. H. Verreussel, N. M. M. Janssen, S. Kerstholt, and T. Boxem, 2017, HYPO-Lias: hydrocarbon potential of the Lias. Toegepast Natuurwetenschappelijk Onderzoek (TNO): 86 pp.

Hougård, I. W., J. A. Bojesen-Koefoed, M. L. Vickers, C. V. Ullmann, C. J. Bjerrum, M. Rizzi, and C. Korte, 2021, Redox element record shows that environmental perturbations associated with the T-OAE were of longer duration than the carbon isotope record suggests – the Aubach section, SW Germany: Newsletters on Stratigraphy, v. 54, no. 2, p. 229–246, doi:10.1127/nos/2020/0630.

Hudson, A., 2015, The Toarcian Oceanic Anoxic Event: a temporary exposure in Lincolnshire: Palaeontology Newsletter, no. 88, p. 74–76.

Katz, B. J., 1995, The Schistes Carton - the Lower Toarcian of the Paris Basin, in B. J. Katz, ed., Petroleum source rocks: New York, Springer, Casebooks in Earth sciences, p. 51–65, doi:10.1007/978-3-642-78911-3_4.

Kemp, D. B., A. L. Coe, A. S. Cohen, and G. P. Weedon, 2011, Astronomical forcing and chronology of the early Toarcian (Early Jurassic) oceanic anoxic event in Yorkshire, UK: Paleoceanography, v. 26, no. 4, p. 1–17, doi:10.1029/2011PA002122.

Langford, F. F., and M.-M. Blanc-Valleron (1990). Interpreting Rock-Eval pyrolysis data using graphs of pyrolizable hydrocarbons vs. total organic carbon: American Association of Petroleum Geologist Bulletin, v. 74, no. 6, p. 799–804.

Lézin, C., B. Andreu, P. Pellenard, J.-L. Bouchez, L. Emmanuel, P. Fauré, and P. Landrein, 2013, Geochemical disturbance and paleoenvironmental changes during the Early Toarcian in NW Europe: Chemical Geology, v. 341, p. 1–15, doi:10.1016/j.chemgeo.2013.01.003.

Littke, R., and J. Rullkötter, 1987, Mikroskopische und makroskopische Unterschiede zwischen Profilen unreifen und reifen Posidonienschiefers aus der Hilsmulde: Facies, v. 17, no. 1, p. 171–180, doi:10.1007/BF02536781.

Littke, R., D. Leythäeuser, J. Rullkötter, and D. R. Baker, 1991, Keys to the depositional history of the Posidonia Shale (Toarcian) in the Hils Syncline, northern Germany, in Tyson, R.V. and T.H. Pearson (eds), Modern and ancient continental shelf anoxia, Geological Society of London Special Publication, v. 58, p. 311–333, doi:10.1144/GSL.SP.1991.058.01.20.

Littke, R., U. Klussmann, B. M. Krooss, and D. Leythäeuser, 1991, Quantification of loss of calcite, pyrite, and organic matter due to weathering of Toarcian black shales and effects on kerogen and bitumen characteristics: Geochimica et Cosmochimica Acta, v. 55, no. 11, p. 3369–3378, doi:10.1016/0016-7037(91)90494-P.

McArthur, J. M., 2019, Early Toarcian black shales: a response to an oceanic anoxic event or anoxia in marginal basins? Chemical Geology, v. 522, p. 71–83, doi:10.1016/j.chemgeo.2019.05.028.

McArthur, J. M., T. J. Algeo, B. van de Schootbrugge, Q. Li, and R. J. Howarth, 2008, Basinal restriction, black shales, Re-Os dating, and the Early Toarcian (Jurassic) oceanic anoxic event: Paleoceanography, v. 23, no. 4, p. 1–22, doi:10.1029/2008PA001607.

Moldowan, J. M., P. Sundararaman, and M. Schoell, 1986, Sensitivity of biomarker properties to depositional environment and/or source input in the Lower Toarcian of SW-Germany: Organic Geochemistry, v. 10, no. 4–6, p. 915–926, doi:10.1016/S0146-6380(86)80029-8.

Montero-Serrano, J.-C., K. B. Föllmi, T. Adatte, J. E. Spangenberg, N.-P. Tribovillard, A. Fantasia, and G. Suan, 2015, Continental weathering and redox conditions during the early Toarcian Oceanic Anoxic Event in the northwestern Tethys: insight from the Posidonia Shale section in the Swiss Jura Mountains: Palaeogeography, Palaeoclimatology, Palaeoecology, v. 429, p. 83–99, doi:10.1016/j.palaeo.2015.03.043.

Monticone, B., M. Duval, R. Knispel, P. Wojciak, and M. H. Dubille, 2012, Shale oil potential of the Paris Basin, France: Search and Discovery, no. 10384, p. 1–30.

Nava Cedillo, A., and G. D. Abbott, 2017, Geochemical study of the Sinemurian Arietites bucklandi Zone in the Blue Lias of Lyme Regis (Dorset, UK): Search and Discovery, no. 51363, p. 1–4.

Neumeister, S., R. Gratzer, T. J. Algeo, A. Bechtel, H.-J. Gawlick, R. J. Newton, and R. F. Sachsenhofer, 2015, Oceanic response to Pliensbachian and Toarcian magmatic events: implications from an organic-rich basinal succession in the NW Tethys: Global and Planetary Change, v. 126, p. 62–83, doi:10.1016/j.gloplacha.2015.01.007.

Neumeister, S., T. J. Algeo, A. Bechtel, H.-J. Gawlick, and R. Gratzer, 2016, Redox conditions and depositional environment of the Lower Jurassic Bächental bituminous marls (Tyrol, Austria): Austrian Journal of Earth Sciences, v. 109, no. 2, p. 142–159, doi:10.17738/ajes.2016.0010.

Neumeister, S., D. Misch, T. J. Algeo, H.-J. Gawlick, R. Gratzer, and R. F. Sachsenhofer, 2020, Early diagenesis of organic-rich marls under shifting suboxic to euxinic conditions: the lower Toarcian of the Bächental basin: Marine and Petroleum Geology, v. 120, no. 104513, p. 1–17, doi:10.1016/j.marpetgeo.2020.104513.

O'Malley, R. & Tyson, R. V. (2012). Oceanic net primary productivity models, pers comms.

Paris, G., V. Beaumont, A. Bartolini, M.-E. Clémence, S. Gardin, and K. N. Page, 2010, Nitrogen isotope record of a perturbed paleoecosystem in the aftermath of the end-Triassic crisis, Doniford section, SW England: Geochemistry, Geophysics, Geosystems, v. 11, no. 8, p. 1–15, doi:10.1029/2010GC003161.

Polgári, M. et al., 2016, Mineral and chemostratigraphy of a Toarcian black shale hosting Mn-carbonate microbialites (Úrkút, Hungary): Palaeogeography, Palaeoclimatology, Palaeoecology, v. 459, p. 99–120, doi:10.1016/j.palaeo.2016.06.030.

Prauss, M. L., B. Ligouis, and H. Luterbacher, 1991, Organic matter and palynomorphs in the "Posidonienschiefer" (Toarcian, Lower Jurassic) of southern Germany, in Tyson, R.V. and T.H. Pearson (eds), Modern and ancient continental shelf anoxia, Geological Society of London Special Publication, v. 58, p. 335–351, doi:10.1144/GSL.SP.1991.058.01.21.

Pross, J., 2012, Acritarchs and prasinophytes: morphology, evolution, paleoecology: Presentation, Frankfurt, University of Frankfurt, p. 1–37. http://servermac.geologie.uni-frankfurt.de/Staff/Homepages/Pross/Mikropal/Acritarchs_Prasinophytes_Micropal_2012.pdf Accessed 29/4/2020.

Quan, T. M., B. van de Schootbrugge, M. P. Field, Y. Rosenthal, and P. G. Falkowski, 2008, Nitrogen isotope and trace metal analyses from the Mingolsheim core (Germany): evidence for redox variations across the Triassic-Jurassic boundary: Global Biogeochemical Cycles, v. 22, no. 2, p. 1–14, doi:10.1029/2007GB002981.

Quesada, S., S. Robles, and I. Rosales, 2005, Depositional architecture and transgressive-regressive cycles within Liassic backstepping carbonate ramps in the Basque-Cantabrian basin, northern Spain: Journal of the Geological Society, London, v. 162, no. 3, p. 531–548, doi:10.1144/0016-764903-041.

Robl, T. L., A. C. Hutton, and D. A. Dixon, 1992, The organic petrology and geochemistry of the Toarcian oil shale of Luxembourg, in Proceedings 1992 Eastern oil shale symposium: Institute for Mining and Minerals Research, University of Kentucky, p. 300–312.

Röhl, H.-J., A. Schmid-Röhl, W. Oschmann, A. Frimmel, and L. Schwark, 2001, The Posidonia Shale (Lower Toarcian) of SW-Germany: an oxygen-depleted ecosystem controlled by sea level and palaeoclimate: Palaeogeography, Palaeoclimatology, Palaeoecology, v. 169, no. 3–4, p. 271–299, doi:10.1016/S0031-0182(01)00224-3.

Röhl, H.-J., and A. Schmid-Röhl, 2005, Lower Toarcian (Upper Liassic) black shales of the central European epicontinental basin: a sequence stratigraphic case study from the SW German Posidonia Shale, in Harris, N.B. (ed.) Deposition of organic-carbon-rich sediments: models, mechanisms and consequences, SEPM Special Publication, v. 82, p. 165–189, doi:10.2110/pec.05.82.0165.

Ruebsam, W., M. Stockhausen, and L. Schwark, 2016, Assessment of temporal source rock variability: an example from the Lower Jurassic Posidonia Shale: Search and Discovery, no. 41974, p. 1–33.

Ruebsam, W., T. Müller, J. Kovács, J. Pálfy, and L. Schwark, 2018, Environmental response to the early Toarcian carbon cycle and climate perturbations in the northeastern part of the West-Tethys shelf: Gondwana Research, v. 59, p. 144–158, doi:10.1016/j.gr.2018.03.013.

Ruhl, M., M. H. L. Deenen, H. A. Abels, N. R. Bonis, W. Krijgsman, and W. M. Kürschner, 2010, Astronomical constraints on the duration of the early Jurassic Hettangian stage and recovery rates following the end-Triassic mass extinction (St Audrie's Bay/East Quantoxhead, UK): Earth and Planetary Science Letters, v. 295, no. 1–2, p. 262–276, doi:10.1016/j.epsl.2010.04.008.

Ruvalcaba Baroni, I., A. Pohl, N. A. G. M. van Helmond, N. M. Papadomanolaki, A. L. Coe, A. S. Cohen, B. van de Schootbrugge, Y. Donnadieu, and C. P. Slomp, 2018, Ocean circulation in the Toarcian (Early Jurassic), a key control on deoxygenation and carbon burial on the European Shelf: Paleoceanography and Paleoclimatology, v. 33, no. 9, p. 994–1012, doi:10.1029/2018PA003394.

Sachse, V. F., D. Leythäeuser, A. Grobe, M. Rachidi, and R. Littke, 2012, Organic geochemistry and petrology of a Lower Jurassic (Pliensbachian) petroleum source rock from Aït Moussa, Middle Atlas, Morocco: Journal of Petroleum Geology, v. 35, no. 1, p. 5–23, doi:10.1111/j.1747-5457.2012.00516.3.

Sælen, G., P. Doyle, and M. R. Talbot, 1996, Stable-isotope analyses of belemnite rostra from the Whitby Mudstone Fm., England: surface water conditions during deposition of a marine black shale: Palaios, v. 11, no. 2, p. 97–117, doi:10.2307/3515065.

Schmid-Röhl, A., H.-J. Röhl, W. Oschmann, and A. Frimmel, 2002, Palaeoenvironmental reconstruction of Lower Toarcian epicontinental black shales (Posidonia Shale, SW Germany): global versus regional control: Geobios, v. 35, no. 1, p. 13–20, doi:10.1016/S0016-6995(02)00005-0.

Scotchman, I. C., 2001, Petroleum geochemistry of the Lower and Middle Jurassic in Atlantic margin basins of Ireland and the UK, in Shannon, P. M., P. D. W. Haughton and D. V. Corocoran (eds) The petroleum exploration of Ireland's offshore basins, Geological Society Special Publication, v. 188, 31–60 p., doi:10.1144/GSL.SP.2001.188.01.03.

Scotchman, I. C., and J. R. W. Thomas, 1995, Maturity and hydrocarbon generation in the Slyne Trough, northwest Ireland, in Croker, P. F. and Shannon, P. M. (eds) The petroleum geology of Ireland's offshore basins, Geological Society of London Special Publication, v. 93, p. 385–411, doi:10.1144/GSL.SP.1995.093.01.30.

Shultz, D. J. & Calder, J. A. (1976). Organic carbon 13C/12C variations in estuarine sediments. Geochimica et Cosmochimica Acta, 40 (4), pp. 381-385.

Silva, R. L., and L. V. Duarte, 2015, Organic matter production and preservation in the Lusitanian Basin (Portugal) and Pliensbachian climatic hot snaps: Global and Planetary Change, v. 131, p. 24–34, doi:10.1016/j.gloplacha.2015.05.002.

Silva, R. L., C. A. M. Carlisle, and G. D. Wach, 2017, A new TOC, Rock-Eval, and carbon isotope record of Lower Jurassic source rocks from the Slyne Basin, offshore Ireland: Marine and Petroleum Geology, v. 86, p. 499–511, doi:10.1016/j.marpetgeo.2017.06.004.

Song, J., R. Littke, and P. Weniger, 2017, Organic geochemistry of the Lower Toarcian Posidonia Shale in NW Europe: Organic Geochemistry, v. 106, p. 76–92, doi:10.1016/j.orggeochem.2016.10.014.

Song, J., R. Littke, P. Weniger, C. Ostertag-Henning, and S. Nelskamp, 2015, Shale oil potential and thermal maturity of the Lower Toarcian Posidonia Shale in NW Europe: International Journal of Coal Geology, v. 151, p. 127–153, doi:10.1016/j.coal.2015.08.011.

Suan, G. et al., 2013, Palaeoenvironmental significance of Toarcian black shales and event deposits from southern Beaujolais, France: Geological Magazine, v. 150, no. 4, p. 728–742, doi:10.1017/S0016756812000970.

Syvitski, J. M. & Milliman, J. (2007). Geology, geography, and humans battle for dominance over the delivery of fluvial sediment to the coastal ocean. Journal of Geology, 115, pp. 1-19.

Trabucho Alexandre, J. P., R. Dirkx, H. Veld, G. Klaver, and P. L. de Boer, 2012, Toarcian black shales in the Dutch Central Graben: record of energetic, variable depositional conditions during an oceanic anoxic event: Journal of Sedimentary Research, v. 82, no. 2, p. 104–120, doi:10.2110/jsr.2012.5.

Trueblood, S., 1992, Petroleum geology of the Slyne Trough and adjacent basins, in Parnell, J. (ed.), Basins on the Atlantic seaboard: petroleum geology, sedimentology and basin evolution, Geological Society of London Special Publication, v. 62, p. 315–326, doi:10.1144/GSL.SP.1992.062.01.24.

Tyson, R. V. (2001). Sedimentation rate, dilution, preservation and total organic carbon: some results of a modelling study: Organic Geochemistry, v. 32, no. 2, p. 333–339.

Tyson, R. V. (2005). The "productivity versus preservation" controversy: cause, flaws and resolution, In: N. B. Harris (ed.), Deposition of organic-carbon-rich sediments: models, mechanisms and consequences, SEPM Special Publication, 82, pp. 17-33.

Tyson, R. V. (2006). Calibration of hydrogen indices with microscopy: a review, reanalysis and new results using the fluorescence scale: Organic Geochemistry, v. 37, no. 1, p. 45–63.

van Bergen, F., M. H. A. A. Zijp, H. Veld, R. M. C. H. Verreussel, and S. Nelskamp, 2011, Looking for sweet spots in shale gas, making good use of an existing database - the example of the Netherlands: Search and Discovery, no. 90122, p. 1–3.

van Bergen, F., M. H. A. A. Zijp, S. Nelskamp, and H. Kombrink, 2013, Shale gas evaluation of the Early Jurassic Posidonia Shale Formation and the Carboniferous Epen Formation in the Netherlands, in Chatellier, J. Y. and D. M. Jarvie (eds) Critical assessment of shale resource plays, American Association of Petroleum Geologists Memoir, v. 103, p. 1–24, doi:10:1306/13401722H53468.

Varga, A., B. Raucsik, M. Hámorné-Vidó, and Á. Rostási, 2007, Az Óbányai Aleurolit Formáció fekete palájának izotópgeokémiai és szénhidrogéngenetikai jellemzése: Földtani Közlöny, v. 137, no. 4, p. 449–472.

Wassmann, P. (1990). Relationship between primary and export production in the boreal coastal zone of the North Atlantic. Limnology and Oceanography, 35 (2), pp. 464-471.

Weedon, G. P., 1986, Hemipelagic shelf sedimentation and climatic cycles: the basal Jurassic (Blue Lias) of South Britain: Earth and Planetary Science Letters, v. 76, no. 3–4, p. 321–335, doi:10.1016/0012-821X(86)90083-3.

Weedon, G. P., and H. C. Jenkyns, 1990, Regular and irregular climatic cycles and the Belemnite Marls (Pliensbachian, Lower Jurassic, Wessex Basin): Journal of the Geological Society, London, v. 147, no. 6, p. 915–918, doi:10.1144/gsjgs.147.6.0915.

Weedon, G. P., H. C. Jenkyns, and K. N. Page, 2018, Combined sea-level and climate controls on limestone formation, hiatuses and ammonite preservation in the Blue Lias Formation, South Britain (uppermost Triassic – Lower Jurassic): Geological Magazine, v. 155, no. 5, p. 1117–1149, doi:10.1017/S0016756816001283.

Wenzhöfer, F., and R. N. Glud, 2002, Benthic carbon mineralization in the Atlantic: a synthesis based on in situ data from the last decade, Deep-Sea Research I, v. 49, no. 7, p. 1255–1279.

Westberry, T. K., Behrenfeld, ,Siegel, & Boss, E. (2008). Carbon-based primary productivity modeling with vertically resolved photoacclimation. Global Biogeochemical Cycles, 22 (2).

4. SOURCE ROCK RISK MAPPING

4.1 INTRODUCTION

Source rock potential risk maps have been constructed by taking into account the palaeogeographic, palaeogeological and palaeocean boundary conditions that would have influenced source rock deposition. They are provided for the five intervals:

- Tithonian
- Toarcian
- Pliensbachian
- Sinemurian
- Hettangian

These maps will provide a spatial understanding of the how and where favourable conditions existed for source rock development at the time of deposition.

4.2 METHODOLOGY

The production of the source rock risk maps involves the stacking of the gross depositional environment maps (Chapter 2), along with organic content (TOC) and richness (HIA) and oxygen levels (Chapter 3) to evaluate how favourable conditions were at the time of deposition for the development of source rocks. The resulting maps represent source rock presence and effectiveness – but only in terms of its potential quality. The risk maps will not take into account:

- Thickness of source rock horizon
- Whether accommodation space was present for accumulation of organic matter
- Maturity
- Volume
- Migration mechanism
- Petroleum charge

Therefore, the resultant risk maps show the extent of favourable to unfavourable conditions for source rock deposition. This does not translate directly as to where there is a mature and effective source rock, as the above factors must also be taken into account.

The maximum extent of the source rock risk mapping covers the area of interest shown in Figure 1.1 of the Introduction Chapter. However, the four Lower Jurassic risk maps will have a more limited extent, as much of the Present Day study area is underlain by oceanic crust that is younger and, therefore, post-dates the Lower Jurassic (Figure 4.1a). As the GDE, HIA and TOC maps are reconstructed from their original palaeopositon (Figure 4.1b) back to Present Day, the reconstructed data will have split across the COB with remaining data being reconstructed on the Moroccan margin as shown in Figure 4.1c.

We have used the following conceptual categories for the risk maps

- Favourable (Green): predicted source-rock parameters clearly demonstrate favourable conditions for source rock development.
- Less Favourable (Yellow): predicted source-rock parameters have less favourable conditions or are ambiguous as source rock development.
- Unfavourable (Red): predicted source-rock parameters do not rule out the presence of source, but they are clearly inadequate to establish an effective source.
- Outside the Source Rock Fairway (White): one or more preconditions for a source rock are lacking.

The assignment of the each category are based purely on the results of the OFP modelling and GDE mapping results.

Figure 4.1 (Below): Extent of Present Day risk maps for the lower Jurassic horizons. a) age of oceanic crust underlying the study area; b) example of a lower Jurassic GDE in its palaeoposition; c) A lower Jurassic GDE reconstructed back to Present Day

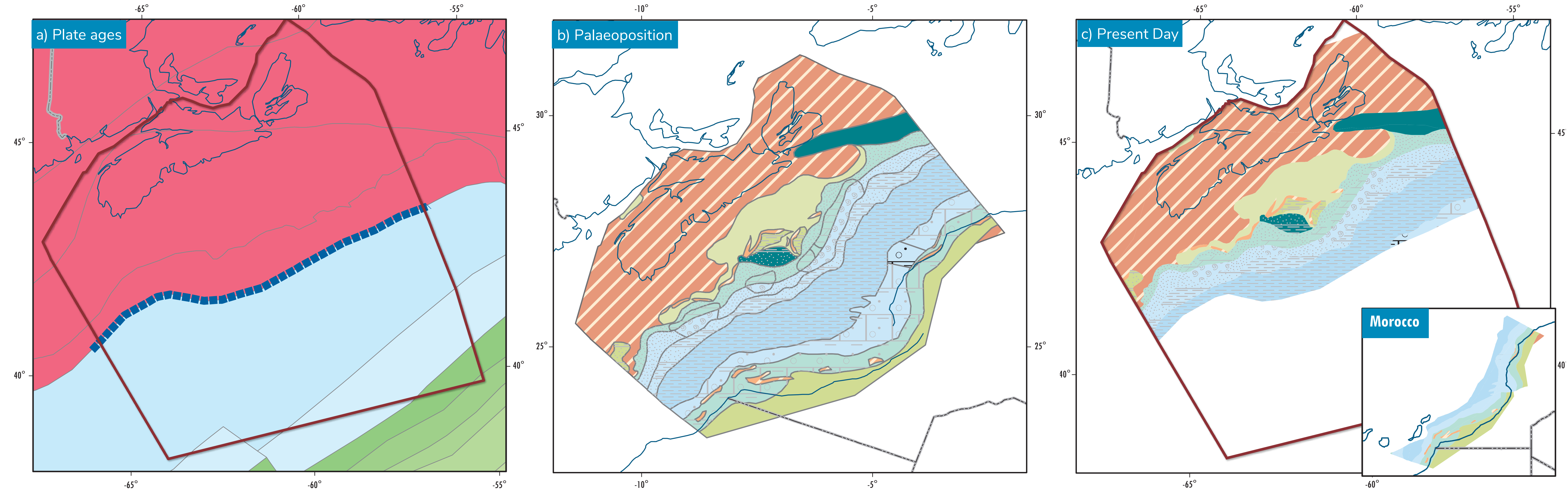

4.2.1 MAPPING/MODELLING RESULTS CONFIDENCE

In the Lower Jurassic strata across the offshore and deep water Scotian Basin, where we have little or no "direct" data in the form of wells, geological models are based on indirect data, such as analogue models from other basins. The construction of the model are supported to a limited extent, but not necessarily confirmed with indirect data, and, therefore, there will be a reasonable degree of uncertainty. According to Otis and Schneidermann (1997), models supported by the presence of indirect data may be described as "encouraging", and in terms of qualitative confidence would allow us to assign a relatively low to moderate risk.

A set of qualitative descriptions of the relative confidence of the modelling and mapping results is shown in Table 4.1. The definition of this chart is empirical and is used to compare uncertainties on different results. For each individual component that produces the source rock risk map, a confidence result is shown for the map.

Analogue or theoretical models confidence chart	
Only possible model applicable for the concerned area. Unfavourable models are impossible	1a
The model is very likely to absolutely certain. Unfavourable models are not impossible	1b
The model is very likely. Only minor chance that unfavourable models can be applied.	2a
The model is likely to very likely. Unfavourable models can be applied.	2b
The model is more likely than all other unfavourable models.	3a
Likely model, however, unfavourable are also likely	3b
Unfavourable models are more likely than applied model.	4a
The model is questionable. and unfavourable models are likely to very likely	4b
The model is unlikely and very questionable. Unfavourable models are very likely.	5a
The model is unlikely and highly questionable. Unfavourable models are very likely to certain.	5b

High Confidence

Low Confidence

Table 4.1 (Left): Mapping and modelling qualitative confidence descriptions (CCOP, 2004).

4.2.2 GDE RISK MAPPING

The risk categorisation for the GDE mapping has taken into account both depositional environment and lithology. The 'favourable' category are areas with the optimum depositional environment conditions for source rocks such as ventilated open ocean on the shelf and slope; and silled basins with the fine-grained sedimentation. While depositional environments that are high-energy with coarse-grained deposition have been categorised as 'unfavourable'. Figure 4.2 shows an example of the risk mapping categorisation for the Toarcian.

Figure 4.2 (Below): Risk mapping categorisation example for the Toarcian GDE.

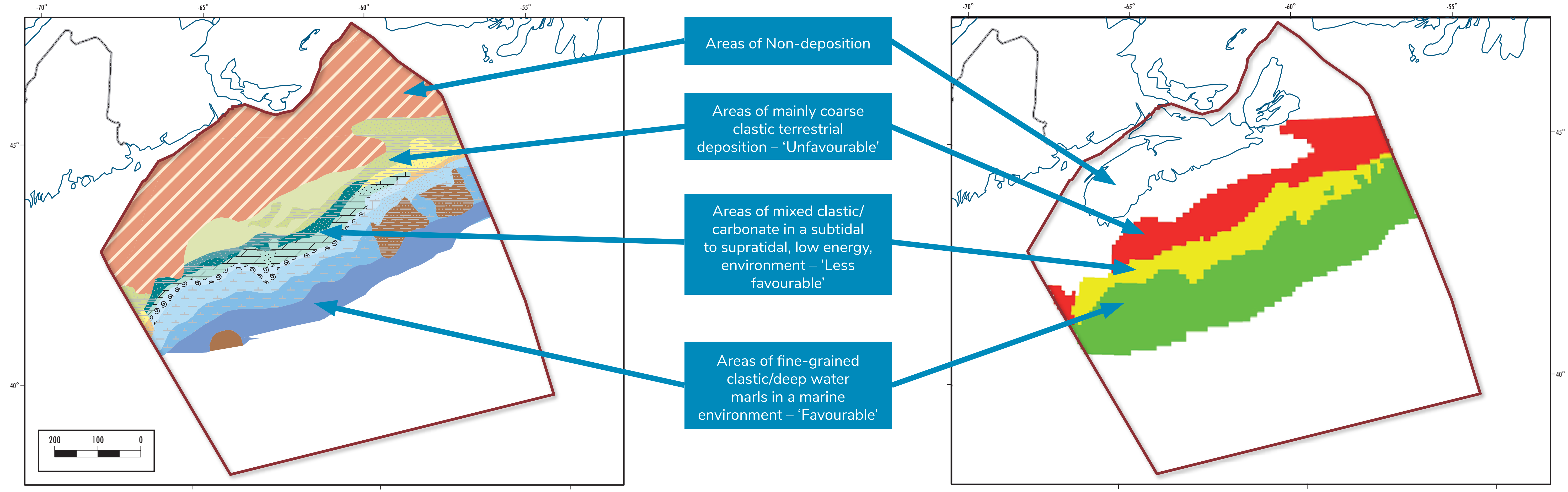

4.2.3 OFP RISK MAPPING

There is no single industry standard of categorising risk values to measured TOC. Many schemes have been developed separately and in parallel in different companies. Classes involving boundaries at 0.5, 1, 2 & 4% are relatively common (Peters & Cassa, 1994; Peters et al., 2005; Baskin, 1997; Cornford, 1998), however some schemes do vary, e.g. Peters & Rodriguez (2017); Curiale 2017; Jarvie, (1991); Law (1999); McCarthy et al., (2011) and Sorkhabi (2016), with variance typically being in the higher value classes. Getech typically uses 6 categories shown in Table 4.2, column 2, these have been grouped into 3 to bring it in line with the proposed 3 categories for this project.

The risk classification needs to honour the model parameters used to generate the TOC and HI maps. Due to the limitations of modern calibration data sets available, a carbon flux cannot be calculated in water depths of <50 m, the OFP model will have set the MTOC (marine TOC) to 1.57% at these depths and applied only TTOC values where present. For this specific region we have a defined oxygen profile that can be used in the risk mapping to provide more clarity in the shallower water, where OFP data is less valid. Therefore, the predicted TOC and O_2 data have been used in conjunction to define risk categories.

According to the Black Sea "PZE" model, everywhere shallower than 40 m is oxic and has been placed in the high risk category, which is thus based on O_2 rather than TOC. This takes precedence where it overlaps with a bathymetry of <50 m deep where a carbon flux cannot be calculated.

The 40-49.99 m depth zone has lowered oxygen in this case, and is thus likely to have slightly better source rock potential than the <40 m zone. Therefore, a medium risk category has been applied in these instances.

The remaining areas that fall within water depths of >50 m use only the OFP model TOC predictions to apply risk categories defined in Table 4.2.

The HI prediction is proportional (non-linearly) with the TOC. Thus, the mapped distribution of the favourable/less favourable/unfavourable categories above should be the same for HI. Therefore, the HI classed in Table 4.2 are directly linked to the limits of the TOC classes.

Once the classification scheme has been defined this can then be applied to the relevant data. As all OFP data is gridded, these grids can be manipulated and reclassified to the relevant risk classes, based on the definitions summarised in Table 4.2. Examples of which are shown in Figure 4.3.

Potential	TOC %	Oxygen zone	HIA equivalent (mgH/gTOC)	Risk mapping value
Excellent	>8	>50 m (TOC risk values take precedence)	>359	Favourable 1
Very Good	4.01-8.00			
Good	2.01-4.00	>40-50 m	150-359	Less favourable 2
Moderate	1.01-2.00			
Fair	0.51-1.00	<40 m	<150	Unfavourable 3
Poor	<0.5			

Table 4.2: Risk classification used for OFP modelling results.

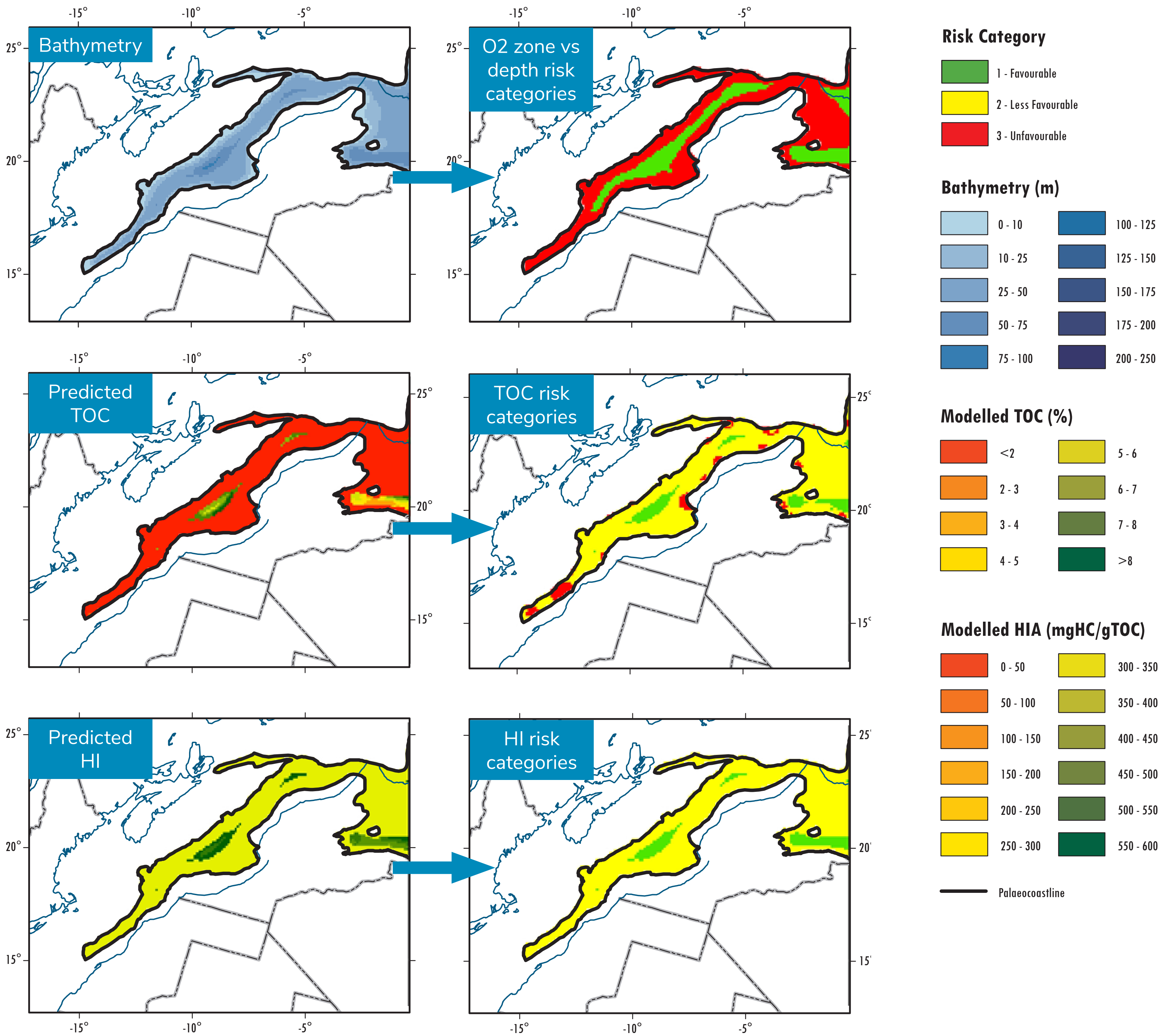

Figure 4.3: Hettangian example of how the risk classification defined in Table 4.2 are applied to the OFP modelling results.

4.3 SOURCE ROCK RISK MAPPING RESULTS

4.3.1 HETTANGIAN

The Hettangian demonstrates some potential for source rock development (Figure 4.4), although the area for favourable conditions is smaller when compared with the other Lower Jurassic intervals.

This is mainly due to water depths being very shallow at this time. Only the deepest central part of the basin falls below 40 m, the PZE depth, with only deepest, most central part reaching ~75m deep.

Although OFP modelling does not cover onshore areas, the GDE mapping suggests limited source rock potential. In the Abenaki, Sable and Huron Sub-basins, playa lake facies are surrounded by low topography.

For source rock facies to be deposited in this environment, the lakes would have needed limited terrigenous input and hydrostatic bottom environments caused by stratification of the water mass. Evidence for the existence of such conditions are inconclusive, however, analysis of oil stains from the Mic Mac J-77 and D-89 wells (Fowler, 2020) demonstrates some evidence of a Lower Jurassic source in this area. Therefore, a medium risk potential has been assigned to these environments.

The other onshore rift basins within the region are unfavourable for source rock development. Leleu et al. (2016) suggest no deep perennial lakes developed, therefore any lakes that may have developed would have been shallow and ephemeral resulting in low preservational potential for organic material. Moreover, many of the onshore grabens were also subsequently eroded.

Figure 4.4 (Below): Hettangian source rock risk.

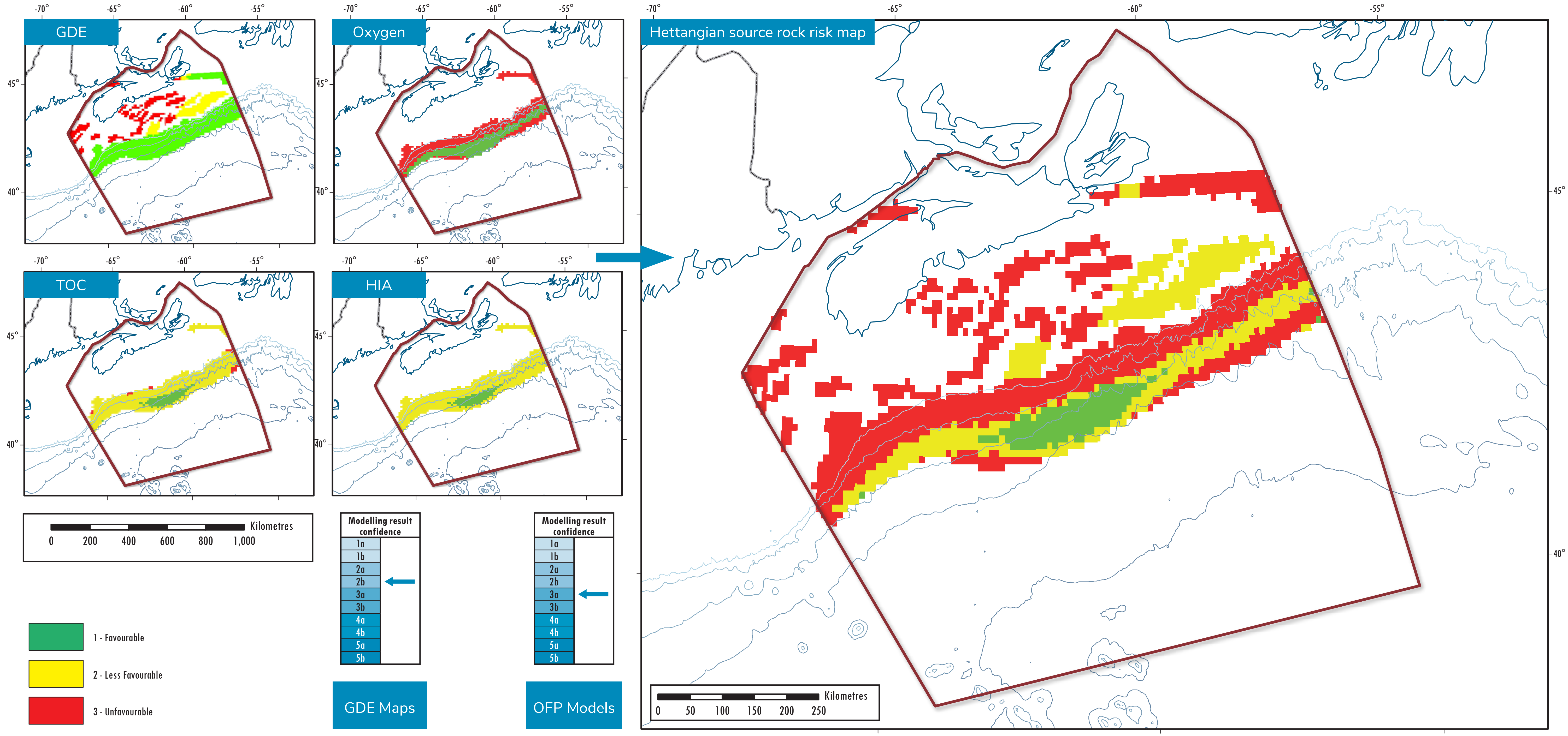

4.3.2 SINEMURIAN

Results of the risk mapping show that the Sinemurian has source rock potential offshore. The less favourable risk assignment along the deepest parts of the basin axis is a result of the sedimentation rate and subsequent CDF flux falling further offshore. TOC values in this central, less favourable, region typically fall between 2.5-3.5%, whereas the more favourable areas surrounding the basin axis are typically just over 4% TOC, hence the more favourable risk categorisation.

On the Moroccan conjugate margin (not visible on this present day risk map), the water depths are predominantly shallower, with the majority of the region not deep enough to fall within the PZE depth, therefore the modelling results are less favourable in this region. This fits well with data from the Mazagan-1 well (MZ-1), where Sinemurian sediments were recovered from the deepest parts of the well; these show little to no source rock potential, with only one very thin TOC rich horizon that is not volumetrically significant to generate economic quantities of hydrocarbons (Fowler, 2018b)

The Tethys Sea had by now encroached the Abenaki, Sable and Huron Sub-basins, however water depth in these sub-basins would have been very shallow (above the PZE depth) with coarse-grained siliciclastic sediments dominating deposition. These conditions would have led to poor preservation of any organic material, therefore this area is unfavourable for source rock development.

Across the remaining Sinemurian onshore area, the source rock potential is poor in the grabens, as only shallow and ephemeral lakes may have existed. These are unfavourable for source rock development, as also seen in the Hettangian.

Figure 4.5 (Below): ***Sinemurian source rock risk.***

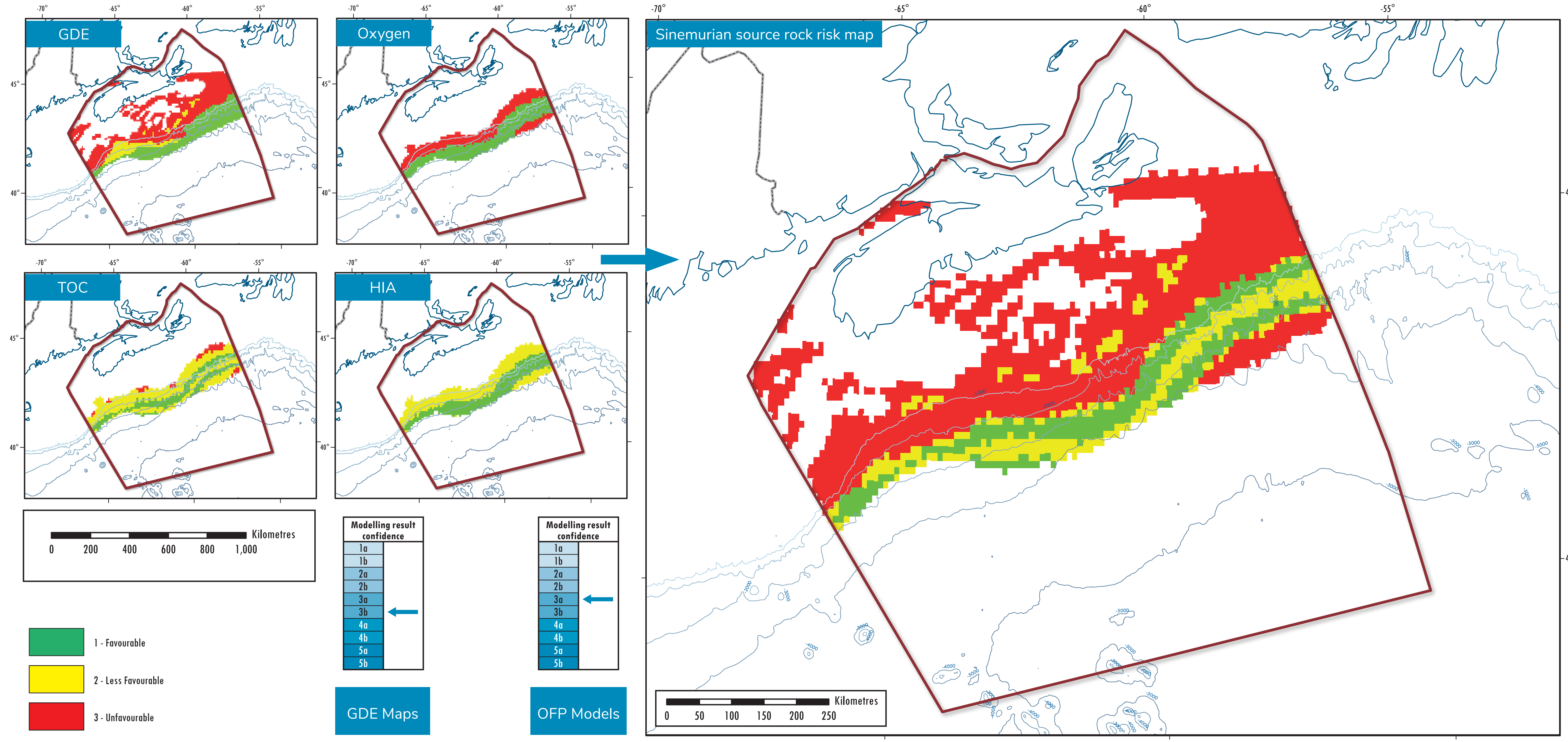

4.3.3 PLIENSBACHIAN

Results of the risk mapping show that the Pliensbachian has source rock potential offshore. As with the Sinemurian, the highest values of predicted TOC sit around the shallower margins of the limit for the PZE zone, with the deeper axis of the basin predicting lower values due to the reduction in sedimentation rate and the CDF reducing distally from the coastline.

Across the Pliensbachian onshore environments, poor preservation of organic matter would exist in the fluvial plain, with much of this area subsequently eroded. In the low energy, high salinity coastal areas away from the clastic input, such as intertidal flats, evaporative embayments, coastal sabkhas and lagoons, fine-grained sediments would have been more favourable to the accumulation of organic material during sedimentation.

These areas have been classified in the medium risk category of 'less favourable' in terms of source rock potential, as there is no direct or modelled data to support a favourable classification. It is important to note that the OFP modelling does not extend over coastal non-marine/transitional areas.

Figure 4.6 (Below): Pliensbachian source rock risk.

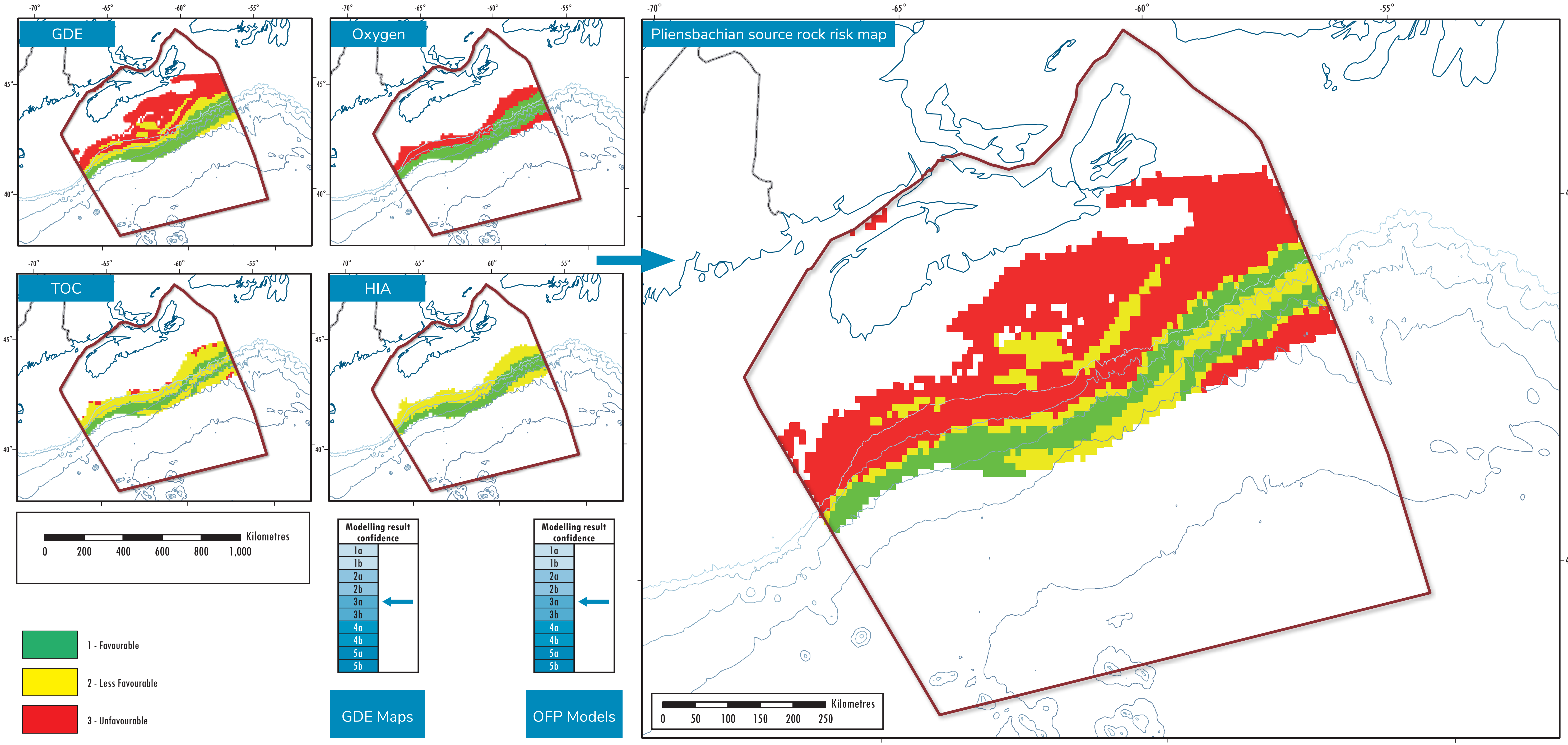

4.3.4 TOARCIAN

Results of the risk mapping show that the Toarcian has source rock potential offshore. As this marks the onset of an early stage mid-ocean ridge formation, the basin axis sits directly on the COB. The furthest outboard, less favourable, region marks the fall in sedimentation and CDF associated with distance from the palaeocoastline.

The expansion of the more proximal shelf into the PZE zone (where the favourable classification is on the oxygen risk map) has generated a thicker band of favourable conditions along the margins of the PZE. This is where oxygen conditions, sedimentation rates and CDF are most likely to produce the richest organic matter deposition in the marine environment.

Across the Toarcian onshore area, poor preservation conditions for organic matter would have existed in the fluvial plain. Additionally, much of this area was subsequently eroded. As in the Sinemurian, but larger in extent, low energy, high salinity coastal areas away from the clastic input, have been classified less favourable in terms of source rock potential, again due to the lack of direct or modelled data to support a favourable classification.

Figure 4.7 (Below): Toarcian source rock risk.

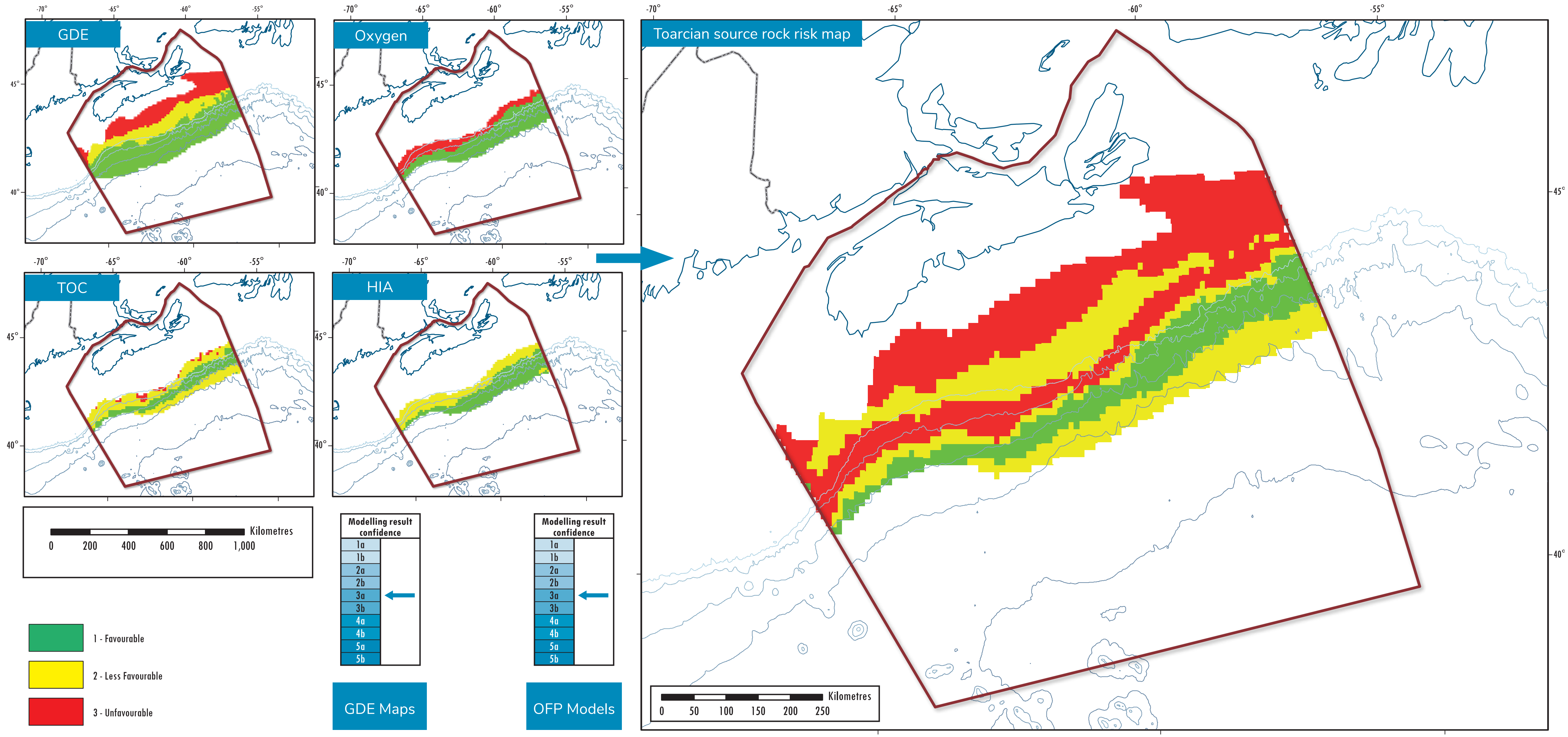

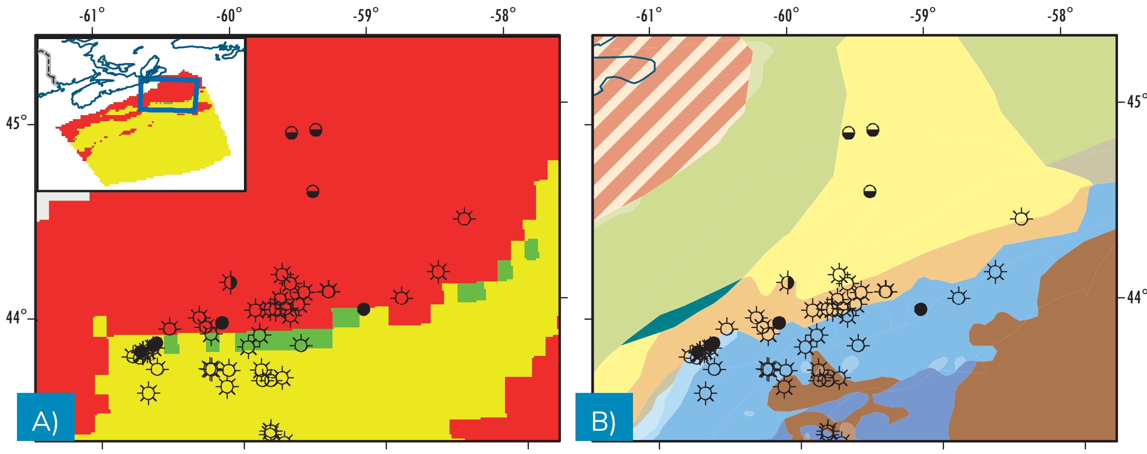

4.3.5 TITHONIAN

Results of the risk mapping for the Tithonian (Figure 4.8) shows only a very limited favourable area for source rock potential. The areas of low risk for the Tithonian are placed across the delta front area of the Sable Delta where Tithonian source rocks have been observed in several wells (Figure 4.9). A second area of low risk is also found across the delta front area of the Shelburne Delta.

Across the rest of the offshore area, the source rock risk mapping result indicates less favourable source rock conditions. This is due to relatively lower predicted TOC and HIA (in the modelling results). However, this does not necessarily preclude the possibility of source rock development, only that these lower TOC and HIA values would equate to moderate source rock potential. While evidence is circumstantial in that no Tithonian source rock has been penetrated in present day deep water, an example of this is the Annapolis discovery.

The assumption for this discovery is that the source of the condensate is of Tithonian age and based on the indirect evidence of the character of the fluid sample being very similar to other Tithonian sourced condensates discovered on the shelf, and that 3D petroleum systems modelling show that any source rock deeper than Tithonian is far too deep present day to be a valid source (Beicep-Franlab, 2016).

Figure4.9 (Left):Tithonian source rock risk map (a) and GDE (b) across the Sable delta where there are known discoveries and observed Tithonian source.

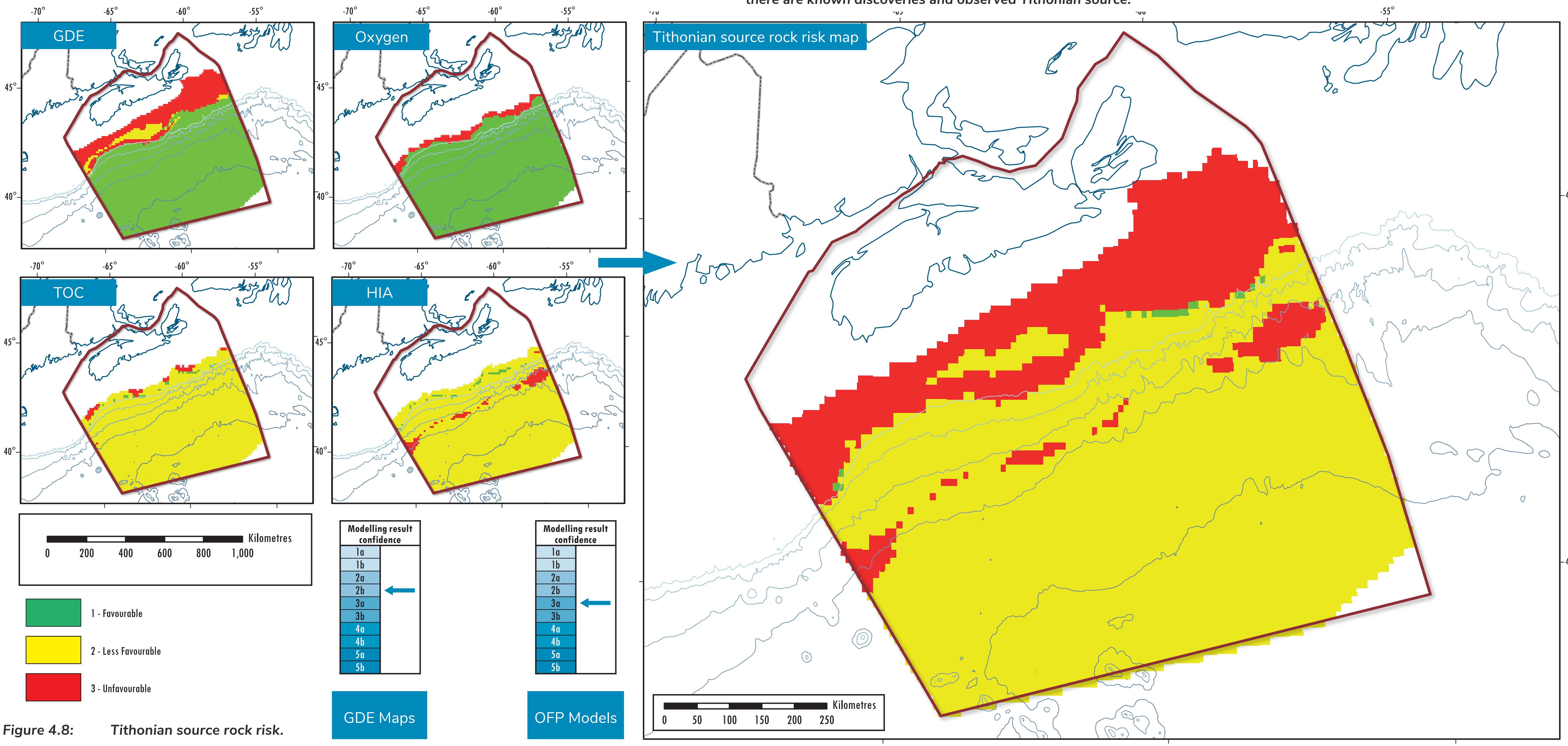

Figure 4.8: *Tithonian source rock risk.*

Across the shelf break there is a very thin band of single cells of high TOC values >4% with some values of >5% around the sable delta (as shown in Figure 4.9). Such a minimal spatial extent of high TOC and HI values are the result of the geometry of the offshore region during the Tithonian. The inboard region consists of a very shallow carbonate platform <40 m deep. This is bounded by a steep foreslope, where water depth dramatically drops to between 1000-2000 m.

As the sedimentation rate and CDF are inherently linked to depth, productivity and distance from coastline, the OPF model will predict significant reduction in sedimentation rate and CDF in deep marine settings, as observed in Present Day marine data.

It is also important to note that the PZE oxygen scenario used in the modelling was devised and considered most suitable for the Lower Jurassic. In the Tithonian, the geography and oceanography has changed from a restricted narrow seaway to an fully open marine setting. Therefore, the modelling results will not be as appropriate for this scenario.

4.4 SOURCE ROCK POTENTIAL RISK MAPPING ANALYSIS

Well data has indicated evidence for a Tithonian source rock deposited in a deltaic environment and contains Type III-II organic matter in the Sable Island area, which the source rock risk map for the Tithonian also highlights as favourable. However, away from the Sable Island area, evidence is less conclusive on how widespread this source rock is. Results from our source rock risk map suggest that source rock potential across most of the Scotian Basin were not overly favourable. An objective of both the Cheshire and Monterey Jack Wells was to penetrate potential Upper Jurassic source rocks. Unfortunately, no oil-prone source rocks were penetrated in either well (Fowler, 2018a). This is not entirely inconsistent with our medium ('less favourable') category on the risk map, as we have not taken into account if there was any sufficient accommodation space or any post depositional process that may have effected source rock development. Indeed, in the Cheshire Well, the Lower Tithonian interval is not represented, as there appears to be an unconformity between middle Tithonian and Kimmeridgian aged sediments, and the whole Tithonian section is very thin (Parthasarathy et al., 2017).

As shown in the previous results section, all four lower Jurassic intervals have favourable conditions for source rock development. Figure 4.10 shows the sum of stacking the "favourable" (green) areas of the four Lower Jurassic intervals. Spatially, these Lower Jurassic horizons are mainly situated above each other, forming a "sweet spot" optimum of multiple intervals that, at the time of deposition, had favourable conditions for source rock development. It does not take into account if there was sufficient accommodation space for sediments to accumulate, or for any post- depositional process that may have perversely (or conversely) affected source rock development and preservation. Geographically, the "sweet spot" is situated beyond the Present Day shelf area. In the east, this area lies in <1,000-3,000 m water depth. in central areas, the sweet spot lies in deep waters of 2,000-4,000 m, but also has all four potential Lower Jurassic source horizons (Figure 4.10). In the western area, the sweet spot is narrower and still lies in relatively deep water. Only a few exploration wells have been drilled in the vicinity of the area where all four horizons overlap, of which, none have penetrated the Lower Jurassic.

As basin modelling was not within the scope of this study, maturity and expulsion data was taken from the Beicep-Franlab PFA studies (2011; 2016). The results of the basin modelling have been overlain onto the Lower Jurassic source rock presence interval map (Figure 4.11). Western and central areas of the Lower Jurassic sweet spot are situated where a potential Lower Jurassic source horizon is oil mature and has a transformation ratio of >10% at Present Day (termed low risk by Beicep-Franlab, 2011). This also coincides with the same area of the tight isotope group of piston-core seeps (of suggested Lower Jurassic origin).

Within the PFA studies (2011; 2014; 2015; 2016; 2019a; 2019b), basin modelling for the lower Jurassic assumed a TOC of 5%, and included areas up to the Present Day water depth of 4,000 m. The modelling did not extend into very deep waters as this area was considered unlikely to be of commercial interest. Renewed petroleum systems modelling of the Scotian deep water area could use the predicted TOC and HIA ranges from the OFP modelling conducted in this study.

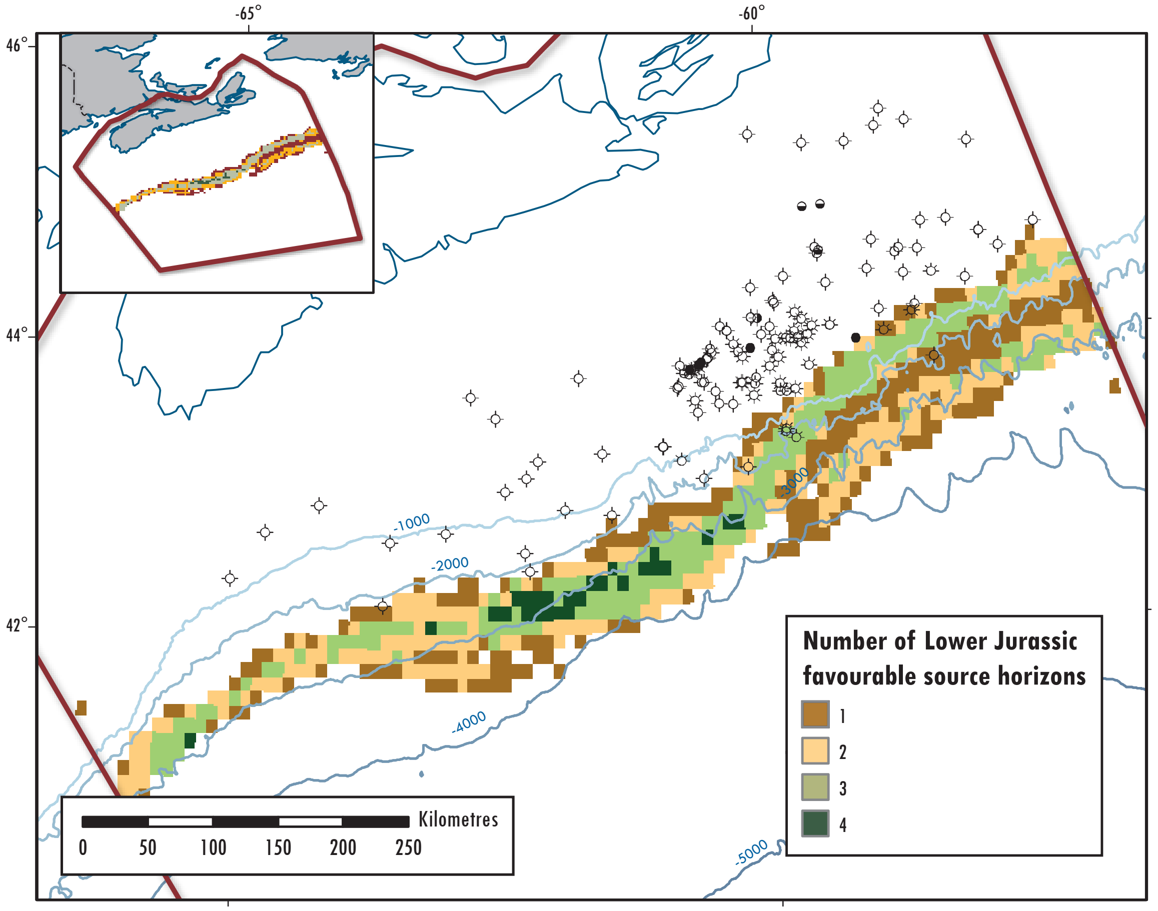

Figure 4.10 (Left): Lower Jurassic sweet spot optimum of favourable conditions.

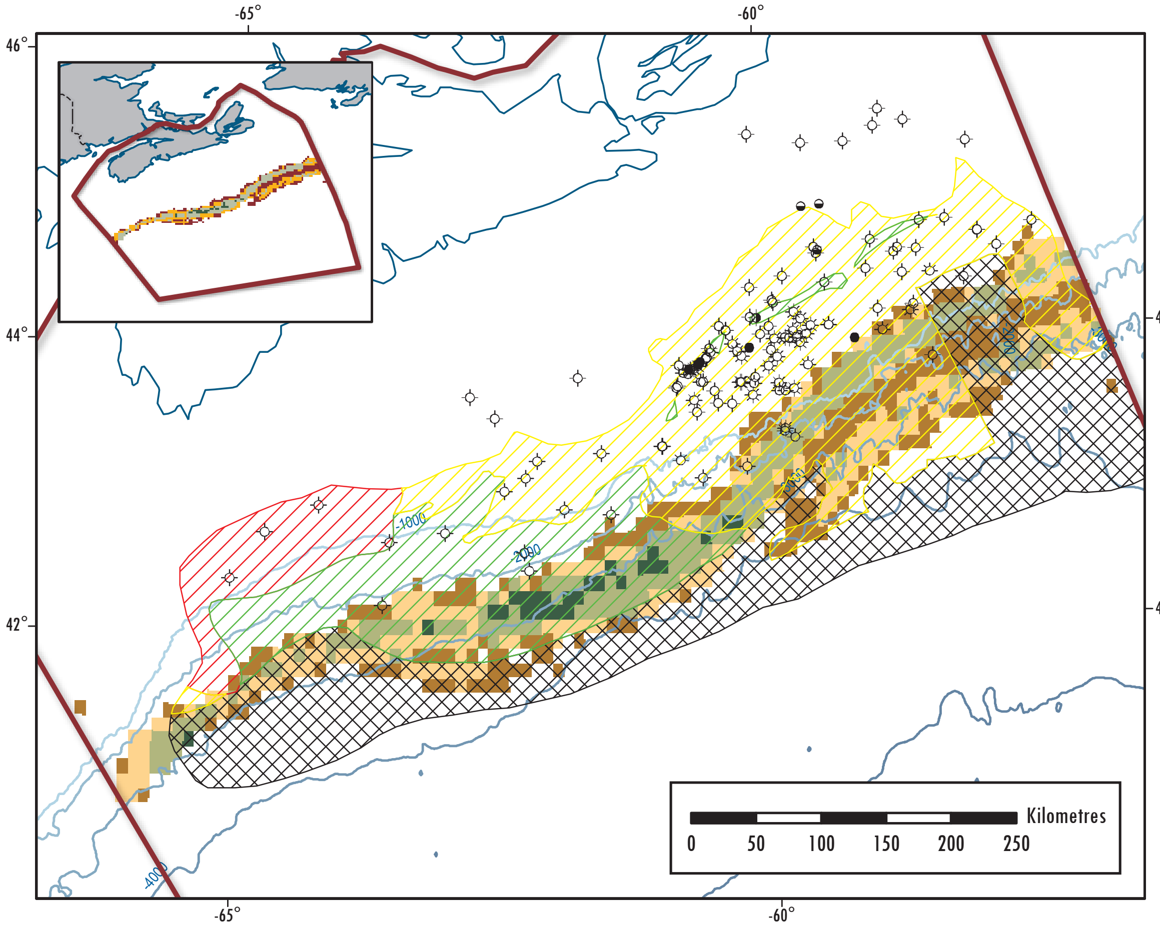

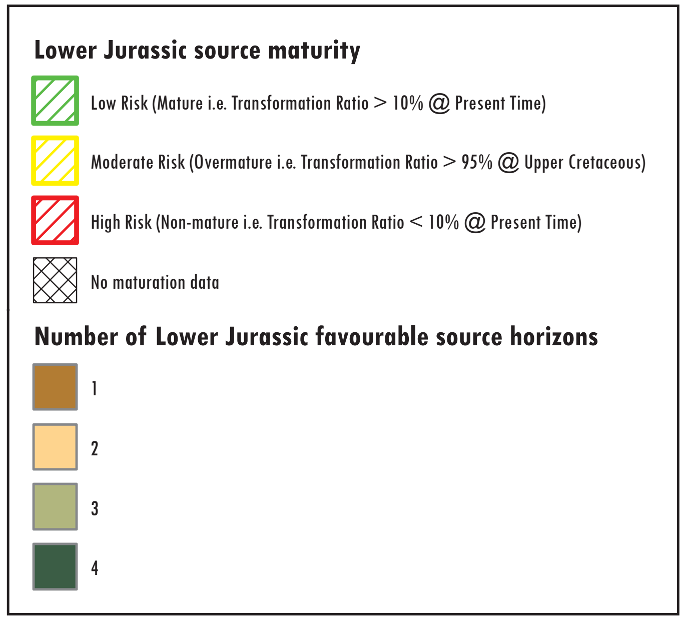

Figure 4.11 (Above): Lower Jurassic sweet spot optimum of favourable conditions and source rock maturity.

The results of the source rock risk-mapping show the extent at the time of deposition and does not account for any post-depositional processes, such as the role of allochthonous salt, which has probably had a significant effect on source rock potential, preservation and maturity. From the Middle Jurassic to the Paleogene, widespread salt deformation and expulsion of salt occurred across the slope area of the Scotian margin, creating a wide range of detached and undetached allochthonous salt bodies. The allochthonous salt structures can be split into three provinces; Diapiric, Canopy and BSW (Banquereau Synkinematic Wedge) as shown in Figure 4.12.

Major salt movement was initiated post Middle Jurassic with the resulting allochthonous salt having possibly had an effect on accommodation space during Tithonian deposition. This would also have impacted all five Jurassic horizons in terms of post-depositional preservation and migration pathways. A large portion of the Lower Jurassic "sweet spot" from this study lies in the Diapiric province, therefore any of the five Jurassic intervals could have potentially been eroded as a result of salt piercement. Conversely, during the Tithonian, mini-basins that may have formed between diapirs (Figure 4.13) may well have experienced increased anoxia, and accommodation space and, therefore, potentially improved source rock depositional conditions.

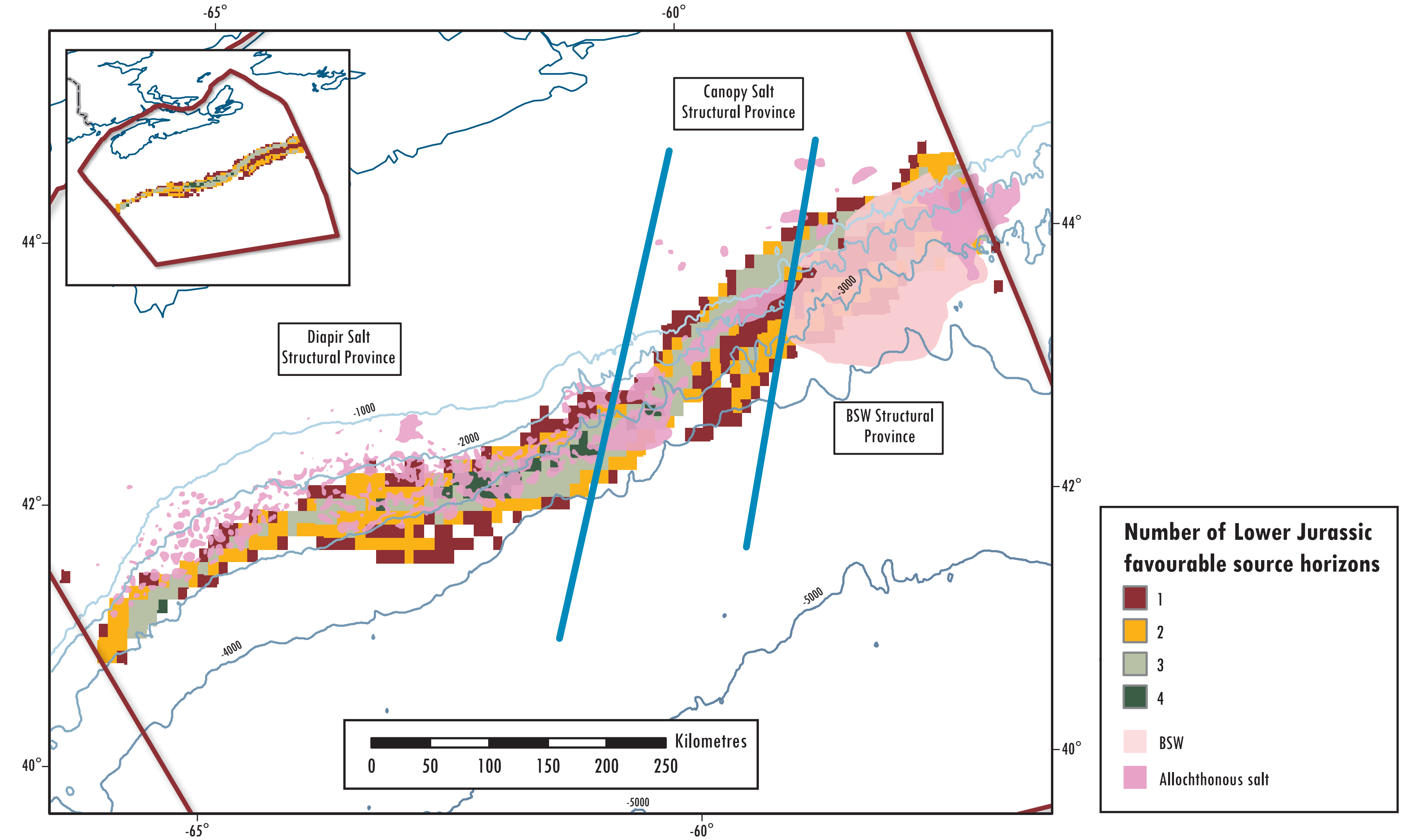

Figure 4.12: Lower Jurassic sweet spot optimum of favourable conditions allochthonous salt.

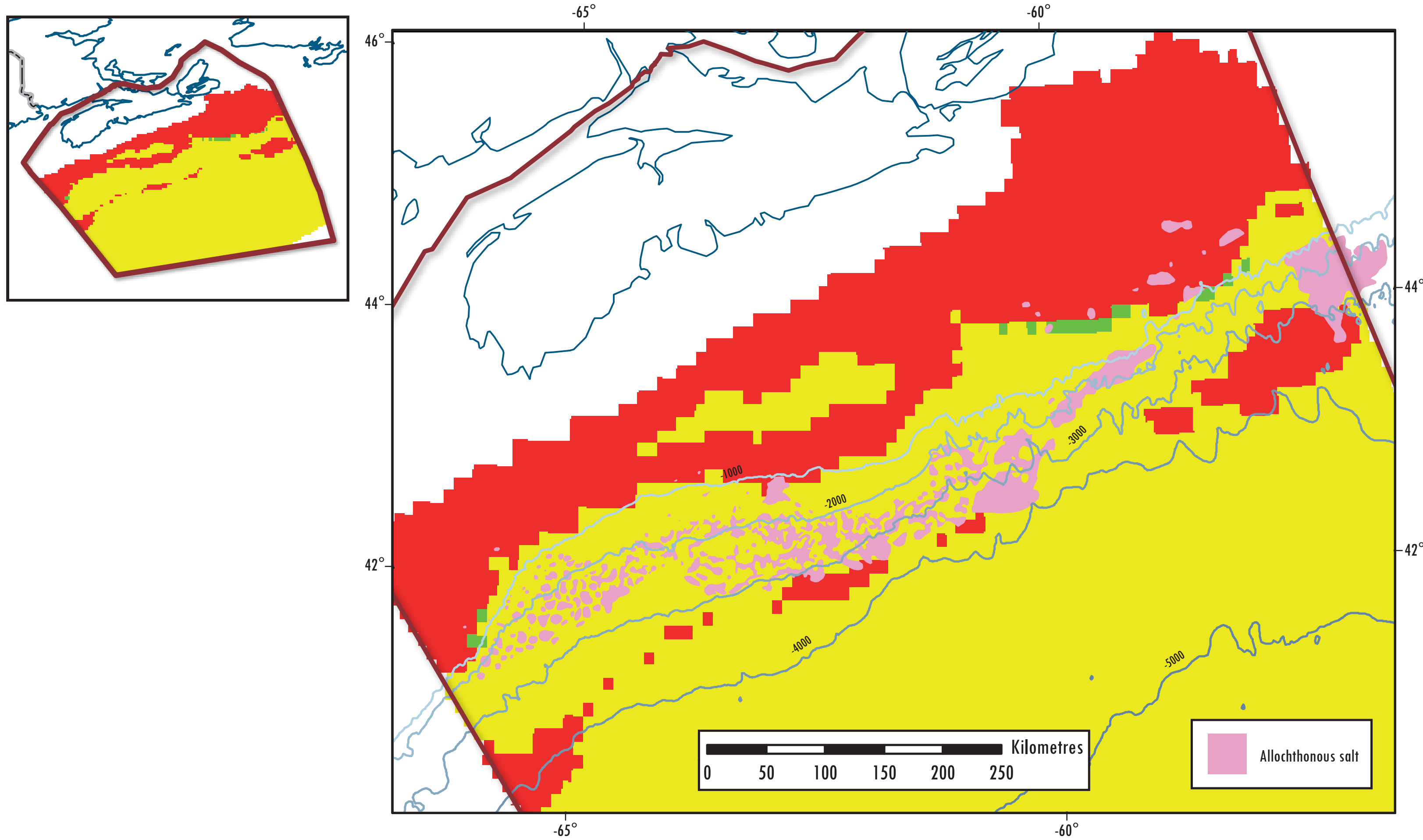

Figure 4.13: Tithonian source risk map and allochthonous salt.

The allochthonous salt would have also created barriers for migration of any hydrocarbons from the Jurassic. In the Diapiric Salt Province (Figure 4.12), the migration of Jurassic hydrocarbons from the salt diapirs structural province would be complex, with the diapirs creating drainage divides. It would, therefore, be unlikely for long-distance migration to have transpired. As a consequence, any of the four Lower Jurassic horizons are unlikely to have charged any plays to the north of the diapiric province, including any prospects situated on the Present Day shelf and upper slope. The existence of relatively permeable faults along the active salt bodies would have also increased and aided vertical migration (Beicep-Franlab, 2011), and could be responsible for the presence of seeps in this area, including the piston cores seep described earlier. Allochthonous salt would also create drainage divides for migration pathways in the Canopy Salt Structure Province, as diapirs and feeders to the canopies are present. The canopies themselves would have also hindered any further vertical migration. However, long distance lateral migration may be possible on the Present Day upper slope region, although this will be dependent on effective carrier beds.

The BSW province represents the area of an Upper Jurassic to Early Cretaceous landslide gliding on top of an allochthonous salt tongue. Ultimately, the salt at the base of this mass transport system would have hindered any vertical migration.

4.5 SOURCE ROCK POTENTIAL RISK MAPPING SUMMARY

- The aim and objectives of this study was to predict the distribution of Tithonian and early Jurassic (Toarcian, Pliensbachian, Sinemurian, Hettangian) source rocks offshore Nova Scotia, based on biogeographic principles derived from modern environments, and palaeoenvironmental interpretations derived from palaeogeographic mapping, and Getech's proprietary organic facies prediction (OFP) modelling.
- Source rock potential risk maps have been constructed by taking into account the output of these models. The resulting maps will provide a spatial understanding of where favourable conditions existed for source rock development **at the time of deposition.**
- Four potential modern analogues were used to model organic facies: Red Sea, Gulf of California, Saanich and Black Sea "PZE" scenarios. Of these scenarios, the latter Black Sea "PZE" scenario was considered the most appropriate. The results from this scenario were applied to the risk maps, along with the gross depositional environments.
- A suitable risk categorisation scheme was selected and the gross depositional environment maps, along with the Black Sea "PZE" model results of organic content (TOC) and richness (HIA) values and oxygen levels were assigned risk categories based on this scheme.
- Although well data has indicated a Tithonian source horizon in the Sable Island area, away from this area, the Tithonian risk map shows less favourable conditions for source rock development across the rest of the basin due to relatively low predicted TOC and HIA (in the modelling results) and are the result of the geometry of the offshore region during the Tithonian. Although the TOC and HI results are lower than the classified "favourable" areas these may still equate to moderate source rock potential within that region.
- Lower Jurassic source horizon recognised across the North Atlantic, along with inconclusive well observations within the Scotian Basin, has led to considerable supposition on the occurrence of a more oil prone Lower Jurassic source rock contributing to hydrocarbons in the Scotian Basin.
- Results from the risk map show that all four Lower Jurassic interval show favourable conditions for source rock development. The Hettangian has the smallest area of favourable conditions as the water depths were too shallow and mainly within the oxic zone, as a result of it being in the early development of the Hispanic Corridor.
- When stacking the spatial areas of the most favourable (green) areas of the Lower Jurassic intervals, this forms a "sweet spot" optimum area of approximately 57,000 km² of multiple intervals that, at the time of deposition, had favourable conditions for source rock development.
- Much of this Lower Jurassic "sweet spot" is beyond the Present Day 2,000 m water depth, as highlighted in Figure 4.14.
- Although basin modelling was not within the scope of this study, overlaying Lower Jurassic source rock maturity data from Beicep-Franlab (2011; 2016) studies over the Lower Jurassic "sweet spot" shows that the best potential for oil maturity is across the central and western parts (Figure 4.14). This area of peak maturity also lies within the diapiric salt structure province, so migration pathways would have been limited to mainly vertical.
- Absence of long distance lateral migration would have more than likely precluded petroleum charge to any accumulation situated on the Present Day shelf and upper slope regions.
- The resultant risk maps show the extent of favourable to unfavourable conditions for source rock deposition but does not take into account if there was sufficient accommodation space for sediment accumulation, any post-depositional process that may have perversely affected source rock development and preservation, and maturity of each source interval. Additionally, potential thickness of any source horizon cannot be clearly defined without well control. When these extra factors are added, the extent of a productive (and effective) source horizon will be smaller. Some examples of these are demonstrated in Figure 4.14, with Lower Jurassic maturation and allochthonous salt overlain onto the Lower Jurassic "sweet spot." A more detailed examination of these factors would further increase our knowledge of the full potential and extent of a lower Jurassic source.

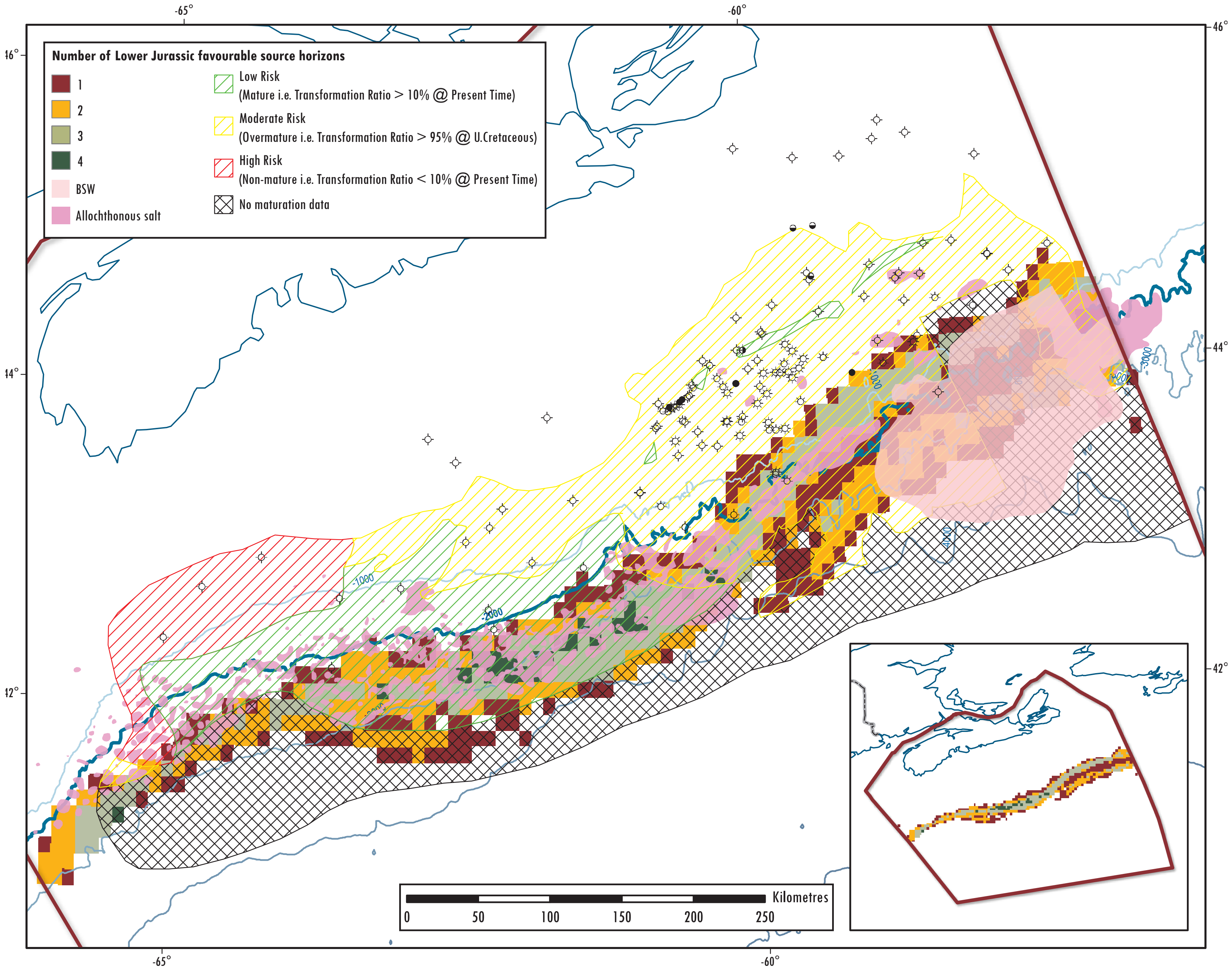

- There is potential for mid Cretaceous turbidites and Middle Jurassic Carbonates (Scataire Formation) prospects to sit above the central area of the Lower Jurassic "sweet spot." Further constraint could be gained from the analysis of these potential plays in terms of their viability as a fully working play.
- Although OFP modelling does not cover the palaeo-onshore areas, the GDE mapping suggest limited favourable conditions for source rock development. The Abenaki, Sable and Huron Sub-basins playa lake that formed part of the Hettangian salt basin, along with Sinemurian and Toarcian low energy, high salinity coastal areas away from the clastic input, could provide limited favourable conditions for source rock development. The other onshore rift basins are unfavourable for source rock deposition, as any lakes that developed were shallow and ephemeral and preservation of organic material would have been low.

Figure 4.14: ***Lower Jurassic sweet spot optimum of favourable conditions summary. The 2,000 m Present Day bathymetry contour is highlighted to show when the main Lower Jurassic "sweet spot" lies.***

4.6 REFERENCES

Baskin, D. K. (1997). Atomic H/C ratio of kerogen as an estimate of thermal maturity and organic matter conversion: AAPG Bulletin 81 (9), pp. 1437–1450.

Beicip-Franlab (2011). Play fairway analysis atlas, offshore Nova Scotia Canada. Offshore Energy Research Association (OERA).

Beicip-Franlab (2014). Play Fairway Analysis: Laurentian Sub-basin, Canada. Offshore Energy Research Association (OERA).

Beicip-Franlab (2015). Play Fairway Analysis: SW Nova Scotia Expansion Atlas. Offshore Energy Research Association (OERA).

Beicip-Franlab (2016). Play Fairway Analysis: Central Scotian Slope Atlas. Offshore Energy Research Association (OERA).

Beicip-Franlab (2019a). Play Fairway Analysis: Shelburne Sub-Basin Play Fairway Analysis Update. Offshore Energy Research Association (OERA).

Beicip-Franlab (2019b). Nova Scotia-Morocco Conjugate Biostratigraphy Project. Offshore Energy Research Association (OERA).

CCOP (2004). The CCOP Guidelines for Risk Assessment of Petroleum Prospects.

Cornford, C. (1998). Source rocks and hydrocarbons of the North Sea. In: Glennie, K. W. ed., Petroleum geology of the North Sea: basic concepts and recent advances: Oxford, Blackwell, pp. 376–462,

Curiale, J. A. (2017). Total Organic Carbon (TOC). In: Sorkhabi, R. ed., Encyclopedia of petroleum geoscience. Springer, pp. 1–5.

Fowler, M. (2020). APT report “Geochemical Evidence for Multiple Source Rocks on the Scotian Shelf https://oera.ca/sites/default/files/2021-01/scotian-shelf-oils-geochemistry-final-report.pdf

Fowler, M. (2018a). Forensic Geochemical Study of Deepwater Shell Wells – Cheshire L-97 and Monterey Jack E-43, Proprietary report for OERA by the APT Group.

Fowlerm M. (2018b). Jurassic Oils and Source Rocks of Morocco. Applied Petroleum Technology (APT) AS Report.

Jarvie, D. M. (1991). Total organic carbon (TOC) analysis. In: Merril, R. K., ed., Source and migration processes and evaluation techniques: AAPG, Treatise of petroleum geology. Handbook of petroleum geology, pp. 113–118,

Law, C. A. (1999). Evaluating source rocks. In: Beaumont, E. A. & Foster, N. H., eds., Exploring for oil and gas traps: AAPG, Treatise of petroleum geology. Handbook of petroleum geology, pp. 1–41.

Leleu, S., Hartley, A. J., van Oosterhout, C., Kennan, L., Ruckwied, K. & Gerdes, K. (2016). Structural, stratigraphic and sedimentological characterisation of a wide rift system: The Triassic rift system of the Central Atlantic Domain. Earth and Planetary Science Reviews 158, pp. 89-124.

McCarthy, K., Rojas, K., Niemann, M., Palmowski, D., Peters, K. & Stankiewicz, A. (2011), Basic petroleum geochemistry for source rock evaluation: Oilfield Review 23, (2), pp. 32–43.

Otis, R. & Schneidermann N., (1997). A process for evaluating exploration prospects. AAPG Bulletin, 81, (7), pp. 1087-1109

Parthasarathy, R., Merker, A.,Tremolada, F., & Gogin, I. (2011). Routine and Wellsite Biostratigraphic Analysis of the Monterey Jack E-43/E-43A Wells, License EL 2424, Shelburne Basin, Offshore Nova Scotia, Canada. Proprietary report for Shell Canada Energy by the RPS Group

Peters, K. E., & Cassa, M. R. (1994). Applied source rock geochemistry: AAPG Memoir, 60, pp. 93–120.

Peters, K. E., & Rodriguez, L. B. (2017). Programmed temperature pyrolysis. In: Sorkhabi, R. ed., Encyclopedia of petroleum geoscience: Springer, Earth Science

Peters, K. E., Walters, C. C. & Moldowan, J. M. (2005). The biomarker guide. Volume 1: biomarkers and isotopes in the environment and human history: Cambridge University Press, 471 p.

Sorkhabi, R. (2016). Back to source rocks: Part II: GEO ExPro Magazine, 13 (6), pp. 22–26.

APPENDIX 1: COASTAL UPWELLING

A1.1. INTRODUCTION

Coastal upwelling occurs when Ekman transport (i.e. where wind-driven currents diverted by the Coriolis effect cause the net movement of ocean surface water at right angles to the wind) takes place away from the coast. As the surface water moves away from the coast, it is replaced by nutrient-rich bottom water. Areas of coastal upwelling are typically characterised by high productivity and are associated with the deposition of organic-rich sediments.

The importance of high primary productivity associated with upwelling as a factor in the origin and distribution of organic-rich marine sediments has been recognised since at least the 1930s (Trask, 1934). Not only did coastal upwelling become one of the key modern analogues for source rock deposition during the 1980s, its predictable relationship to wind patterns and the Coriolis force means that it also became the primary palaeoclimatological-palaeogeographic approach to large scale modelling of marine source rock distribution (e.g. Barron, 1985; Barron & Moore, 1994; Kruijs & Barron, 1990; Miller, 1989; Moore et al., 1993, 1995; Parrish, 1982, 1995; Parrish & Curtis, 1982; Scotese & Summerhayes, 1986). The primary focus of this effort has been the coastal upwelling associated with the major Eastern Boundary Upwelling Systems (EBUS), as seen in the modern California Current, Humboldt Current (Peru-Chile), Canary Current (northwest Africa) and Benguela Current (Namibia), plus monsoon-related upwelling, as seen in the modern Arabian Sea. These areas appear to be the ones most associated with the SiPC association in the fossil record (i.e. sediments enriched in biogenic silica, phosphorus and organic carbon). There has been less focus on upwelling linked to equatorial divergence as this process is not linked to coastlines; instead, it occurs mostly over deep oceanic waters, and its relevance to effective ancient source rocks (i.e. those likely to reach maturity and whose generated hydrocarbons are likely to encounter accessible potential reservoirs) has yet to be clearly demonstrated.

For coastal upwelling to occur at all, there are two essential oceanographic conditions that must be present (Figure 1):

- Vertical upward movement of stratified nutrient-rich bottom water into the mixed ocean layer (MOL); this results in nutrient-rich bottom water being brought into the photic zone.
- Horizontal movement of the surface water in an offshore direction; this draws mixed surface water away from the coast and redeposits the organic matter in stratified water offshore.

Furthermore, these two essential conditions must coexist during the same part of the year; if they do not, then coastal upwelling will not occur. For example, if one of the conditions existed from January to June and the other condition only existed from July to December, an annual average of these conditions would show moderate values for coastal upwelling; however, this would actually be a false result as no coastal upwelling would occur at all if there was no cross-over between the two essential conditions being in place at the same time of the year. Therefore, it is crucial to assess where these conditions exist on monthly basis.

Two additional oceanographic conditions also need to be considered as they have a direct impact on coastal upwelling and can restrict it: latitudinal light limitation (as upwelling without light will not be expressed in palaeoproductivity) and sea ice coverage (as sea ice will both inhibit light penetration and reduce the depth of the photic zone).

This document will outline the technical theory used to create Getech's Coastal Upwelling Model, describe the model principals and the methodology used, and give examples of the data that the model produces.

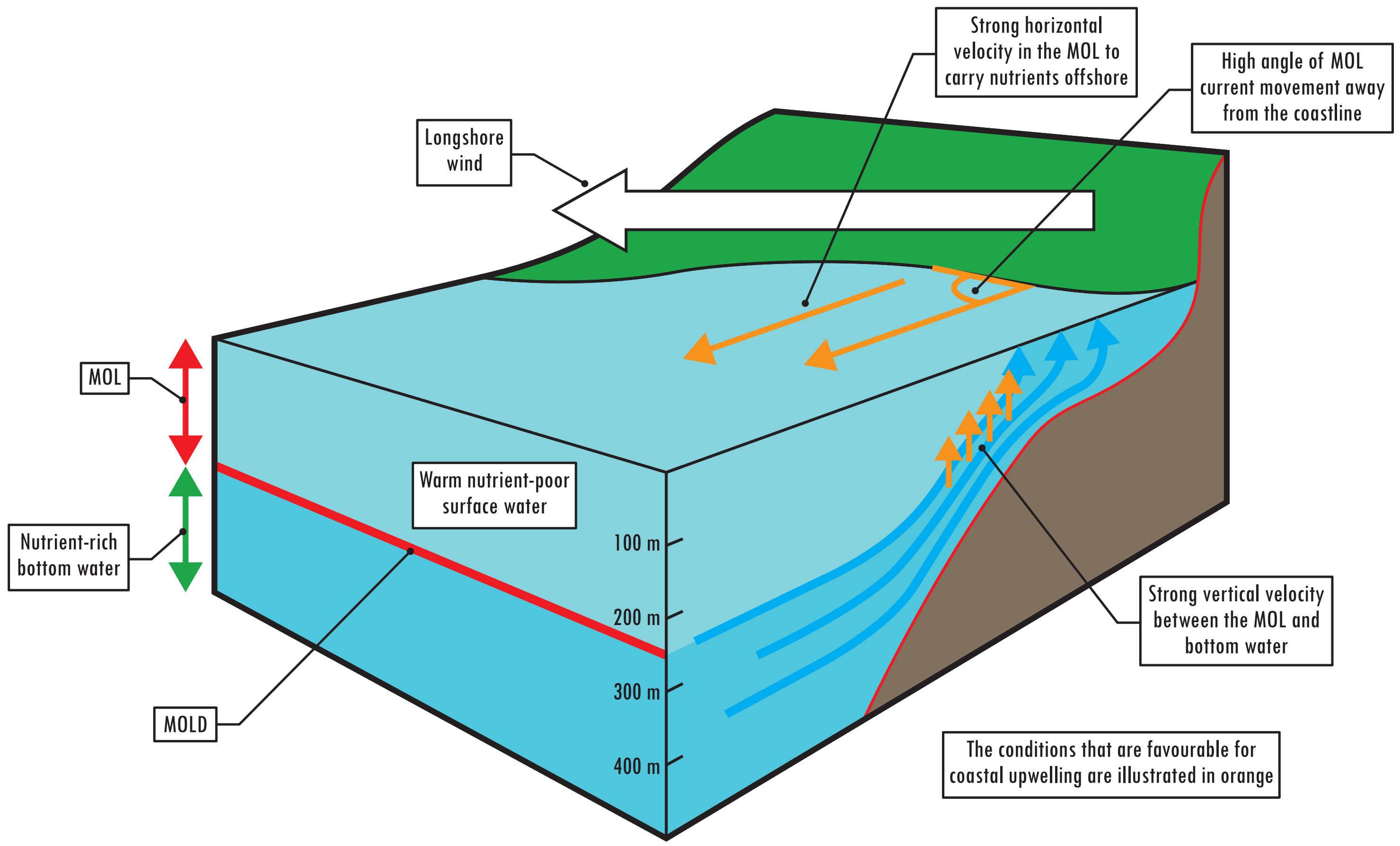

Figure A1.1: The key oceanographic conditions required for effective coastal upwelling to take place.

A1.2. THE MODELLING PRINCIPALS USED TO DEFINE THE COASTAL UPWELLING SIGNAL

The four key oceanographic conditions that provide the best potential for coastal upwelling to occur are as follows:

1. The vertical upward movement of stratified water across the MOL: This is critical as it supplies stratified nutrient-rich bottom water to the photic zone, allowing organic matter to be produced in this zone.
2. An offshore current: The movement of the surface water in an offshore direction is important as it draws mixed surface water away from the coast and redeposits the organic matter in stratified water offshore.
3. Daylight length of 8 hours or more per day: This amount of light is enough to allow photosynthesis to occur in phytoplankton.
4. Less than 50% sea ice cover: Sea ice cover of 50% or less does not restrict light penetration into the photic zone; therefore, photosynthesis in phytoplankton is not inhibited by this level of sea ice cover.

The width of the upwelling-influenced zone in classic modern coastal upwelling areas (e.g. the areas affected by the Benguela, Canary, Humboldt and California Currents) varies spatially and temporally and can extend up to 300 km offshore (e.g. Hagen et al., 2001). Within this zone, the upwelling signal will decrease with distance offshore ('downstream'), as the frequency of events that extend beyond a given distance decreases (although those events that extend furthest will be more intense). The mixed layer nutrients become progressively depleted by plankton growth with time and downstream distance, and the impacts on the sediment record will be diminished by any increase in water depths that would result in decreased carbon delivery fluxes. It is therefore necessary to apply a spatial mask as this lets us focus our upwelling predictions more specifically on coastal or shelf-break zones.

Based on the above observations, a 250 km wide upwelling zone has been defined. We could simply use the coastline to define this zone however, in the case of palaeogeographic configurations with wide shallow shelves where the water is too shallow to be stratified, the locus of upwelling will be displaced offshore to the shelf/slope boundary, which may lie more than 250 km from the coastline, and thus would be excluded from consideration if a fixed distance of 250 km was used. We have thus utilised a 'pseudo-coastline' based upon the boundary between stratified and mixed waters (i.e. where the depth becomes deeper than the ocean mixed layer (MOLDcor). This boundary will vary seasonally and with bottom gradient, the width of the potential upwelling zone being defined by its spatial range, the woffshore limit where the depth is always >MOLD, and the onshore limit where it is always <MOLD (i.e. during all 12 months). At any one time (month), the upwelling front will be located along the landward edge of the stratified zone, but with its influence extending offshore. This is undoubtedly a simplification but is probably a realistic one given the 0.5° spatial resolution of the GCM. Lateral variation within the zone of potential upwelling is not explicitly taken into account, other than that produced by the lateral annual migrations of the edge of the stratified zone.

There are several important caveats to this approach of modelling potential source rocks:

- Not all source rocks are products of upwelling or of upwelling alone; most are probably not.
- There remain significant methodological uncertainties with regard to the robustness of reported levels of agreement between predicted upwelling and source rock occurrence that is potentially explicable by upwelling (i.e. the type of statistic used, exactly how it is calculated and its genuine significance).
- Upwelling is a widespread phenomenon that occurs at a wide range of spatial scales, intensities, frequencies and persistence; therefore, generalisations should be treated with caution.
- Upwelling addresses only the supply of nutrients by Ekman divergence (although it is made more relevant to phytoplankton productivity by also considering the availability of light); consequently, not all upwelling results in the production of organic-rich (or oil-prone) sediments due to the influence of other regional or local factors (e.g. water depth, oxygen levels, current strengths, sediment grain size, siliciclastic dilution and biogenic autodilution).
    - Onshore aridity and areas of low fluvial discharge are factors that can be used in conjunction with predicted upwelling to help define areas of favourably low dilution by siliciclastic sediment.
- Any organic-rich sediment produced is not necessarily permanently preserved (e.g. due to subsequent erosion or reworking of the outer shelf and upper slope), and it may also not acquire an adequate thickness.

A1.3. METHODS

For modelling purposes, it is assumed that modelled palaeo-oceanographic data from Globe's Earth system model (ESM) can be used to depict the oceanographic conditions that define coastal upwelling; therefore, the data can also be used to indicate the locations of areas that had potentially high ocean productivity throughout geological history.

The model defines areas of potential coastal upwelling during any given month as being:

- In water deep enough to be stratified
- Within 250 km of the frontal zone
- Where there is a net upward movement of water across the base of the OML
- Where there is a net offshore movement of the surface water (relative to the local coastline generalised at a 0.5° level)
- Where daylight length is not limiting (i.e. at least 8 hours of daylight per day)
- Where sea ice cover is limited to less than 50%

The conditions listed above are combined to show the spatial distribution of the occurrence of upwelling conditions, but the combination will not give a sense of the intensity of its signal. To obtain a measure of the intensity of the coastal upwelling signal, the strength of both the offshore current and the vertical upward movement of the ocean must be assessed. The greater the velocity of these currents, the greater the influx of nutrients into the photic zone and the greater the volume of organic matter carried away from the coastal ocean mixed zone, resulting in an increased likelihood of organic matter being deposited.

The model produces three annual summary layers of coastal upwelling frequency/intensity per timeslice:

1. Upwelling annual frequency: Showing only the number of months upwelling exists regardless of its intensity.
2. Upwelling annual average intensity: Showing an upwelling index that integrates the vertical and horizontal velocities, the transport direction and the available light for all 12 months.
3. Average intensity of upwelling months: Showing the annual intensity index values averaged over the number of months an upwelling signal is present.

The following sub-sections show how Globe's palaeo-oceanographic and palaeogeographic data have been combined to produce the annual frequency and intensity data. The sub-sections also 1) describe how each of the six key upwelling conditions listed above are defined using Globe's palaeo-oceanographic data, 2) depict the necessary workflows undertaken by the model to depict each of the key upwelling conditions, and 3) outline how the key upwelling conditions are combined spatially and temporally to produce annual and monthly summary maps.

A1.3.1 METHODS FOR DETERMINING THE KEY UPWELLING CONDITIONS FROM EXISTING GLOBE DATA

All of the Globe ESM data used in the modelling process are monthly. As a first step, it is critical to assess the monthly data to determine 1) spatially where the upwelling conditions required existed in a given month and 2) the strength of that upwelling signal. This accomplishes two things: 1) it preserves information on the seasonality of the signal that can then be assessed at a later stage in the modelling process, and 2) it eliminates any data values being included in annual summaries where the conditions for upwelling were not all met. The following sub-sections describe the processes applied by the model to determine the spatial extent of the upwelling conditions defined for each month. Once the monthly data have been analysed, they can be combined to produce annual summaries.

A1.3.1.1 DETERMINING THE FRONTAL ZONE AND THE 250 KM AREA OF UPWELLING

Data required:

- Globe palaeobathymetry layers
- Globe ESM palaeoclimate monthly mixed ocean layer depths (MOLDs)

Here, the frontal zone is defined as the area where the MOLD intersects with the bathymetry (Figure 2). Water shallower than this point will be completely mixed and will not have any stratified nutrient-rich bottom water to bring to the surface. As the MOLD varies by month, the point of intersection with the bathymetry will also vary by month; it is therefore essential to assess the frontal zone and 250 km area of upwelling on a monthly basis.

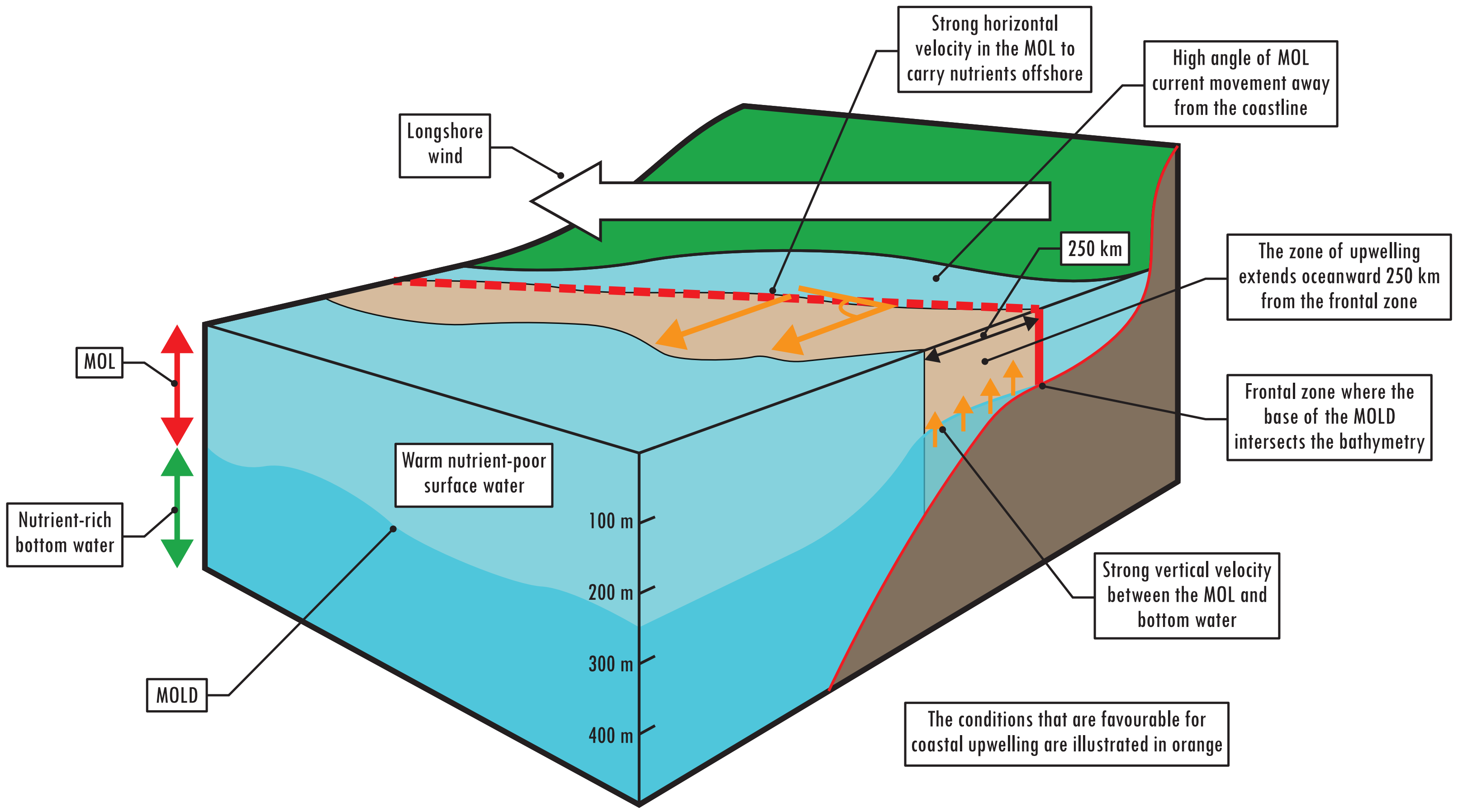

Figure A1.2: Box diagram showing how the frontal zone and the 250 km area of upwelling are defined.

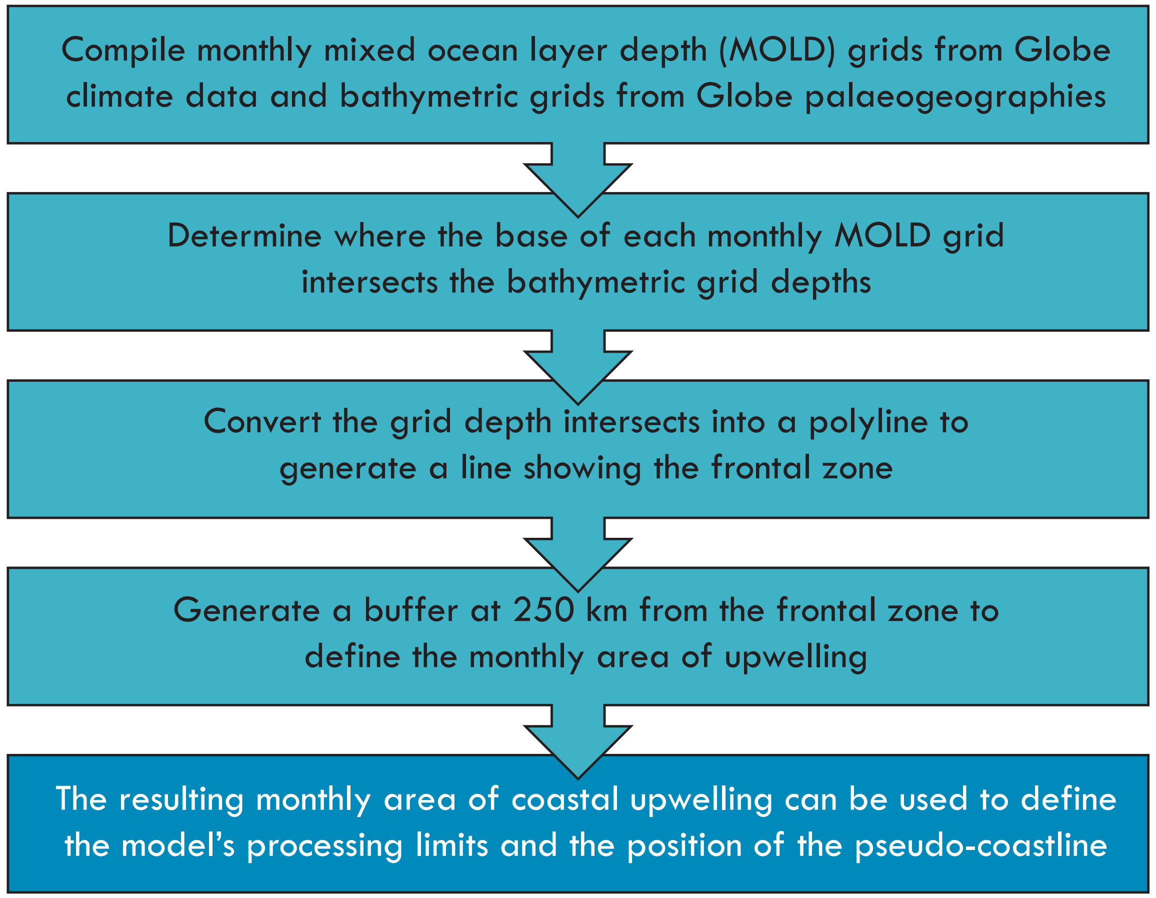

Figure A1.3: ***Workflow for determining the frontal zone and the 250 km area of upwelling.***

Once the frontal zone line is determined, it is then possible to generate a 250 km buffer from this line that extends in a seaward direction; this buffer will define the 250 km zone of coastal upwelling for each month. Any data positioned outside this zone will be masked out as they are considered beyond the offshore extent of upwelling (based on Present Day observations). The workflow outlined in Figure 3 shows the necessary steps taken to determine the frontal zone and the 250 km area of upwelling.

A1.3.1.2 DETERMINING IF STRATIFIED WATERS ARE BROUGHT INTO THE OCEAN MIXED LAYER

Data required:

- Globe ESM palaeoclimate monthly MOLDs
- Globe ESM palaeoclimate monthly ocean vertical velocity depth layers
- Monthly area of coastal upwelling (calculated in previous step)

The next stage in the modelling process is to determine if there is vertical upward movement of nutrient-rich stratified ocean waters into the MOL. This can be done using the monthly MOLDs (as they represent the boundary between the stratified deeper ocean water and the oxygenated mixed layer) and the vertical velocity data (as these data show the net vertical movement of water in the ocean). The model isolates the relevant vertical velocity grid values for all depth layers that intersect with the MOLD (Figure 4); this generates a single grid with the velocity values at the MOLD.

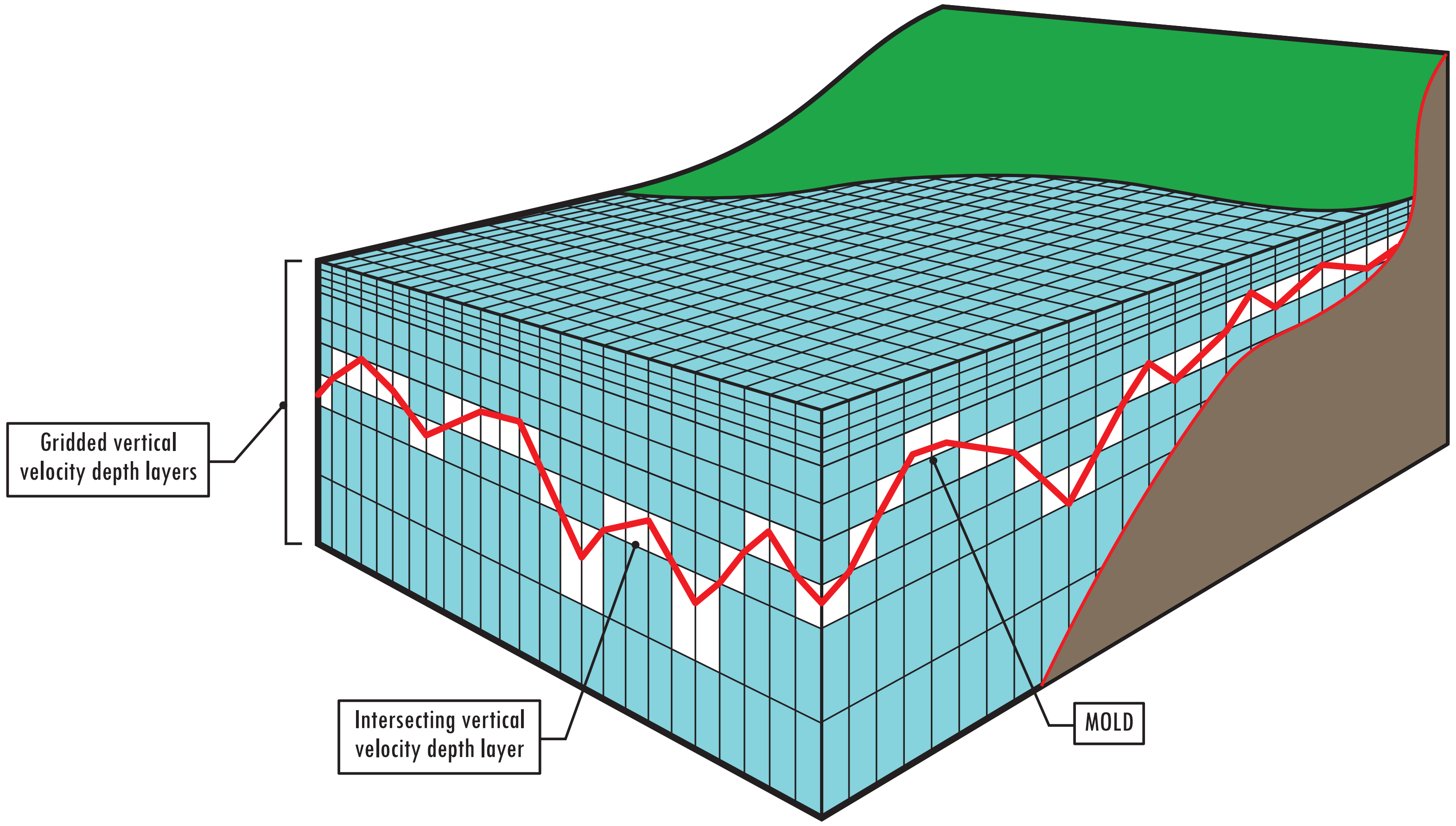

Figure A1.4: ***Schematic box diagram showing how the model intersects the mixed ocean layer depth (MOLD) with different vertical velocity depth grids.***

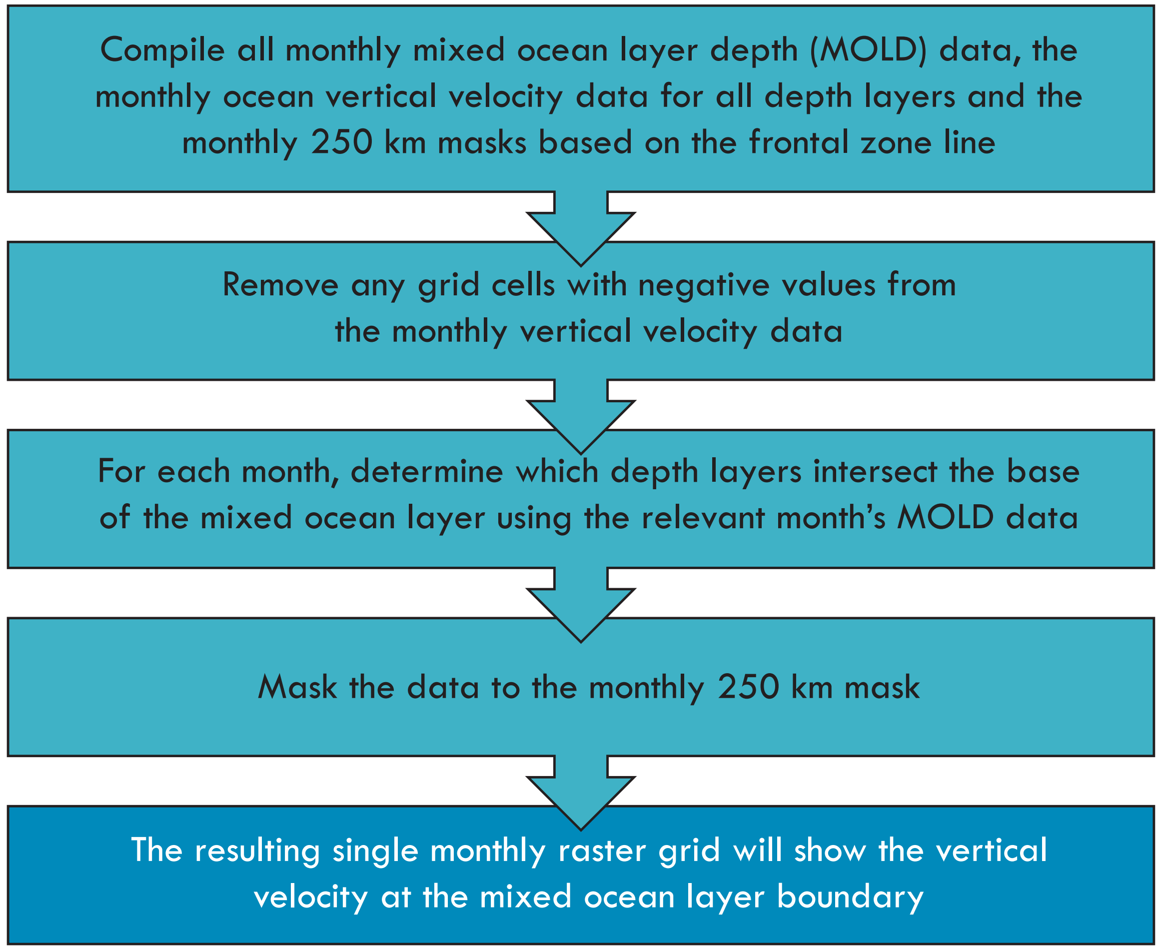

Figure A1.5: ***Workflow for determining the vertical velocity at the mixed ocean layer boundary.***

The velocity values are positive for the upward movement of water and negative for the downward movement of water; as upwelling requires the upward movement of water, the model filters out any negative values, leaving only the velocity values for upward moving water. The data are then masked against the monthly extent of upwelling determined by the 250 km masks described in the previous sub-section.

The workflow used for this part of the modelling is shown in Figure 5. The final layer from this process shows the spatial extent of vertical upward movement through the MOL boundary; this layer is used in the modelling for both the monthly and annual summaries.

A1.3.1.3 DETERMINING IF THERE IS AN OFFSHORE CURRENT IN THE SURFACE WATER

Data required:

- Frontal zone polylines (calculated in a previous step)
- Monthly zone of coastal upwelling (calculated in a previous step)
- Globe ESM palaeoclimate monthly ocean horizontal velocity depth layers

It is essential to establish if the nutrient-rich waters that were brought to the surface at a specified point in time were carried offshore away from the frontal zone. If these waters were driven from the frontal zone in an onshore direction, then there will have been no stratified bottom water available for the organic matter produced to have been deposited and preserved within the sediment. Any organic matter that remained in the shallow mixed oxygenated water is likely to have been oxidised and not preserved in the sediments deposited. Therefore, the model considers the frontal zone to be a pseudo-coastline, and the 'offshore' current is calculated relative to this instead of the coastline (Figure 2).

Figure A1.6: ***Workflow to determine if an offshore current exists relative to the pseudo-coastline.***

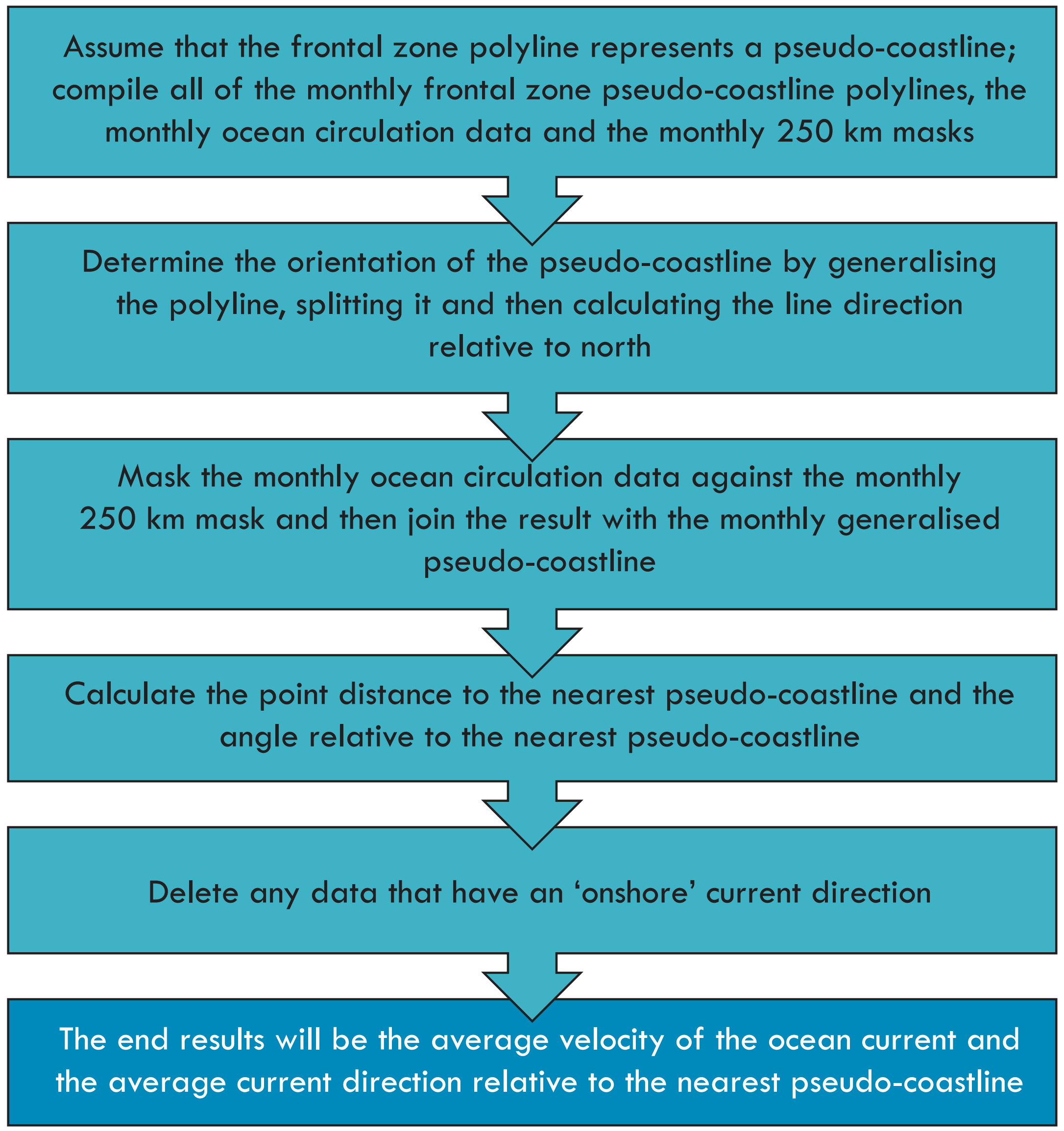

In order to determine if an offshore current existed at a certain point in time, a number of steps must be taken (Figure 6). Initially, the frontal zone polyline (acting as a pseudo-coastline) is generalised to 0.5 degrees; this converts the polyline into a series of straight lines from which its orientation relative to north can be calculated.

The next step in the modelling process is to establish the direction of the current in the surface water. The surface water in this model encompasses the upper five depth layers of the ocean circulation data. These depth layers correspond to the upper 50 m of the water column and are considered the most significant ones as this where the majority of photosynthesis takes place. These data are masked to the relevant monthly 250 km area of upwelling (determined in a previous step in Section 3.1.1). The data are then joined to the nearest section of the monthly pseudo-coastline, based on the point distance to the pseudo-coastline.

Once the data have been joined to the pseudo-coastline, the angle relative to the pseudo-coastline can be calculated. The data are then filtered to leave only the offshore current values (i.e. values between 0 and 90 relative to the pseudo-coastline). These values are then averaged through the five surface depth layers to generate a single point data set with the average offshore current direction and velocity in the surface water. These data values are exported to produce two separate raster grids, with one showing the average current direction relative to the pseudo-coastline and the other showing the average velocity of the current. These raster grids will be used in the modelling for both monthly and annual summaries.

A1.3.1.4 FILTERING FOR DAYLIGHT LENGTH LIMITATIONS & SEA ICE COVER

As upwelling can only influence productivity where and when light is available, the mean monthly daylight length variation with latitude and season is used to determine whether daylight is likely to be limiting or not for the month(s) of predicted upwelling. The objective is to help identify the likely distribution of effective (non-light-limited) upwelling productivity.

The mean monthly length of daylight is calculated from the formula of Forsythe et al. (1995), which corrects for latitude and the Julian day of the year (seasonality) for both hemispheres (arbitrary fifteenth day of the month values are used for monthly calculations). Present Day orbital parameters are assumed. Spatial filtering of the predicted coastal upwelling is applied according to a minimum required daylight length of 8 hours for plankton blooming, based upon Ardyna et al. (2013) for the modern Arctic Ocean. At least some of the upwelled nutrients that cannot be utilised at the time of physical upwelling because of low light levels (or too deep a MOLD) may be utilised later in the year, boosting productivity once light improves and the MOLD is reduced. However, the nutrient-rich cold water may sink or be exported. No such effects are included in the model.

The GCM estimated sea ice coverage ('concentration') is also used as a spatial filter to further constrain the distribution of productivity-effective upwelling. High latitude productivity is likely to be positively correlated with the proportion of open water (Ardyna et al., 2014). In the absence of data, we have assumed a maximum permissible sea ice concentration of 0.5 (i.e. 50% of a grid cell).

The productivity of upwelling zones will be greatest where the MOLD is less than the thickness of the euphotic zone. Under such circumstances the phytoplankton are never light-limited. When the mixed layer is deeper (as happens in winter), mixing will carry the phytoplankton below the euphotic zone for part of the time, limiting the primary productivity. Of course, during winter the euphotic zone will also be shallower (especially at higher latitudes) and daylight length will be shorter. At the moment, we have not yet included the euphotic depth in our model, although generalised algorithms are available that could be utilised for this purpose. Its inclusion would further constrain productivity-effective upwelling to the spring to autumn period (i.e. not winter) and would amplify latitudinal gradients.

To summarise, both seasonal daylight length and sea ice have limiting effects on photosynthesis. For modelling purposes, it is assumed that photosynthesis becomes limited if an area receives less than 8 hours of daylight per day and if it has over 50% sea ice cover. These parameters roughly correspond with the limits of high-latitude productivity blooms. Daylight length is determined by latitude and the time of year, while sea ice cover is derived directly from the climate model. Any data that either do not meet the required minimum number of daylight hours or exceed the sea ice cover limits are removed by the model.

A1.3.2 GENERATING MONTHLY AND ANNUAL SUMMARY LAYERS

A1.3.2.1 UPWELLING ANNUAL FREQUENCY SUMMARY LAYER

Once the model has determined where each of the coastal upwelling conditions existed on a monthly basis, it is possible to stack these monthly conditions to determine the spatial extent of areas where all of the requirements for an upwelling signal were met each month.

These 12 monthly frequency layers can be combined to show the number of months the upwelling signal was present for each year (Figure 7). This is the first annual summary layer provided to users and it is named 'upwelling annual frequency'; it consists of a grid that shows values ranging from 1 to 12, with the numbers representing the number of months in a year that the upwelling signal was present, irrelevant of its intensity.

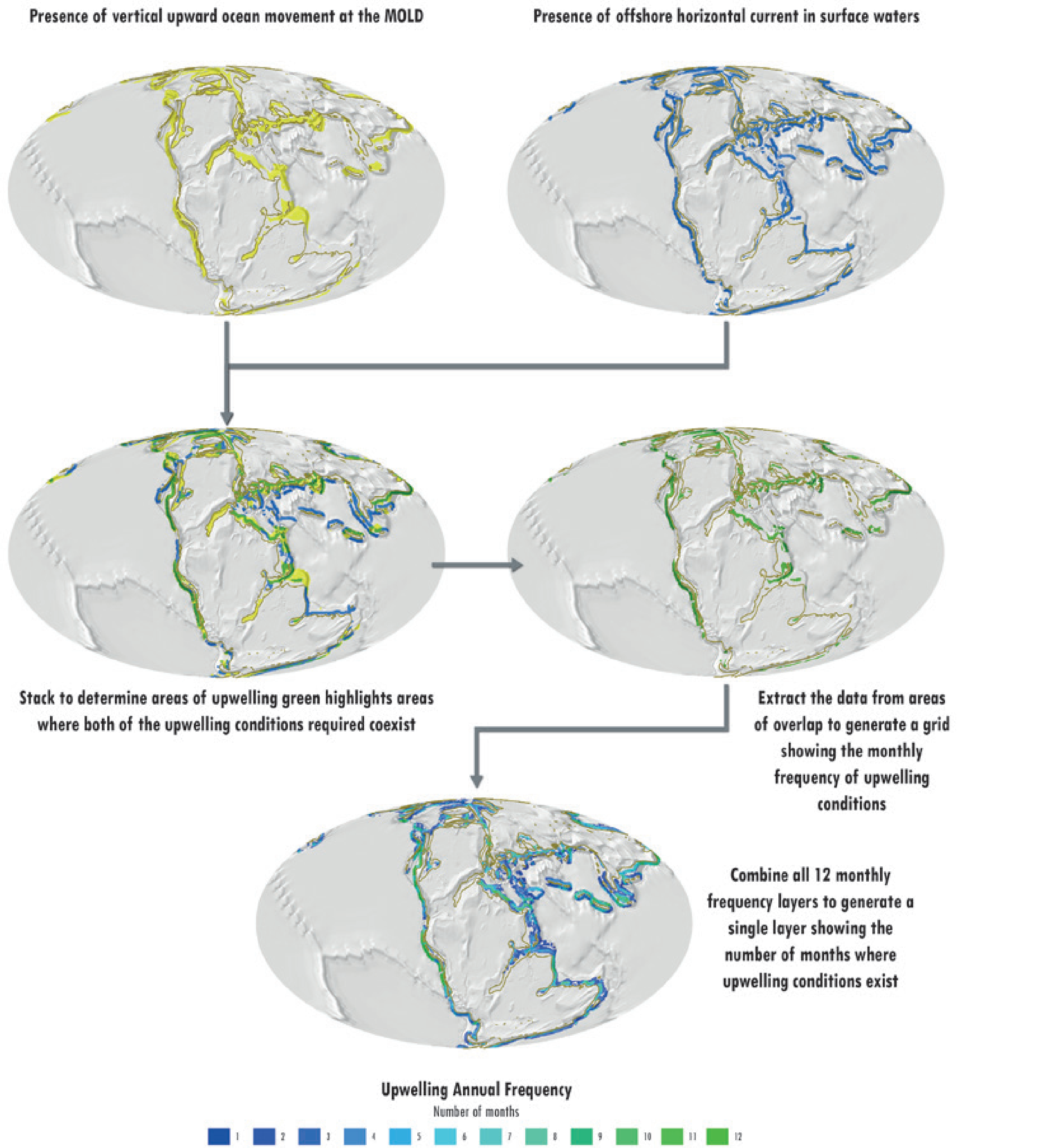

Figure A17: ***Workflow for determining the number of months where upwelling conditions existed to produce an upwelling annual frequency data layer.***

A1.3.2.2 UPWELLING MONTHLY INTENSITY SUMMARY LAYER

The monthly summaries for the vertical velocity at the MOLD, the offshore current velocity and the surface ocean current direction relative to the nearest pseudo-coastline all contain velocity/vector values within the data. These values can be used to generate a sense of the monthly intensity of the upwelling signal.

To evenly weight the values of the data, they are converted into a percentage of the maximum value. This brings all the data values for each of the three conditions down to a value of between 0 and 100. Once they are filtered by the various masks (i.e. the 250 km extent of upwelling, sea ice and daylight filters), the resulting intensity grids can be stacked and combined to show a monthly intensity of the coastal upwelling signal; the resulting data layer is called ‘upwelling monthly intensity’ (Figure 8). The model will only combine values where all three conditions exist. This layer allows the user to assess the strength of the coastal upwelling signal on a monthly basis.

A1.3.2.3 UPWELLING ANNUAL AVERAGE INTENSITY LAYER AND AVERAGE INTENSITY OF UPWELLING MONTHS LAYER

Once the monthly intensity values of all the upwelling conditions have been combined, it is then possible to summarise them as an annual average. This has been achieved in a simple way by summing the values of the 12 monthly layers and then dividing the total by 12 to return the intensity values back to a single percentage value that ranges from 0 to 100. The resulting data layer is called ‘upwelling annual average intensity’; it gives an overall average of the strength of the coastal upwelling signal throughout the year, but it does not distinguish whether that signal strength/weakness is down to a few months of strong upwelling or down to several months of weak upwelling. This is where the monthly intensity data can become useful.

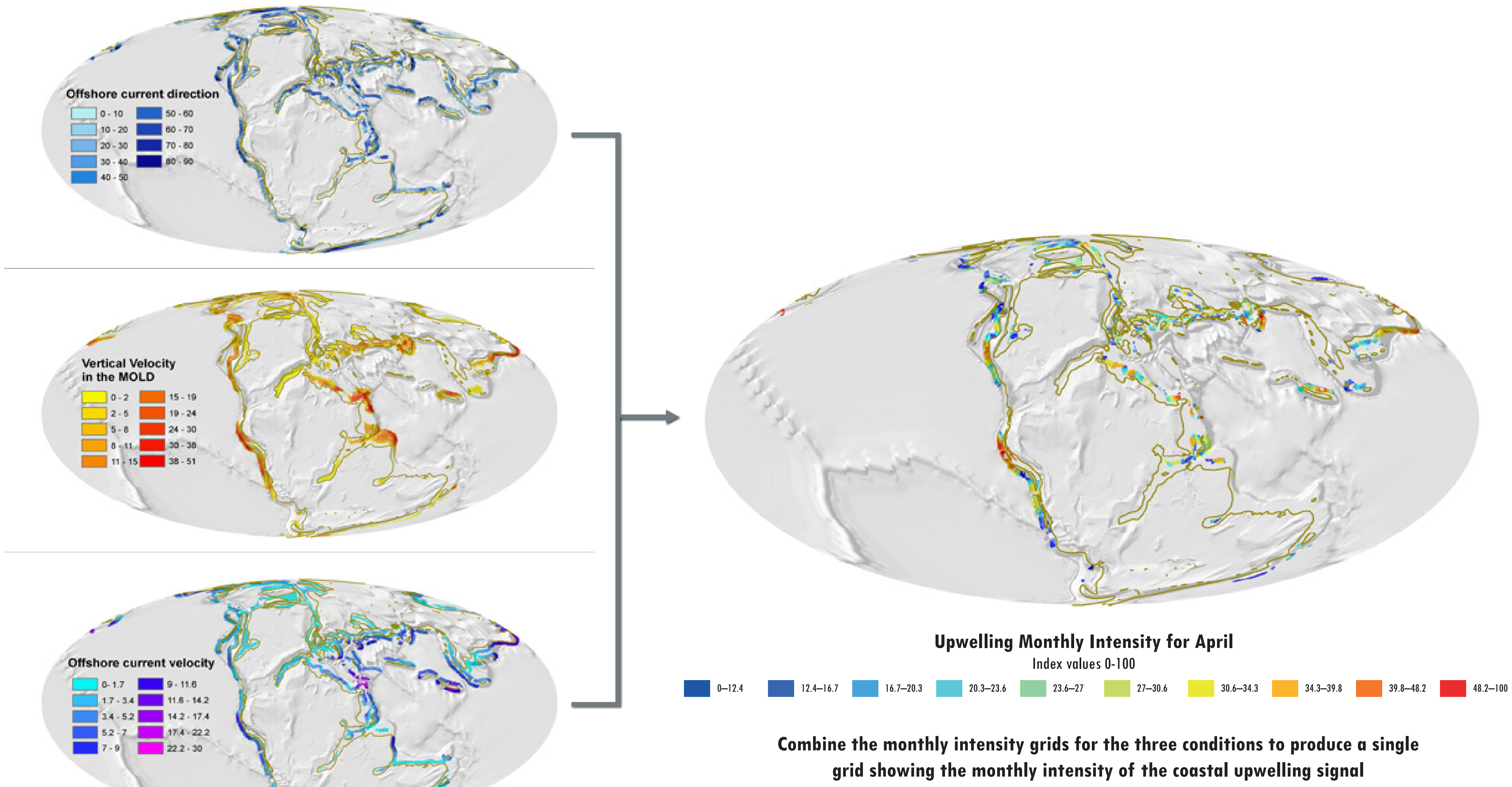

Figure A1.8: Workflow used to produce an upwelling monthly intensity data layer.

A further useful summary of these data is provided by taking the annual intensity sum and dividing this by the number of months the upwelling signal existed. The resulting data layer is called ‘average intensity of upwelling months’; it shows the average intensity for the months of the year where the upwelling conditions actually existed, rather than being averaged over the entire year. This will give a more informed metric for the strength of the upwelling signal when it existed, without the need to search through all 12 monthly summaries.

A1.3.3 OVERVIEW OF THE MODELLING PROCESSES

Figure 9 provides a summary workflow of the modelling methods applied by Getech's Coastal Upwelling Model. In particular, the workflow outlines the input data used in the modelling, the simplified steps applied in the modelling processes and the output summary data generated.

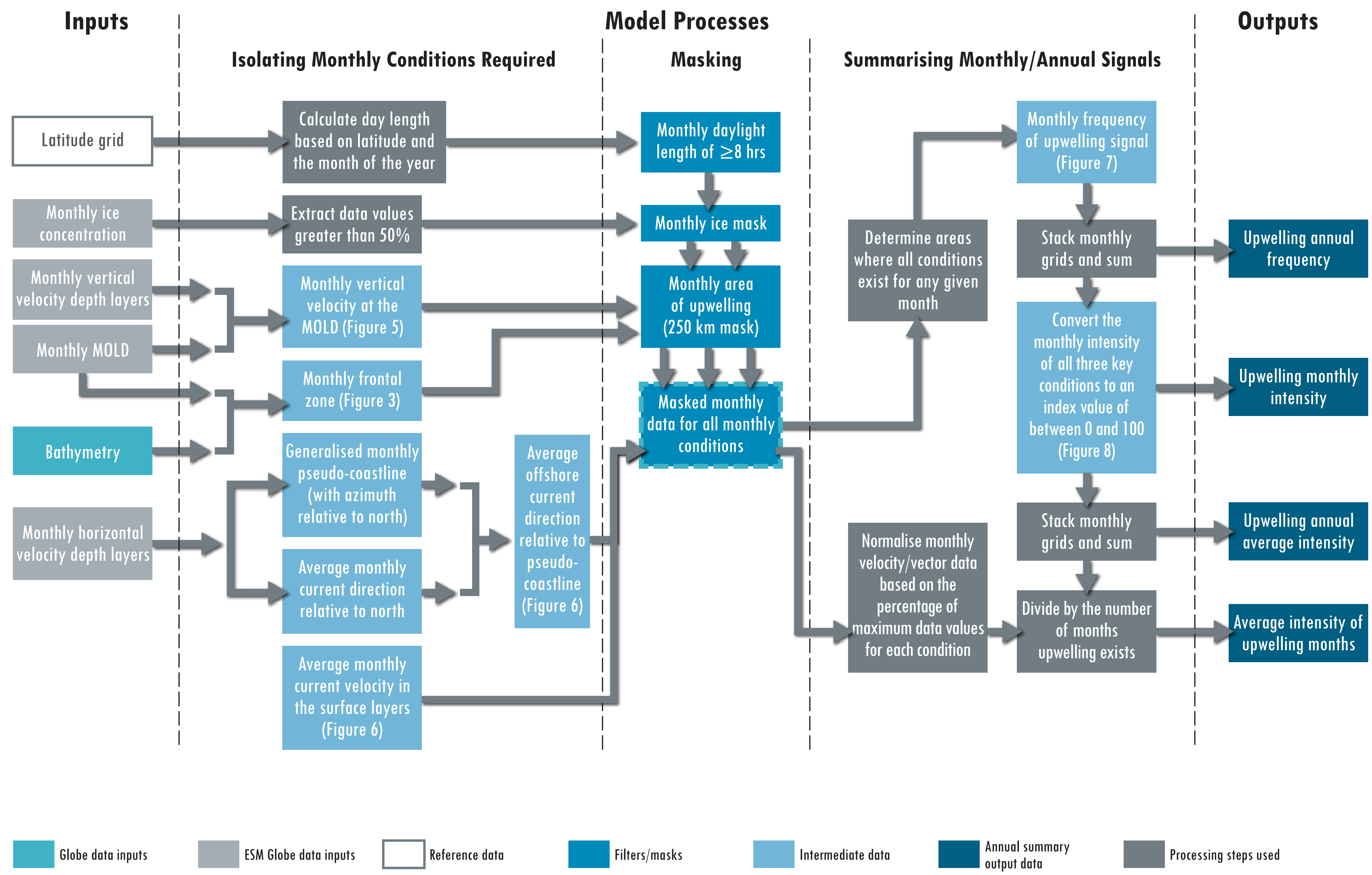

Figure A1.9: Summary workflow of the modelling methods applied by Getech's Coastal Upwelling Model.

A1.4 WEST TETHYS COASTAL UPWELLING RESULTS

The coastal upwelling model was run for all Lower Jurassic stages (Hettangian to Toarcian) and Tithonian to supplement the OFP modelling results. The results are presented in Figure 10.

These results show low to moderate conditions for upwelling within the Hispanic Corridor region. However, due to the limited width and length of the corridor during the Early Jurassic the results are limited to a few grid cells and do not provide adequate information regarding potential spatial patterns. Moreover, the shallow restricted nature of the Hispanic Corridor basin during the early Jurassic means it is unlikely to have well established open oceanographic conditions that typify present day coastal upwelling regions. Therefore, the influence of coastal upwelling on productivity is likely to limited in the Hispanic Corridor during the Lower Jurassic.

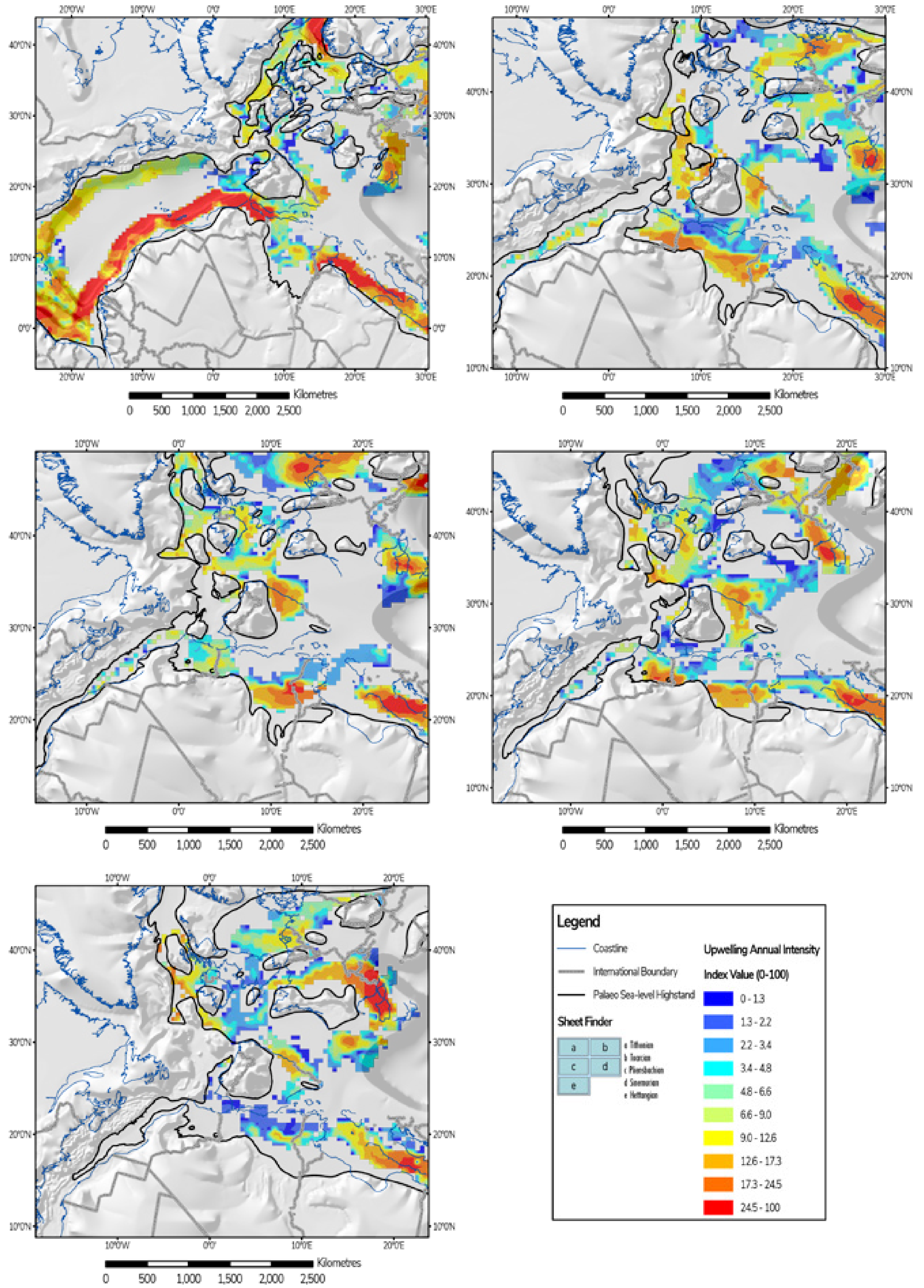

Figure A1.10: ***Modelling results for annual average intensity of coastal upwelling for the Lower Jurassic and Tithonian.***

A1.5. REFERENCES

Ardyna, M., Babin, M., Gosselin, M., Devred, E., Bélanger, S., Matsuoka A. & Tremblay, J.-É. (2013). Parameterization of vertical chlorophyll a in the Arctic Ocean: impact of the subsurface chlorophyll maximum on regional, seasonal, and annual primary production estimates. Biogeosciences, 10 (6), pp. 4383-4404, doi: 10.5194/bg-10-4383-2013.

Ardyna, M., Babin, M., Gosselin, M., Devred, E., Rainville, L. & Tremblay, J.-É. (2014). Recent Arctic Ocean sea ice loss triggers novel fall phytoplankton blooms. Geophysical Research Letters, 41 (17), pp. 6207-6212, doi: 10.1002/2014GL061047.

Barron, E. J. (1985). Numerical climate modeling, a frontier in petroleum source rock prediction: results based on Cretaceous simulations. AAPG Bulletin, 69 (3), pp. 448-459, doi: 10.1306/ad46250b-16f7-11d7-8645000102c1865d.

Barron, E. J. & Moore G. T. (1994). Upwelling prediction. In: E. J. Barron & G. T. Moore (Eds.) Climate Model Applications in Paleoenvironmental Analysis, SEPM Short Course Notes, 33, pp. 109-129, doi: 10.2110/scn.94.03.0109.

Forsythe, W. C., Rykiel, E. J., Stahl, R. S., Wu, H.-I. & Schoolfield, R. M. (1995). A model comparison for daylength as a function of latitude and day of year. Ecological Modelling, 80 (1), pp. 87-95, doi: 10.1016/0304-3800(94)00034-F.

Hagen, E., Feistel, R., Agenbag, J. J. & Ohde, T. (2001). Seasonal and interannual changes in intense Benguela upwelling (1982–1999). Oceanologica Acta, 24 (6), pp. 557-568, doi: 10.1016/S0399-1784(01)01173-2.

Kruijs, E. & Barron, E. J. (1990). Climate model prediction of paleoproductivity and potential source-rock distribution. In: A.-Y. Huc (Ed.) Deposition of organic facies, AAPG Studies in Geology, pp. 195-216, doi: 10.1306/St30517C13.

Miller, R. G. (1989). Prediction of ancient coastal upwelling and related source rocks from palaeo-atmospheric pressure maps. Marine and Petroleum Geology, 6 (3), pp. 277-283, doi: 10.1016/0264-8172(89)90007-x.

Moore, G. T., Barron, E. J., Bice, K. L. & Hayashida, D. N. (1995). Paleoclimatic controls on Neocomian-Barremian (Early Cretaceous) lithostratigraphy in northern Gondwana's rift lakes interpreted from a general circulation model simulation. In: A.-Y. Huc (Ed.) Paleogeography, Paleoclimate, and Source Rocks, AAPG Studies in Geology, 40, pp. 173-189, doi: 10.1306/St40595C8.

Moore, G. T., Hayashida, D. N. & Ross, C. A. (1993). Late Early Silurian (Wenlockian) general circulation model-generated upwelling, graptolitic black shales, and organic-rich source rocks - an accident of plate tectonics? Geology, 21 (1), pp. 17-20, doi: 10.1130/0091-7613(1993)021<0017.

Parrish, J. T. (1982). Upwelling and petroleum source beds, with reference to Paleozoic. AAPG Bulletin, 66 (6), pp. 750-774, doi: 10.1306/03b5a30e-16d1-11d7-8645000102c1865d.

Parrish, J. T. (1995). Paleogeography of Corg-rich rocks and the preservation versus production controversy. In: A.-Y. Huc (Ed.) Paleogeography, paleoclimate, and source rocks, AAPG Studies in Geology, 40, pp. 1-20, doi: 10.1306/St40595C1.

Parrish, J. T. & Curtis, R. L. (1982). Atmospheric circulation, upwelling, and organic-rich rocks in the Mesozoic and Cenozoic eras. Palaeogeography, Palaeoclimatology, Palaeoecology, 40 (1-3), pp. 31-66, doi: 10.1016/0031-0182(82)90084-0.

Scotese, C. R. & Summerhayes, C. P. (1986). Computer model of paleoclimate predicts coastal upwelling in the Mesozoic and Cenozoic. Geobyte, 1 (3), pp. 28-42.

Trask, P. D. (1934). Deposition of organic matter in recent sediments. In: W. E. Wrather & F. H. Lahee (Eds.) Problems of Petroleum Geology, AAPG Special Publication, 6, pp. 27-33, doi: 10.1306/SV6334C3.